Copyright is owned by the Author of the thesis. Permission is given for a copy to be downloaded by an individual for the purpose of research and private study only. The thesis may not be reproduced elsewhere without the permission of the Author.

PREDICTION OF THE GLASS TRANSITION TEMPERATURE OF FRUIT JUICE POWDERS



A thesis presented in partial fulfilment of the
requirements for the degree of

Doctor in Philosophy
in
Process Engineering

At Massey University, Manawatu, New Zealand

Sebastian Linnenkugel

2019

To

My Family

&

My Flower and Moon

Abstract

To overcome the limited shelf life of fresh fruit juice, manufacture aim to reduce the juice to a powdered form that can be available all year around. One technique of powder formulation is the use of spray dryer. However fruit juices are rich in fruit sugars and organic acids, which make them difficult to spray dry. Their low glass transition temperatures lead to stickiness problems in the spray dryer. This work investigates the prediction of the glass transition temperature (T_g) of fruit juice powders and mixtures including high molecular weight components often used as drying aids of their mixtures. The ability to predict glass transition temperatures enables optimization of powder formulations and spray dryer operation to avoid sticking problems.

A semi-empirical model is presented to predict the glass transition temperature of fruit juice powders on the basis of the chemical composition and the T_g values of the individual pure components. The Flory-Huggins Free Volume theory is used to describe the relation between the water activity of the powders and the glass transition temperature based on the composition of the powders. These prediction models were tested for different freeze dried multicomponent systems and validated against the glass transition temperatures measured by Differential Scanning Calorimetry (DSC).

The model was then applied to predict the T_g of values freeze dried juice and vegetable powders prepared from commercial juice concentrate. The six fruit and vegetable juice powders exhibited higher measured T_g values at zero water activity those that predicted from the model. The 6-14˚C difference between the measured and predicted T_g values cannot be explained purely by the main sugar and organic acid components, but are rather linked to the presence of residual breakdown products of pectins and other polysaccharides from the base fruit. For several powders, a second glass transition temperature was visible in the DSC thermogram, which can be attributed to these additional components. The prediction of the glass transition temperature of the pure juice powders at various water activities showed better agreement with the experimental data the closer the predicted and measured T_g value of the powders was at zero water activity.

The T_g values of different low molecular weight components and the polysaccharide maltodextrin DE 9-13 often used as a drying aid was studied. The T_g for the binary and multicomponent systems was well estimated by the prediction model at zero water activity. The addition of higher amounts of maltodextrin DE 9-13 up to a weight fraction

of 0.7 in the mixture resulted in a widening of the transition observed in the DSC thermogram, which can be attributed to dynamic heterogeneity of the samples due to the dynamic response times of different domains in the solid matrix. This could be demonstrated by annealing the samples below their glass transition temperatures for 16 hours. The analytical semi-empirical model proved to be a viable method for predicting the glass transition temperature of mixtures of low and high molecular mixtures.

Multicomponent systems consisting of more than one high molecular weight component in the form of various soluble polysaccharides and the monosaccharide glucose were investigated for their T_g values at zero water activity. The different mixtures of the low molecular weight components and polysaccharides showed a shift in the glass transition temperature that depended strongly on the T_g value of the pure polysaccharide. However, the overall trend of T_g values for the mixtures of low and high molecular weight components was found to be similar for all mixtures. The T_g values of all systems with various polysaccharides were well predicted. It also highlighted that a weight fraction of above 0.5 for the polysaccharides with a degree of polymerization of sugar units above 5 is necessary in the solid matrix to have a significant impact on the glass transition temperature.

Salts were tested as an alternative drying aid to high molecular weight components at various ratios to the monosaccharide glucose. The salts increased the glass transition temperature of the blends at lower concentrations. A weight fraction of 0.2 of salts in the system has the same effect on the T_g values as a 0.5 weight fraction of a higher molecular weight component. The difference in necessary amount to increase T_g can be attributed to the different mechanisms of salts and polysaccharide in the solid matrix.

To demonstrate the utility of the model, it was applied to optimize the spray drying of blackcurrant juice concentrate, with the aid of maltodextrin DE 9-13. It has been reported that sticking can be avoided during drying if the operating temperature does not exceed $T=T_g + 25^{\circ}C$. By combining the prediction of the T_g of the solid mixture at various water activities and a mass and energy balance over the spray dryer, reasonable feed composition and operational conditions were found. This allowed the successful conversion of blackcurrant juice into a powder in a single trial without relying on trial-and-error approaches.

Acknowledgements

I greatly appreciate the support of the Food Industry Enabling Technology (FIET) programme, which made this project possible and funded me during my time at Massey University. Besides the financial support, I would like to mention the great involvement of the FIET commodity, which stimulated the exchange between the researchers and provided us with an insight of the commercial side of the R&D work.

I am so grateful for all what my supervisors have done for me and how they helped me develop my research skills, but also helped me develop as a person and made me feel welcomed in New Zealand. I will miss the fruitful discussions on Wednesday mornings, which help me to discover my journey of my PhD. Thanks, to Tony Paterson, I finally know what "a red herring" is, after I had to hear it several times. But I am so very grateful that he pulled me out some of my rabbit holes and helped me to get back on track. Before coming to New Zealand, I think I never used the word "why" that often, but throughout our discussions Tony always emphasized the importance of the asking the question "why" and really trying to dig deep to try to fully understand a topic. Now I cannot look at something without asking the question why does it work like this and I believe it helps me a lot to tackle new challenges in the future.

Thanks to my supervisor Lee Huffman, I learned to look beyond the research. She introduced me to the commercial side of R&D and really sharpened my skill to communicate my research. My supervisor, John Bronlund allowed me to live a "true Kiwi experience" by introducing me to a hay day adventure and I appreciate all the good ideas and comments that improve the quality of my work. I am grateful for all the input I received and I believe I have to thank everyone that worked with me over that time, contributing to my personal and professional development.

Especially, thanks belong to my fiancée, who supported me throughout my PhD with lots of love and motivated me to keep pushing forward even in hard times. I am also grateful for the support of my family and friends, who made the long journey to New Zealand to discover the beautiful islands together with me.

Table of Contents

Table of Contents **5**

Index of Abbreviations **9**

Index of Symbols **12**

Index of Figures **16**

Index of Tables **22**

1. Project Overview **24**

1.1 Introduction 24

1.2 Objectives of the study 26

2. Literature Review **28**

2.1 Amorphous Solids 28

2.2 Composition of fruit juices 30

2.3 Powder production 33

2.3.1 Spray drying 33

2.3.2 Freeze drying 35

2.4 Physical stability of food product 37

2.4.1 Stickiness 37

2.5 Glass transition 39

2.5.1 Miscibility and the glass transition temperature 41

2.6 Effects on the glass transition temperature 43

2.6.1 Plasticizer 43

2.6.2 Molecular weight 48

2.6.3 Crystallinity 49

2.6.4 Filler effects 52

2.7 Mathematical models 53

2.7.1 Glass transition of linear polymers 53

2.7.2 Binary blends 54

2.7.3 Multicomponent systems 60

2.8 Glass transition temperature of components 63
2.8.1 Preparation of amorphous solids for DSC measurement 63
2.8.2 Melt quenching 63
2.8.3 Freeze drying 64
2.8.4 T_g of solids in fruit juices 65
2.8.5 T_g of anhydrous binary systems 69
2.8.6 T_g of anhydrous ternary mixtures 75
2.9 Drying aids 78
2.10 Analysis of the glass transition temperature 83
2.10.1 Differential Scanning Calorimetry 84
2.10.2 Dynamical Mechanical and Dielectric Analysis 88
2.11 Water Activity 89
2.12 Water activity and glass transition temperature 92
2.13 Conclusion 93
3. Materials and methods 95
3.1 Materials 95
3.2 Methods 96
3.2.1 High Pressure Liquid Chromatography 96
3.2.2 Fast Pressure Liquid Chromatography 97
3.2.3 Freeze drying 97
3.2.4 Water activity and moisture content 98
3.2.5 Differential Scanning Calorimetry 100
3.2.6 Spray drying 100
3.2.7 Error calculations 101
4. Modelling of fruit juice powders 102
4.1 Introduction 102
4.2 Prediction of the T_g of fruit juice powders with polysaccharides 102
4.2.1 Testing of the approach on literature data 112
4.3 Flory-Huggins Free Volume theory (FHVT) 114
4.3.1 Absorption into a material in the rubbery state 117
4.3.2 Absorption into a glassy matrix 120

4.4 Test on literature values 123
4.4.1 Test of component with increasing molecular weight 124
4.4.2 Freeze dried grapefruit puree powders 128
4.4.3 Freeze dried mango puree powders 130
4.4.4 Spray dried lemon juice powders 135
4.4.5 Freeze dried strawberry puree powder 137
4.4.6 Deviation of the FHVT models 138
4.5 Conclusion 143
5. Pure fruit juice powders 144
5.1 Introduction 144
5.2 Composition of fruit juices 144
5.3 T_g of juice and vegetable powders at zero water activity 148
5.3.1 Second glass transition temperature in fruit powders 149
5.4 Water activity and T_g of juice powders 152
5.4.1 Predicted sorption isotherms of the powders by the FHVT model 152
5.4.2 Blackcurrant juice powder 154
5.4.3 Kiwifruit juice powder 157
5.4.4 Clear apple juice powder 159
5.4.5 Cloudy apple juice powder 162
5.4.6 Lemon juice powder 164
5.4.7 Carrot juice powder 166
5.4.8 Second glass transition temperature 170
5.5 Conclusion 171
6. Blends with maltodextrin DE 9-13 173
6.1 Introduction 173
6.2 Glass transition temperature of anhydrous powders 173
6.2.1 Prediction of T_g values of the maltodextrin DE 9-13 blends 179
6.2.2 Dynamic heterogeneity in maltodextrin DE 9-13 blends 184
6.3 Water activity and T_g of powders 193
6.3.1 Glucose and maltodextrin DE 9-13 powder 193
6.3.2 Citric acid and maltodextrin DE 9-13 powder 196

6.3.3 Fructose and maltodextrin DE 9-13 powder 198
6.3.4 G/F/C and maltodextrin DE 9-13 powder 200
6.3.5 Blackcurrant and maltodextrin DE 9-13 powder 202
6.4 Phase separation at low water activities 204
6.5 Conclusion 207
7. Polysaccharide and salt mixtures 209
7.1 Introduction 209
7.2 Polysaccharides 210
7.2.1 Glucose with one polymer 214
7.2.2 Glucose with two polymers 216
7.2.3 Glucose with three polymers 218
7.3 Salts 220
7.4 Conclusion 224
8. Case study of spray drying fruit juice 226
8.1 Introduction 226
8.2 Determination of the operational conditions range 226
8.3 Conclusion 234
9. Conclusions and future work 235
9.1 Conclusions 235
9.2 Future work 237
Appendices 239
References 258

Index of Abbreviations

BET	Brunauer-Emmett-Teller equation
BL	Blackcurrant
C	Citric acid
CCP	Calcium caseinate
DE	Dextrose equivalent
DEA	Dielectrical Analysis
DMA	Dynamical Mechanical Analysis
dn/dc	Refractive index increment
DP	Degree of polymerisation
DSC	Differential Scanning Calorimetry
DTA	Differential Thermal Analysis
EDTA	Ethylenediaminetetraacetic acid
F	Fructose
FD	Freeze drying
FH	Flory-Huggins
FHVT	Flory-Huggins Free Volume theory
FPLC	Fast Pressure Liquid Chromatography
FTIR	Fourier Transform Infrared Spectroscopy
G	Glucose
GAB	Guggenheim-Anderson-DeBoer equation
HCP	Hydrolysed caseinate
HPLC	High Performance Liquid Chromatography
HWP	Hydrolysed whey protein
IN	Inulin
M	Molar
MALLS	Multi-Angle Laser Light Scattering
MD	Maltodextrin
Mid	Midpoint
M_n	Number average molecular weight
MQ	Melt quenching
MT	Modulated temperature
M_w	Molecular weight

NaCl	Sodium chloride
NaOAc	Sodium acetate
ND	Not detected
NMR	Nuclear Magnetic Resonance Spectroscopy
PALS	Positron Annihilation Lifetime Spectroscopy
PCL	Polycuproeactone
PE	Pectinesterase
PET	Polyethylene terephthalate
PG	Polygalacturonase
pH	Potential of hydrogen
PiPMA	Poly(isopropyl methacrylate)
PL	Pectinlyase
PMMA	Poly(methyl methacrylate)
PPI	Pea protein isolate
PS	Polystyrene
PVC	Poly(vinylchloride)
PVMA	Poly(vinyl methyl acetate)
PVME	Poly(vinyl methyl ether)
PVPh	Poly(vinyl phenol)
q_m	Melting rate of the crystals
RH	Relative humidity
RPC	Rice protein concentrate
RT MD	Resistance Maltodextrin
S	Sucrose
SD	Standard deviation
SEC	Size Exclusion Chromatography
SPI	Soy protein isolate
t	Time
T	Operating temperature
T_{FM}	Final melting temperature to melt the crystals
T_g	Glass transition temperature
T_g'	Glass transition temperature of the maximal unfrozen amorphous state
TMA	Thermomechanical analysis

T_s	Sticky point temperature
UC	Uncontrolled heating or cooling
UV	Ultraviolet
WLF	Willam-Landel-Ferry equation
WPI	Whey protein isolate
5-HMF	5-Hydroxylmethylfurfural

Index of Symbols

Symbol	Name	Unit
a_0, a_1, a_2	Coefficients of the Brostow equation	K
A_0,A_1,A_2	Polynomial coefficient	J/g
A_{norm}	Normalized coefficient for Redlich-Kister equation	J/g·˚C·
A_{BR},	Coefficient of the Bartenev-Ritland equation	1/K
a_w	Water activity	-
a_{Ai},	Coefficient of the Askadaskii equation	1/K
b	Coefficient of the Orford equation	J/mol·K
b_{Aj}	Coefficient of the Askadaskii equation	$Å^3$/K
b_J	Coefficient of the Jenckel-Heusch equation	-
B_K	Constant for k value determination	-
B_{BR}	Coefficient of the Bartenev-Ritland equation	s/K^2
c	Surface heat constant	-
C_1 , C_2	Coefficient of the WLF equation	-
c_{LW}, b_{LW}	Coefficient of the Lu-Weiss equation	-
C_p	Heat capacity	J/g·˚C
$C_{p,SCL}$	Heat capacity in supercooled liquid state	J/g·˚C
$C_{p,g}$	Heat capacity in glassy state	J/g·˚C
ΔC_p	Difference of heat capacity in glassy and supercooled liquid state	J/g·˚C
$E_{11,12}$	Contact specific interaction enthalpy of intra- and intermolecular interactions	J/g
$E^{'}$	Young's storage modulus	Pa
$E^{''}$	Young's loss modulus	Pa
E_r	Average error	˚C
f_w	Fugacity of water in system	Pa
$f_{w,0}$	Fugacity of pure water	Pa
f_C, n_C, p_C,	Coefficients of the Cowie-Harding equation	-
ΔG_{mix}	Gibbs free energy of mixing	J/g
H	Enthalpy	J/g
H^0	Enthalpy of pure component	J/g

H_g	Enthalpy in glassy state	J/g
H_{SCL}	Enthalpy in supercooled liquid state	J/g
ΔH_{mix}	Enthalpy of mixing	J/g
$\Delta H_{mix,E}$	Difference of enthalpy of mixing in glassy and supercooled liquid state	J/g
k	Coefficient of the Gordon-Taylor equation	-
K_F	Coefficient of the free volume Flox and Flory equation	˚C·g/mol
K_{BS1}, K_{BS2}	Coefficients of the Schneider-Brenker-Cantow equation	-
K^*	Coefficient of the Utracki equation	˚C
M	Moisture content	g/100g
M_0	Monolayer moisture content	g/100g
M_w	Molecular weight	g/mol
M_n	Number average molecular weight	g/mol
N	Ratio of molar volume of solute to solvent	-
p	Pressure	Pa
p_w	Vapour pressure of water in system	Pa
$p_{w,0}$	Vapour pressure of pure water	Pa
q	Heating/cooling rate	˚C/min
q_c	Coefficients of the Cowie-Harding equation	K
q_K	Coefficient of the Kwei equation	˚C
q_m	Heating rate to melt crystals	˚C/min
Q	Heat	J
Q_s	Excess heat of sorption	J/mol
r_b	Bridge radius between two particles	m
R_p	Particle radius	m
R	Gas constant	J/mol·K
R^2	Coefficient of Determination	-
s	Standard deviation	-
s_m	Standard error	-
S	Entropy	J/g˚C
S^0	Entropy of pure component	J/g˚C
S_{SCL}	Entropy in supercooled liquid state	J/g˚C
S_g	Entropy in glassy state	J/g˚C
ΔS_{mix}	Excess entropy of mixing	J/g˚C

t	Time	s
T	Absolute temperature	˚C
T_α	Transition temperature of semi-crystalline materials	˚C
T_a	Temperature of second relaxation peak (DMA)	˚C
T_b	Onset set point transition	˚C
T_c	Crystallisation temperature	˚C
T_{cc}	Cold-crystallisation temperature	˚C
T_e	Endpoint of transition	˚C
T_{1e}	Extrapolated onset point of transition	˚C
T_{2e}	Extrapolated endpoint of transition	˚C
T_g	Glass transition temperature	˚C
$T_{g,mix}$	Glass transition temperature of mixture	˚C
T_g'	Maximally freeze-concentrated amorphous matrix	˚C
T_m	Melting temperature	˚C
T_s	Sticky temperature	˚C
U	Internal energy	J
V	Volume	m^3
V_0	Volume of complete amorphous material	m^3
V_g	Volume in glassy state	m^3
V_{SCL}	Volume in supercooled liquid state	m^3
x	Weight fraction	-
X_s	Sublimation interface in freeze drying	m
$\overline{X}$	Sample mean	-
X	Sample data point (DSC)	˚C
$X^E{}_{ij}$	Variable for excess properties	-
Y	Indicator of successful drying	-

Greek Symbols

α	Volumetric thermal expansion coefficient	1/˚C
$\alpha_{A,B,C...}$	Coefficient of polynomial equation	-
$\alpha_{0\text{-}8}$	Coefficients of Scheffe cubic model	˚C
β	Coefficient of intramolecular forces	m^3/mol·J
ε	Indicator of ideal mixing	-
ε'	Dielectric permittivity	F/m
ε''	Dielectric loss factor	F/m
μ	Dynamic viscosity	Pa·s
μ_g	Dynamic viscosity at T_g	Pa·s
ρ	Density	kg/m^3
ρ_a, ρ_{cr}	Density of amorphous and crystalline phase	kg/m^3
σ	Surface tension	N/m
σ_Θ	Phase angle (DMA/DEA)	˚
φ	Volume fraction	-
χ	Flory-Huggins binary interaction parameter	-

Index of Figures

Figure 2.1.1. Adjusted schematic drawing of enthalpy, entropy and volume diagram (Kalogeras, 2016) 28

Figure 2.3.1. Adjusted schematic drawing of various physical changes of a droplet during spray drying. The T_g is the glass transition temperature and $T_{surface}$ the temperature of the particle's surface adapted from (Cheuyglintase & Morison, 2010). 34

Figure 2.3.2. Schematic illustration of the process of a substance on a tray during freeze drying (Liapis & Bruttini, 2014). 35

Figure 2.5.1. Schematic presentation of the effects of glass transition on dielectric constant, specific heat, expansion coefficient, viscosity, enthalpy, and volume when an amorphous glass is heated over its glass (Roos, 2006) 39

Figure 2.5.2. Thermal history different heating rates (Roos, 2006). 41

Figure 2.5.3. Illustration of the glass transition temperature plots dependent on the composition for a) miscible, b) partial miscible and c) immiscible binary polymer blends (Kalogeras, 2016). 42

Figure 2.6.1. a) Change of the free volume between polymer due to hydrogen interference of water molecule and b) hole size distribution in a glassy matrix with increased water content, adapted from (Ubbink, 2010). 44

Figure 2.6.2. Normalized T_g values of experimental data and predicted with Gordon-Taylor equation. Data and k values of fructose, glucose and sucrose (Ruiz-Cabrera & Schmidt, 2015), data of maltodextrin DE 5 (Arvanitoyannis et al., 1993; Roos & Karel, 1991c) and k values (Adhikari et al., 2005; Ruiz-Cabrera et al., 2016; Truong, 2003). 45

Figure 2.6.3. DSC thermogram of the dextrin and glucose mixtures (Kawai & Hagura, 2012). 46

Figure 2.6.4. Schematic drawing of the effect of increased plasticizer in the system (Kawai & Hagura, 2012). 46

Figure 2.6.5. DSC thermograms of the various dextran blends with a M_w of 970 Da and 2,000,000 Da (Icoz et al., 2005). 47

Figure 2.6.6. Dependency of the glass transition temperature on the molecular weight of polystyrene (Blanchard et al., 1974; Hitac-Hightech, 1995). 48

Figure 2.6.7. Illustration of a semi-crystalline polymer. The amorphous phase is embedded between crystalline regions. a) response to the true amoprhous bulk region, b) represents the amorphous rigid fraction and c) the conjunction of the crystalline region by longer polymer chains (Kalogeras, 2016). 50

Figure 2.6.8. Dependency of the glass transition temperature in Kelvin of the amorphous region on the degree of crystallinity in polyethylene (Askadaskii et al., 2014). 51

Figure 2.7.1. Based on the illustration of the principle of the analytical model of Truong (Truong, 2003). 62

Figure 2.8.1. Glass transition temperature at various weight fraction of fructose for glucose and fructose mixtures. Authors from top to down: (Truong, 2003), (Arvanitoyannis et al., 1993), (Finegold et al., 1989), (Ruiz-Cabrera & Schmidt, 2015) and (Wungtanagorn & Schmidt, 2001a). 69

Figure 2.8.2. Glass transition temperature at various weight fraction of fructose for sucrose and fructose mixtures. Authors from top to down: (Finegold et al., 1989), (Truong, 2003) and (Saavedra-Leos et al., 2012). 70

Figure 2.8.3. Glass transition temperature at various weight fraction of glucose for sucrose and sucrose mixtures. Authors from top to down: (Truong, 2003), (Seo et al., 2006) and (Ruiz-Cabrera & Schmidt, 2015)..... 72

Figure 2.8.4. Glass transition temperature of binary citric acid-sugar mixtures adapted by (Truong, 2003)..... 73

Figure 2.8.5. Experimental design for sucrose, fructose and glucose mixtures (left) and three-dimensional response surface of the measured glass transition temperature during heating (right) (Saavedra-Leos et al., 2012)..... 75

Figure 2.8.6. Glass transition temperature of ternary sugar mixtures (sucrose, glucose and fructose). The ratio between sucrose and glucose is set to 5/3, 4/4, 3/5. Data from (Truong et al., 2002)..... 77

Figure 2.9.1. Percentage of powder recovery and the glass transition temperature of various orange juice concentrates and maltodextrin DE 6 ratios (Shrestha et al., 2007). 80

Figure 2.9.2. Glass transition temperature measurements and predictions of the binary systems of sucrose and maltodextrins with different average molecular weights (Roos & Karel, 1991c). 81

Figure 2.9.3. Schematic drawing of the distribution of added whey protein (left) or maltodextrin DE 10 (right) in spray dried bayberry powder (Fang & Bhandari, 2012). 82

Figure 2.9.4. Comparison of the glass transition temperatures of spray dried bayberry powder at various whey protein and maltodextrin DE 10 ratios obtained by Fang and Bhandari (2012). 82

Figure 2.10.1. Overview of the most common possible transitions and reactions observed in a DSC thermogram obtained by (Kalogeras, 2016). 85

Figure 2.10.2. Determination of the various possible temperatures associated with the glass transition for a DSC heating scan obtained by (Kalogeras, 2016). 86

Figure 2.11.1. Schematic drawing based on the various types of sorption isotherms in food by Heiss and Eichner (1971). 90

Figure 2.12.1. Stability/mobility diagram displaying the water activity, moisture content, glass transition temperature and sticky point for mango powder (left) and tomato powder (right) (Jaya & Das, 2009)..... 93

Figure 3.2.1. Sealable storage box for equilibrating powders at various relative humidities. 99

Figure 3.2.2. DSC TA Q2000. 100

Figure 4.2.1. Binary system of glucose and maltodextrin DE 6. The experimental data are from (Truong, 2003)..... 105

Figure 4.2.2. T_g of binary system of glucose and maltodextrin DE 6 with fitted θ. The experimental data are from (Truong, 2003). 107

Figure 4.2.3. T_g of binary system of glucose, sucrose, fructose and citric acid with maltodextrin DE 6. The experimental data are from (Truong, 2003). 107

Figure 4.2.4. Replotted normalized T_g values of the binary maltodextrin DE 6 mixtures. 108

Figure 4.2.5. Representation of the binary maltodextrin DE 6 systems using the individual fitted A_0 and A_1 coefficients. 109

Figure 4.2.6. Prediction of binary system with Maltodextrin DE 6 using the average coefficients. 111

Figure 4.2.7. Normalized T_g value of binary mixtures of sucrose and polymer data from (Roos & Karel, 1991c; Shamblin & Zografi, 1998; Truong, 2003). 112

Figure 4.2.8. Prediction of T_g values of mango powder with various content of maltodextrin DE17-19. The experimental data is from (Fongin et al., 2017)..... 113

Figure 4.3.1. Concept of the GAB and Flory-Huggins Free Volume theory adapted from (Ubbink et al., 2007). 115

Figure 4.3.2. Flory-Huggins interaction χ parameter as a function of number average molecular weight. Representation of the data from van der Sman (2017). 119

Figure 4.3.3. Data and prediction of the constant k value of the Gordon-Taylor equation for solid water systems from the literature (Orford et al., 1989; Roos & Karel, 1991a; Roussenova et al., 2014; Ruiz-Cabrera et al., 2016; Ruiz-Cabrera & Schmidt, 2015; Truong, 2003; Ubbink et al., 2007). 122

Figure 4.4.1. Prediction of the relation of the water activity and glass transition temperature for maltodextrin DE 10 using a fixed and changing interaction parameter. Experimental data from (Roos & Karel, 1991c)..... 125

Figure 4.4.2. Prediction of the relation of the water activity and glass transition temperature for maltose and maltopolymers with increasing number average molecular weight. Data from (Roos & Karel, 1991c; Ubbink et al., 2007)..... 127

Figure 4.4.3. Prediction of the relation of the water activity and glass transition temperature for data of the grapefruit powders presented by (Telis & Martínez-Navarrete, 2009). 129

Figure 4.4.4. Prediction of the relation of the water activity and glass transition temperature for data of the mango powders with various maltodextrin DE 17-21 fractions presented by (Fongin et al., 2017). 132

Figure 4.4.5. Sorption isotherms of mango soluble solids with various maltodextrin DE 17-21 fractions from A) 0 to 0.8 water activity and B) an enlargement at low water activity from 0 to 0.4. 134

Figure 4.4.6. Predicted stability curves of spray dried lemon juice powder with 0.6 weight fraction of maltodextrin DE 10. The experimental data are from (Paterson & Bröckel, 2015)..... 136

Figure 4.4.7. The relation of water activity and glass transition temperature of pure strawberry puree and in combination with maltodextrin DE 16.5-19.5 and gum arabic. The experimental data are from Mosquera et al. (2012). 137

Figure 4.4.8. Prediction of the relation of the water activity and glass transition temperature for data of the acai powders with various drying aids presented by (Tonon et al., 2009)..... 139

Figure 4.4.9. T_g values of mango powder and acai powder with similar maltodextrin DE 20 contents at various water activities. 140

Figure 4.4.10. Modelled sorption isotherm of the mango and acai powders at high maltodextrin amounts using the GAB and FHVT models. 140

Figure 4.4.11. Prediction of the relation of the water activity and glass transition temperature for data of the orange juice powders with fractions of MD DE 10. In A, only the predicted values are used. In B, the T_g solid values of the mixture of powder from the study by Islam et al. (2016) are utilized. 142

Figure 5.2.1. FLPC chromatogram of the total carbohydrate content and galacturonic acid in blackcurrant in combination of various dextran standards. 147

Figure 5.3.1. (A) The second cycle of the DSC heating curve of the various juice powders at zero water activity. (B) Both heating cycles of the DSC signal of cloudy apple juice powder. 151

Figure 5.4.1. Moisture content of the six juice powders at different water activities and the predicted corresponding sorption isotherm using the FHVT model. 153

Figure 5.4.2. Visual changes in blackcurrant juice powder stored at 30˚C at different relative humidities. 155

Figure 5.4.3. Prediction of the effect of water on the T_g depression of blackcurrant juice powder on the basis of the chemical composition and using the DSC value of blackcurrant juice powder at zero water activity. The error bars refer to the 95% confidence interval for n=3. 156

Figure 5.4.4. Visual changes in kiwifruit juice powder stored at 30˚C at different relative humidities. 158

Figure 5.4.5 Prediction of the effect of water on the T_g depression of kiwifruit juice powder on basis of the chemical composition and using the DSC value of kiwifruit juice powder at zero water activity. The error bars refer to the 95% confidence interval for n=3. 159

Figure 5.4.6. Visual changes of clear apple juice powder stored at 30˚C at different relative humidities. 160

Figure 5.4.7 Prediction of the effect of water on the T_g depression of clear apple juice powder on the basis of the sugar and organic acid composition and using the DSC value of clear apple juice powder at zero water activity. The error bars refer to the 95% confidence interval for n=3. 161

Figure 5.4.8. Visual changes in cloudy apple juice powder stored at 30˚C at different relative humidities. 163

Figure 5.4.9. Prediction of the effect of water on the T_g depression of cloudy apple juice powder on the basis of the sugar and organic acid composition and using the DSC value of cloudy apple juice powder at zero water activity. The error bars refer to the 95% confidence interval for n=3. 164

Figure 5.4.10. Visual changes in lemon juice powder stored at 30˚C at different humidities. 165

Figure 5.4.11. Prediction of the effect of water on the T_g depression of lemon juice powder on the basis of the sugar and organic acid composition and using the DSC value of clear apple concentrate powder at zero water activity. The error bars refer to the 95% confidence interval for n=3. 166

Figure 5.4.12. Visual changes in carrot juice powder stored at 30˚C at different relative humidities. 168

Figure 5.4.13. Prediction of the effect of water on the T_g depression of carrot juice powder on the basis of the sugar and organic acid composition and using the DSC value of clear apple concentrate powder at zero water activity. The error bars refer to the 95% confidence interval for n=3. 169

Figure 5.4.14. Second glass transition temperature of the blackcurrant, kiwi, clear apple and cloudy apple juice powders at different water activities. The error bars refer to the 95% confidence interval for n=3. 170

Figure 6.2.1. Enthalpy recovery peak of the powder containing 0.7 fructose and 0.3 maltodextrin DE 9-13. 174

Figure 6.2.2. DSC thermogram of 0.7 glucose + 0.3 maltodextrin DE 9-13 with various final heating temperatures. 175

Figure 6.2.3. Heat flow signal of 0.7 fructose + 0.3 maltodextrin DE 9-13 with various final heating temperatures. 176

Figure 6.2.4. Heat flow signal of 0.7 G/F/C + 0.3 maltodextrin DE 9-13 with various final heating temperatures. 177

Figure 6.2.5. Predicted and measured T_g values of various blends with various ratios of maltodextrin DE 9-13 at zero water activity. The error bars refer to the 95% confidence interval for n=3. 180

Figure 6.2.6. DSC heat flow signal of fructose and maltodextrin DE 9-13 blends with various ratios. 183

Figure 6.2.7. Onset, offset and midpoint T_g data for the fructose and maltodextrin DE 9-13 blends at zero water activity. The error bars refer to the 95% confidence interval for n=3. 184

Figure 6.2.8. DSC thermogram after removal of their thermal history of 0.3 fructose and 0.7 maltodextrin DE 9-13. 186

Figure 6.2.9. DSC thermogram after annealing at 30˚C for 16 h of the 0.3 fructose and 0.7 maltodextrin DE 9-13 blend. 187

Figure 6.2.10. DSC thermogram after annealing at 50˚C for 16h of the 0.3 fructose and 0.7 maltodextrin DE 9-13 blend. 188

Figure 6.2.11. DSC thermogram of 0.3 fructose and 0.7 maltodextrin DE 9-13 in combination with the different relaxation response of the different domains in the blend after annealing at 50˚C for 16h. 189

Figure 6.2.12. DSC thermogram after annealing at 90˚C for 16 h of the 0.3 fructose and 0.7 maltodextrin DE 9-13 blend. The bottom graph includes the characterization of the enthalpy peak. 190

Figure 6.2.13. DSC thermogram of the thermal history of various fructose and maltodextrin DE 9-13 blends after the first heating cycle at zero water activity. 191

Figure 6.2.14. DSC thermogram after annealing at 50˚C for 16 h of the 0.3 blackcurrant juice and 0.7 maltodextrin DE 9-13 blend shown in the first two graphs. The bottom graph shows the thermal history of various blackcurrant juice and maltodextrin DE 9-13 blends after the first heating cycle. 192

Figure 6.3.1. Effect of the moisture content on the glass transition temperature of the various glucose and maltodextrin DE 9-13 blends 194

Figure 6.3.2. Prediction of the effect of water on the T_g depression of glucose and maltodextrin DE 9-13 using the measured and estimated T_g value for the FHVT model. The error bars refer to the 95% confidence interval for n=3 195

Figure 6.3.3. Prediction of the effect of water on the T_g depression of citric acid and maltodextrin DE 9-13 using the measured and estimated T_g value for the FHVT model. The error bars refer to the 95% confidence interval for n=3 197

Figure 6.3.4. Prediction of the effect of water on the T_g depression of fructose and maltodextrin DE 9-13 using the measured and estimated T_g value for the FHVT model. The error bars refer to the 95% confidence interval for n=3 199

Figure 6.3.5. Prediction of the effect of water on the T_g depression of one third glucose, one third fructose and one third citric acid with maltodextrin DE 9-13 using the measured and estimated T_g value for the FHVT model. The error bars refer to the 95% confidence interval for n=3. 201

Figure 6.3.6. Prediction of the effect of water on the T_g depression of blackcurrant juice with maltodextrin DE 9-13 using the measured and estimated T_g value for the FHVT model. The error bars refer to the 95% confidence interval for n=3. 203

Figure 6.3.7. Prediction of the effect of water on the T_g depression of maltodextrin DE 9-13 using the measured T_g value for the FHVT model. The error bars refer to the 95% confidence interval for n=3. 204

Figure 6.4.1. DSC thermogram of the different maltodextrin DE 9-13 blends at 0.11 water activity. 205

Figure 6.4.2. DSC thermogram of 0.5 glucose and 0.5 maltodextrin DE 9-13 blend at various water activities. 206

Figure 7.2.1. Molecular structure and chromatogram of inulin, as well as the representation of the observed transition of pure inulin in the DSC thermogram. 211

Figure 7.2.2. Molecular structure and chromatogram of digestive resistant maltodextrin, as well as the representation of the observed transition of pure digestive resistant maltodextrin in the DSC thermogram 212

Figure 7.2.3. Molecular structure and chromatogram of maltodextrin DE 9-13, as well as the representation of the observed transition of pure maltodextrin DE 9-13 in the DSC thermogram 213

Figure 7.2.4. Representation of the measured and predicted T_g values of the binary blend of glucose and various polysaccharides at zero water activity. The error bars refer to the 95% confidence interval for n=3. 215

Figure 7.2.5. DSC thermogram of the thermal history of various glucose and inulin blends. 216

Figure 7.2.6. Representation of the measured (left) and predicted (right) T_g values of glucose and various polysaccharides blends at zero water activity. The error bars refer to the 95% confidence interval for n=3. 217

Figure 7.2.7. Representation of the measured (top) and predicted (bottom) T_g values of glucose and 1/1/1 inulin, digestive resistant maltodextrin and maltodextrin DE 9-13 a various ratios at zero water activity. The error bars refer to the 95% confidence interval for n=3. 219

Figure 7.3.1. Outlined mechanism of monovalent salts in their interaction with other molecules in comparison to monovalent salts. 221

Figure 7.3.2. Molecular structures and weights of disodium carbonate, trisodium citrate and trisodium phosphate. 221

Figure 7.3.3. Measured T_g values of glucose with various salt blends at zero water activity. The error bars refer to the 95% confidence interval for n=3. 222

Figure 7.3.4. Comparison of the effect of salt and polysaccharide addition on the T_g values of mixture with glucose at zero water activity. The error bars refer to the 95% confidence interval for n=3. 223

Figure 7.3.5. Schematic drawing of the possible different mechanisms by which salts and polysaccharides affect the molecular structure of mixtures containing low molecular components such as glucose. 224

Figure 8.2.1. Prediction of blackcurrant juice and maltodextrin DE 9-13 blend with various ratios at zero water activity, as presented in Chapter 5. 228

Figure 8.2.2. T-T_g values as a function of the estimated outlet temperatures for 0.45 blackcurrant and 0.55 maltodextrin DE 9-13 blend estimated at various feed flows. 230

Figure 8.2.3. Characterization of the operating regions regarding the outlet temperature and T-T_g. 231

Figure 8.2.4. Final operating conditions during spray drying. 231

Figure 8.2.5. Prediction of the effect of water on the T_g depression of 0.45 blackcurrant and 0.55 maltodextrin DE 9-13 using the estimated T_g value for the FHVT model. The error bars refer to the 95% confidence interval for n=3 232

Figure 8.2.6. T-T_g values as a function of the estimated outlet temperatures for blackcurrant and various blends with maltodextrin DE 9-13 at a fixed feed flows of 0.9kg/h. 233

Index of Tables

Table 2.2.1. Chemical composition of various fruit juices (Dietrich et al., 2007; Eisele & Drake, 2005; Elkins et al., 1996; Kelebek et al., 2009). 31

Table 2.7.1. List of the most common analytical models for predicting the glass transition of binary blends. 59

Table 2.8.1. Glass transition temperature of the main solids in fruit juices: sucrose, fructose, glucose, citric acid and malic acid measured by DSC. 65

Table 2.8.2. Melting and thermal degradation temperature at different heating rates for D-fructose, D-glucose and D-sucrose (Hurtta et al., 2004). 67

Table 2.8.3. Glass transition temperature for binary citric acid-sugar system adapted by (Truong, 2003). 73

Table 2.8.4. Characterizing of the mixing conditions in various anhydrous binary mixtures adapted by (Truong et al., 2002). 74

Table 2.8.5. Comparison of the efficiency of the various models to predict the glass transition temperature of the ternary sugar mixtures with distinct sucrose and glucose ratios. Data obtained from (Truong et al., 2002). 78

Table 2.10.1. Common used techniques to determine the glass transition temperature in polymers and other substances (Kalogeras, 2016). 84

Table 4.2.1. ΔC_p for sugar, organic acid and polysaccharides from (Truong, 2003). 106

Table 4.2.2. Coefficient of the Redlich-Kister equation of the normalized binary systems. 110

Table 4.2.3. T_g and ΔC_p values of pure components used for the prediction of fruit juice powders. 113

Table 4.4.1. Density, number average molecular weight and interaction parameter χ used in the FHVT model (Duvallet et al., 1989; Takeiti et al., 2010; Truong, 2003). 124

Table 4.4.2. Number average molecular weight, Flory-Huggins interaction parameter and coefficent of determination of the prediction for maltose and maltopolymers. 127

Table 4.4.3. Predicted and measured glass transition temperatures of grapefruit powders (Telis & Martínez-Navarrete, 2009). 128

Table 4.4.4. The predicted and measured $T_{g,solid}$ values used for the FHVT model Fongin et al. (2017). 130

Table 4.4.5. Coefficient of determination of the estimated stability curves of the various mango powders. 131

Table 4.4.6. Predicted and presented glass transition temperatures of acai powders by Tonon et al. (2009). 138

Table 4.4.7. Predicted and presented glass transition temperatures of orange powders from Islam et al. (2016). 141

Table 5.2.1. Sugar and organic acid profile of the different fruit and vegetable juices. 145

Table 5.2.2. Distribution of the sugar and organic acid composition in the fruit and vegetable juices. 146

Table 5.3.1. T_g of fruit and vegetable powders at zero water activity. 148

Table 5.3.2. Comparison of predicted and measured T_g values of pure juice powders at zero water activity. 149

Table 5.3.3. Second transition of the cloudy apple, clear apple, kiwifruit and blackcurrant juice powders detected in the second cycle of the DSC heating curve. 152

Table 5.4.1. Glass transition temperature of blackcurrant juice powder at different water activities. 154

Table 5.4.2. Glass transition temperature of kiwifruit juice powder at different water activities. 157

Table 5.4.3. Glass transition temperature of clear apple juice powder at different water activities. 160

Table 5.4.4. Glass transition temperature of cloudy apple juice powder at different water activities. 162

Table 5.4.5. Glass transition temperature of lemon juice powder at different water activities. 165

Table 5.4.6. Glass transition temperature of carrot juice powder at different water activities. 167

Table 6.2.1. Glass transition temperature of pure components at zero water activity. 174

Table 6.2.2. Effect of final heating temperature on the glass transition temperature of the 0.7 glucose and 0.3 maltodextrin DE 9-13 blend at zero water activity..... 176

Table 6.2.3. Effect of final heating temperature on the glass transition temperature of the 0.7 fructose and 0.3 maltodextrin DE 9-13 blend at zero water activity. 177

Table 6.2.4. Effect of final heating temperature on the glass transition temperature of the 0.7 G/F/C and 0.3 maltodextrin DE 9-13 blend at zero water activity. 178

Table 6.2.5. Predicted T_g values of the different components with various weight fractions of maltodextrin DE 9-13 at zero water activity. 179

Table 6.2.6. Measured T_g values of the different components with various ratios of maltodextrin DE 9-13 at zero water activity. 182

Table 6.3.1. Glass transition temperature of glucose and maltodextrin DE 9-13 at different water activities. 194

Table 6.3.2. Glass transition temperature of citric acid and maltodextrin DE 9-13 at different water activities. 197

Table 6.3.3. Glass transition temperature of fructose and maltodextrin DE 9-13 at different water activities. 198

Table 6.3.4. Glass transition temperature of G/F/C and maltodextrin DE 9-13 at different water activities. 200

Table 6.3.5. Glass transition temperature of blackcurrant juice and maltodextrin DE 9-13 at different water activities. 202

Table 8.2.1. Estimation of the outlet temperature glass transition temperatures at different inlet temperatures at a fixed feed flow and composition of blackcurrant and maltodextrin DE 9-13. 229

1. Project Overview

1.1 Introduction

Fruits and fruit juices are a common part of our daily diet and a great source of various natural vitamins, minerals, fibres and phytochemicals (Sanchez-Moreno et al., 2012). The nutrients and bioactive compounds in the fruits have antioxidant capacities and the capability to inhibit cell proliferation. These properties are associated with having a positive effect on the prevention of several cerebral and cardiovascular illnesses and cancer (Vanamala et al., 2006). Since consuming fruits can contribute to our health and well-being, there is a great interest from industry to supply natural beneficial juices.

The issue with fruits is that they are seasonal products with limited shelf life, restricting their natural availability to a short period over the year. In order to provide accessibility, great effort is put into preservation of juices over the year or to import juices from abroad. On the market, fruit juices are generally available in the form of pasteurized fresh juice or juice reconstituted from a concentrate. The concentrate allows for the reduction of the storage volume and preservation of the juice. The next logical improvement is the transformation of the fruit juices into a powder, decreasing the storage and transport volume and limiting the water content to a minimum. This reduces further the storage and transport costs, while at the same time improving the shelf-life stability and quality. Furthermore, it allows for the direct incorporation into new consumable products without the addition of residual water.

Common techniques for transforming a liquid food product into a powder are drying processes such as spray, air, vacuum, drum and freeze drying. The high drying rates and rapid cooling of these techniques turn the carbohydrates components into an amorphous state. Minor components such a flavours, minerals, vitamins and enzymes can be trapped and preserved in the amorphous matrix. Food products contain components, which in terms of drying can categorized into two types: non-sticky and sticky. The former, including maltodextrins, gums and proteins, are easy to handle and produce less hygroscopic and free flowing powders. Sticky products such as fruit juices, honey and vegetable juices, on the other hand, can be impossible to process without additives and turn into a sticky non-free flowing clump. The stickiness is attributed to the high content of low molecular weight components, especially sugars such as fructose, glucose and

sucrose and organic acids such as citric, malic acid, tartaric and succinic acid. These components contribute over 90% of the solids in fruit juices (Dolinsky et al., 2000).

Stickiness is the main factor limiting the drying of sugar and acid-rich food products without additives. The phenomenon of stickiness is directly related to the viscosity of the material. In the glassy state the amorphous material's viscosity is greater than $10^{12\text{-}14}$ Pa·s, however once the material surpasses a critical temperature, known as the glass transition temperature (T_g), the viscosity decreases abruptly and a glassy microstructure can no longer be supported. Issues such as stickiness, caking, collapsing and undesirable crystallisation of the product can occur. The temperature at which particles start to stick instantaneously can be described by a critical difference of the operating temperature and the glass transition temperature $T\text{-}T_g$. The critical difference is dependent on the contact time of particle-particles or particle-surface to allow for viscous flow to form liquid bridges. The contact time coupled with the surface composition of the particle define the critical limit for $T\text{-}T_g$. By understanding the relation between the drying of amorphous products and their sticky point, it is possible to optimize the drying process (Chatterjee, 2004; Paterson et al., 2007).

Different attempts have been made over the years to solve this problem by either modifying the drying equipment or by altering the chemical composition of the product. The modifications include features such as the cooling of the chamber wall, which showed no improvement to the particle sticking to the wall (Ozmen & Langrish, 2003). Other methods concentrated on the air flow in the chamber, where cool air was introduced at the bottom of the drying chamber, a second air stream near the wall being implemented, or the humidity of the air being reduced to increase the evaporation of water in the particles. All modifications to the spray drying equipment have been proven to be much less effective than the approach of changing the properties of the materials by adding a drying aid such as maltodextrin, which increases the T_g of the product.

The quantity of added drying aids that is needed to dry fruit juices reliably is in the range of 40-70% of the fruit solids (Masters, 1991). Over the years, many fruits have been tested with different spraying aids and drying techniques, as summarized by Telis and Martínez-Navarrete (2012). Drying aids are generally high molecular weight polymers, with maltodextrin as the most common food additive. Maltodextrin possesses a neutral colour and taste, while being inexpensive. At the same time it increases the T_g and a solution with high maltodextrin content can still be sprayed due to the low viscosity (Adhikari &

Bhandari, 2008). However due to the high quantity of drying aid in the powders, the natural beneficial components in the juice are reduced.

The common practice for the determination of the glass transition of fruit juice powders is time consuming and provides only limited results for a fixed composition. In most cases, fruit juices with known composition are mixed with various amounts of drying aids and dried by different drying techniques. The glass transition temperature of the powder is measured at various water activities and the Gordon-Taylor equation as well as sorption isotherm model are fitted to the experimental data to predict the glass transition temperature over a range of various water activities (Jaya & Das, 2009; Khalloufi et al., 2000). Roos, Bandhari, Adhikari and others used the Gordon-Taylor equation to predict the T_g values of binary systems of carbohydrates and water (Adhikari et al., 2003, 2004; Bhandari, Datta, & Howes, 1997; Rahman, 2009; Roos, 1993a; Roos, 1995). In more recent years, the prediction of the glass transition has been extended to ternary sugar mixtures ratios with and without water. Little attention has been given to further predictions of glass transition of higher order mixtures from their pure components. The established models are limited to only the interaction of one component, usually water, with the remaining other components. This results in an overestimation or underestimation of T_g values of multicomponent systems (Arvanitoyannis et al., 1993). Reliable prediction of T_g for real fruit powders (with or without drying aids) without the need for the expensive empirical measurement will provide a significant advantage for design of powder formulation and dryer operation; and allow for cost-effective delivery of the nutritional benefits of fruit juice powders.

1.2 Objectives of the study

The aim of this study was to develop a prediction model for a multicomponent system consisting of low and high molecular weight carbohydrates components. The relationship between the water activity and the glass transition temperature of these mixtures was then further investigated and used to find the optimal conditions that addressed the stickiness issues during spray drying. The following objectives were identified to reach these goals:

Development of a model to predict the glass transition temperature of low and higher molecular weight carbohydrate components on the basis of the chemical composition

- The extension of the model to the prediction of the glass transition temperatures as a function of moisture content at various water activities

- Application of the model to fruit juice powders and predict the glass transition temperature based on their chemical composition
- Extension to predict the mixing of low and high molecular carbohydrate components and their effect on the glass transition temperature of the mixtures
- Test of salts as an alternative drying aids
- Demonstration of the optimization of spray drying of fruit juice powders on the basis of the glass transition temperature

2. Literature Review

2.1 Amorphous Solids

The state of matter is commonly divided into gas, liquid and solid. These states differ mainly in their molecular configuration and their molecular mobility. Gas is the state in which the molecules have the highest mobility and can move independently over distance with low activity of interaction compared to time of free motion. The free volume of particles can be approximated to be equal to the volume of the system. Liquids exhibit a higher density due to their reduction of free volume. The molecules can still rearrange randomly in space, but because of the lower free volume, the rate of the interaction between the molecules increases, affecting the properties of the liquid (Gutzow et al., 2011).

As a liquid is cooled below its melting point, it is considered to exist as a supercooled liquid with a very high viscosity. At this stage the melt can solidify discontinuously or continuously (Figure 2.1.1). When the cooling is slow enough and nucleation sites are present to initiate the crystallisation process, a discontinuity is displayed in the thermodynamic potentials with respect to the temperature and the molecules organize themselves in a well-ordered periodic pattern and form a crystal. In contrast to this, if the melt is cooled rapidly from its melting temperature to below the glass transition temperature, the molecules have no time to rearrange and are locked in their original melt

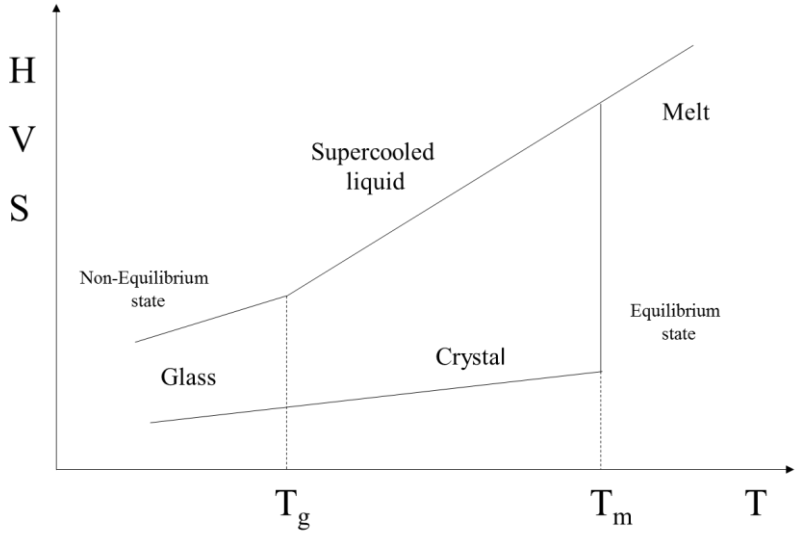


Figure 2.1.1. Adjusted schematic drawing of enthalpy, entropy and volume diagram (Kalogeras, 2016) .

configuration (Figure 2.1.1). This solid state is called an amorphous solid or glassy state and possesses a liquid-like randomized structure. Amorphous configurations can maintain their structure and withstand external shear without flowing. This is mainly due to limitation of the any translation motion of the molecules and the increase of the viscosity, which increases to 10^{12} Pa·s at the glass transition temperature (Biroli & Bouchaud, 2012).

Both the liquid and crystal are in a thermodynamic equilibrium state. As the liquid falls under its melting temperature, the crystal configuration is the energetically more favourable state, thus this transition is thermodynamically driven. However the formation to an amorphous solid is a kinetically controlled process and the cooling rate defines the temperature at which the molecules are constrained in their configuration. Since the molecules did not rearrange themselves to form a more stable configuration, but rather are trapped in their previous liquid arrangement, the amorphous solid is in a metastable state and relaxation processes are still taking place. Other than for crystals, the changes of the thermodynamic potentials are continuous over a temperature range. The fundamental difference between an amorphous solid and a crystal is molecular structure at the microscopic scale. In a crystalline solid the atoms arrange themselves in a periodic reoccurring lattice structure over a long ranged order. In the amorphous state short ordered, ranged regions are present, in which molecules have the same distance and number of neighbour molecules. This short ranged order matches the local order of the molecules in the liquid state and is not continued over a longer range. The amorphous solid lacks the translation orientated symmetry of crystals and can be considered as a heterogeneous system with distinct high and low density regions (Liu et al., 2006).

Many industrial products contain amorphous solids from ceramics, glasses, fibres, polymers to pharmaceuticals and food (Yu, 2001). In food processing, various techniques can cause the partial or complete destruction of an ordered molecular structured arrangement to transform it into a disordered amorphous solid. The formation of amorphous solid structure in food products can arise from mechanical shear, gelatinization, rapid removal of solvent, denaturation or depolymerisation of large polymers. The most commonly used techniques involving these mechanisms are drying processes such as spray, freeze and hot-air drying, extrusion, and milling such as ball grinding (Bhandari & Hartel, 2005; Kim et al., 2001; Liapis & Bruttini, 2014).Many processed food products exist in a partial or fully amorphous state, from hard candy to food powders such as instant coffee, dairy, tea, spice. Since the amorphous solid is in a metastable state, these products can be affected by internal relaxation processes, as well

as external effects such as moisture adsorption. This stands in direct relation to the quality and the stability of the product during storage.

2.2 Composition of fruit juices

Fruits juices consist mainly of the carbohydrates, acids, nitrogen compounds, polyphenols, vitamins, aromas and minerals. Especially, high contents of low molecular weight carbohydrates and organic acids attributed to the physical changes such as stickiness or caking during processing and storage of food (Adhikari et al., 2003). In order to optimize the quality and stability of the end product, the distribution of the components in the juices has to be known.

The natural composition of fruit juices over the year is influenced by several factors such as the weather conditions, the variety of fruits, geographical location, the soil, the maturity of the fruit and the post-harvest handling. The sheer number of these factors make an accurate determination of the composition a difficult task and mostly a composition range is given for the juices. Various fruits were analysed for their nutrition values in different countries and put together into databases over the years such as the national nutrient database for standard reference of the United States Department of Agriculture, the New Zealand Food Composition Database, McCance and Widdowson's the Composition of foods integrated datasets.

Raw fruits juices consist primarily of 70-95% water and around 6-12% solids, apart from some exceptions such as avocado and banana (Cassano et al., 2003; Gunko et al., 2006; Sanchez-Moreno et al., 2012). The soluble solids contain mainly carbohydrates, organic acids, nominal amounts of amino acids and other components. The partially insoluble portions are polysaccharides located in the cell structure of the pulp composed of lignin, hemicellulose and cellulose. After water, carbohydrates are the main components of fruit juices. Glucose and fructose are the major monosaccharides in fruits. The composition of these monosaccharides varies with the majority of the fruit and their natural composition. Peaches, plums, and apricots exhibit higher concentrations of glucose than fructose, whereas for apples and pears the opposite is the case (Sanchez-Moreno et al., 2012). In apples the highest concentration of glucose can be detected about seven weeks after full bloom; after this time the glucose content reduces due to accumulation of starches up to 12-13 weeks after full bloom and rises again when the starch content decreases (Berüter, 1985). Other monosaccharides, such as galactose, arabinose and xylose can only be found in extreme low concentration. Besides the two monosaccharides, the disaccharide sucrose

is the most common sugar in fruits and these three sugars are associated with the sweetness of the fruits, whereas the order of sweetness listed from lower to higher is glucose < sucrose < fructose. Additional to the disaccharide sucrose, some fruits also have smaller amounts of maltose, melibose, raffinose and stachyose. The starch content is commonly low in the total composition due to a decrease during maturation; only bananas exhibit a starch content over 3%. Dolinsky et al. (2000) stated that the carbohydrates contribute over 90% to the solid. The other larger fraction of fruit juices are the organic acids citric and malic acid, with citric acids occurring mostly in citrus fruits (Kefford & Chandler, 1970), and malic acid in apples (Tucker, 1993). In grapes, tartaric acid as well as malic acid contribute to over 90% of the organic acids (Ford, 2012). Apart from a high amount of citric acid, oranges can sometimes contain succinic acid in their juice (Liu et al., 2012). The rest of the solids are a mixture of smaller proportional nitrogen compounds, lipids and fibres. Fruits are a low source of proteins, having a low percentage (0.1-1.5% of total juice), and exist in the form of enzymes or free amino acids.

Table 2.2.1. Chemical composition of various fruit juices (Dietrich et al., 2007; Eisele & Drake, 2005; Elkins et al., 1996; Kelebek et al., 2009).

Compound	**Non-commercial apple juice[a,b]**	**Commercial apple juice concentrate[a,b]**	**Cloudy pear juice**	**Orange juice[c]**
Brix°	14.24	57.0-72.9 (69.8)	16.15	11.8
pH	3.37-4.24 (3.71)	3.2-4.1 (3.6)	4.16	3.35
Ash	0.25% w/w	0.26	-	3.7 g/L
Fructose	3.84-8.01 (5.69) g/100ml	5.03-6.80 (6.07)%	86.4 g/L	28.55±0.94 g/L
Glucose	1.05-3.23 (2.01) g/100ml	1.46-3.55 (2.42)%	21.5 g/L	32.30±0.86 g/L
Sucrose	0.38-5.65 (2.16) g/100ml	0.56 -3.29 (1.66)%	5.4 g/L	59.34±2.04 g/L
Sorbitol	0.17-1.40 (0.45) g/100ml	0.17-0.66 (0.39)%	51.36 g/L	-

L-Malic acid	193-1738 (847.7) mg/100ml	0.12-0.83 (0.46)%	3.66 g/L	1.06±0.01 g/L
Citric acid	0.8-27.4 (11.9) mg/100ml	0.0063-0.045 (0.012)%	0.11 g/L	12.66±0.16 g/L
Polyphenolics	133.1 ppm	86.22 ppm	492.33 mg/L	60.3 mg/L
Minerals	1883.2 ppm	121.52 mg/100g	1425.33 mg/L	-
Proteins/Amino Acids	-	68.27 mg/100g	-	-

a) All values are standardized to 11.5 Brix° except for Brix° and pH.

b) Sugars and organic acid were analysed by HPLC method.

c) Sugars and organic acid were analysed enzymatically.

The dietary fibres are mostly polysaccharides and are part of the cell structure. These polysaccharides are set free once the juice is extracted from the fruit, where pectin substances and hemicellulose make up most of the fibre content. Lipids can be found either in the seeds or in the peel of the fruits and play a minor role in juices with the exception of avocados, where lipids make up most of the solids.

The composition of raw juice differs from the industrial processed and concentrated juice (Table 2.2.1). During production the fruit juices undergo an enzyme treatment, therefore enzyme inhibitors such as polyphenols are oxidised in advance to improve the treatment. The addition of pectinase and other enzymes is an established step in the fruit industry. It enhances the juices extraction and modifies the juice of berries, citrus fruits, stone fruits, grapes, apples, pears and even vegetables (Lozano, 2006). Commercial enzyme preparations for apple processing are a combination of Pectinesterase (PE), Polygalacturonase (PG), and Pectinlyase (PL) enzymes. The correct proportion of all three enzymes is vital for the complete breakdown of pectin (Ceci & Lozano, 1998). The treatment can take from 15 min to 2 h depending on the exact enzyme preparation, the temperature conditions and the fruit. The pectinase breaks down the soluble pectin in the pulp making the juice more free flowing. Insoluble pectin is also treated, enhancing the juice extraction, since pectin holds the cell structure together and thus impedes the juice extraction (Lozano, 2006). The yield of the fruit juice can be increased up to 20% by performing enzyme treatment prior to pressing. If a clear juice is desired after the centrifugation, a clarification step is added to remove residual insoluble components.

Once more enzymes are added to juices, they have the effect of degrading the soluble pectin and forming of cluster of suspended particles. The pectin creates a coat around the enzymes due to their different electric charge. The enzyme breaks the coating and sets part of the enzymes free, promoting the agglomeration of these partially coated enzymes. These agglomerates can be separated by filtration. The treatment of the fruit juices, especially clear juice, reduces the amount of other components in the concentrate than the main sugars and organic acid to a minimum (Table 2.2.1).

2.3 Powder production

Dehydration is the most commonly used method to transform a solution into a free-flowing powder. The main objective of the dehydration in food production is the removal of the moisture to reduce the microbial activity and prevent product deterioration. The removed water decreases the weight and allows for more efficient packaging, handling and reduced transportation cost. Many conventional methods are used in food drying including hot air drying, vacuum drying, drum drying, spray drying, freeze-drying: in the following the spray and freeze drying will be presented in regard to the formation of amorphous solids and the accompanied effects.

2.3.1 Spray drying

In a spray dryer the concentrated solution is introduced into a hot dry gaseous medium by atomizer, usually a nozzle. The small droplets exhibit a great ratio of surface area to mass of the droplet. This allows the water at the surface to evaporate rapidly from the droplet on contact with the hot medium. The driving force of the process is the difference in vapour pressure on the surface of the droplet to the external vapour pressure in the hot air. The evaporation of the water at the surface of the droplet cools the air in the spray tower and keeps the temperature of the droplet below the outlet temperature of the spray dryer at the same time (Bhandari, Datta, & Howes, 1997). This fact makes the application valuable for the food industry, since heat-sensitive components can be handled. Products can be split into two groups, the non-sticky and the sticky. On the one hand is the non-sticky group such as milk, egg and protein powder where the final product can be obtained without major complications. However sticky products like low molecular weight carbohydrates and organic acids will stick to the chamber wall or will leave the spray chamber as a syrup. The major problem for spray drying fruit juice is the contact zone at the bottom part of the chamber where the particles are collected. Through airflow

adjustment, the collision of highly viscous particles in mid-air can be reduced, however as soon as the particles get in contact at the bottom, agglomerates can be formed (Adhikari et al., 2003; Bhandari & Howes, 1999).

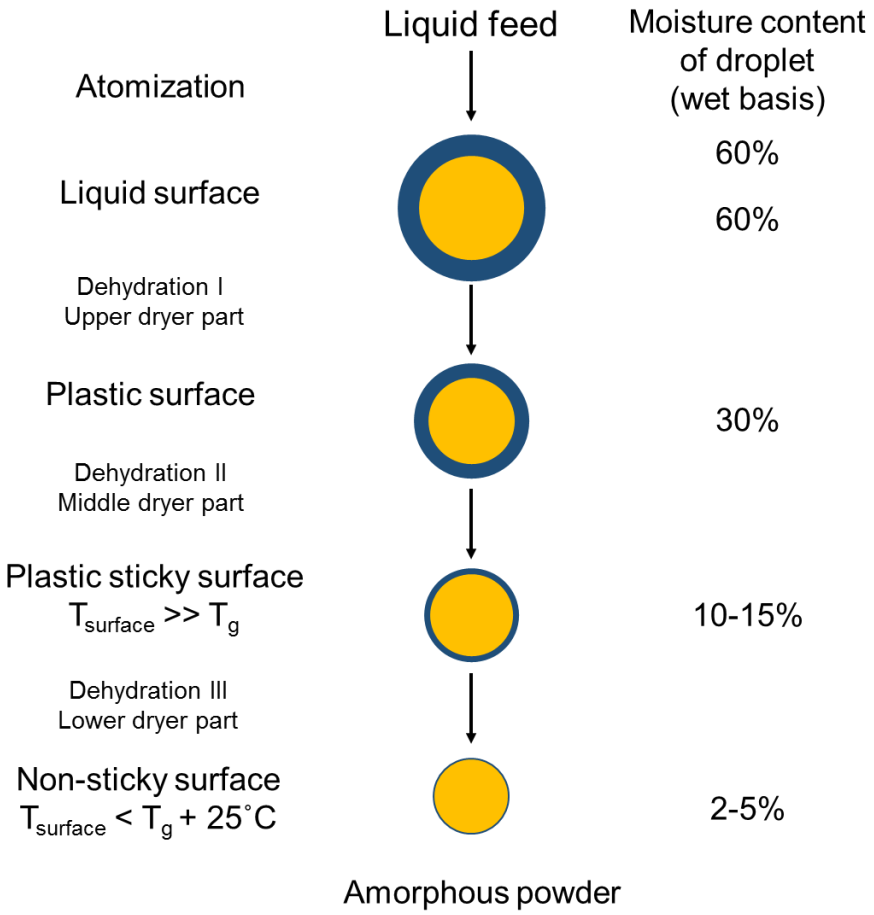


Figure 2.3.1. Adjusted schematic drawing of various physical changes of a droplet during spray drying. The T_g is the glass transition temperature and $T_{surface}$ the temperature of the particle's surface adapted from (Cheuyglintase & Morison, 2010).

Bhandari, Datta, and Howes (1997) classify the drying mechanism into four steps (Figure 2.3.1). First, the concentrated solution is atomized into small droplets. As soon as the atomized droplets are in contact with the hot medium gas, the solvent starts to evaporate. The hot gas temperature results in a heat exchange from the hot gas medium to the droplet and the difference of vapour pressure leads to a moisture transfer to the surface of the droplet. During the evaporation step the droplet starts to shrink. Once the solute almost reaches the saturation level, a thin shell is formed on the surface of the particle and the evaporation rate slows down. The process becomes dependent on the water diffusion rate through the surface shell; at this point the surface is still sticky. With a decrease of moisture content at the surface, the components at the surface transform from a rubber to a glassy state. In the case of the sticky group, the glassy state is never reached, as their

glass transition temperature lies far below the operating conditions of the spray drier (Adhikari & Bhandari, 2008). In order to make it possible to still spray dry sugar-rich foods, additives are used. Commonly, the quantity of added spraying aids is based on empirical studies. Bhandari, Datta, and Howes (1997) introduced an index-based drying model for sugar-rich foods to predict the amount of drying aid to obtain a recovery of 50%.

$$\sum_{i=1}^{n} I_i x_i = Y_i \tag{2.1}$$

Where I is the index of the component, x is the weight fraction and Y is the indicator of the success where 1 represents a recovery of 50%. Sucrose, glucose, fructose, citric acid and maltodextrin DE 6 have been given an index of 0.85, 0.51, 0.27, -0.4 and 1.6 respectively for inlet and outlet temperatures of 150˚C and 65˚C. The model has been validated for honey and pineapple juices.

2.3.2 Freeze drying

Freeze drying is a process in which a product is separated from a solvent. In food products the solvent is usually water, by sublimation and desorption under reduced pressure. The process is divided in accordance to their physical effect into three stages: freezing, primary drying, where the sublimation of the solvent is achieved, and secondary drying stage, where the rest of the solvent is removed by desorption. In the first step the product is cooled till the initial water is frozen (65-90%) and the residual water (10-35%) is in the unfrozen (sorbed) state. The amount of unfrozen water strongly depends on the

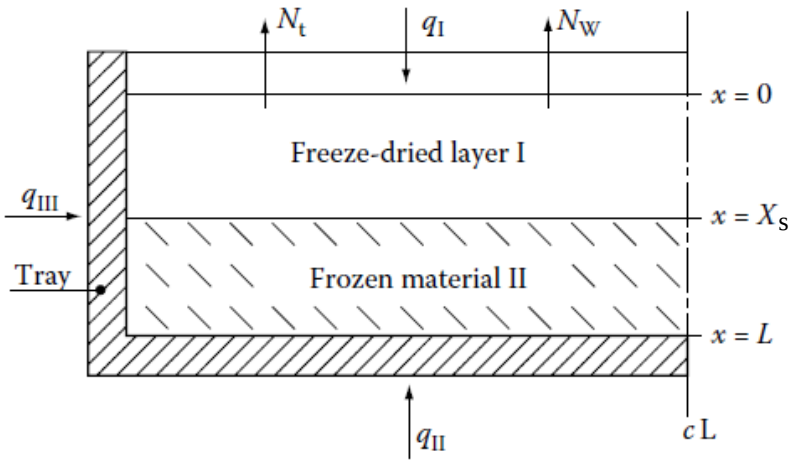


Figure 2.3.2. Schematic illustration of the process of a substance on a tray during freeze drying (Liapis & Bruttini, 2014).

components and their hydroscopic nature. Studies of partially dried strawberries (a_w < 0.7) and water in sugar (moisture ~ 16%) proved to be unfreezable, suggesting the strong influence of sugars and organic acid in inhibiting the ice crystallisation (Sopade et al., 2002). For sublimation to take place, the pressure has to be reduced to be equal or lower than the vapour pressure of the solvent. The sublimation of pure water (ice) is only possible below its triple point at a temperature of 0.0098˚C and an absolute pressure of 610.8 Pa. However food consists of various solids, thus lower temperatures are required to keep the water in a frozen state. With a reduction of temperature commonly to -10˚C or lower, the pressure is set to < 270 Pa to allow the ice to sublimate. Figure 2.3.2 illustrates the sublimation procedure in freeze dried material. The necessary latent heat of sublimation is supplied by radiation and conduction. At the outer surface of the material the ice starts to sublimate leaving the material as vapour. The Xs in Figure 2.3.2 displays the sublimation interface between the freeze dried layer and the remaining frozen material. The sublimation starts at the outer surface and proceeds till only a single layer of freeze dried materials remains.

For materials with a eutectic point, the operating conditions for drying should be chosen to be below it to avoid melting. Any melting in the frozen layer can cause shrinkage, puffing or structural topologies filled with liquid water (Liapis & Bruttini, 2014). Once the ice is melted, it is impossible to separate it from the bulk by sublimation. For materials without a detectable eutectic point, a state diagram of the system can give insight into the glass transition temperature of the maximal unfrozen amorphous state T_g'. If during freeze drying T_g' is surpassed, the material structure can collapse. Since, in the sublimation process, the change of ice to water vapour is obtained in one step, the empty space of the evaporated ice crystals makes the structure very porous. Once the amorphous state has changed into a viscous liquid, the porous structure cannot hold its own weight and collapses (Roos, 2006). The temperature at which collapsing occurs is dependent on the composition of the food product. Fruits and materials with higher sugar content exhibit a low collapse temperature (Bhandari & Hartel, 2005). Collapsing is a relaxation process due to the flow of the viscous liquid, which can be described using the WFL equation (Levi & Karel, 1995). With the complete sublimation of the ice, the second drying stage is initiated and the rest of the bound unfrozen water is removed from the system.

The bound water exists in the material due to the mechanisms of physical and chemical adsorption and water of crystallisation. By applying heat to the system under vacuum, the rest water of the water can be slowly removed. The drying rate is restricted by the amount

of heat provided, since it influences the structural and product stability during and after drying.

For the structural stability, the same mechanism as in the primary drying stage is responsible, while the product stability is an interplay of the moisture concentration and temperature profile during the drying. Since many products are temperature sensitive, the temperature is a limiting factor and the moisture content has to be checked at the end of drying. Usually temperatures of 10 to 35˚C for heat sensitive products and 50˚C for less sensitive ones are applied. Freeze dried products keep most of their nutrition, aromas and flavours, and dissolve quickly. It is very important to avoid collapsing during drying, otherwise the quality of the product can be degraded and the dissolubility is reduced.

2.4 Physical stability of food product

For the cause of stability issues in products, a distinction has to be made between matrix structure and viscosity-related stability issues. For instance, the molecular packing of the matrix is linked the barrier properties against oxygen, which can be modified by minimising the molecular size hole between molecules and therefore control the product stability. The viscosity-related issues, on the other hand, are related to the T_g of a system and the transition from a solid-like state to a highly viscous liquid. Since, the production issues are connected to the viscosity and T_g, the main phenomena of stickiness are discussed in more detail.

2.4.1 Stickiness

The stickiness of amorphous powders can be distinguished into two categories. If a fine powder needs to be changed into a coarse and highly porous agglomerate, the inducing of stickiness can be utilized as an initiation process for agglomeration. Agglomerates exhibit better flow ability, intensified colour, improved appearance and reduced dustiness with respect to a fine powder (Boonyai et al., 2004; Downton et al., 1982; Hartmann & Palzer, 2011). The agglomeration process is performed after a spray dryer in a fluidized or vibro-fluidized bed, where the fine powder is intentionally exposed to steam, moist air or a fine mist of water. After the agglomerates have been formed, the residual moisture is removed for shelf life improvement (Downton et al., 1982).

On the other hand, uncontrolled stickiness during the drying process is the cause of quality degradation, lower product yield, plant shutdowns, frequent cleaning requirements and safety hazard (Bhandari, Datta, Crooks, et al., 1997). The particles stick to the chamber

wall and form lumps at the bottom of the dryer. The stickiness of the particles is attributed to the surface properties and viscosity. If the viscosity on the particle's surface is reduced from commonly 10^{12} Pa·s to 10^{7} Pa·s, liquid bridges can be formed between contiguous particles that results in an agglomeration (Bhandari & Roos, 2017). The decrease of viscosity is attributed to the exceeding of the glass transition of the components at the surface. This can be the case if the operating temperature is above the glass transition or a plasticizer, usually water, reduces the glass transition temperature of the mixture below the operating temperature (Foster, 2002; Palzer, 2005). The temperature above T_g at which the critical viscosity is surpassed is called the sticky point temperature (T_s). The change of the viscosity in accordance to the increase of temperature or the decrease of T_g due to moisture uptake can be expressed by the Williams-Landel-Ferry (WLF) equation.

$$\log\left(\frac{\mu}{\mu_g}\right) = \frac{C_1\left(T - T_g\right)}{C_2 + \left(T - T_g\right)} \tag{2.2}$$

Where μ is the viscosity in the rubber like state at the temperature T, μ_g is the viscosity at the T_g and C_1 and C_2 are constant with the general values of -17.44 and 51.6K, which seem to correlate to the viscosity of sugar solutions (Downton et al., 1982; Soesanto & Williams, 1981). Frenkel's equation, links the interparticle bridge radius with the time of coalescence because of the surface energy driven viscous flow.

$$r_b^2 = \frac{3R_p\sigma t}{2\mu} \tag{2.3}$$

r_b is the bridge radius, R_p is the particle diameter, μ is the viscosity, σ is the surface tension and t is the time. As the definition of the strength of a liquid-bridge is proportional to the cross-sectional area (πr_b^2), which makes the strength in Frenkel's equation proportional to r_b^2/t. Paterson et al. (2005) combined the equations (2.2) and (2.3).

$$\log\left(\frac{r_b^2}{t}\right) = \log\left(\frac{3R_p\sigma}{2\mu_g}\right) - \frac{C_1\left(T - T_g\right)}{C_2 + \left(T - T_g\right)} \tag{2.4}$$

Plotting log (r_b^2 / t) versus $\left(T - T_g\right) / \left(C_2 + T - T_g\right)$ should give a straight line with slope of C_1 and an intersection point equal to $\left(3R_p\sigma t\right) / \left(2\mu_g\right)$. Paterson et al. (2005) tested the stickiness of amorphous lactose with a blow tester at different temperatures and humidity

conditions, but with similar T-T_g values. The results showed that the increase of stickiness is directly connected to the magnitude of T-T_g.

2.5 Glass transition

The mechanism of the glass transition has been the subject of many studies, however there is not one general explanation, but rather various theories, which form different perspectives on the complex mechanism and do not necessarily contradict each other.

Simon (1930) defined glasses as kinetically frozen in a thermodynamically non-equilibrium state. The relaxation process in the melt becomes so slow due to the sharp increase of viscosity that it cannot keep up with changes of the external parameters. Therefore a certain molecular configuration is frozen in the glass. The glass transition temperature defines the temperature in which a material, during heating in the amorphous state, turns into a viscous liquid (syrup, rubbery, etc.). This phenomenon is reversible and the transition occurs as well by rapid cooling of a supercooled liquid to the point where the substance is vitrified in the non-equilibrium glassy state (Figure 2.5.1). The transformation of the physical state of the system is characterized by the relaxation time, which indicates the experimental measurable response time of the molecules in the system to adapt their configuration to the external changes. The relaxation time varies strongly during the cooling process; in the case of a liquid, the response of the molecules is of a high magnitude. Near the glass region the relaxation time overlaps with the experimental time scale and below T_g, the relaxation time exceeds the possible measurement (Zallen, 2007). The kinetic effect on T_g can be detected during calorimetry

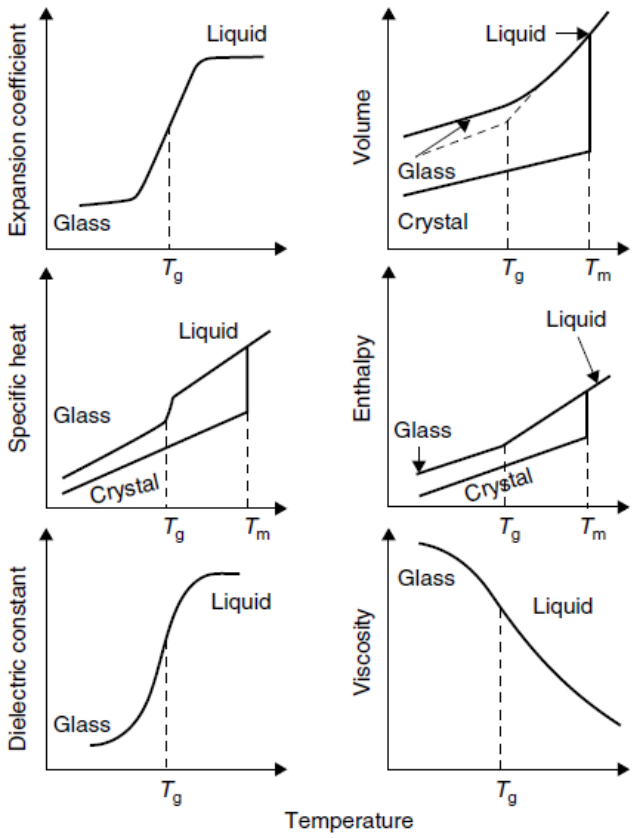


Figure 2.5.1. Schematic presentation of the effects of glass transition on dielectric constant, specific heat, expansion coefficient, viscosity, enthalpy, and volume when an amorphous glass is heated over its glass (Roos, 2006) .

experiments with different heating or cooling rates (Figure 2.5.2). Along with the immense increase of the relaxation time, for specific material properties such as the heat capacity, expansion coefficient and compressibility, a step-like increase can be observed over the transition region. The variation of these physical properties are detected over a temperature range and the spectrum varies strongly depending on the food's components. Low molecular weight amorphous carbohydrates show a temperature range of 10-20˚C for the shift of the properties, whereas for carbohydrate polymers like starch and gluten the alteration is measured over a broader temperature scale (Hoseney et al., 1986; Zeleznak & Hoseney, 1987).

The determination of the glass transition temperature of pure substances or systems is carried out by the heat and cooling measurement of the change of the referred physical properties. The T_g is usually obtained by the inflection point of the measured curve of the properties (Figure 2.5.1).

It is important to note the glass transition temperature as a non-equilibrium transition and it is dependent on the kinetics of the measurement. The dependency of T_g on the cooling or heating rate q and the T_g is described by the Bartenev-Ritland equation.

$$\frac{1}{T_g} = A_{BR} - B_{BR} \log q \qquad \text{with} \quad q = -\frac{dT}{dt} \tag{2.5}$$

Where A_{BR} and B_{BR} are component specific coefficients and q the heating or cooling rate. Using the same heating and cooling rates, no hysteresis in the measured curve for the properties is observed. However, a variation of the rates results in a shift of the curve and a hysteresis is seen. A fast cooling rate leads to a configuration with a higher energy state and the energy is released by slow heating. For the opposite case of slow cooling and fast heating, the system is of lower energy and additional heat is needed over the transition region (Figure 2.5.2). The obtained hysteresis of the various thermodynamic properties can provide information of the thermal history of the substances (Roos, 2006).

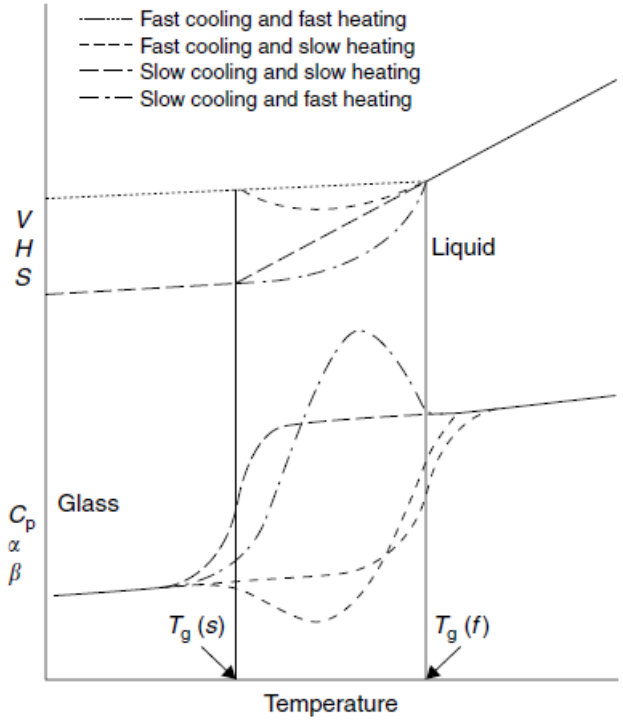


Figure 2.5.2. Thermal history different heating rates (Roos, 2006).

2.5.1 Miscibility and the glass transition temperature

The determination of the glass transition temperature is an easy and popular method to test the miscibility of polymers. The detection of one glass transition temperature is usually an indicator for full miscibility. Several studies suggest that in DSC measurements two glass transition temperature are measured, if the level of heterogeneity described by a domain size is within the range of 15-20 nm. In order to measure smaller domain size, analysing techniques with a higher sensitivity and resolving powder have to be used. For example, X-ray scattering supplies a much higher resolution, allowing the identification of structural heterogeneities down to molecular level with domain sizes in the range of 0.1-1 nm (Kalogeras, 2016). The problem with the glass transition temperature as an indicator for miscibility is that different preparation methods and measurements protocols can affect the morphological characteristics, making a general comparison of the data difficult.

However, if the blend morphology is decoupled from the evaluation technique and the impact of the experimental method is minimized, the number and compositional dependence of glass transition temperature can be a viable indicator for miscibility, partial miscibility or immiscibility. Figure 2.5.3 describes schematically the variations of the glass transition temperature for binary mixtures with different compositions and their responses in dynamical mechanical and dielectric measurements. For fully miscible materials, the single glass transition is declared as the "blend average T_g", whereas the interactions between the components and induced variation of the free volume determine the temperature of the transition. For compatible or partial misciblity, usually two glass transitions are detected with a convergence of both phases and an alteration in width and strength of the signal. Totally immiscible blends show no convergence at all and exhibit two completely independent peaks.

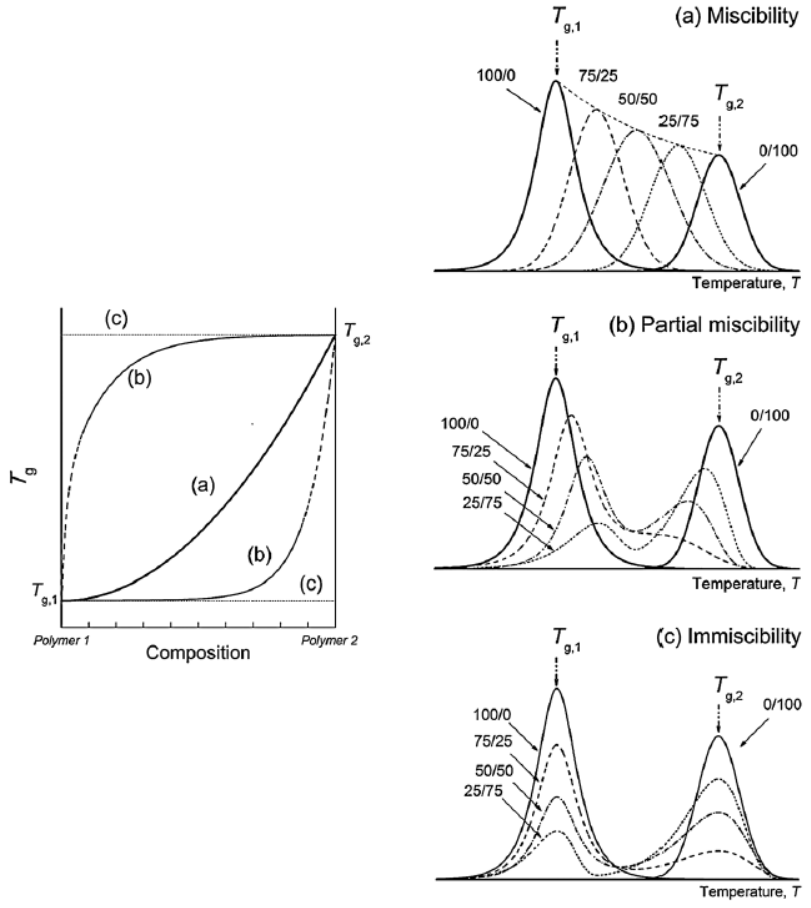


Figure 2.5.3. Illustration of the glass transition temperature plots dependent on the composition for a) miscible, b) partial miscible and c) immiscible binary polymer blends (Kalogeras, 2016).

A single glass transition temperature in a DSC thermogram is not a reliable indicator for complete homogeneity. Because of self-association of polymers and the dynamic fluctuation of various length scales, the blend components exhibit different dynamic environments that may result in different temperature dependences of their relaxation rates. This dynamic heterogeneity can be observed as a wide glass transition temperature range, a broad distribution of the relaxation modes as well as two separated glass transition temperatures. For instance, the polymer blend PMMA + PVPh blends appears to be completely homogeneous when analysed at a domain-size scale around ~20–30 nm by DSC and a single glass transition is determined for all blend compositions. With lower scaling of the domain-size to 1-15 nm by DMA, the blend is heterogeneous (Barrat et al., 2010). As stated above, dynamic heterogeneity is linked to the different relaxation behaviour of the phases for each component in the mixture even if the substances are completely miscible on a molecular level.

2.6 Effects on the glass transition temperature

2.6.1 Plasticizer

Plasticizers are the main reason for the observed decrease of T_g value in a system, which can be classified into two parts. On the one hand are the internal plasticizers, where additional monomers with low temperature properties are copolymerized into the main chain of the polymer. The monomer prohibits the chains from matching closely together, thus inducing the polymer to soften and reducing its glass transition temperature (Immergut & Mark, 1965). On the other hand are the external polymers. these small molecules with low temperature properties are added to a polymer and lower the glass transition temperature of amorphous polymers. In crystalline and semi-crystalline structures, the plasticizer has the effect of reducing the crystallinity and melting temperature, and the glass transition of amorphous regions (Sperling, 2005). In polymer

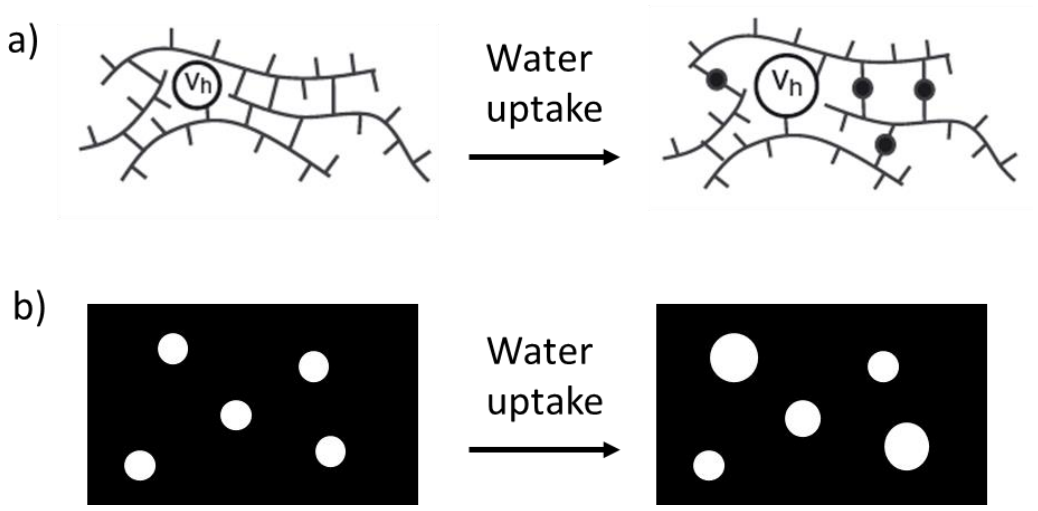


Figure 2.6.1. a) Change of the free volume between polymer due to hydrogen interference of water molecule and b) hole size distribution in a glassy matrix with increased water content, adapted from (Ubbink, 2010).

technology, plasticizers are common ingredients to modify the flexibility, ductility and extensibility, as well as the mechanical resistance of polymers (Kern Sears & Darby, 1982). Slade stated that each solvent miscible with a polymer acts as a plasticizer, however the converse is not the case as not every plasticizer has to be a solvent for a polymer. It clarifies that the phenomenon of plasticization is not reduced to solvents, but every small, miscible molecule can act as a plasticizer.

Three common theories try to cover the mechanisms of plasticisation: the gel, the lubricity and the free volume theory. In the gel theory the main effect of the plasticizer is attributed to the interruption of hydrogen bonds and Van der Waals forces between the polymers (Di Gioia & Guilbert, 1999). The lubricant theory is based on the assumption that the plasticizer functions as a lubricant between the molecules and enhances the motion of the macromolecules relative to each other (Di Gioia & Guilbert, 1999). The most prevalent explanation of plasticization is the linkage to the free volume theory. The introduced plasticizer increases the free volume in the system and allows for more free motion of the molecules (Kelley & Bueche, 1961).

In food systems, water is the most common plasticizer and the effect on the glass transition has been shown in many studies: starch (Biliaderis, 1991; Kalichevsky et al., 1992; Liu et al., 2009; Zeleznak & Hoseney, 1987), gelatine (Reutner et al., 1985), glucose, fructose, sucrose (Arvanitoyannis et al., 1993; Izard et al., 1996; Ruiz-Cabrera et al., 2016; Ruiz-Cabrera & Schmidt, 2015), lactose (Roos & Karel, 1991d), trehalose

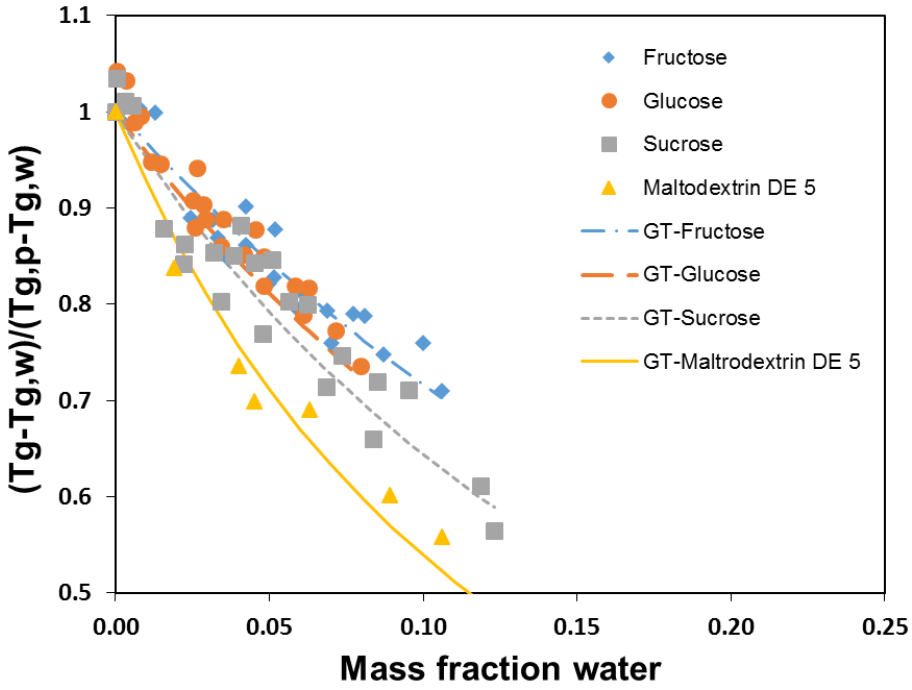


Figure 2.6.2. Normalized T_g values of experimental data and predicted with Gordon-Taylor equation. Data and k values of fructose, glucose and sucrose (Ruiz-Cabrera & Schmidt, 2015), data of maltodextrin DE 5 (Arvanitoyannis et al., 1993; Roos & Karel, 1991c) and k values (Adhikari et al., 2005; Ruiz-Cabrera et al., 2016; Truong, 2003).

(Miller et al., 1997) and maltodextrins (Roos & Karel, 1991c). At very low moisture contents, water has the opposite effect. It fills the free holes in the network and decreases the free volume, which is known as anti-plasticization (Benczdi et al., 1998). With further water uptake, it assumed that the water molecules interfere with the hydrogen bonds of the polymers, changing the hole size distribution in a glassy polymer matrix (Ubbink, 2010).

In Figure 2.6.2, the T_g values of experimental data and predicted values using the Gordon-Taylor equation are presented for various carbohydrates-water mixtures. For a better comparison, all values are normalized $(T_g - T_{g,w}) / (T_{g,p} - T_{g,w})$, where the indices p and w refer to the glass transition temperature of the pure polymer and water. The prediction of the Gordon-Taylor equation agrees well with the experimental data. The noticeable effect of the plasticization is increased with larger ΔT_g difference of the components, which is also represented by order of T_g and the k values for the Gordon-Taylor equation of the mixtures: fructose (T_g=15.4˚C and k=3.61) < glucose (T_g=34.2˚C and k=4.4) < sucrose (T_g=65.8˚C and k=4.98) < maltodextrin DE 5 (T_g=188˚C and k=7.7). Besides water, especially low weight molecules such as sugars, glycerol and sugar alcohols also

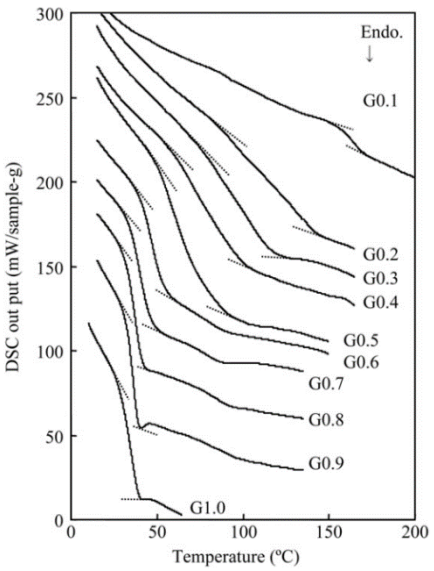


Figure 2.6.3. DSC thermogram of the dextrin and glucose mixtures (Kawai & Hagura, 2012).

act as a plasticizer in food systems. Other than water the small sugars do not alter the interaction between the higher molecular weight carbohydrates, but rather reduce the average number of entanglements of a polymer chain and allows molecular rearrangements at temperatures, where the polymer chains would be normally in a frozen state (Ubbink, 2010). However, Shamblin et al. (1998) stated their studies of sucrose and polymers with Fourier Transformed Raman Spectroscopy proved the establishment of hydrogen bonds between sucrose and the polymers. It is assumed the formation of the hydrogen bond enforces steric constraint on contiguous hydroxyl-groups and the decrease of T_g of the system is related to the overall loss of hydrogen bonds (Kawai & Hagura, 2012). If the influence of the interaction is neglected then a clear trend can be observed with the difference of the size and molecular weight. Kawai and Hagura (2012) investigated the heterogeneous system glucose and dextrin. The DSC thermograms of the mixture change abruptly with the increase of the glucose concentration Figure 2.6.3. A concentration of 0.2 glucose is sufficient to broaden the glass transition temperature. After a glucose

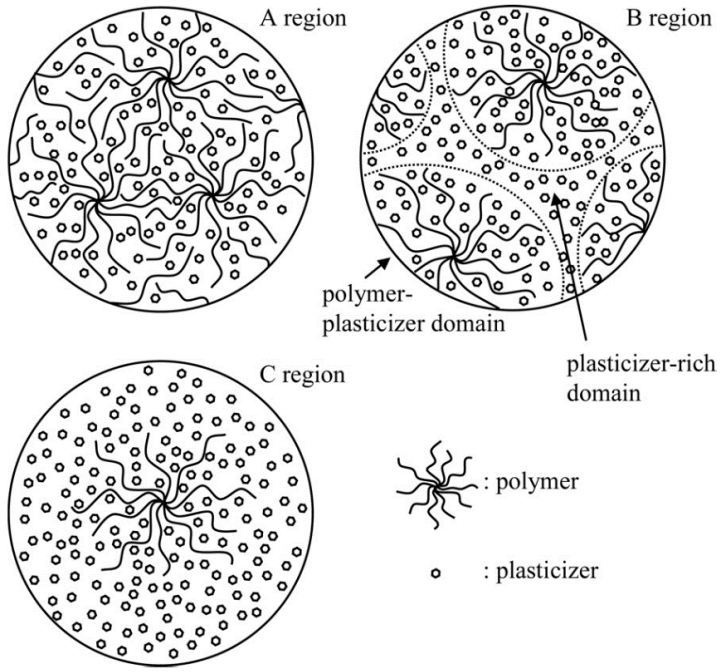


Figure 2.6.4. Schematic drawing of the effect of increased plasticizer in the system (Kawai & Hagura, 2012).

concentration of 0.5, the thermograms resemble that of pure glucose. This phenomenon is not attributed to a phase separation of the components, otherwise individual T_g values for each component would be detected. It is best explained in Figure 2.6.4 where region A represents the weight fraction of 0-0.1 for glucose in the system. The plasticizer is spread around the polymer and interaction between the polymer and plasticizer takes place. With higher glucose weight fraction, $0.2 \leq 0.5$ two regions are formed: one a polymer-plasticizer region and a plasticizer rich region. The assembly of the region B is initiated by a shift of the onset point of T_g closer to that of glucose and the transition to region C at a glucose weight fraction < 0.5 is accompanied by a shift of T_g offset to pure glucose. In region C the polymer is embedded in the plasticizer (glucose) rich domain and the mobility of the molecules is affected by the plasticizer alone. Icoz et al. (2005) could demonstrate when mixing two dextrans with different molecular weights of 970 Da and 2,000,000 Da, the DSC signal of the blend resembles the DSC signal of the dextran with M_w of 970 Da, but broadens out with increased concentration of the dextran with M_w of 2,000,000 Da (Figure 2.6.5).

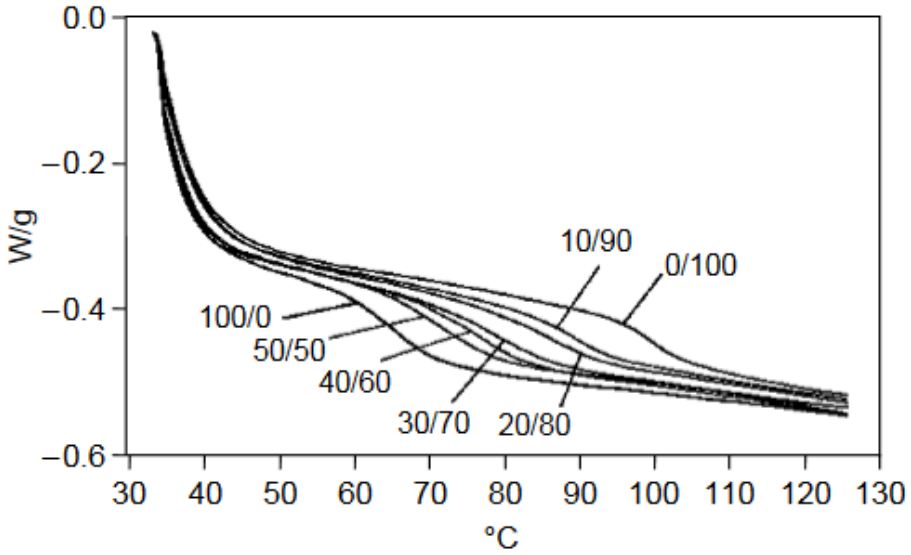


Figure 2.6.5. DSC thermograms of the various dextran blends with a M_w of 970 Da and 2,000,000 Da (Icoz et al., 2005).

At a concentration of 80%, of the dextran with M_w of 2,000,000 Da in the mixture the signal of the DSC heat flow signal is similar to the signal of the pure dextran with M_w of 2,000,000 Da. This effect can explain the high amount of high molecular weight additives needed to notice a relevant increase of the glass transition temperature (Roos & Karel, 1991c). The impact of plasticizers on T_g in a mixture has been studied by many people, however to explain the effect of water and other plasticizers on the molecular mobility of the system, more evidence has to be provided to support the listed theories (Di Gioia & Guilbert, 1999; Kawai & Hagura, 2012; Kelley & Bueche, 1961; Ubbink, 2010). The

combination of Molecular Dynamic simulations, FTIR, NMR and PALS techniques can give a more accurate picture of the microstructure of the molecules, explaining the influence of plasticizer on the molecular interaction and the structure of the matrix.

2.6.2 Molecular weight

The correlation of an increase of the glass transition temperature with increasing molecular weight has been proved by several authors (Ruan et al., 1999; Shaw & MacKnight, 2005; Sperling, 2005) and it was put into a theoretical relation by (Fox & Flory, 1950). For linear polymers the relation is expressed as:

$$T_g = T_{g\infty} - \frac{K_F}{M_w} \tag{2.6}$$

Where K_F is a polymer specific constant, M_w the molecular weight, increases with molecular mass, $T_{g\infty}$ is the glass transition temperature at infinite molecular weight and T_g is the glass transition temperature. The influence of the molecular weight results from the decrease of the free volume in systems caused by a higher connection of monomers between the polymers and inhibition of independent motion of the end segments (Shaw & MacKnight, 2005; Sperling, 2005). As soon the polymer exceeds a critical mass, the end segment cannot perform thermal motion without interfering with other parts of the polymer.

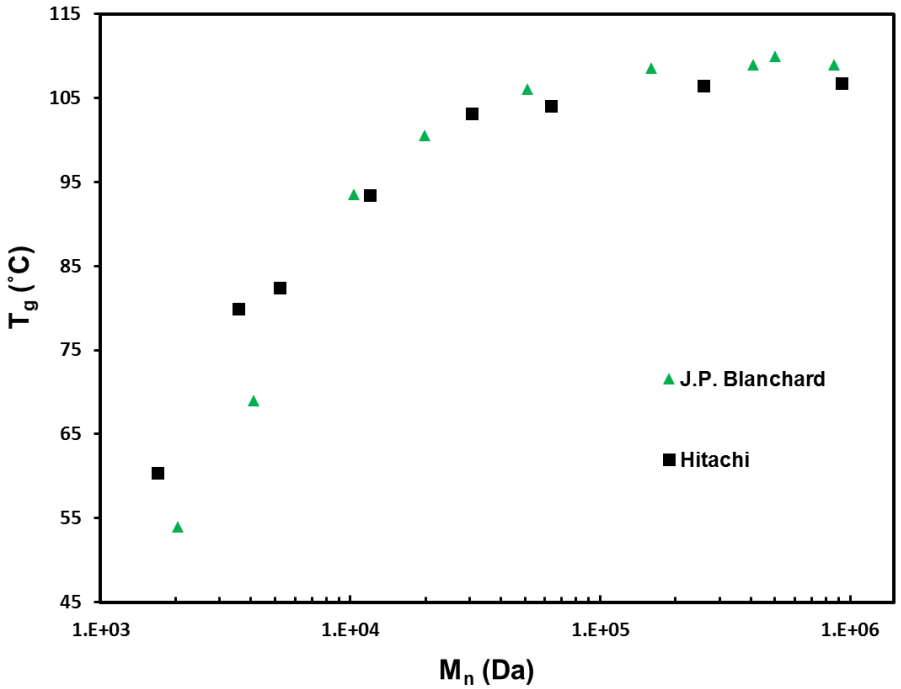


Figure 2.6.6. Dependency of the glass transition temperature on the molecular weight of polystyrene (Blanchard et al., 1974; Hitac-Hightech, 1995).

At this point an increase in molecular weight has no additional effect on the transition of the polymer in the rubbery state. Polystyrene is a well-studied linear polymer and the relationship between the molecular weight to the glass transition is proven by Figure 2.6.6. On the other hand the temperature of the viscous flow is increased with molecular weight to higher values, because with increased length of the molecules more heat is required to set the relative motion of the molecules to each other in to place. This is because flow is nothing but the slide of separate molecules relative to each other in the system (Askadskii, 2003). For maltodextrins with various dextrose equivalents (DE) from 2 to 100, Busin et al. (1996) found a reasonably linear correlation between the glass transition and the molecular weight.

$$T_g = -1.4DE + 449.5 \tag{2.7}$$

2.6.3 Crystallinity

The glass transition is a property associated with amorphous solids, however food systems are seldom fully amorphous and exhibit crystalline regions. Mandelkern (2002) stated that with advanced crystallinity of the polymer, the density of the crystalline phase increases, which is linked to strains on the amorphous phase. The deformation of the amorphous phases is accountable for minimizing the macromolecular formation and decreasing the mobility of the molecules in the amorphous regions entrapped between crystalline phases, which increases the relaxation time of the amorphous phase and hence the glass transition temperature. For highly crystalline polymers the glass transition may be masked by the melting peak of the crystals. Many semi-crystalline polymers display two T_g values, the lower one corresponding to the fully amorphous region being without the restraints of the crystalline region (Boyer, 1975). The upper value correlates with the entrapped region. Only the lower T_g shall be used in regard of the chemical structure, because it displays the true mobility of the molecules (Boyer, 1975).

Most recent research on macroscopic structure of semi-crystal polymers gave a more detail explanation of the effect of crystalline regions on the amorphous phases. It was discovered that the transition temperature phase is not only controlled by the degree of crystallinity, but also by the so-called “rigid amorphous fraction” (Cheng & Jin, 2002). This related to the chains being firmly coupled to the crystalline interface (Figure 2.6.7 (b)). Once the crystalline region reaches the size of micro or nanometre, the longer polymer chains in the amorphous regions will form connections between the different

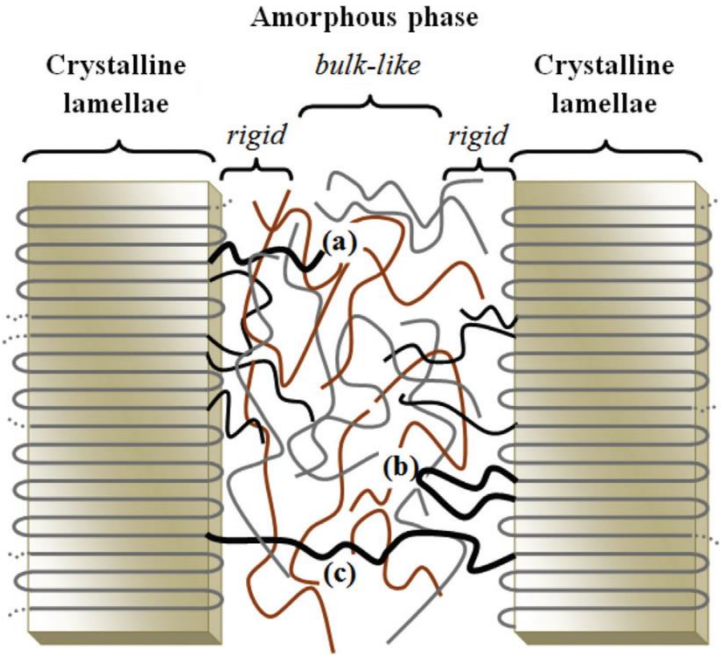


Figure 2.6.7. Illustration of a semi-crystalline polymer. The amorphous phase is embedded between crystalline regions. a) response to the true amoprhous bulk region, b) represents the amorphous rigid fraction and c) the conjunction of the crystalline region by longer polymer chains (Kalogeras, 2016).

crystalline interfaces (Figure 2.6.7 (c)). These strong engagements of the polymer segments with the crystalline interface affect the molecular mobility, which is displayed by a broader main glass transition temperature in semi-crystalline polymers and a shift to higher temperatures (Struik, 1978). In many polymers the formation of "rigid amorphous fractions" results in a separation of the glass transition of the bulk amorphous and the "rigid amorphous fractions", as observed by (Boyer, 1975). Interestingly, the crystalline region can increase as well as decrease the glass transition temperature. For example, in polyethylene terephthalate (PET) the glass transition temperature shifts from 65˚C in a fully amorphous state to 95˚C for high degrees of crystallinity (DSC measurements) (Alves et al., 2002), whereas for poly (4-methyl-1-pentene) an increase of crystallinity from 0% to 67% results in a reduction of T_g from originally 29˚C to 18˚C (dilatometric measurements) (Griffith & Rånby, 1960). The reason for this unusual behaviour of the amorphous phase is not fully understand yet; one possible explanation is the relative densities of the amorphous and crystalline phase play an important role in this phenomenon (Kalogeras, 2016).

Askadaskii et al. (2014) studied polymers such as polyethylene and developed a formulation to predict the alteration of the glass transition temperature of the amorphous region for polymers dependent on the degree of crystallinity and their chemical structure.

$$\ln \frac{T_\alpha}{T_g} = \frac{1}{2} \frac{V_0}{\beta U} \frac{(\rho_a - \rho_{cr})}{\rho_a^2} \alpha_{cr}^2 \tag{2.8}$$

T_α is the modified temperature of the amorphous region, α_{cr} is the fraction of crystals, V_0 is the volume of the complete amorphous polymer, ρ_a and ρ_{cr} are the densities of the pure amorphous and crystalline polymer respectively, β is a coefficient accounting for the intramolecular forces and U is the internal energy. The term βU can be determined at full crystallinity, since T_α becomes equal to the melting temperature (T_m) at $\alpha_{cr} = 1$, which leads to following expression:

$$\beta U = \frac{1}{2} V_0 \frac{(\rho_a - \rho_{cr})}{\rho_a^2 (\ln T_m - \ln T_g)} \tag{2.9}$$

The necessary parameters for equation (2.9) can be obtained by experiments or if no experimental data are available, various prediction methods to calculate polymer properties were presented by Askadskii (2003).

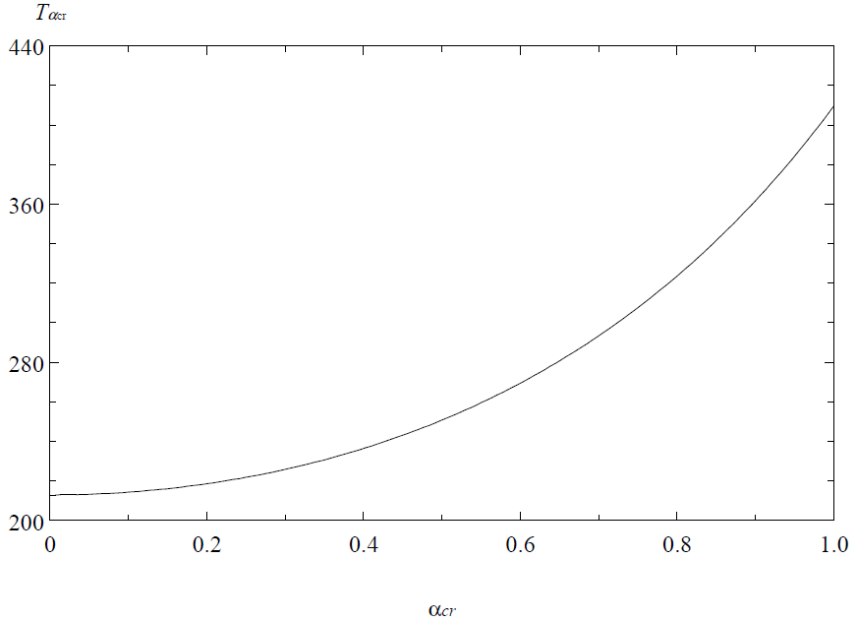


Figure 2.6.8. Dependency of the glass transition temperature in Kelvin of the amorphous region on the degree of crystallinity in polyethylene (Askadaskii et al., 2014).

Figure 2.6.8 illustrates the impact of crystal domains on the amorphous regions in polyethylene. At low proportions up to 30% the crystal domains have no effect on the

relaxation temperature, since the crystals domains are too small to restrict the molecular motion of the amorphous phase. However, with increased crystallinity the glass transition temperature of the remaining amorphous phase is enhanced (Figure 2.6.8).

2.6.4 Filler effects

Inorganic micro and nanoparticles fillers are dispersed in polymers to adapt their properties. The dispersed fillers control the mechanical strength, thermal stability and electrical conductivity of the polymer. Common inorganic fillers are clays, alumina, silica, silver or gold nanoparticles, carbon blacks, carbon nanofibers, and single-wall or multiwall carbon nanotubes. The impact of fillers on the properties of the polymer are driven by various factors, implying their size and the amount of fillers, their surface chemistry and the degree of interaction between the polymer and the fillers as well as their own material properties. For many polymers the fillers loosen up the molecular packing of the polymer enhancing the molecular mobility and hence, shifting the glass transition temperature to lower temperatures (Koppensteiner et al., 2010; Krüger et al., 1999). On the other hand, wetted surface fillers have the ability to form positive "attractive interactions" with the polymer chain via hydrogen bonds and raise the T_g of the polymer system. However, if the attraction forces between the fillers and the molecules in the matrix are smaller than the filler "repulsive attractions" are provoked, causing a lowering of T_g (Djemour et al., 2015). The interactions at the interface of the filler are the driving force of the jump in the glass transition temperature due to the formation of "rigid amorphous fractions" around the filler particle (Davtyan et al., 2014; Klonos et al., 2010). Similar to what has been described for partial crystalline polymers, the constraint on the molecular mobility extends in a gradual away from the interface layer of the filler. This can be seen by a one upshifted T_g, since the whole matrix is immobilized, or the separation of the bulk and rigid amorphous regions seen by two T_g values in calorimetric and dielectric thermograms (Davtyan et al., 2014).

2.7 Mathematical models

Once the glass transition temperature of a system is available, important conclusions about the changes of the morphology and properties can be drawn for the systems. In food processing or preservation the known glass transition serves as a reference parameter to be able to control of effects such as collapsing, stickiness or caking. On the bases of the introduced theoretical models researchers attempt to predict the Tg of linear polymers and explain the composition dependency on T_g for polymer blends.

2.7.1 Glass transition of linear polymers

The prediction of the glass transition temperature of a linear homopolymer was established by Askadskii (2003).

$$T_g = \frac{\sum_i \Delta V_i}{\sum_i a_{A,i} \Delta V_i + \sum_j b_{A,j}} \tag{2.10}$$

$\sum_i \Delta V_i$ is the sum of the Van der Waals volumes of the repeating segment in the polymer chain, $a_{A,i}$ is a constant representing the weak dispersion forces from each atom in the segment and $b_{A,j}$ characterizes the energy of strong specific interactions in the segment (dipole-dipole, hydrogen bonds etc.). The constants $a_{A,i}$ and $b_{A,j}$ were obtained by the regression fitting to 50 polymers (Askadskii et al., 2016b). The scheme is further advanced for copolymerization and to account for polymer networks (Askadskii, 2003; Askadskii et al., 2016a). The method has been applied to predict the glass transition temperature of various proteins with reasonable success, by considering only the involved amino acids (Matveev et al., 1997). Over the years other group contribution methods for polymers or ionic liquids have been developed, however the use of these group contribution schemes is till now limited and cannot be applied to general systems (Camacho-Zuñiga & Ruiz-Treviño, 2003; Lazzús, 2012).

2.7.2 Binary blends

The earliest approach came from Gordon and Taylor which was derived from the difference of the expansion coefficients $\alpha = \left(\partial V / \partial T\right)_p$ at T_g for the components in binary polymer blends (Gordon & Taylor, 1952).

$$T_g = \frac{x_1 \Delta\alpha_1 T_{g1} + \Delta\alpha_2 x_2 T_{g2}}{x_1 \Delta\alpha_1 + x_2 \Delta\alpha_2} \tag{2.11}$$

By putting the expansion coefficients in ratio, the equation can be reduced to the commonly known form:

$$T_g = \frac{x_1 T_{g1} + k x_2 T_{g2}}{x_1 + k x_2} \quad with\, k = \frac{\Delta\alpha_2}{\Delta\alpha_1} \tag{2.12}$$

In general the index 1 is assigned to the component with the higher and 2 for the one with the lower T_g value for anhydrous and aqueous system.

Over the years, different model specific methods have been proposed to determine the parameter k in equation (2.12). Kelley and Bueche (1961) adjusted the parameter to the free volume to be additive $k = (\rho_1 / \rho_2) / \left(\Delta\alpha_2 / \Delta\alpha_1\right)$, where ρ is the density and $\Delta\alpha = \left(\alpha_{melt} - \alpha_{glass}\right)$ the difference of the volumetric expansion coefficient at T_g of the component. By applying the Simha-Boyler rule (Simha & Boyer, 1962), which states that $\Delta\alpha \approx const.$, this permits an estimate of the coefficient from the density ρ and the glass transition temperature T_g of the blends $k = \rho_1 T_{g1} / \rho_2 T_{g2}$. The simplification works well for polymer-polymer and polymer-diluent blends, however the method fails to predict solute-diluent mixtures, where the solute is not a high molecular weight polymer but rather a low molecular weight polymer such as sugars (Chen et al., 2000; Roos, 1993b). Therefore it is recommended to obtain the coefficient by empirically fitting to experimental data. In this case the coefficient is uncoupled of its corresponding property and an interaction contribution from the polymer blends is included in the parameter. The parameter *k* becomes an empirical fitting parameter of the experimentally seen T_g deviations, which can be obtained by the least square method.

$$\frac{d}{dk} \sum_{i=1}^{n} \left(\frac{x_{1,i} T_{g1} + k x_{2,i} T_{g2}}{x_{1,i} + k x_{2,i}} - T_{gmeasured,i} \right)^2 \tag{2.13}$$

Originally designed for polymer blends, the Gordon-Taylor equation is commonly applied for the prediction of the glass transition in food systems such as sucrose-maltrodextrin (Roos & Karel, 1991c), glucose-fructose (Arvanitoyannis et al., 1993), corn syrup solids-maltrodextrin and solute-dilute systems of carbohydrate-water (Roos, 1993b).

Fox proposed the relation between the two components could be approximately expressed by $k \approx T_{g1} / T_{g2}$ leading to the transformation to the Fox equation (Fox, 1956).

$$\frac{1}{T_g} = \frac{x_1}{T_{g1}} + \frac{x_2}{T_{g2}} \tag{2.14}$$

Schneider and Di Marzio compared the Fox and Di Marzio equations for 30 compatible polymer blends (1992). Both equations show the same composition dependence for miscible polymer blends and can provide a valid rough approximation. However, they fail to predict experimentally observed strong negative and positive deviations of T_g for the blends (Schneider, 1988; Schneider & Di Marzio, 1992).

An equation based on the classic thermodynamic theory was introduced by Couchman and Karasz (1978). They proposed the glass transition as a function of the entropy of the compatible polymer blends.

$$S = S_1 x_1 + S_1 x_2 + \Delta S_{mix} \tag{2.15}$$

Where S is the entropy, x the mass fraction the index referring to the pure components and ΔS_{mix} is the excess entropy of the mixture. The entropy S_i is composed of the entropy of the pure components S_i^0 at their glass transition temperature and the entropy difference $S_i = S_i^0 + (S_i - S_i^0) = S_i^0 - \Delta S_i$

$$C_{pi} = \frac{dQ}{dt} = dS_i \left(\frac{T}{dT} \right) \tag{2.16}$$

$$\Delta S_i = \int_{T_{gi}}^{T} dS_i = \int_{T_{gi}}^{T} \frac{C_{pi}}{T} dT \tag{2.17}$$

$$S_i = S_i^0 + \int_{T_{gi}}^{T} \frac{C_{pi}}{T} dT \tag{2.18}$$

The idea is the same as for the Gordon-Taylor equation. The entropy of the components is additive and a true second order transition is assumed, as in the definition of a second order transition by Ehrenfest (1933), the thermodynamically potentials are continuous. Furthermore, it is assumed that at the transition the entropy of the glass and rubbery state are identical $S_i^{0,g} = S_i^{0,SCL}$.

$$x_1 \int_{T_{g1}}^{T_g} \frac{\Delta Cp_1}{T} dT + x_2 \int_{T_{g2}}^{T_g} \frac{\Delta Cp_2}{T} dT + \Delta S_{mix,SCL} + \Delta S_{mix,g} = 0 \tag{2.19}$$

Where $\Delta C_{p,i} = C_{p,iSCL} - C_{p,ig}$ is the difference of the heat capacity between the supercooled liquid and the glass state of the pure components. Since the entropy is continuous at T_g and the excess entropy ΔS_{mix} is only configurational without taking any interaction into account, the excess entropies are assumed to be equal $\Delta S_{mix,SCL} = \Delta S_{mix,g}$. The final form of the equation varies depending on the definition of the relation of the heat capacity to the temperature. Originally, Couchman and Karasz (1978) defined the heat capacity to be independent of temperature leading to the first expression.

$$\sum \left\{ x_i \Delta C_{pi} (lnT_g + lnT_{gi} \right\} = 0 \tag{2.20}$$

Brinke et al. (1983) declared the independence of the heat capacity from the temperature to be incorrect and proposed the assumption to be proportional to the temperature.

$$\sum \left\{ x_i \Delta C_{pi} (T_g + T_{gi} \right\} = 0 \tag{2.21}$$

By solving the equation for T_g one receives the same form as the Gordon-Taylor equation.

$$T_g = \frac{x_1 T_{g1} + k x_2 T_{g2}}{x_1 + k x_2} \quad with\, k = \frac{\Delta C_{p2}}{\Delta C_{p1}} \tag{2.22}$$

Both equations have the identical form, since they rise from the same assumption of ideal additivity of the properties and an Ehrenfest second order phase transition at the glass transition, in which the entropy, enthalpy and volume are continuous. However, the physical meanings of the equations differ strongly from each other, where one takes the ratio of the incremental changes of the heat capacity at T_g into account while the other is based on the free volume of the components in the blend.

The changes of the heat capacity for the Couchman-Karasz equation can be obtained by DSC measurements for the pure components. The equation was successfully used to describe solid-solid mixtures, where the difference of the glass transition between the

components is comparably low and the temperature dependency of the heat capacity can be considered negligible (Brinke et al., 1983). In the case of dilute-solute system, the difference can be so great that the assumption is not valid any more. In the studies of Arvanitoyannis regarding fructose, glucose and water systems, he found that the systems with a high amount of solid, over 70%, the prediction method was more accurate. In general, it is stated that the T_g values for aqueous sytems are underestimated and for anhydrous systems overestimated (Arvanitoyannis et al., 1993).

In the given equations the physical properties are assumed to be additive. This allows only to predict monotonous deviations from additivity, either negative or positive. Not for all polymer blends can the T_g deviations be described by these equation, such as sugar and salt blends (Weng et al., 2014). By strong deviation from additivity the effect of intra- and inter-molecular interaction of the components has to be accounted for in the mixture.

Over the years, many empirical concentration second order power equations have been introduced. Kwei (1984) interpreted that the strong deviations come from the dissipation and merging of hydrogen bonds of the components. To account for these effects, he extended the Gordon-Taylor equation by the additional parameter q_K. Both coefficients are treated as empirical fitted parameters, which can be determined from experimental data (Kwei, 1984).

$$T_g = \frac{x_1 T_{g1} + k x_2 T_{g2}}{x_1 + k x_2} + q_K x_1 x_2 \tag{2.23}$$

The Kwei equation allows the sigmoidal shaped behaviour of the T_g blended curves to be described, but it cannot be applied to all polymer systems due to the limitation of capture of positive deviation in the low T_g range and negative deviation in the high T_g range. The same holds for the equation of Jenckel and Heusch (1953), Di Marzio (1990) or Kanig (1963), who linked the shift in interaction energies in the polymer melt to the respective Gibbs functions and hence, created free volume in the glassy state.

In order to describe the T_g changes over the whole composition range in a blend, the equations were advanced to third order. Brekner et al. (1988) stated the conformational mobility and the free volume are linked to the probability of the arrangement of hetero-molecular contacts in the blends due to the specific interactions of the components. Thus, an additional coefficient $K_{SB,1} = (2E_{12} - (E_{11} + E_{22}) / (T_{g,2} - T_{g,1})$ was introduced, with E_{ij} being the contact specific interaction enthalpy either of the homo- or heteromolecular enthalpy.

$$T_g = T_{g,1} + \left(T_{g,2} - T_{g,1}\right)\left[\left(1 + K_{SB,1}\right) x_{2,c} - K_{SB,1} x_{2,c}^2\right]$$
$$x_{2,c} = \frac{k x_2}{\left(x_1 + k x_2\right)} \qquad (2.24)$$

Where x is the mass fraction and the index 2 refers to the polymer with the higher T_g value, k has the same physical meaning as in the Gordon-Taylor equation, by which $x_{2,c}$ relates to the difference of density and expansivity of the components. From the thermodynamic view of mixing the Gibbs free energy $\Delta G_{mix} = \Delta H_{mix} - T\Delta S_{mix} < 0$ has to be fulfilled for miscibility of the polymers. It is assumed that the combinatorial entropy of mixing for polymer is negligible, the enthalpy of mixing has to be exothermic to assure $\Delta H_{mix} < 0$. This means the energy of homo-molecular interactions has to be overcome by the heteromolecular interactions, which only explains positive deviations. Shamblin et al. (1998) showed in their study of mixing of various sugars with additives that the excess enthalpy of the mixture is positive. If only the interaction of hydrogen bonds are accounted for, this means in respect to the enthalpy more hydrogen bonds are broken than new ones are formed. At the same time, the conformational entropy increases because of the higher number of non-bonded-hydrogen groups resulting in miscibility of the components (Shamblin et al., 1998). In order to take into account the influence of hetero-molecular interaction on the changes of conformational entropy in the adjacent contacts, the equation (2.24) was extended in accordance with Schneider, Benker and Cantow to a virial concentration power equation (Schneider, 1997).

$$T_g = T_{g,1} + \left(T_{g,2} - T_{g,1}\right)\left[\left(1 + K_{SB,1}\right) x_{2,c} - (K_{SB,1} - K_{SB,2}) x_{2,c}^2 + K_{SB,2} x_{2,c}^2\right] \qquad (2.25)$$

The parameters $K_{SB,1}$ and $K_{SB,2}$ are identical to the ones in equation (2.24) with the additional $K_{SB,1}$ coefficient. The $K_{SB,2}$ coefficient characterizes the energetic effect on the interaction in a binary system in accordance with the entropy changes caused by the hetero-molecular interaction in the compatible polymer blend (Schneider, 1997). Table 2.7.1 gives an overview of the most common T_g functions for a binary system. It has to be mentioned that all the presented coefficients, even though they are based on a thermodynamic theory, are mostly empirical fitted parameters.

Table 2.7.1. List of the most common analytical models for predicting the glass transition of binary blends.

	Name	Functional form	Coefficients
1.	Gordon-Taylor	$T_g = \frac{x_1 T_{g1} + k x_2 T_{g2}}{x_1 + k x_2}$	k
2.	Fox	$\frac{1}{T_g} = \frac{x_1}{T_{g1}} + \frac{x_2}{T_{g2}}$	-
3.	Couchman-Karasz	$\ln T_g = \frac{x_1 \Delta C_{p,1} \ln T_{g,1} + x_2 \Delta C_{p,2} \ln T_{g,2}}{\Delta C_{p,1} x_1 + \Delta C_{p,2} x_2}$	-
4.	Jenckel-Heusch	$T_g = x_1 T_{g,1} + x_2 T_{g,2} + b_{JH}\left(T_{g,2} - T_{g,1}\right) x_1 x_2$	b_{JH}
5.	Kwei	$T_g = \frac{x_1 T_{g1} + k x_2 T_{g2}}{x_1 + k x_2} + q_K x_1 x_2$	q_K
6.	Utracki	$T_g = \left[1 + K^* x_1 x_2\right]\left[x_1 T_{g,1}^{3/2} + x_2 T_{g,2}^{3/2}\right]^{2/3}$	K^*
7.	Pinal	$T_g = \frac{x_1 \Delta C_{p,1} T_{g,1} + x_2 \Delta C_{p,2} T_{g,2}}{\Delta C_{p,1} x_1 + \Delta C_{p,2} x_2} \exp\left(-\frac{\Delta S_m^c}{\Delta C_{p,m}}\right)$	-
8.	Painter	$\left[x_1 \Delta C_{p,1}\left(T_g - T_{g,1}\right) + x_2 \Delta C_{p,2}\left(T_g - T_{g,2}\right)\right] + x_2\left[\left(H_B^{H,L}\right)_{T_{g,mix}} - \left(H_B^{H,L}\right)_{T_{g,2}}\right] + \Delta H_{mix}^{H,L} = 0$	-
9.	Lu-Weiss	$T_g = \frac{x_1 T_{g,1} + k x_2 T_{g,2}}{x_1 + k x_2} + \frac{A x_1 x_2}{\left[x_1 + k x_2\right]\left[x_1 + b_{LW} x_2\right]\left[x_1 + c_{LW} x_2\right]^2}$ $A = \frac{-\chi_{12} R (T_{g,1} - T_{g,2}}{M_1 \Delta C_{p,1}} \quad k = \frac{\Delta C_{p,2}\, x_1 C_p^l}{\Delta C_{p,1} - x_2 \delta C_p^g}$	C_{LW}, b_{LW}
10.	Cowie-Harding	$T_g = \frac{(x_1 + f_C) T_{g1} + k(x_2 - f_C) T_{g2}}{(x_1 + f_C) + k(x_2 - f_C)} + \left[q_C\left(x_1 + f_C\right)\left(x_2 - f_C\right)\right]^{n_C}$	f_C,n_C, q_C, k_C
11.	Brekner-Schneider-Cantow	$T_g = T_{g,1} + \left(T_{g,2} - T_{g,1}\right)\left[\left(1 + K_{SB,1}\right) x_{2,c} - (K_{SB,1} - K_{SB,2}) x_{2,c}^2 + K_{SB,2} x_{2,c}^2\right]$ $x_{2,c} = \frac{k x_2}{\left(x_1 + k x_2\right)}$	$K_{SB,1}$ $K_{SB,2}$
12.	Brostow	$T_g = x_1 T_{g,1} + x_2 T_{g,2} + x_1 x_2\left[a_0 + a_1\left(2x_1 - 1\right) + a_2\left(2x_1 - 1\right)^2\right]$	$a_{,0}$, a_1, a_2

Authors: 1. (Gordon & Taylor, 1952), 2. (Fox, 1956), 3. (Brinke et al., 1983) 4. (Jenckel & Heusch, 1953), 5. (Kwei, 1984), 6. (Utracki & Favis, 1989), 7. (Pinal, 2008) 8. (Painter et al., 1991), 9. (Lu & Weiss, 1992), 10. (Cowie et al., 1989), 11. (Schneider, 1997), 12. (Kalogeras & Brostow, 2009).

2.7.3 Multicomponent systems

The direct transfer of an equation for binary systems to systems of higher order is complicated and requires a large amount of experiments. For instance, for a ternary two sugars with water systems, several experiments with different sugar ratios and water fractions have to be performed to obtain the corresponding k values. The easiest way to combine the T_g values is the extension form of the Fox equation. Identical to the procedure for a binary system, only the T_g values of the pure components are necessary and the mass or mole fraction of the component to predict the T_g of the multicomponent system.

$$\frac{1}{T_g} = \sum_{i=1}^{n} \frac{x_i}{T_{g,i}} \tag{2.26}$$

Similar to the binary systems, the Fox equation cannot give a detailed description of strong deviations, especially systems containing moisture (Hancock & Zografi, 1994). Another approach is the extension of the Gordon-Taylor and Couchman-Karasz equation, where the Gordon-Taylor equation takes up the following form.

$$T_g = \frac{x_1 T_{g,1} + \sum_{i=2}^{n} x_i k_{1i} T_{g,i}}{x_1 + \sum_{i=2}^{n} x_i k_{1i}} \tag{2.27}$$

Where $T_{g,1}$ refers to the component with the lowest T_g in food system, mostly water due to a T_g of -135˚C, the coefficient k_{1i} describes the deviation of the component with the component of the lowest T_g. That means the component with the lowest T_g is set as a plasticizer and the other components as solids and are plasticised by it. The values for k can either be estimated using the Simha-Boyer rule or from binary experiments of the solid and plasticizer. The constants of the extended version of the Couchmann-Karasz equation are easier to obtain, since only the ΔC_p of the pure components are required to predict the T_g of the mixture.

$$T_g = \frac{\sum_{i=1}^{n} x_i \Delta C_{p,i} T_{g,i}}{\sum_{i=1}^{n} x_i \Delta C_{p,i}} \tag{2.28}$$

In the work of Foster (2002) a slightly different approach has been taken. The T_g of the mixture was estimated by the weight average additive method of each component´s T_g, in accordance to the water activity in the system.

$$T_g = \sum_{i=1}^{n} x_i T_{g,a_w,i} \tag{2.29}$$

It can be understood as the sum of Gordon-Taylor equations of each component with the amount of bonded water. Water is not equally distributed in the solid matrix structure of a mixture. Therefore the correlation of the water activity and moisture content via sorption isotherm allows prediction of the glass transition temperature associated with the right amount of moisture for each component in the mixture. This method proved to be effective in a ternary sugar-water system and showed better results than the Couchmann-Karasz extended version (Foster, 2002). All the methods for multicomponent systems only consider the effect of one plasticizer, usually water, on the components. Since the T_g of water is low it has the greatest impact on the system as a plasticizer (Matveev et al., 2000), however studies of binary or ternary sugar systems show the plasticizing effect of the sugar molecules on each other (Cheuyglintase & Morison, 2010; Finegold et al., 1989; Seo et al., 2006). In a study from Kalichevsky et al. (1992), the plasticizing effect of several mono- and disaccharides on amylopectin gave the following order on the degree of plasticisation: sucrose < glucose < xylose < fructose, which accords with their T_g values. Truong´s analytical model is the only model taking the plasticising effect of each component on the components with higher T_g values into consideration (Truong et al., 2002). In the model, each component is plasticised separately by the component with the lowest T_g. The new obtained T_g values are then considered to be plasticised by the plasticizer next in order. For instance, a mixture of sucrose, fructose and glucoses is chosen, the order of plasticisation is identical, as mentioned above, sucrose < glucose < fructose, since with a lower T_g value the plasticising effect increases. First of all glucose and sucrose would be plasticised by the fraction of fructose equally Figure 2.7.1.

$$T_{g,SF} = \frac{(1-x_F)T_{g,S} + k_{SF}x_F T_{g,F}}{(1-x_F) + k_{SF}x_F} \qquad T_{g,GF} = \frac{(1-x_F)T_{g,G} + k_{GF}x_F T_{g,F}}{(1-x_F) + k_{GF}x_F}$$
$$T_{g,SGF} = \frac{x_S T_{g,SF} + k_{SG}x_G T_{g,GF}}{x_S + k_{SG}x_G} \tag{2.30}$$

This assumption is made on the basis that the glass transition of the mixture has to be in the range of the highest and lowest glass transition temperature for the plasticizer combinations. In case of the ternary sugar system, the glass transition of the ternary system has to be between the lines corresponding to the binary system with fructose, which is represented in Figure 2.7.1 by the dashed line. In the following step, the new estimated T_g values are transferred into a binary system of glucose and sucrose and the plasticizing effect of glucose is accounted for. For each additional component a further step is added and the sequence is determined starting from the plasticizer with the lowest T_g value to the highest. The advantages of this model are that only the k values of each binary system are needed for the prediction, furthermore it combines the plasticization effect of all components in a system. This method proved to be in good accordance with DSC measurements of ternary sugar mixtures with various sugar ratios (Truong et al., 2002). However, the model has not been applied to anhydrous quaternary system or in combination with low water, and evidence has to be provided the assumption of separate plasticization is valid. The results of Foster's work indicate that care has to be taken to consider the different distribution of water between the components in a food system (Foster, 2002).

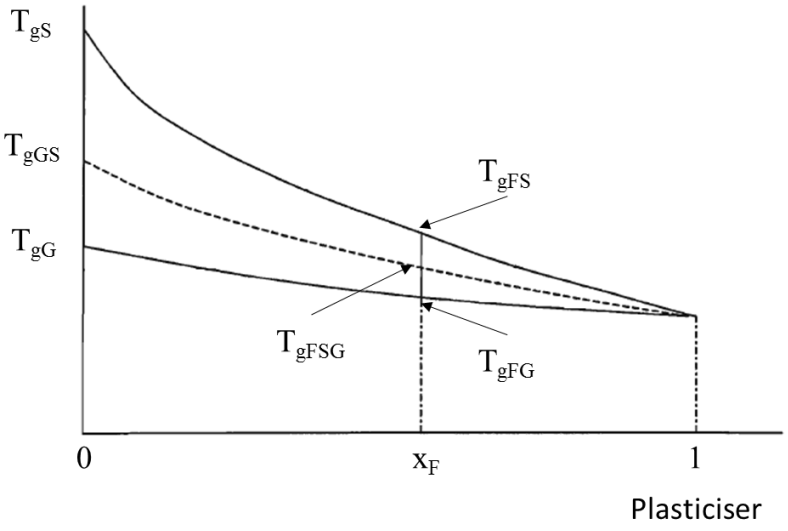


Figure 2.7.1. Based on the illustration of the principle of the analytical model of Truong (Truong, 2003).

2.8 Glass transition temperature of components

2.8.1 Preparation of amorphous solids for DSC measurement

The formation of amorphous solids in food and pharmaceutical products is a result of the rapid removal of a solvent or when a concentrated solution is cooled quickly without sufficient time for the dissolved components to reach an equilibrium state. This general principle is adopted to transfer pure components or mixtures into amorphous solids and study the thermophysical properties. Melt quenching and freeze drying are common methods for the production of amorphous samples, since both allow good control over the products and are applicable to solids with low glass transition temperatures.

2.8.2 Melt quenching

In melt quenching pure or a mixture of crystals are heated over their melting temperature and then cooled fast enough to transfer the melt into an amorphous solid (Finegold et al., 1989; Fukuoka et al., 1989; Jeong-Ah et al., 2005; Ruiz-Cabrera et al., 2016; Ruiz-Cabrera & Schmidt, 2015; Saavedra-Leos et al., 2012). The melting of the crystals can be directly performed in a DSC pan or in a beaker. Previous to the melting, the crystals can be dried in a vacuum oven at 70˚C under a pressure of 20-70 kPa for 1-2 days and stored over phosphorous pentoxide at room temperature to reduce the residual moisture in the crystals (Saavedra-Leos et al., 2012; Truong, 2003). The moisture content of crystal is generally and Truong (2003) measured only for glucose monohydrate, obtaining a moisture content of 10% db. For fructose, citric acid, sucrose, malic acid crystal it was near 0% db. Wungtanagorn and Schmidt (2001b) analysed fructose and glucose crystals by applying the Karl-Fischer titration method to measure their moisture content, drying at 60˚C for 12h. The determined moisture content was around 0.0232% db. for fructose and 0.0346% db. for glucose, which demonstrates that vacuum drying can be considered to be sufficient to produce completely anhydrous crystals.

2.8.3 Freeze drying

Roos and Karel (1990) proved this method could be used to obtain completely amorphous solids for 10 and 20% solute concentrations of sucrose, α-lactose, maltose, maltodextrin (MD) with various DE and sucrose-MD mixtures (Roos & Karel, 1990, 1991b, 1991c, 1992). The solution was frozen to -20˚C for 24 h, held over dry ice for 3 h and freeze dried for 48 h. Saleki-Gerhardt and Zografi (1994) produced amorphous products from 10% (w/v) aqueous solutions of the pure substance sucrose, trehalose, lactose, raffionose and sucrose mixture with the previously listed sugars. The freeze drying was done over several steps, where the solutions were frozen at -45˚C, primarily freeze dried at 6 Pa for 72 h and slowly heated up to 0˚C over a period of 4 days. The secondary drying was performed at 25˚C for 1 day followed by drying of the lyophilized powder at 60˚C for 2 days. Arvanitoyannis et al. (1993) freeze dried 50% aqueous sugar solutions of fructose and glucose at -60˚C for 4 days. Truong (2003) adopted in his work the solute concentration of 50% (w/w) for binary and multicomponent mixtures. The solutions were frozen at either -18 or -40˚C for 20 h and then freeze dried for 2 days and dried at 60˚C for an additional 2 days. This approach produced mostly complete amorphous powder, however in the case of binary systems of sucrose/fructose and glucose/fructose partial crystallisation of sucrose and glucose was detected for concentrations below 40% (w/w) of solid mixtures. Similar results were obtained for binary systems of sucrose/glucose, if the concentration of one of the components was below 12.5% (w/w) and for sugar and citric acid mixtures once the concentration of citric acid exceeded 80% (w/w). No crystallisation was found for ternary sucrose, fructose and glucose mixture independent of their composition.

After optimal freeze drying the residual moisture content in the amorphous product is around 1-2% (Pikal et al., 2005; Tang & Pikal, 2004). In order to decrease the moisture content further, Roos and Karel (1990) transferred the amorphous powders into a vacuum desiccator and dried them over phosphorous pentoxide for a least a week. Brooks (2000) studied the additional moisture content loss of spray dried and freeze dried amorphous lactose over phosphorous pentoxide for 3 weeks. In the first week, a rapid moisture loss was detected from the original 3.75% db. spray dried and 6.3% db. freeze dried amorphous lactose to 1.65% and 3.3% db., respectively. With further drying over phosphorous pentoxide up to 3 weeks a decrease of only 0.5% for spray dried and 1% db. freeze dried for amorphous lactose could be achieved. It is assumed the driving force of

the moisture desorption is quite low due to the low moisture content in the sample making the process very slow. Another explanation could be that after one week only water molecules remain that are weakly bound to the α-lactose molecules and are harder to remove (Brooks, 2000). Truong (2003) compared the impact of the freeze drying time, applying heat on the product after freeze drying for 2 days and drying it over phosphorous pentoxide for 15 days on the residual moisture content of various concentrations of glucose/fructose and sucrose/citric acid mixtures. The study showed that the samples dried over phosphorous pentoxide had a moisture content of 1.5-2% db. and were partially crystallised with higher citric acid concentrations. Freeze dried samples dried for 2 days without applying heat had high moisture contents with up to 11% db. for sucrose/citric acid and 3% db. for glucose/fructose mixtures. The lowest moisture content of 0.1-0.2% db. for all samples could be achieved by applying heat to 60˚C for 2 days.

2.8.4 T_g of solids in fruit juices

The glass transition is a time-dependent property of the glassy state and the relative rate of glass formation determines the measured temperature by the DSC. Nevertheless, the approximated T_g value of the components can be reproduced and different authors have investigated the main solid component of the fruit juices over the years. Table 2.8.1 gives an overview of the range of the measured glass transition temperatures in relation to the applied preparation method as well as the various heating and cooling rates.

Table 2.8.1. Glass transition temperature of the main solids in fruit juices: sucrose, fructose, glucose, citric acid and malic acid measured by DSC.

Material	**T_g (˚C)**		**ΔC_p**	**Sample preparation**		**Scan rate (˚C/min)**	
	Onset	**Mid**	**(J/g)**	**Size**	**Method – [T_{FM}] (˚C) q_m (˚C/min)**	**Cooling**	**Heating**
Fructose		7.5 ± 0.59			MQ[(a)] [160]- 20 ˚C/min	20	10
		7	0.84		MQ[(b)] [157]- 50 ˚C/min	50	10
		6.8 ± 1.07		10	MQ[(c)] [168]	10	10
		16.2 ± 0.8	0.62	10-30	MQ[(d)] [143]- 10 ˚C/min	50	10
		18.1 ± 0.6		10-30	MQ[(d)] [160]- 50 ˚C/min	50	10
		23 ± 1.2		10-30	MQ[(d)] [UC]	50	10
		15.8 ± 0.6		10-30	FD[(d)]	50	10
		15 ± 2.0		5-12	MQ[(e)] [125]- 20 ˚C/min	20	10
		10.4 ± 0.3		5-12	MQ[(f)] [125]- 20 ˚C/min	20	10
		11		10-30	FD[(g)]		2.5-10

Material	T_g (˚C)		ΔC_p	Sample preparation		Scan rate (˚C/min)	
	Onset	Mid	(J/g)	Size	Method – [T_{FM}] (˚C) q_m (˚C/min)	Cooling	Heating
		13		5-10	MQ[h] [UC]	UC	10
	5	10	0.75	3-20	MQ[i] [UC]	UC	5
Glucose		38	0.88	5-10	MQ[b] [167]	50	10
		41		10-30	FD[g]		2.5-10
		39		5-10	MQ[h] [UC]	UC	10
		39	0.77	10	MQ[c] [168]	10	10
		35.4 ± 0.3			MQ[a] [180]- 20 ˚C/min	20	10
		40.3 ± 0.7	0.58	10-30	MQ[d] [170]- 10 ˚C/min	50	10
		40.4 ± 0.8		10-30	MQ[d] [185]- 50 ˚C/min	50	10
		44 ± 1.3		10-30	MQ[d] [UC]	50	10
		38 ± 0.5		10-30	FD[d]	50	10
		34.2 ± 3.7		5-12	MQ[e] [160]- 20 ˚C/min	20	10
		31.8 ± 0.23		5-12	MQ[f] [160]- 20 ˚C/min	20	10
	31	36	0.75	3-20	MQ[i] [UC]	UC	5
Sucrose	56.6			2-3	FD[j]		5
	62	67	0.6	10-25	FD[k]		5
		70	0.68	5-10	MQ[b] [157]- 50 ˚C/min	50	10
	62	67	0.6	2-3	MQ[i] [UC]	UC	5
		72.2 ± 0.2			MQ[l] [190]	10	10
		68.6 ± 1.0	0.43	10-30	MQ[d] [205]- 10 ˚C/min	50	10
		72.8 ± 1.2		10-30	MQ[d] [215]- 50 ˚C/min	50	10
		72.9 ± 1.4		10-30	MQ[d] [UC]	50	10
		65.8 ± 2.9		5-12	MQ[e] [185]- 20 ˚C/min	20	10
		64.8 ± 0.28		5-12	MQ[f] [185]- 20 ˚C/min	20	10
	62	67	0.6	3-20	MQ[i] [UC]	UC	5
Citric		13.6 ± 0.3	0.43	10-30	MQ[d] [175]- 10 ˚C/min	50	10
acid		13.8 ± 0.5		10-30	MQ[d] [185]- 50 ˚C/min	50	10
		14.5 ± 0.9		10-30	MQ[d] [UC]	50	10
		12 ± 0.6		10-30	FD[d]	50	10
	11			10-20	MQ[m] [154]	30	10
	11				FD		20
Malic		-16.1 ± 0.6	0.82	10-30	MQ[d] [175]- 10 ˚C/min	50	10
acid		-12.1 ± 0.8		10-30	MQ[d] [190]- 50 ˚C/min	50	10
		-8.6 ± 1.1		10-30	MQ[d] [UC]	50	10

Symbols: Mid=midpoint, MQ=melt quenching, FD=freeze drying, q_m=melting rate of the crystals, T_{FM}=final melting temperature to melt the crystals, UC=uncontrolled heating or cooling.

Authors: (a) (Liu et al., 2006), (b) (Orford et al., 1990), (c) (Wungtanagorn & Schmidt, 2001a), (d) (Truong, 2003), (e) (Ruiz-Cabrera & Schmidt, 2015), (f) (Ruiz-Cabrera et al., 2016), (g) (Arvanitoyannis et al., 1993), (h) (Finegold et al., 1989), (i) (Roos, 1993b) (j) (Roos & Karel, 1991c), (k) (Roos & Karel, 1991d), (l) (Vanhal & Blond, 1999), (m) (Lu & Zografi, 1997).

In Table 2.8.1, it is evident that melt quenching is the most common method to investigate the glass transition temperature of pure components. This is because it involves less preparation effort, since the crystal can be direct melted in the DSC and no long preparation steps as in freeze drying are required. However, care has to be taken to avoid decomposition and mutarotation of the components (Arvanitoyannis et al., 1993). Therefore, the melting point should always be validated for the chosen heating rate. Hurtta et al. (2004) investigated the effect of the melting rate of D-fructose, D-glucose and D-sucrose on the melting and the thermal degradation temperature (Table 2.8.2). Especially, at lower heating rates, thermal degradation can occur at lower temperatures than the melting temperature.

Table 2.8.2. Melting and thermal degradation temperature at different heating rates for D-fructose, D-glucose and D-sucrose (Hurtta et al., 2004).

Sugar	**Rate of heating (˚C/min)**	**Melting temperature (˚C)**	**Thermal degradation temperature (˚C)**
Sucrose	0.5	182.7	167.0
	1	186.6	171.3
	2	189.3	178.8
	10	191.5	189.2
	20	192.9	200.7
	50	196.1	214.9
	100	196.5	228.4
Glucose	0.5	147.5	147.0
	1	149.3	152.0
	2	151.9	159.0
	10	159.4	170
	20	163.8	183.5
	50	168.9	201.1
	100	173.8	204.3
Fructose	0.5	113.0	110.4
	1	116.7	113.9
	2	121.0	119.0
	10	131.7	136.8
	20	136.0	147.1
	50	139.8	157.0
	100	142.0	165.4

This phenomenon can not only be seen for glucose, but also for fructose, where a heating rate of 10˚C/min is sufficient to overcome the degradation temperature. The heating rate also shifts the melting temperature to higher temperatures, particularly for glucose and fructose where the melting temperature is raised ~30˚C and for sucrose ~14˚C. The difference in the melting temperature makes it difficult to co-melt these three sugars together without avoiding any degradation (Jiang et al., 2008).

The heating of fructose at 10˚C/min up to a final melting temperature 168˚C results in a glass transition temperature of 6.8˚C (Wungtanagorn & Schmidt, 2001a). A similar low glass transition temperature of 7.48˚C for fructose could be observed at a final melting temperature of 160˚C heated at 20˚C/min (Liu et al., 2006). Although, the preparation method and the DSC protocol vary between the authors, the temperature difference between the lowest and highest measured glass transition temperature (midpoint) is ~9˚C for fructose and glucose, ~8˚C for sucrose, ~3˚C for citric acid and -8.6˚C for malic acid in Table 2.8.1. This fact shows that it is impossible to reduce the glass transition temperature to exactly one temperature due to the time dependency, but the narrow temperature range allows one to approximate the glass transition well enough to be used as a reference parameter for related physical changes.

2.8.5 T_g of anhydrous binary systems

The preparation method of the binary systems is the same as for pure substances, however in the case of melt quenching, the crystals have to be co-melted to obtain an amorphous mixture. As previously described, this procedure has disadvantages for binary or higher order systems. Truong (2003) demonstrated for binary sugar and organic acid mixtures that by heating them up, interaction in the form of hydrolysis occurs between the components as well as degradation of the components is observed. For the study fructose, glucose and sucrose crystals were individually combined with either malic, citric or tartaric acid crystals and heated over the melting temperature of the component with the higher melting temperature. Depending on the intensity of the change in colour of the mixture, Truong (2003) divided the interaction into, no, slight, intermediate and strong interaction. Only binary mixtures of glucose and fructose with citric acid show no interaction; all other systems exhibit slight to strong interaction, especially for the combination with tartaric acid, showing that melt quenching cannot be considered for these mixtures.

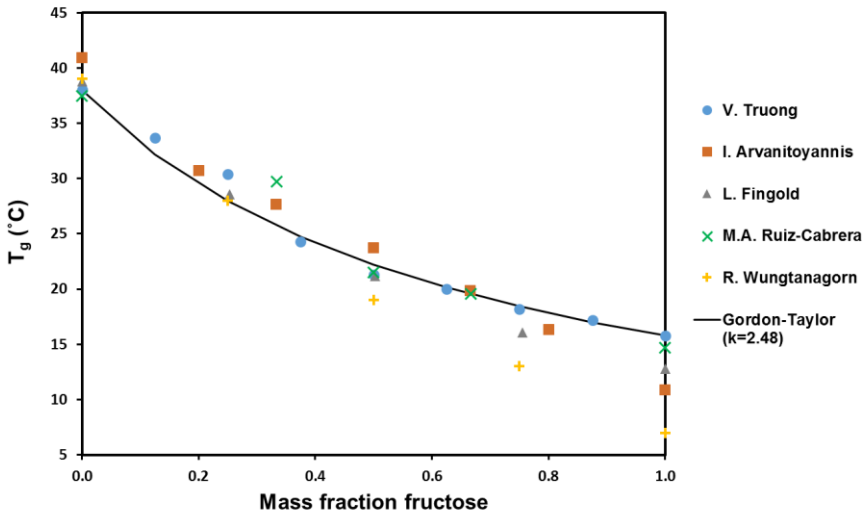


Figure 2.8.1. Glass transition temperature at various weight fraction of fructose for glucose and fructose mixtures. Authors from top to down: (Truong, 2003), (Arvanitoyannis et al., 1993), (Finegold et al., 1989), (Ruiz-Cabrera & Schmidt, 2015) and (Wungtanagorn & Schmidt, 2001a).

Binary systems of mono- and disaccharides and the effect of the various weight fractions on the common glass transition temperature were studied by several authors using either freeze drying (Arvanitoyannis et al., 1993; Truong, 2003) or melt quenching (Finegold et al., 1989; Ruiz-Cabrera & Schmidt, 2015; Saavedra-Leos et al., 2012; Seo et al., 2006; Wungtanagorn & Schmidt, 2001a) as a preparation method to obtain amorphous mixtures. The glass transition temperature was measured using a DSC and the midpoint as a reference point, whereby Arvanitoyannis et al. (1993) and Seo et al. (2006) employed a heating rate of 1.25 and 4 ˚C/min respectively and the rest used the standard heating rate of 10˚C/min. The common glass transition temperature at various weight fractions of glucose and fructose can be seen in Figure 2.8.1. Scattered data for the glass transition of the mixture are expected due to the kinetic nature of the glass transition and the difference in preparation method. Despite, the difference in the measured glass transition from various authors, a general trend can be observed for all data points with the increase of the weight fraction of fructose in the mixture. The Gordon-Taylor equation is suitable to represent the negative deviation from linearity of the common glass transition temperature for the binary system of fructose and glucose. The k coefficient for the Gordon-Taylor equation is fitted to the data from Truong (2003) and the glass transition temperature of the pure components is also adopted from the same study. Only the glass transition temperature obtained by Wungtanagorn and Schmidt (2001a) varies strongly from the data of the other authors at higher weight fractions > 0.5 for fructose. Wungtanagorn and Schmidt (2001a) prepared the amorphous mixture by melt quenching

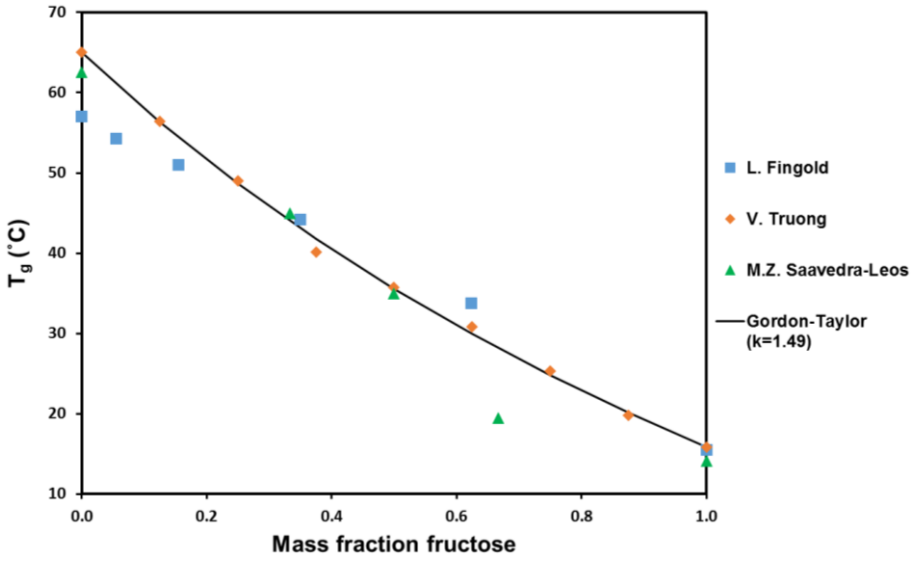


Figure 2.8.2. Glass transition temperature at various weight fraction of fructose for sucrose and fructose mixtures. Authors from top to down: (Finegold et al., 1989), (Truong, 2003) and (Saavedra-Leos et al., 2012).

the crystals directly in the DSC. However, no indication as to the final heating temperature is given in their trial, whereas a too high final melting temperature could be the reason for the degradation of fructose and the lower response seen for the glass transition at higher fructose contents.

The glass transition for the mixtures of fructose and sucrose is quite similar for the various compositions (Figure 2.8.2). The reason for the close spacing between the first data points of Finegold et al. (1989) is that mole fraction was considered in the study instead of weight fraction and since the molar mass of sucrose is almost double that of fructose, the conversion of mole fraction to mass fraction has a great effect, whereas the molar mass of glucose and fructose are almost identical and no change is observed (Figure 2.8.2). Similar to the previous binary systems, the Gordon-Taylor equation models the tendency of the glass transition of the binary mixture well.

The glass transition temperature for the binary system of glucose and sucrose follows a different trend compared to the two other binary systems. Unlike the negative deviation from mass additivity observed for fructose/sucrose and glucose/fructose mixtures, the binary system of sucrose and glucose displays an alternating convex-concave plot of the glass transition temperature over the composition range. This indicates that the interaction and the scale of the mixing are different and change for different blend compositions. Seo et al. (2006) defined the shape and size of molecules responsible for this behaviour. In their study, they compared the glass transition temperature of binary systems for mono/monosaccharide (glucose/sorbitol), di/disaccharide (sucrose/trehalose), mono/disaccharide (sorbitol/sucrose and glucose/sucrose) and mono/trisaccharide (glucose/maltotriose) mixtures. All binary systems of monosaccharides in combination with di or trisaccharides exhibit the sigmoidal trend for the glass transition temperature. The binary system of mono/disaccharide fructose and sucrose does not present irregular trends of the glass transition for different blend compositions. Furthermore the irregular compositional dependence on the glass transition temperature can be found in polymer blends such as PVMA/PVPh, PMMA/PVPh and PCL/PS, where the size factor between the molecules becomes minor (Kalogeras & Brostow, 2009). More likely is that the balance between inter and intramolecular interaction is shifted at a crucial compositional threshold. FTIR studies of the PVMA/PVPh blends displayed strong intermolecular hydrogen bonds between the phenolic -OH group in PVPh and the ether oxygen of PVME, which exceed the intrachain interaction of the repeating PVPh segment in strength. This is seen as a positive deviation from mass additivity for the glass transition

temperature of the mixture. At a weight fraction of 0.4 (Zhang et al., 2004) or 0.5 (Pedrosa et al., 1994) for PVME in the blend the positive deviation invert to a negative response, since the amount of the PVPh molecules is not sufficient to keep the dense structure and a shift of intermolecular to intramolecular interaction is observed. The variance in the hydrogen bonds has an effect on the enthalpy of the systems and simultaneously provokes changes in the entropy, which results in the observed plot for the glass transition temperature.

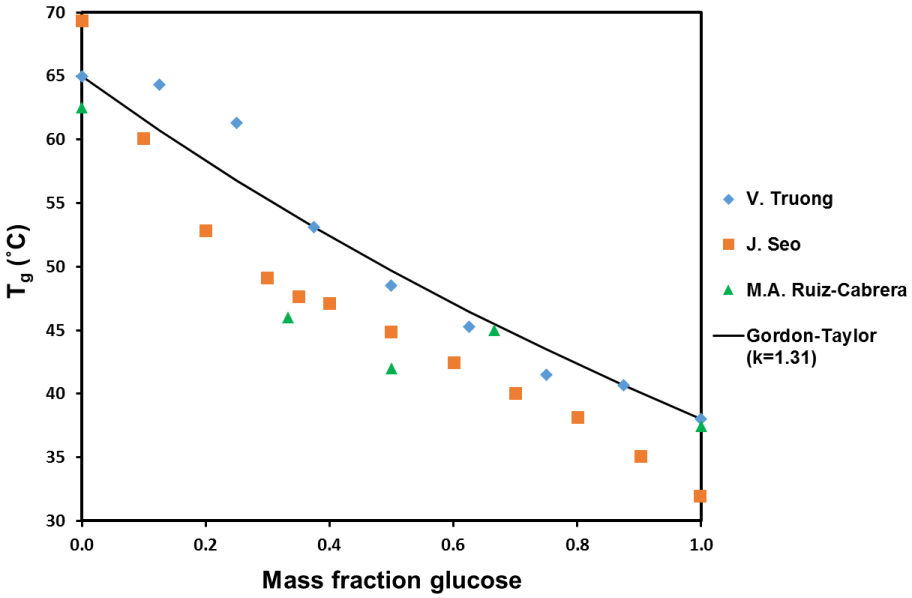


Figure 2.8.3. Glass transition temperature at various weight fraction of glucose for sucrose and sucrose mixtures. Authors from top to down: (Truong, 2003), (Seo et al., 2006) and (Ruiz-Cabrera & Schmidt, 2015).

Interestingly, in Figure 2.8.3 for the authors Truong (2003) and Seo et al. (2006), the observed positive and negative deviations for the glass transition plot is reversed. The inflection point is for both studies at weight fraction of around 0.35 of glucose, however, for Truong (2003) first a positive and then a negative deviation can be observed and for Seo et al. (2006) the reverse. An additional trial for this binary system should give further indication on the compositional dependence of the glass transition temperature.

For organic acids, only citric acid in combination with carbohydrates has been studied for binary systems so far. Tartaric (T_g~18.5˚C) and succinic acid (T_g~30˚C) possess moderate glass transition temperatures, which would allow one to investigate them without overly great precaution against recrystallization. However, due to the low concentration in natural products, not much attention has been given so far to the interaction between these two organic acids and carbohydrates, and the corresponding effect on the blend glass transition temperature. In the case of L-malic acid, the glass transition of the pure

component is ~ -16˚C. This makes it hard to study, since according to an annealing study of amorphous L-malic acid at ambient temperature (22˚C), 60% of the L-malic acid was crystallized after only one day of annealing (Truong, 2003). The high portion of crystallinity will have an impact on the detected transition temperature in DSC runs.

Table 2.8.3. Glass transition temperature for binary citric acid-sugar system adapted by (Truong, 2003).

Mass fraction Citric acid	**T_g of binary citric acid-sugar system in ˚C**		
	Sucrose	**Glucose**	**Fructose**
0	65	38	16
0.2	51.4 ± 0.9	30.6 ± 0.9	14.3 ± 0.5
0.4	39.6 ± 1.0	23.9 ± 0.6	13.3 ± 0.6
0.6	28.7 ± 0.8	20.1 ± 0.8	12.8 ± 0.4
0.8	19.9 ± 0.7	15.8 ± 0.7	12.2 ± 0.4
1	12	12	12

The citric acid-sugar mixtures (Table 2.8.3 and Figure 2.8.4) do not display a strong offset from mass additivity. Truong (2003) compared the fitting ability of the Couchman-Karasz equation, Gordon-Taylor equation with Simha-Boyer rule, Fox equation, Linear equation and Gordon-Taylor equation with an empirical coefficient to predict the glass transition temperature of binary systems. The Fox and Linear equations were in almost all cases not capable of describing the trend of the glass transition temperature for the binary systems

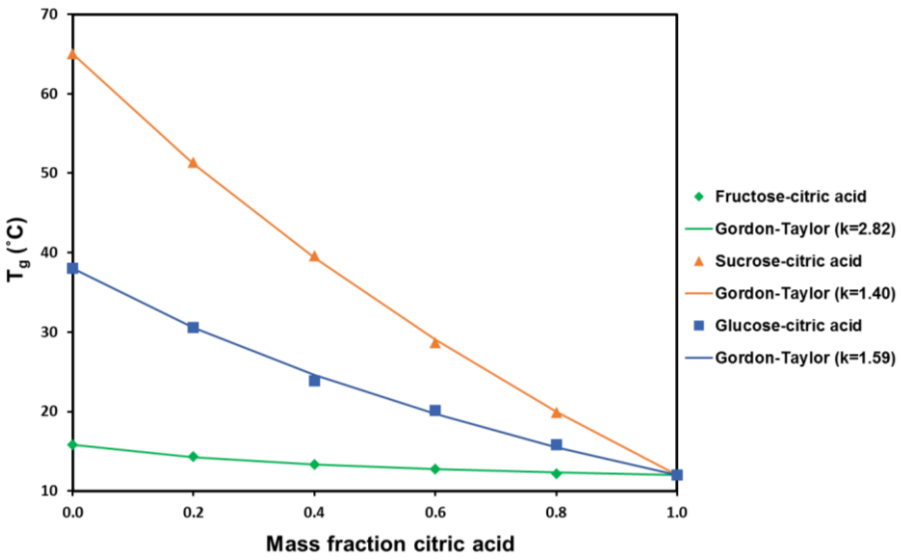


Figure 2.8.4. Glass transition temperature of binary citric acid-sugar mixtures adapted by (Truong, 2003).

presented above. The Simha-Boyer rule and the Couchman-Karasz performed much better in characterizing the binary systems, however in some binary systems these equations lack the ability to cover interactions between the components. Therefore, Truong (2003) compared the empirical coefficient k for the Gordon-Taylor equation with the coefficient of the Couchman-Karasz $k = \Delta Cp_2 / \Delta Cp_1$ and introduced an interaction factor ε to quantify the deviation from ideal mixing of binary systems. The latter coefficient only represents the ideal mixing of the components, whereas due to the fitting of the k coefficient in the Gordon-Taylor to experimental data, it also accounts for the interaction between the components.

$$\varepsilon = \frac{k_{GT}}{k_{CK}} = \begin{cases} k_{CK} = k_{GT} & \text{(ideal mixing)} \\ k_{CK} \neq k_{GT} & \text{(non-ideal mixing)} \end{cases} \tag{2.31}$$

$$\mathrm{I_{mix}} = |1 - \varepsilon| \leq 0.05 \tag{2.32}$$

Where ε is the interaction factor, k_{GT} and k_{CK} are the empirical coefficients of the Gordon-Taylor and the Couchman-Karasz equation and $\mathrm{I_{mix}}$ is the parameter characterizing the mixing. The system was defined as ideal, if the empirical coefficient is in the range of 5% from the ratio of the change in heat capacity of the pure components the system (Table 2.8.4).

Table 2.8.4. Characterizing of the mixing conditions in various anhydrous binary mixtures adapted by (Truong et al., 2002).

Parameter	**Anhydrous binary mixtures**					
	S/G	**G/F**	**S/F**	**C/S**	**C/G**	**C/F**
k_{GT}	1.31	2.48	1.49	1.41	1.59	2.82
k_{CK}	1.35	1.06	1.44	1.63	1.21	1.13
ε	0.97	1.72	1.03	0.86	1.31	2.15
$\mathrm{I_{mix}}$	0.03*	0.72	0.03*	0.14	0.31	1.15

Note: * ideal mixing

Only the binary systems sucrose/fructose and sucrose/glucose can be considered ideal mixtures by this definition. It is still open to argument whether this is really the case for the binary system of sucrose and glucose due to the sigmoidal trend of the glass transition

temperature (Figure 2.8.3) or whether a more diverse data collection would show actually a similar trend to the other binary sugar blends.

2.8.6 T_g of anhydrous ternary mixtures

The information on the glass transition temperature of food components in ternary mixtures is relatively limited; only two research groups have addressed the topic with the focus on the main carbohydrates sucrose, glucose and fructose. The approach around the research from Saavedra-Leos et al. (2012), Ruiz-Cabrera and Schmidt (2015) and Ruiz-Cabrera et al. (2016) differentiates strongly from the work of Truong (2003). Truong (2003) constructed the study of the glass transition temperature of ternary sugar mixtures to prove the reliability of his presented analytical model whereas Saavedra-Leos et al. (2012), Ruiz-Cabrera and Schmidt (2015) and Ruiz-Cabrera et al. (2016) did a statistical analysis using a Scheffe cubic model to evaluate the compositional dependence of the glass transition temperature.

$$\begin{aligned} y = {} & \alpha_0 x_G + \alpha_1 x_F + \alpha_2 x_S + \alpha_3 x_G x_F + \alpha_4 x_G x_S \\ & + \alpha_5 x_F x_S + \alpha_6 x_G x_F x_S + \alpha_7 x_G x_F (x_G - x_F) \\ & + \alpha_8 x_G x_S (x_G - x_S) + \alpha_8 x_F x_S (x_F - x_S) \end{aligned} \tag{2.33}$$

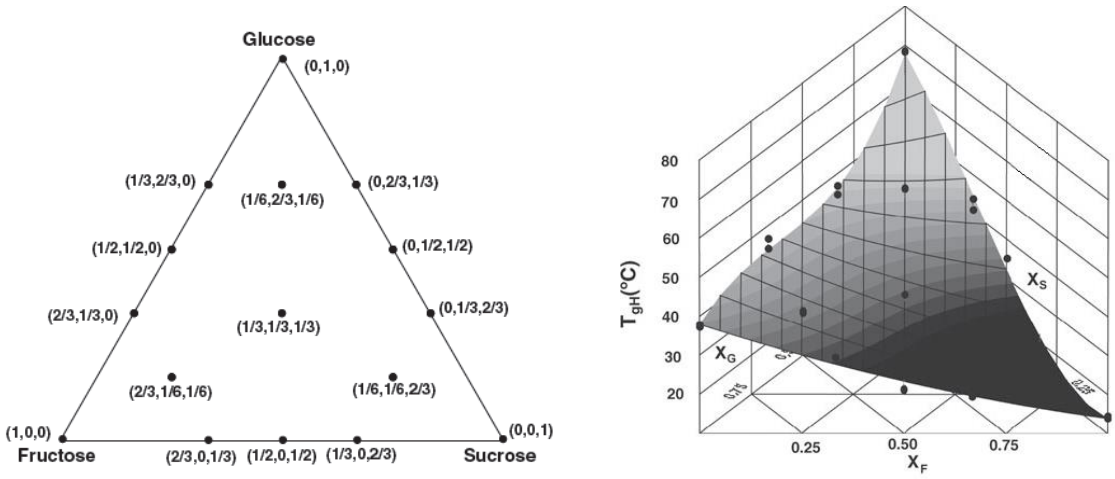


Figure 2.8.5. Experimental design for sucrose, fructose and glucose mixtures (left) and three-dimensional response surface of the measured glass transition temperature during heating (right) (Saavedra-Leos et al., 2012).

The regression analysis shows that only the linear model and the binary mixtures have a statistically relevant impact on the T_g of the mixture (Ruiz-Cabrera & Schmidt, 2015). At the same time Saavedra-Leos et al. (2012), Ruiz-Cabrera and Schmidt (2015) and Ruiz-Cabrera et al. (2016) used direct melt quenching in the DSC to obtain amorphous mixtures

and measure their glass transition temperature (Figure 2.8.5). Saavedra-Leos et al. (2012) proposed in their research a calorimetric methodology to prevent thermal decomposition and degradation for the ternary sugar mixtures. In their study, it was stated that no degradation in form of thermal browning of the mixtures could be observed by visual inspections, since the colour of the sample was unchanged after the heat treatment. However, Ruiz-Cabrera and Schmidt (2015) applied the same calorimetric protocol for the ternary sugar mixtures and a few samples were analyzed via HPLC for possible thermal decomposition products (fructose, glucose, 5-HMF). In every sample, an increase of decomposition products was detected, which again emphasizes the problematic nature of the melt quenching technique for precise measurements of the compositional dependence of the T_g measurements of mixtures with widely spaced melting temperatures. See for instance the binary mixture of 2/3 fructose and 1/3 sucrose, which was heated up to 160-190˚C in the study of Ruiz-Cabrera and Schmidt (2015). The glass transition temperature during the heating cycle was ~14˚C. In comparison, pure fructose had a T_g of ~15˚C but was only heated up to maximal 135˚C. In the trial of Saavedra-Leos et al. (2012), for the same composition and final heating temperature of 200˚C, a T_g of ~20˚C was detected and for the freeze dried sample of Truong et al. (2002) a T_g of ~30˚C. This makes a difference of 15˚C between the glass transition in the study of Ruiz-Cabrera and Schmidt (2015) and (Truong et al., 2002). Figure 2.8.5 displays the experimental design for the sugar mixtures and the response surface of the statistical model for the glass transition temperature for the chosen mixtures. The statistical model allows one to predict the T_g for all possible compositions in a ternary system, however it is only of limited usefulness, since it is only fitted to the defined systems. If the T_g of a higher ordered system needs to be estimated or one component is exchanged for another one, the model fails to predict the new T_g value and a new experimental design has to be created to cover the new formulation.

The analytical model for the prediction of the glass transition temperature from Truong et al. (2002) (Section 2.7.3) relies only on the binary data to predict the glass transition of the mixture. In his three trials of ternary sugar mixtures, the ratio between sucrose and glucose (5/3, 4/4 and 3/5) were kept identical for each trial and scaled in correlation to the increasing mass fraction of fructose (Figure 2.8.6).

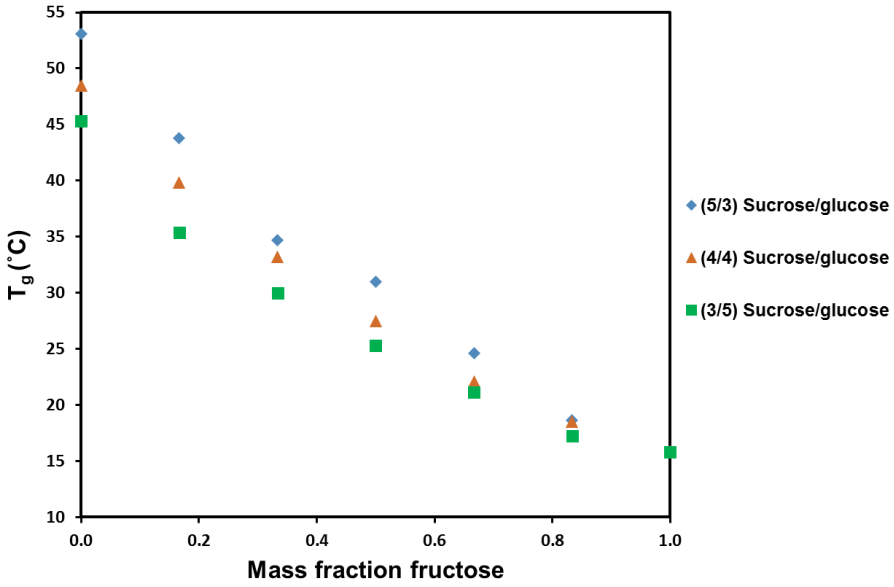


Figure 2.8.6. Glass transition temperature of ternary sugar mixtures (sucrose, glucose and fructose). The ratio between sucrose and glucose is set to 5/3, 4/4, 3/5. Data from (Truong et al., 2002).

The empirical coefficient for the Gordon-Taylor of the binary mixtures (Table 2.8.4) were used in the analytical model to predict the T_g of the mixtures. Additionally, the results were compared to the prediction accuracy of the extended the Couchman-Karasz equation, the extended Gordon-Taylor equation using Simha-Boyer rule and an empirical second-order polynomial equation. The addition of a third-order interaction coefficient to the polynomial equation $\alpha_{GFS} x_F x_G x_S$ showed a maximum difference less than 0.6˚C to the polynomial equation with only second order interactions.

$$T_g = \alpha_G x_G + \alpha_F x_F + \alpha_S x_S + \alpha_{GF} x_G x_F + \alpha_{GS} x_G x_S + \alpha_{FS} x_F x_S \qquad (2.34)$$

This agrees well with the results the regression analysis of Ruiz-Cabrera and Schmidt (2015) stating the statistical insignificance of the higher order interaction terms.

As expected, the fitted polynomial equation represents the experimental data in the best way. However, just like the fitted polynomial from the study of Saavedra-Leos et al. (2012), the estimated coefficients cannot be applied to a new component systems and are limited to the prediction of the pre-defined ternary system. The extended Gordon-Taylor

equation and the Couchman-Karasz equation do not provide a consistent prediction for different ternary systems. The average error of the Gordon-Taylor equation with Simha-Boyler rule for the ternary system with a ratio of sucrose to glucose of 5/3 is 3.61˚C, which is much higher in comparison to the other models for the same systems. The same is true for the Couchman-Karasz equation, which has an average error of 3.78˚C for a ratio of sucrose to glucose of 3/5. On the other hand, the analytical approach from Truong (2003) estimates the glass transition temperature almost with the same accuracy as the polynomial equation. With an overall small average error and high coefficient of determination R^2 (Table 2.8.5). In future studies, the applicability of the presented analytical equation has to be validated for higher order systems and in combination with low moisture contents to represent the particles of the spray dryer.

Table 2.8.5. Comparison of the efficiency of the various models to predict the glass transition temperature of the ternary sugar mixtures with distinct sucrose and glucose ratios. Data obtained from (Truong et al., 2002).

Ratio	**Maximum Difference in ˚C**			**Average Error in ˚C**			**Coefficient of Determination R^2**		
Sucrose/Glucose	5/3	4/4	3/5	5/3	4/4	3/5	5/3	4/4	3/5
Analytical model	1.41	1.34	2.60	0.70	0.96	1.57	0.993	0.991	0.967
G-T (Simha-Boyler)	6.24	3.90	1.56	3.61	2.02	0.79	0.867	0.940	0.989
Couchman-Karasz	3.89	3.61	5.12	1.85	2.84	3.78	0.965	0.915	0.810
Poly. equation	1.98	0.75	2.40	0.87	0.41	0.98	0.992	0.998	0.983

Note: G-T (Gordon-Taylor)

2.9 Drying aids

The transformation of fruit juices into a powder by the two typical dehydration methods, freeze and spray drying, is quite difficult due to the presence of high amount, ca. 90%, of low molecular weight molecules with relatively low T_g values. During the rapid drying process the product will not be in its crystal state, but rather transformed into an amorphous product. Because of the high temperature operating conditions the components will be above their glass transition temperature involve a decrease in viscosity and various time-dependent structural changes may occur such as collapsing, stickiness, caking and recrystallization.

A common practice to prevent the operational problems is the addition of a drying aid or so-called carrier agent to the fruit juice previous to the dehydration process (Adhikari et al., 2002; Bhandari, Datta, & Howes, 1997; Jaya & Das, 2009). A drying aid has to be capable of reducing the hygroscopic properties, modifying the thermoplastic properties by increasing the overall T_g of the fruit juice, while the quality and solubility of the produced powder must be maintained (Verma & Singh, 2015). High molecular weight materials such as maltodextrin have been commonly used drying aids for the production of fruit juice powder since the 1970s (Brennan et al., 1971). Maltodextrin is a product of starch hydrolysis by either an acid or enzyme; it consists of β-D-glucose units linked by glycosidic bonds (1-4) and is a mixture of monosaccharide (D-glucose), disaccharide (maltose) and other malto-oligosaccarides with various chain lengths. In order to distinguish the different maltodextrin types from each other, the dextrose equivalency was introduced, where dextrose with DE of 100 serves as the reference value. The dextrose equivalency states the percentage of the reducing sugars in the mixture and is inversely related to its average molar weight (BeMiller & Whistler, 1996). In general, compounds with a $DE \leq 20$ are referred to as maltodextrins and between $20 \leq DE \leq 60$ as corn syrup solids. Maltodextrins are naturally in their amorphous state and manifest high glass transition temperature. Roos and Karel (1991c) studied the various anhydrous maltodextrins with a DE of 5, 10, 20, 25, 36 and maltose and measured T_g values of 188, 160, 141, 121, 100 and 86˚C respectively. As described in Section 2.6.2, the increased degree of polymerisation and thus higher molecular weight corresponds to a higher glass transition temperature. In industrial applications, maltodextrins are high popular due to their sweet taste, low viscosity even at high solid ratios, low production cost and their effectiveness as drying aids (Telis & Martínez-Navarrete, 2012). Nevertheless, maltodextrins are not the only possible option for a drying aid; there are also corn syrup, methylcellulose and gum Arabic, to name a few. Gum arabic in particular has been a popular subject of several studies regarding the use as an additive in the drying process. Gum arabic is a heteropolysaccaride, which is characterized by its high solubility, low viscosity, emulsification characteristics and high capability of enclosing volatile compounds. However, high fluctuation rates in the availability and costs have shifted towards maltodextrins as the most common carrier agent (McNamee et al., 2001).

In recent years most fruits and vegetable juices and pulps have been transformed by the help of drying aids into powders. Two works give a good overview of the state of the art on this topic. In the first one, Telis and Martínez-Navarrete (2012) listed the work of

various authors on the drying of fruit juices and pulp with the focus on the ratio of drying aid to juice and the applied dehydration method. The second review focuses on the research of fruit and vegetable juices using spray drying as the main drying technique (Verma & Singh, 2015). Predominately maltodextrins have been the used by the authors to produce fruit and vegetable powders.

The use of maltodextrins as a drying aid also has its downsides, since large quantities ranging from 30% MD DE 6 for bayberry juice (Fang & Bhandari, 2012) or 60% MD DE 6 for orange juice concentrate (Shrestha et al., 2007) are needed to have a positive impact on the powder recovery. Shrestha et al. (2007) compared the powder recovery of different orange juice concentrates and maltodextrin DE 6 ratios (Figure 2.9.1).

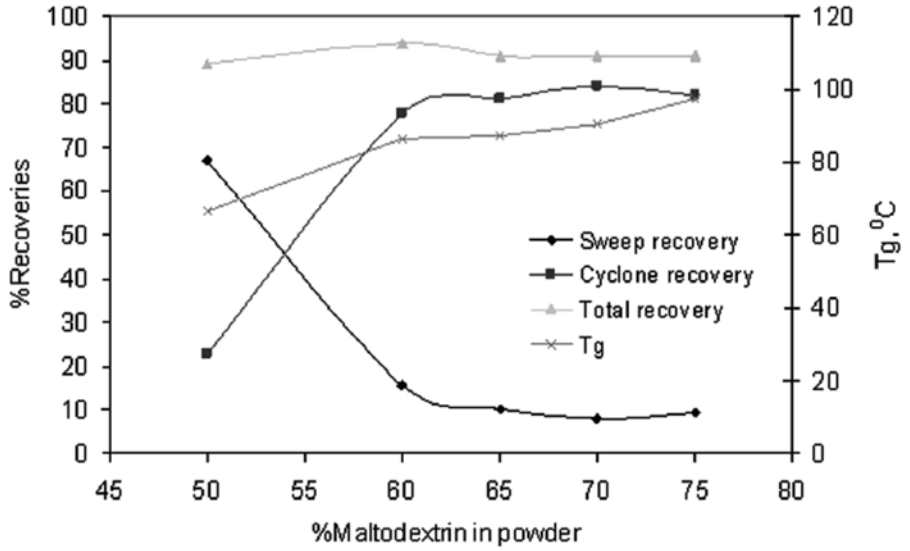


Figure 2.9.1. Percentage of powder recovery and the glass transition temperature of various orange juice concentrates and maltodextrin DE 6 ratios (Shrestha et al., 2007).

At a ratio of 50/50 the cyclone recovery is only at around 20% while a spray drying trial with a cyclone recovery of 50% is considered to be efficient (Bhandari, Datta, Crooks, et al., 1997). The outlet temperature of the spray dryer was set to 65˚C, which is around 10˚C higher than the glass transition temperature of the powder mixture of 55˚C. The difference of T_g + 10˚C is usually the limit for stickiness of the particles to occur, which explains the low recovery of the powder. As soon as the T_g of the powder is above the outlet temperature at a weight fraction of 60% MD, the powder recovery in the cyclone increases to almost 80% and further addition of maltodextrin has no major effect on the recovery rate (Figure 2.9.1). This agrees well with the results of Roos and Karel (1991c),

in which the glass transition temperatures of the binary system of sucrose and maltodextrin with various DE are presented in Figure 2.9.2.

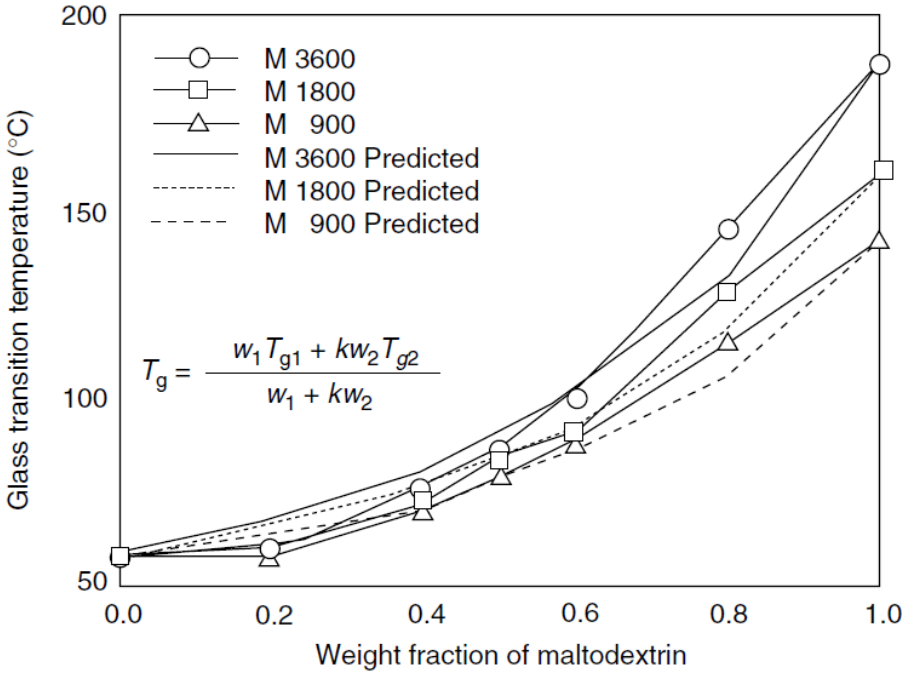


Figure 2.9.2. Glass transition temperature measurements and predictions of the binary systems of sucrose and maltodextrins with different average molecular weights (Roos & Karel, 1991c).

Up to a weight fraction of 0.2 for the various maltodextrins no change in the glass transition temperature is detected and even at a higher portion of maltodextrin of 0.4 the increase is only minor. As described in Section 2.6.1, the polymer has no effect on the glass transition at low concentrations, as the molecular mobility of the mixture is dominated by the low molecular weight components. For the easier case of a binary system with sucrose, the starting temperature is already relatively high compared to other low molecular weight solids in the fruit juice. The high amount of additional fructose, glucose and citric acid in orange juice in combination with residual water decreases the glass transition temperature significantly due to their low glass transition temperature making it necessary to use high ratios of maltodextrin to raise the overall T_g of the mixture.

Looking at a particle during the spray drying process maltodextrin is evenly distributed, which means the glass transition temperature is affected by maltodextrin over the whole particle. An alternative is the use of a surface active agent for example proteins, which assembles at the water/air interface.

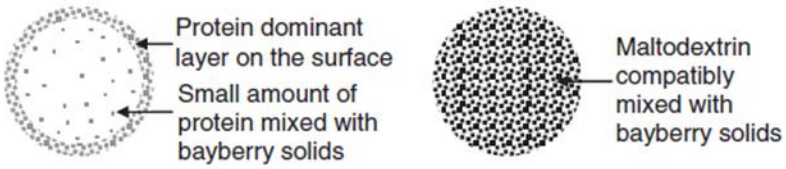


Figure 2.9.3. Schematic drawing of the distribution of added whey protein (left) or maltodextrin DE 10 (right) in spray dried bayberry powder (Fang & Bhandari, 2012).

Fang and Bhandari (2012) compared the efficiency of whey protein and maltodextrin DE 10 as a drying aid for spray drying of bayberry juice. As illustrated in Figure 2.9.3, the mechanisms of proteins and maltodextrins are completely different, since the protein will accumulate at the particle's surface and form a surface barrier during drying and the core of the particles will be left almost in their original form. This reduces the particle/particle and particle/wall stickiness during the drying process, whereas maltodextrin increases the overall glass transition temperature (Figure 2.9.4).

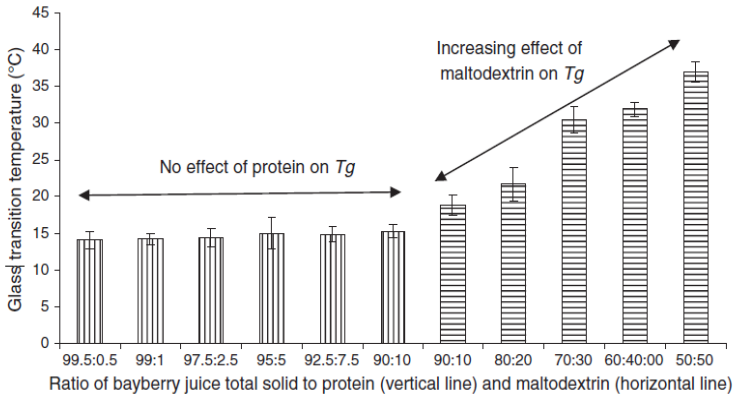


Figure 2.9.4. Comparison of the glass transition temperatures of spray dried bayberry powder at various whey protein and maltodextrin DE 10 ratios obtained by Fang and Bhandari (2012).

Figure 2.9.4 illustrates that increasing the portion from 0.5 to 10% of protein in the powder has no effect on the overall glass transition temperature measured after the spray drying trial, while the T_g values rise with different maltodextrin ratios from 10 to 50%. The advantage of using protein is that only a very low quantity of 1% is needed to avoid stickiness in comparison to 30% of maltodextrin DE 10 and to achieve a powder recovery of 50% in the cyclone during spray drying (Fang & Bhandari, 2012). Fang et al. (2013) tested the various proteins (WPI, whey protein isolate; HWP, hydrolysed whey protein; CCP, calcium caseinate; HCP, hydrolysed caseinate; SPI, soy protein isolate; PPI, pea protein isolate; RPC, rice protein concentrate) on their surface activity by measuring the surface tension of sucrose solutions upon addition of various amounts of protein, as well

as detecting the powder recovery of the these samples after spray drying. The comparison stated that animal proteins have higher surface activities than plant proteins. This is yet again linked to the proportion of protein migrating to the surface of the particle and therefore responsible for higher powder yield in the cyclone. The percentage of protein on the surface can be estimated by analysing the amount of nitrogen on the surface of the particle, as long as protein is the only component containing nitrogen. In the case of sucrose solution, a maximum concentration of 60% protein on the surface could be detected at an addition of 2.5%. A further increase had no great impact on the surface coverage and therefore on the powder recovery. The experiments with bayberry show almost identical results for surface coverage and powder yield. Despite the promising ability of protein to prevent stickiness of fruit juices during spray drying at very low quantities, some difficulties still exist. For instance, the long-term stability of the produced powder could be compromised, since the encapsulated mixture is most likely at ambient temperature above the glass transition temperature, which could lead to stickiness of the particle once the protein barrier is ruptured. More studies have to be done in this field to guarantee a completely stable powder product and to prove the efficiency of protein as a drying aid.

2.10 Analysis of the glass transition temperature

A variety of different analysing instruments for the glass transition exist. The instruments distinguish themselves in their basic method and the measured properties. This makes it important to know in advance if the focus of interest is on thermodynamic, mechanical, physical or rheology properties. Table 2.10.1 provides a summary of the most frequently used techniques to determine the glass transition temperature in materials and following that some of these techniques are explained in more depth.

Table 2.10.1. Common used techniques to determine the glass transition temperature in polymers and other substances (Kalogeras, 2016).

Technique[1)]	Analysed property	Definition of T_g	Resolution, sensitivity
DTA	Temperature difference	Onset, midpoint or endpoint of step change in ΔT versus T plot [2)]	Low/ moderate
DSC/ MTDSC	Heat flow (differential heat flow (sample/reference), heat capacity)	Onset, end or midpoint of the step change in C_p versus T plot or the inflection point (maximum peak in first derivative of the reversing heat flow versus T plot) [2)]	Moderate/ high
TMA/ MTTMA	Dimension changes (thermal expansion coefficient) or softening	Point of the intersection of the glassy and rubbery expansion versus T plots[2)]	Moderate/ high
DMA	Viscoelastic properties (mechanical strength and energy loss)	α-relaxation of peak in the loss modulus (E″) versus T plot. Onset temperature of the storage modulus (E′) drop at the transition[3)]	High
DEA	Dielectric properties and electrical relaxation (permittivity, dialectical loss, polarisation change rate)	α-relaxation of peak in the loss factor (ε″) versus T plot. Onset temperature of the real part permittivity (ε′) rise at the transition[3)]	Moderate/ high

1) DTA=Differential Thermal Analysis, DSC=Differential Scanning Calorimetry, MT=Modulated temperature, TMA=Thermomechanical Analysis, DMA=Dynamical Mechanical Analysis, DEA=Dielectrical Analysis.

2) Temperature change rate dependent.

3) Oscillation frequency dependent.

2.10.1 Differential Scanning Calorimetry

The DSC is a method for the estimation of thermal properties systems (Privalov & Plotnikov, 1989). It was originally applied in polymer science, but nowadays it is a common method to study food systems (Nakamura et al., 1988). The power compensation DSC is composed of a furnace with a sample carrier. The sample carrier consists of two sample holders, one for a pan with the sample and one empty reference pan. Both samples are heated and cooled at the same rate and the heat flow into the pans and the substance is measured. The temperature of both samples is recorded over the time and each holder is connected to a circuit detecting the temperature difference between them. If a

temperature difference is presented, the heater adjusts it to keep both temperatures identical. The difference in detected heat flow between the sample and empty pan is plotted over the temperature and provides information about physical changes and phase transition occurring in the sample (Wunderlich, 2005).

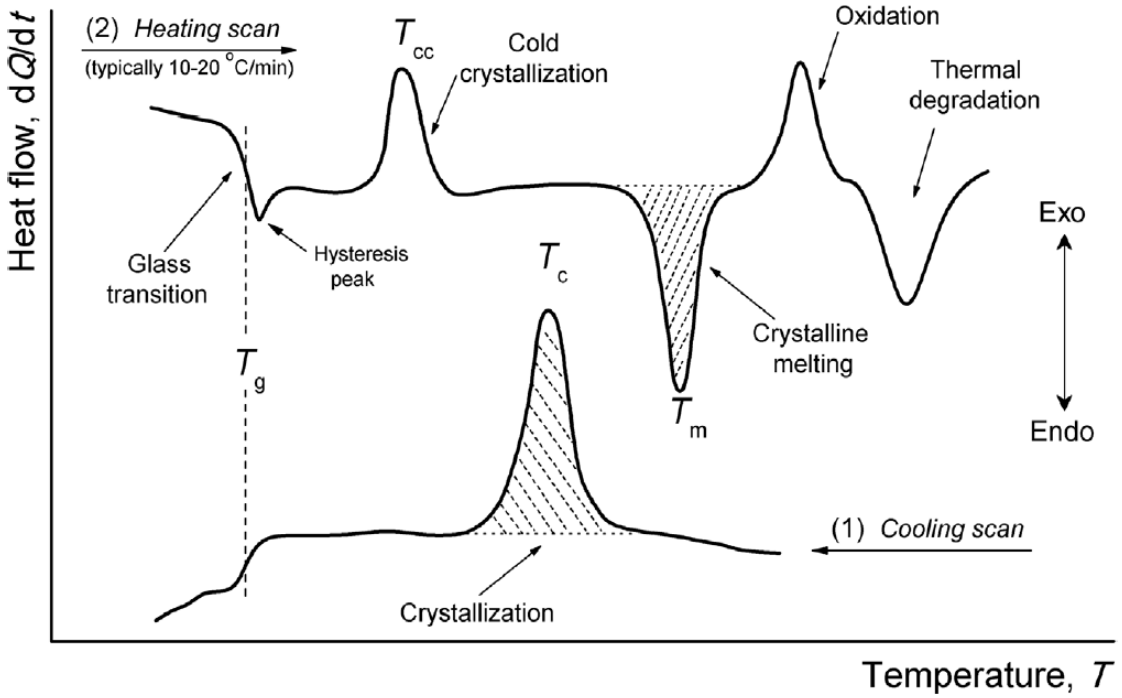


Figure 2.10.1. Overview of the most common possible transitions and reactions observed in a DSC thermogram obtained by (Kalogeras, 2016).

Figure 2.10.1 shows the common measured transitions and reactions for polymers in DSC measurements. First order phase transitions are accompanied by absorption or release of heat without any temperature changes. Both melting and crystallisation are first-order transitions that are identified by exothermal and endothermal peaks of the heat flow. Crystallisation is an exothermal process releasing heat at transition, whereas melting requires heat to proceed which is seen as an endothermic peak. The area of the peaks is equal to the latent heat of the transition. Because of the resemblance of a second order transition, a step of the heat flow at the glass transition is detected. The glass transition occurs over a broad temperature range and there are various ways of defining the glass transition temperature. As displayed in Figure 2.10.2, the first possible temperature is the onset point (T_b), in which the first change in heat flow is detected. In some cases, this can be a quite difficult task, for which reason the more reproducible extrapolated onset point (T_{1e}) is commonly stated, which is the intersection of the extrapolated baseline with the tangent through the midpoint of the curve. In literature, the midpoint of the slope (T_g) is most frequently defined as the glass transition temperature, as it allows the highest

reproducibility. In semi-crystalline polymer and polymer blends the transition can be very broad, making it harder to detect the location of the midpoint of the slope. Therefore, the temperature peak of the first derivative is used as an indicator for the glass transition temperature, which is known as the inflection point and is close to the value of the midpoint T_g. The extrapolated endpoint (T_{2e}) and the endpoint (T_e) are rare options to define the glass transition temperature.

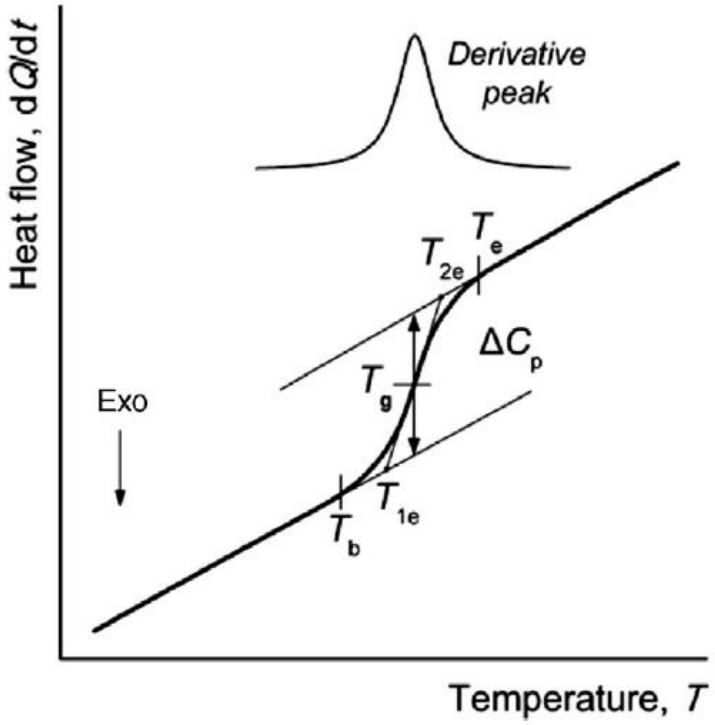


Figure 2.10.2. Determination of the various possible temperatures associated with the glass transition for a DSC heating scan obtained by (Kalogeras, 2016).

The size of the transition region is strongly dependent on the substance. For amorphous sugar, a narrow regime of 10-20˚C can be observed, whereas a range of 50˚C for other polymers in food can be expected (Jasim, 2010; Roos, 2006). There exists no universal consensus on which point characterizes the glass transition in the best manner, but the importance of the reproducibility of the values makes the extrapolated onset point and the midpoint/inflection point common choices for the definition of the glass transition temperature. In combination with the temperature range of the transition, it can give a good general framework of the glass transition (Champion et al., 2000). Roos (2006) stated in his research that the onset point is of great importance, since it can be associated with rapid property changes in the food system.

As mentioned, the DSC monitors the fixed heating rate or cooling rate as well as the heat flow. The two parameters can be used to get the heat capacity of the material. Since heat capacity determines the ability on how well a material can store heat, it is defined as the amount of energy needing to be applied to the material to increase temperature one degree. Once the heat capacity is estimated, other thermodynamic properties such as enthalpy can be derived.

$$\begin{aligned} heat\ flow &= \frac{Q}{t} \\ heating\ rate &= \frac{increase\,of\ temperature}{time} = \frac{\Delta T}{t} \\ \frac{heat\ flow}{heating\ rate} &= \frac{Q/t}{\Delta T/t} = heat\,capacity \end{aligned} \tag{2.35}$$

The way the properties are measured has been modified for various DSCs. In heat-flux DSC the sample and the inert reference material are placed on a heat-sensitive plate in a furnace. Thermocouples are connected to the samples, the furnace and the heat-sensitive plate. During a phase transition the heat flux through the plate is varied, which leads to an incremental temperature difference of the heat-sensitive plate and the furnace. The heat capacity is measured as a function of the temperature and the enthalpy transition can be evaluated by the temperature difference of the plate and the furnace (Hatakeyama & Quinn, 1999). The issue with this type of DSC is, because of the way it is constructed, the sample temperature can vary dramatically from the furnace temperature, which can make the heat capacity measurements difficult. The power compensation method has an advantage over the heat flux method in that isothermal experiments and heat capacity measurements can be performed more easily. At the same time, the method is more vulnerable to moisture condensation at the sample carrier which has to be taken into account for experiments below ambient conditions.

In recent years, DSC measurement has been advanced by the modulated temperature DSC (MT DSC). The idea is to superpose the linear temperature profile by a sinusoidal temperature modulation, where the amplitude and the period of the modulation can be adjusted. Typical values for heating rates of 1-5 ˚C/min are 0.5-1˚C for the amplitude and an oscillation time of 40-60 s. Higher resolution can be achieved by decreasing the heating and oscillation rate and amplifying the amplitude. In conventional DSC only the total heat flow of the samples is measured, thus time-dependent phenomena can overlap thermal events during a DSC run. This problem is solved in the MT DSC by dividing the total

heat flow in reversible and non-reversible heat flows, making it effective to detect irreversible and reversible processes at the same time (Hatakeyama & Quinn, 1999).

2.10.2 Dynamical Mechanical and Dielectric Analysis

Elastic and viscoelastic substances are exposed to sinusoidal mechanical stress at a set frequency. The materials experience a strain and the recovery is measured as a function of the frequency and temperature. Part of the absorbed stress is stored as elastic energy, the other part dissipates as heat. The response of strain can be formulated in Hooke's Law of the Young's storage modulus E′ and the modulus related to energy converted to heat as the loss modulus E″ (Jung et al., 2014). The phase angle (δ_θ) is the difference between the monitored stress and resulting strained wave and is commonly derived as the ratio between the loss and the storage modulus.

$$\frac{E''}{E'} = \tan \delta_\theta \tag{2.36}$$

As the material passes the glass transition, a decrease of the storage modulus is detected and a peak for the loss factor and the loss modulus occurs. The maxima for E″ and δ are described as the α-relaxation and are associated with the glass transition temperature of the material (Gernigon et al., 2013). Both peaks are separated by a few degrees, giving some indication of the state of the material and the molecular mixing of blends (Sperling, 1986).

The Dielectric Analysis resembles the DMA method. The difference between the methods is instead of exposing the material to stress, the sample is placed between two parallel conductors and an electric field with a set frequency is applied. The Young's modulus is replaced by the dielectric permittivity ε′ and the dielectric loss factor ε″. By running the experiments either isothermally or dynamically, the collected data can provide a broader understanding of the molecular motion at the glass transition. Also mechanical dumping problems such as vibrational control are mitigated (Roos, 2006; Sperling, 2005).

2.11 Water Activity

Water plays an important role in foods, having a direct effect as a plasticizer and solvent on mechanical diffusional properties of foods and controlling the growth of microorganisms. The water content alone cannot provide sufficient information relating the energetics and the equilibrium state of water and the influence on the properties of the system. Therefore the thermodynamic description of water as water activity was defined by Lewis and Randall (1924).

$$a_w = \left(\frac{f_w}{f_{w,0}} \right)_T \tag{2.37}$$

Where f_w is the fugacity of water in the system at the given temperature and $f_{w,0}$ is the fugacity of pure water at the same temperature conditions. Fugacity is a measure of the escaping tendency of a substance. It is measured in the units of pressure and describes an effective pressure regarding the non-ideality in the gas phase. In food science it is assumed the water vapour behaves like an ideal gas, which allows us to replace the fugacity with the equilibrium vapour pressure. The error of the approximation is less than 0.1% under normal conditions. Therefore, the water activity can be expressed as the vapour pressure of water above the system p_w at the temperature T, divided by the vapour pressure of pure water at the same temperature.

$$a_w = \left(\frac{p_w}{p_{w,0}} \right)_T \tag{2.38}$$

Food solids exist mostly in a steady state, but they are non-equilibrium systems and these undergo changes with time to reach equilibrium (Chirife & Buera, 1995; Roos, 1995). The properties of the food solids can be time-dependent depending on the state of the solids, which can be seen in changes of the microstructure and the water activity during storage. The water activity at which stability issues occur may vary strongly for each component from hours to years. A food powder with sucrose as a main component becomes sticky and may crystallise at a water activity of 0.3, whereas dairy powder with lactose as its main sugar will continue to be stable for years at the same a_w and under normal storage conditions (Roos, 2008).

In solid bodies surface molecules and atoms are exposed to unbalanced forces of attraction. The surface of solids tends to bind molecules from the surroundings to lower the free surface energy and reach an equilibrium state. The acting surface forces can be

chemical or physical. For food solids especially, the physical ones are of relevance and can be attributed to dispersion, repulsion and electrostatic forces. These surface forces are responsible for pulling the surrounding molecules to the solid and adsorbing it on the surface. Other than in adsorption, in absorption the component is fully dispersed in the bulk phase of the other substance, the general term sorption covers the principle of adsorption as well as absorption. Sorption is a spontaneous process, however due to adsorption on the surface, the degree of freedom of the solid is reduced, and with it the entropy and the Gibbs free energy of the system. The amount of the sorption and the partial pressure of the ab- or adsorbed molecules at constant pressure and temperature can be put into a relationship which is called sorption isotherm (Piotr, 2009). In food, the sorption of water from the surroundings is crucial for the system. The shape of the water sorption isotherm of the food solid depends on the physical-chemical structure state and

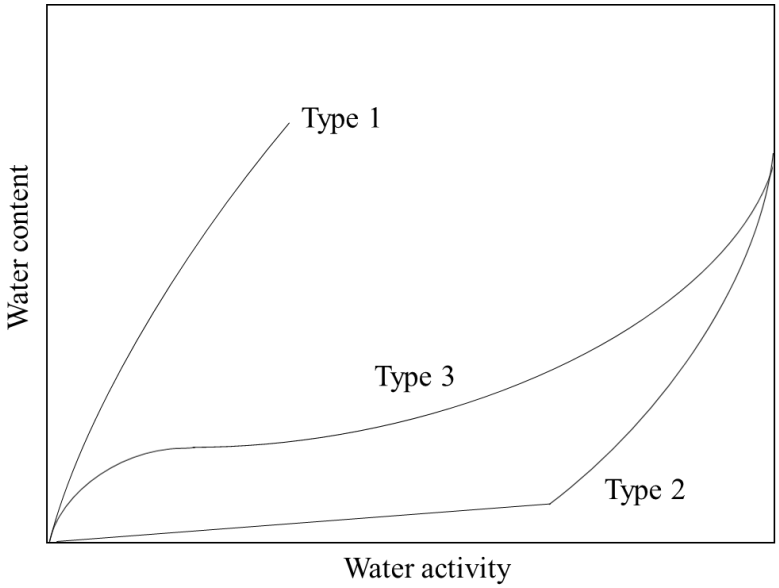


Figure 2.11.1. Schematic drawing based on the various types of sorption isotherms in food by Heiss and Eichner (1971).

the physical structure of the solid. In general three forms are adopted for food systems, which was proposed by Heiss and Eichner (1971) (Figure 2.11.1).

Type 1 corresponds to highly hygroscopic components mostly anti-caking agents, which can hold large amounts of water at low water activities. These components bind water via chemisorption onto specific sites and the increase of water content is low at exposure to higher humidity, since most pores are already filled. Type 2 is the most common sorption isotherm for food and is represented by a sigmoid-shaped curve. The shape of the curve is the result of additive effects such as Raoult's law, capillary effect and surface water interaction. Three critical water activities can be identified, which imply a change of

magnitude because of the different chemical and physical effects. First, small pores are filled and a multilayer of water is built up on the surface up to a_w of 0.2-0.4, followed by swelling and filling of larger pores up to 0.6 to 0.7 and finally the solute dissolution in the upper region. The last type represents mostly crystalline components such as sugars and salt. The increase of moisture content is very low up to the point where the crystal starts to dissolve in the adsorbed water at the surface of the crystal (Labuza & Altunakar, 2008).

Usually the food solid samples are equilibrated over different saturated salt solutions with a constant relative humidity to obtain at least five experimental data and then a sorption model is fitted to the data. The Guggenheim-Anderson-DeBoer (GAB) or the Brunauer-Emmett-Teller (BET) sorption models are commonly used to fit the experimental sorption data (van der Berg & Bruin, 1981). In the BET models, it is assumed the sorption is predominated by adsorption of the water molecules on the surface of the system. Thus, heat of adsorption is limited to one monolayer of water on the surface and no interaction of the adsorbed molecules occurs.

$$M = \frac{M_0 c a_w}{(1-a_w)\left[1+(c-1)a_w\right]} \tag{2.39}$$

Where M is the moisture content in solids at a_w and temperature T, and M_o is the monolayer value in the same units and c is the surface heat constant expressed by:

$$c = constant = e^{Q_s/RT} \tag{2.40}$$

R is the real gas constant, Q_s is the excess heat of sorption. The constant c varies depending on the characteristics of adsorbing site. For type 1 chemisorption, the excess is large and varies from 50-200, for type 2 it is much lower in the range of 2-50 and type 3 the value becomes 0-2. The BET model is in a good agreement for solids with low water activities, however it performs weakly to capture the whole range. Therefore the GAB model was developed as an improved version of the BET model taking into account multilayer adsorption. It has been proven to represent experimental data in the water activity range of 0-0.95. This improvement is achieved by introducing an additional parameter kb, which has a value between 0.7 to 1 (Labuza & Altunakar, 2008). Piotr (2009) summarized in his work most of the known equations based on physical phenomena, semi-empirical models and empirical models. Furthermore the required coefficients for the models are given for a broad range of foods.

Foods are always heterogeneous systems with various ingredients. In mixtures, the individual isotherms are used to determine the multicomponent sorption isotherms. It is assumed the isotherms are additive and no interactions take place between the components. Primarily, the moisture content of each component is predicted at one water activity. In the next step, the moisture content of multicomponent system is calculated by adding the individual moisture contents in respect to their solid weight fraction in the system (Labuza & Altunakar, 2008). This simplification of the multicomponent systems is valid for several systems. Berlin et al. (1973) stated in various milk protein mixtures the additivity of individual sorption isotherms. Lang and Steinberg (1980) also proved for binary and ternary mixtures that the components act independently of each other. Foster (2002) found in her studies the approximation of additivity of various sugars mixtures to be valid. Not all systems can be described by a simply additive approach. Studies of sugar beet roots (Iglesias et al., 1975), dried lactose hydrolysed milk (Jose et al., 1977), and sucrose and starch mixture (Chinachoti & Steinberg, 1986) contradicted the results of other works. The deviation of the experimental data and the predicted sorption isotherm are related to various effects such as assembly of water on the macromolecular surface, swelling, conformational changes caused by water adsorption, inter-polymer hydrogen bonds, binding of ions, cross-linking, competition for water, and plasticization of amorphous regions. Hence, the validity of the additive method is more an exception than the regular case (Labuza & Altunakar, 2008).

2.12 Water activity and glass transition temperature

The importance of the water activity regarding the glass transition temperature is the linkage of the water activity to the moisture content of a substance at a specific temperature. This is especially helpful in cases where it is not possible to measure the water content directly, for example during spray drying. With the assumption that the surface of the particle is in equilibrium with gas outlet flow, the sorption isotherm of the material can be used to approximate the moisture content on the surface of the particle. With the known moisture content the glass transition temperature can be predicted, if the impact of water on the glass transition of the product has been studied previously (Timothy, 2010). The water activity is often displayed with the corresponding moisture content and glass transition temperature in the same diagram to show the correlation between the parameters. Jaya and Das (2009) investigated the glass transition temperature and sticky point of mango and tomato powder at various moisture contents (Figure

2.12.1). The two diagrams demonstrate the correlation between the glass transition and the sticky temperature. Up to a value of 0.3 for the water activity, the difference between the parameters is almost identical for the range. This agrees well with the study of Paterson et al. (2005), indicating only the difference in $T-T_g$ is related to the sticky phenomena of homogenous powders.

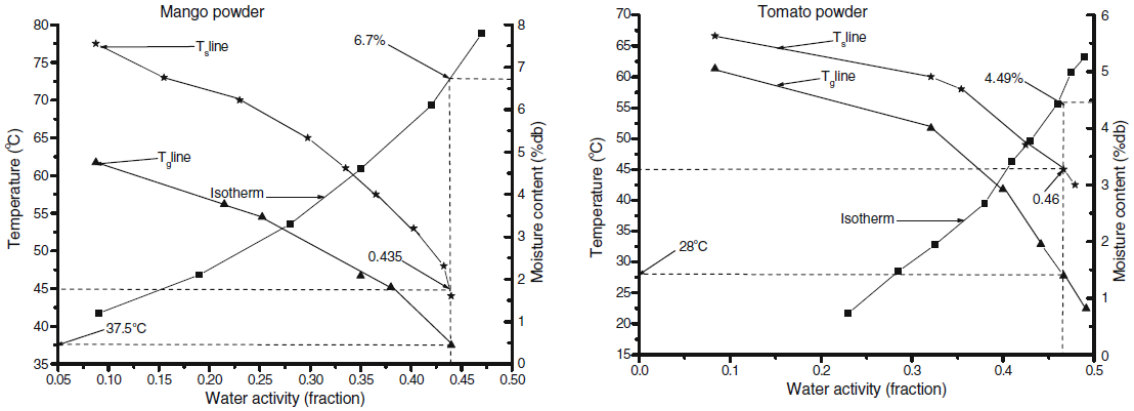


Figure 2.12.1. Stability/mobility diagram displaying the water activity, moisture content, glass transition temperature and sticky point for mango powder (left) and tomato powder (right) (Jaya & Das, 2009).

2.13 Conclusion

Over the years, many researchers have applied drying techniques on various fruit juices in combination with additives. However, the focus of the studies has been mainly on different drying methods and their modifications, as well as the utilization of various drying aids. Little attention has been given so far on the physical and chemical aspect of the whole fruit juice composition. The correlation between the stability issues during the process and storage to the glass transition temperature has been demonstrated in many cases for low molecular weight components. The emphasis in many DSC measurements of the glass transition temperature has been on pure components, binary blends or fruit juices with a fixed composition and especially the influence of water. In several studies, only the sugars and water are stated to influence the glass transition of the fruit juices, but due to the low T_g value, other components such as organic acid and sorbitol have to be considered to predict the overall glass transition temperature of the juice. This gap has to be filled in order to account for all the possible interaction between the components. The established extended prediction models of Gordon-Taylor and Couchman-Karasz describe the compositional dependency of the glass transition temperature poorly for higher order mixtures, if water is not predominant in the system. The plasticisation model

of Truong et al. (2002) is the only model so far taking into account binary interactions between all components and is extendable to higher order mixtures. It has to be proven, if this method is capable of predicting the glass transition temperature of fruit juice with known chemical composition and low moisture content or other methods might have to developed. It is only if the glass transition temperature of the fruit juices is known that the right amount of drying aids can be added to increase the glass transition temperature to the necessary value avoiding stability issues. However, the reason why high quantities are needed to observe a major increase in the glass transition temperature is not yet fully understood and it has to be accounted for in the prediction of the T_g of the mixture. Combining the insights of the molecular miscibility of polymers and low molecular weight components, as well as the molecular mobility of the components might provide a clearer picture of the structure of the matrix and the connection to the measured glass transition temperature. This gives the opportunity to modify the matrix in the powder particles of fruit juices during drying and further improve their shelf life stability.

3. Materials and methods

3.1 Materials

Anhydrous D-glucose analytical grade (Unilab, Thermo Fisher Scientific, Massachusetts, USA, M_w=180.16 g/mol), anhydrous D-fructose analytical grade (Thermo Fisher Scientific, Massachusetts, USA, M_w=180.16 g/mol), monohydrate D-(+)-maltose analytical grade (Sigma-Aldrich, St Loius, USA), anhydrous citric acid food grade (PureNature, Henderson, Auckland, M_w=192.12 g/mol), anhydrous L-malic acid analytical grade (Sigma-Aldrich, St Loius, USA, M_w=134.08 g/mol), maltodextrin DE 9-13 hydrolysed from corn starch (Clintose© maltodextrin CR10, ADM, Minnesota, USA), inulin (Orafti© HIS, Beneo, Mannheim, Germany, supplier(Invita NZ, Auckland, New Zealand)), digestive resistant maltodextrin (Fibersol©-2, Matsutani chemical industry, Itami, Japan , supplier (Hawkins Watts, Penrose, New Zealand)), trisodium citrate analytical grade (Labserv, M_w=294.10 g/mol), anhydrous disodium carbonate analytical grade (Univar, M_w=105.98 g/mol), sodium phosphate tribasic dodecahydrate (Sigma-Aldrich, M_w=380.12 g/mol), phosphorous pentoxide (Sigma-Aldrich), dextran 9.3 kDa analytical grade (Sigma Aldrich), dextran 526 kDa analytical grade (Sigma Aldrich), bovine serum albumin analytical grade (BSA) (Gibco, Thermo Fisher Scientific, Massachusetts, USA), potassium carbonate analytical grade (Prolabo, VWR Chemicals, Leuven, Belgium), lithium chloride (Unilab, M_w=42.39 g/mol), magnesium chloride (Labserv, M_w=95.21 g/mol), potassium acetate (Sigma-Aldrich, M_w=98.142 g/mol) and deionised water were used in this research.

Commercially produced blackcurrant juice concentrate, clear apple juice concentrate, cloudy apple juice concentrate, kiwifruit juice concentrate and carrot juice concentrate (Enzafood, Hawke’s Bay, New Zealand) and lemon juice (St. Andrews Limes, Hawke’s Bay, New Zealand) were utilized in this research.

3.2 Methods

3.2.1 High Pressure Liquid Chromatography

The sugars of the juices were analysed using the HPLC Dionex system (Dionex, Thermo Fisher Scientific, Massachusetts, USA) combined with the Sugar Pak© 1 column (Waters Corporation, Massachusetts, USA). The eluent was monitored by refractive index (R-101 Shodex, Showa Denko KK., Kawazaki, Japan). The flow rate was 0.5 ml/min with a buffer solution of 50 mg/L Ethylenediaminetetraacetic acid (EDTA) and the column temperature was set to 65˚C. A sample of 100 µl was injected. A standard set of fructose, glucose and sucrose (0.5, 0.4, 0.3, 0.2 and 0.1 g/100ml) was prepared and run. One g of each juice was diluted in 100 ml deionised water. The samples were filtered through a 0.25 filter before filling them in 2 ml screw thread vials (HPLC). The concentration of the sugars in the juices was analysed using the Chromeleon software (Chromeleon version 6.80, Dionex, Thermo Fisher Scientific, Massachusetts, USA).

The organic acids of the juices were analysed using the HPLC Dionex system (Dionex, Thermo Fisher Scientific, Massachusetts, USA) combined with the Metacarb H PLUS column (Waters Corporation, Massachusetts, USA). The eluent was monitored by UV (UVD340U Dionex, Thermo Fisher Scientific, Massachusetts, USA). The flow rate was 0.6 ml/min with a 2 M sulphuric acid buffer and the column temperature was set to 55˚C. A sample of 100 µl was injected. A standard set of citric acid, L-malic acid (0.5, 0.3, 0.2, 0.1, 0.05, 0.01 and 0.001 g/100ml) was prepared and run. One g of each juice was diluted in 100 ml deionised water. The samples were filtered through a 0.25 filter before filling them in 2 ml screw thread vials (HPLC). The concentration of the organic acids in the juices was analysed using the Chromeleon software (Chromeleon version 6.80, Dionex, Thermo Fisher Scientific, Massachusetts, USA).

The molar mass of the polysaccharides, highly soluble inulin (Orafti© HIS), resistant digestive maltodextrin (Fibersol©-2) and maltodextrin DE 9-13 (Clintose© maltodextrin CR10) were characterized by Size Exclusion Chromatography (SEC) with a series of three columns. The columns with an exclusion limit of 1×10^4, 1×10^5 and 4×10^5 g/mol (Shodex SB-802.5 HQ, SB-803 HQ and SB-804 HQ, Showa Denko KK., Kawazaki, Japan) coupled with the Shimadzu HPLC system (UFLC, Shimadzu, Kyoto, Japan) was selected. The eluent was monitored by refractive index (RID-20A, Shimadzu, Kyoto, Japan) combined with a Multi-Angle Laser Light Scattering (MALLS) detector

(DAWN8$^+$, Wyatt technology, Santa Barbara, USA). The flow rate was 0.4 ml/min with a buffer solution of 0.1 M NaOAc and 0.1 M NaCl (pH 4.5) and the column temperature was set to 35˚C. A sample of 100 µl was injected. Ten mg/ml of maltose, dextrans with 9 kDa and 526 kDa and bovine serum albumin were used as standards. A dn/dc value of 0.146 ml/g was used for all samples. The number average (Nanasombat et al.) and average molecular weight were determined by the software (Astra, version 6.1.1, Wyatt technology, Santa Barbara, USA) by fitting the Debye model (second order).

3.2.2 Fast Pressure Liquid Chromatography

The blackcurrant sample was diluted 1:1 with deionised water, 200 µl was pipetted in an Eppendorf container and mixed with 800 µl of pure ethanol. The sample was stored for 45 min over ice and centrifuged at 14000 rpm for 5min. The sample was washed with 80% ethanol with 1 ml, two more times, and finally mixed with 2 ml deionised water. The sample was analysed using the Fast Protein Liquid Chromatography (FPLC) combined with the Superose S HR (GE Healthcare, Chicago, USA). The mobile phase buffer contained 30 mM NaOAc (pH 6.5), 20 mM NaCl and 10 mM EDTA at a flow rate of 0.5 ml/min. One ml aliquots of sample containing 7.7 mg/ml pectin were injected and 44 fractions of 0.5 ml/1 min collected. Dextrans with a M_w of 3, 40, 500, 500 and 4500 kDa and glucose with a concentration of 1 mg/ml were used as standards. The collected fractions were analysed for their total carbohydrate content using the method described by Agrawal et al. (2016) and the total galacturonic acid content was measured using the method by Blumenkrantz and Asboe-Hansen (1973).

3.2.3 Freeze drying

In order to investigate the glass transition temperature of different mixtures, they were freeze dried to create amorphous powders. The various fruit juices were diluted to 10% solid concentration. Glucose, fructose, citric acid (1/3 glucose, 1/3 fructose and 1/3 citric acid) and blackcurrant juice were mixed with maltodextrin DE 9-13 at the ratios of 3/7, 1/1, 7/3 and deionised water was added to reach a 30% solid concentration.

Glucose was combined with inulin, digestive resistant maltodextrin and maltodextrin DE 9-13 at a ratio of 7/3, 1/1, 3/7, 2/8, 1/9 and 1. Moreover, a blend of the polysaccharides was created by mixing two polysaccharides together at a ratio of 1/1 so the blended combinations of inulin with digestive resistant maltodextrin, inulin with maltodextrin DE 9-13 and digestive resistant maltodextrin with maltodextrin DE 9-13 were produced.

These blends were combined with glucose at the same ratios (0, 7/3, 1/1, 3/7, 2/8, 1/9 and 1). Finally, a blend of all three polysaccharides was produces with 1/1/1 inulin, digestive resistant maltodextrin and maltodextrin DE 9-13 and mixed with glucose with the identical ratios as the other blends. Deionised water was added to obtain a 10% solid concentration.

Glucose was mixed with disodium carbonate, trisodium citrate and trisodium phosphate at the ratios 1/99, 1/19, 1/9 and 2/8. Since trisodium citrate and phosphate are not available in their anhydrous form, the ratios are accounted for the hydrate form of the salts. The final mixtures were filled up with water to obtain a 10% solid concentration.

All the mixtures were filled into Petri dishes (150 mm x 15 mm) up to a height of 10 mm. Following this, the samples were immersed in liquid nitrogen to reduce the freezing time. Afterwards the samples were stored in a -80˚C freezer for 12 h, then the frozen samples were crushed with a pestle to increase the surface where the water vapour can escape the porous structure to aid with the freeze drying procedure. The samples were stored for an additional 12 h in the freezer at -80˚C. Then, the samples were transferred to a tray freeze dryer (FD-10F-TP2, Lab-Kits, Xiangtan City, China), which was cooled down to -50˚C and the freeze drying process was initiated. The samples were freeze dried for four days at 10-15 Pa, whereas the freeze dryer shelf was slowly heated up over the 4 days period to a final temperature of 20˚C to help with the removal of additional water.

After the freeze drying step the samples were directly removed and transferred to a drying box with a relative humidity below 5%. The samples were treated with a pestle to reduce the particle size further and placed in sealed boxes filled with phosphorous pentoxide. The samples were stored over phosphorous pentoxide for four weeks to assure the sample had a water activity around zero before the samples were treated or analysed further. The samples showed a water activity lower than 0.03, when tested in the water activity meter (Aqualab 4TE, Meter Group, Pullman, USA).

3.2.4 Water activity and moisture content

Saturated salt solutions were used to create the desired relative humidities in sealable boxes to equilibrate the samples. The salts were lithium chloride (11% RH), potassium acetate (22% RH), magnesium chloride (32% RH) and potassium carbonate (43% RH). Deionised water was added to the salts until a slurry was prepared. The slurry solution was tested in the water activity meter to assure the right relative humidity was reached.

Temperature and humidity data loggers (Ibutton, Maximum Integrated, San Jose, USA) were also added to monitor the temperature and relative humidity in the humidity boxes.

About 1-2 g of the freeze dried samples were placed in a Petri dish (60 mm x 15 mm) and weighed to provide the weight at zero water activity. The samples were prepared as triplicates (n=3). Afterwards the samples were placed over the saturated salt solutions in the humidity boxes (Figure 3.2.1) and stored in the temperature control room at 30˚C. The sample weight was monitored every two days for three weeks, when all samples reached equilibrium and a weight change of less than 0.3% occurred.

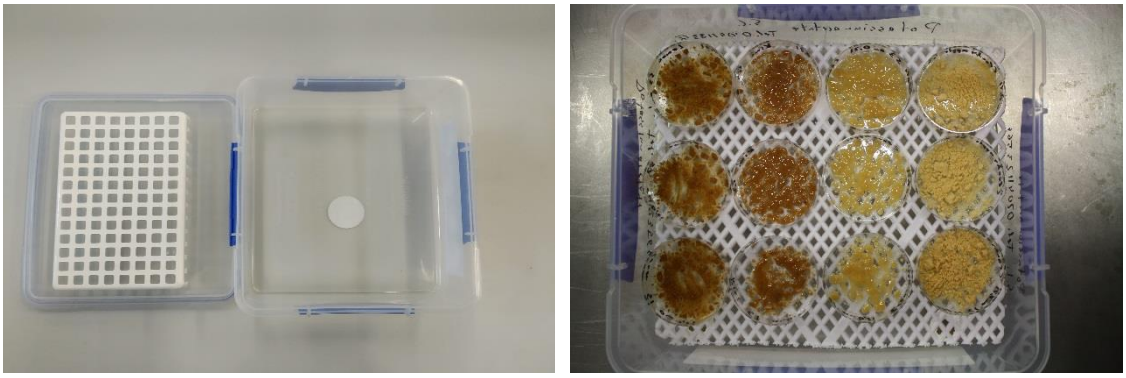


Figure 3.2.1. Sealable storage box for equilibrating powders at various relative humidities.

The moisture content of the pure fruit juice was also determined by gravimetrical vacuum oven drying method using the vacuum oven (EV 018, NÜVE, Ankara, Turkey). Therefore ca. 5 g of fruit juice was weighted and placed in aluminium dishes and dried at 60˚C and 80 Pa for 3 h with n=3. About 1-2 g of the equilibrated powders at the different water activities were weighed, placed in aluminium pans and dried at 70˚C and 80Pa for 48h n=3. The vacuum dried samples showed signs of decomposition and the weight changes were not consistent, especially for the pure fruit juice powders. Therefore the gravimetrically monitored moisture content from zero water activity to the final relative humidity was considered as the moisture contents.

3.2.5 Differential Scanning Calorimetry

For the determination of the glass transition temperature, a sample size between 5-20 mg was filled in an aluminium pan (Tzero Pan) and sealed with a hermitic lid (Tzero hermetic lid). Samples with zero water activity were sealed in the drying box to minimize the exposure to the ambient relative humidity. The DSC (Figure 3.2.2) (DSC Q2000, TA Instrument, New Castle, USA) was calibrated using water (melting point, 0˚C and ΔH_m, 335 J/g), gallium (melting point, 29.8˚C and ΔH_m, 80 J/g), indium (melting point, 156.59˚C and ΔH_m, 28.57 J/g), tin (melting point, 231.93˚C and ΔH_m, 60.6 J/g) and bismuth (melting point, 271.44˚C and ΔH_m, 53.07 J/g). An empty pan was used as a reference pan in all runs. The DSC was checked regularly for any irregularities by melting indium to see if any shift in the baseline or the melting peak could be detected. Triplicate samples were scanned and the heating and cooling cycle was defined in the Thermal Advantage program (Thermal Advantage Q Version 5.5.23), where the sample was first cooled to -35˚C and heated at 10 ˚C/min over the glass transition to remove the thermal history of the sample. It was then cooled to -35˚C and the onset, mid and endset points of the transition of the second heating cycle were documented. The T_g value was determined by the Thermal Advantage Universal Analysis software (Universal Analysis 2000, TA Instruments, Version 4.5A).



Figure 3.2.2. DSC TA Q2000.

3.2.6 Spray drying

A Niro mobile pilot scale spray drier (GEA Group AG, Düsseldorf, Germany) with a 0.6 m diameter x 1.8 m high chamber, a two fluid nozzle in fountain mode and a 0.9 kg/h feed flow was used in the spray drying experiment. The blackcurrant juice was mixed slowly with maltodextrin DE 9-13 to avoid the formation of any lumps. The final solid concentration was 40% with a ratio of maltodextrin DE 9-13 to blackcurrant solid (11/9). The inlet temperature was set to 120˚C and the outlet temperature was 68˚C. The powder was collected in the chamber and cyclone and directly heat sealed in aluminium foil bags, before it was stored for further usage.

3.2.7 Error calculations

The coefficient of determination (R^2) and average error (E_r) in ˚C is calculated by:

$$E_r = \frac{1}{n}\sum_{i=1}^{n}\left|T_{gp,i} - T_{gDSC,i}\right| \tag{3.1}$$

$$R^2 = \frac{\sum_{i=1}^{n}(T_{gDSC,i} - \bar{T}_{gDSC})^2 - \sum_{i=1}^{n}(T_{gp,i} - T_{gDSC,i})^2}{\sum_{i=1}^{n}(T_{gDSC,i} - \bar{T}_{gDSC})^2} \tag{3.2}$$

Where T_{gp} is the predicted glass transition temperature, T_{gDSC} the measured value and $\bar{T}_{gDSC}$ the average measured T_g value of the data set. The 95% confidence interval is calculated with a t distribution with df=2 of z=4.303.

$$\bar{X} = \frac{1}{n}\sum_{i=1}^{n} X_i \tag{3.3}$$

$$s = \sqrt{\frac{\sum_{i=1}^{n}(X_i - \bar{X})^2}{n-1}} \tag{3.4}$$

$$s_M = \frac{s}{\sqrt{n}} \tag{3.5}$$

$$\bar{X} \pm z \cdot s_m \tag{3.6}$$

Where $\bar{X}$ is the sample mean, X_i a data point, n the sample size, s the standard deviation, s_m the standard error and z is the value of the t-table for a 95% interval.

4. Modelling of fruit juice powders

4.1 Introduction

In the literature, several fruit juices and purees have been dried with various drying aids and studied for the stability of the powder by relating the glass transition temperature of the powders to the corresponding water activities. This procedure has to be done for each individual combination of fruit juice and drying aid. In this work, it was assumed that each of the fruit juice powders exhibits a similar thermoplastic behaviour, which can be estimated by using only the chemical composition of the powder. Therefore a new analytical empirical model for the prediction of the glass transition temperature of low molecular mixtures with polysaccharides is proposed. The Flory-Huggins Free Volume theory is presented to correlate the glass transition temperature to water activity. Both models are tested on available literature data to show, if the presented approach is valid.

4.2 Prediction of the T_g of fruit juice powders with polysaccharides

In Chapter 2, the different models for the prediction of the glass transition have been discussed, especially for binary, but also for multicomponent systems. The mixture of low molecular weight components, such as sugars and organic acids, is almost ideal and can be represented by the Couchman-Karasz equation, which has been demonstrated by Truong (2003). On the other hand, the mixing of low molecular weight components with polymers such as polysaccharides strongly deviates from the ideal behaviour (Truong, 2003; Ubbink et al., 2007). Truong (2003) presented a model to determine the glass transition temperature of mixtures by nesting the Gordon-Taylor binary systems from the component with the lowest T_g value to the highest (see Section 2.7.3). The problem with this approach is that the k values of the binary systems are projected on to mixtures, which might behave differently from the binary systems on their own. In this work, a different approach has been taken to obtain the glass transition temperature of the mixture between low molecular weight components and polysaccharides.

The glass transition temperature is defined by the relaxation time of the system and therefore is a kinetic property. However, in order to describe and compare the composition dependency of the glass transition temperatures of multicomponent systems the kinetic component is not considered in this approach. The usual similar heating rates

between 2-20 ˚C/min show quite similar glass transition temperatures for various materials from different literature sources (Section 2.8.4) and allow for a comparison between varying compositions. From a purely thermodynamic concept, the glass transition can be characterised as a second order phase transition that means $V_g = V_{SCL}$, $H_g = H_{SCL}$, $S_g = S_{SCL}$. In an ideal system, the enthalpy of the glass and the supercooled liquid can be described as:

$$H_g = x_1 H_{g1} + x_2 H_{g2} \tag{4.1}$$

$$H_{SCL} = x_1 H_{SCL1} + x_2 H_{SCL} \tag{4.2}$$

$$H_{\mathrm{i}} = H_{\mathrm{i}}^0 + (H_i - H_{\mathrm{i}}^0) = H_{\mathrm{i}}^0 + \Delta H \tag{4.3}$$

$$H_{\mathrm{i}} = H_{\mathrm{i}}^0 + \Delta H_i = H_{\mathrm{i}}^0 + \int_{T_{g,i}}^{T_g} C_{p,i} dT \tag{4.4}$$

The enthalpy H_i can be written as the enthalpy of the pure component and an enthalpy difference. Since the enthalpy of mixing is not equal to zero, due to interactions between the components, it is introduced as the enthalpy of mixing ΔH_{mix} for the glass and the supercooled liquid as $H_g = H_{SCL}$.

$$x_1 H_{g1} + x_2 H_{g2} + \Delta H_{mix,g} = x_1 H_{SCL1} + x_2 H_{SCL2} + \Delta H_{mix,SCL} \tag{4.5}$$

$$x_1 H_{SCL1} - x_1 H_{g1} + x_2 H_{SCL2} - x_2 H_{g2} + \Delta H_{mix,SCL} - \Delta H_{mix,g} = 0 \tag{4.6}$$

$$\begin{aligned} x_1 (H_{SCL,1}^0 - H_{\mathrm{g},1}^0) + \mathrm{x}_1 \int_{T_{g1}}^{T_g} (C_{p,\mathrm{SCL}1} - C_{p,g1}) dT x_2+ x_2 (H_{SCL,2}^0 - H_{\mathrm{g},2}^0) \\ + \mathrm{x}_2 \int_{T_{g2}}^{T_g} (C_{p,\mathrm{SCL}2} - C_{p,g2}) dT + \Delta H_{mix,SCL} - \Delta H_{mix,g} = 0 \end{aligned} \tag{4.7}$$

The enthalpy, volume and entropy are continuous at Tg, $H_{SCL,1}^0 = H_{\mathrm{g},1}^0$ and the equation can be summarized to:

$$x_1 \int_{T_{g1}}^{T_g} (C_{p,\mathrm{SCL}1} - C_{p,g1}) dT + x_2 \int_{T_{g2}}^{T_g} (C_{p,\mathrm{SCL}2} - C_{p,g2}) dT + \Delta H_{mix,\mathrm{SCL}} - \Delta H_{mix,g} = 0 \tag{4.8}$$

$$\Delta C_{p,1} = C_{p,\mathrm{SCL}1} - C_{p,g1} \text{ (isobaric)}$$

$$\Delta H_{mix,E} = \Delta H_{mix,SCL} - \Delta H_{mix,g}$$

$$x_1 \Delta C_{p,1} (T_g - T_{g,1}) + \mathrm{x}_2 \Delta C_{p,2} (T_g - T_{g,2}) + \Delta \mathrm{H}_{mix,E} = 0 \tag{4.9}$$

$$\mathrm{x}_1 \Delta C_{p,1} T_g + \mathrm{x}_2 \Delta C_{p,2} T_g = x_1 \Delta C_{p,1} T_{g,1} + \mathrm{x}_2 \Delta C_{p,2} T_{g,2} - \Delta H_{mix,E} \tag{4.10}$$

$$T_g = \frac{x_1 \Delta C_{p,1} T_{g,1} + \mathrm{x}_2 \, \Delta C_{p,2} T_{g,2}}{x_1 \Delta C_{p,1} + \mathrm{x}_2 \, \Delta C_{p,2}} - \frac{\Delta H_{mix,E}}{x_1 \Delta C_{p,1} + \mathrm{x}_2 \, \Delta C_{p,2}} \quad (4.11)$$

$\Delta H_{mix,\mathrm{E}}$ is the overall excess enthalpy in high order systems and is composed of the $\Delta H_{mix,\mathrm{E}\,ij}$ of the binary systems. Since it is hard to identify the excess properties of the binary systems, excess properties for binary systems are usually fitted to experimental data and the following three methods have been used:

Redlich and Kister (1948):

$$X_{ij}^{E} = x_i x_j \sum_{k=0}^{n} A_k (\mathrm{x}_i - x_j)^k = x_i x_j [A_0 + A_1 (x_i - x_j) + A_2 (x_i - x_j)^2] \quad (\mathrm{n} = 2) \quad (4.12)$$

Hwang et al. (1991):

$$X_{ij}^{E} = x_i x_j [A_0 + A_1 x_i^3 + A_2 x_j^3] \quad (4.13)$$

A series of Legendre polynomials:

$$X_{ij}^{E} = x_i x_j \sum_{k=0}^{n} a_k L_k (x_i) = x_i x_j [A_0 + A_1 (x_i - x_j) + A_2 (6x_i^2 - 6x_i + 1)] \quad (\mathrm{n} = 2) \quad (4.14)$$

A_0 , A_1 , A_2 are polynomial adjustable coefficients, $\mathrm{x_i}$ and $\mathrm{x_j}$ are the weight fraction of the components and X_{ij}^{E} represents the excess property of the binary system. As Hillert (2008) recommended to fit the binary excess properties to the Redlich-Kister expression, this approach has been implemented in this model. One of the recent empirical equations for binary systems was developed by (Brostow et al., 2008) and showed the best fit to complex binary systems.

$$T_g = x_1 T_{g,1} + x_2 T_{g,2} + x_1 x_2 \left[a_0 + a_1 (2x_1 - 1) + a_2 (2x_1 - 1)^2 \right] \quad (4.15)$$

Where $\mathrm{a_o}$, $\mathrm{a_1}$, $\mathrm{a_2}$ are polynomial adjustable coefficients similar to A_0 , A_1 , A_2 defined by (Brostow et al., 2008) as presented in section 2.7.2 , $\mathrm{x_1}$ and $\mathrm{x_2}$ are the weight fraction of the components and $\mathrm{T_{g,i}}$ are the glass transition temperatures of the pure components.

The first term $x_1 T_{g,1} + x_2 T_{g,2}$ is the linear combination of the glass transition temperature (weight average) and the second term accounts for the deviation from linearity. The second term is identical to the Redlich-Kister expression as

$(x_i - x_j) = (x_i - (1 - x_i) = (2x_i - 1)$. The expression allows representation of even sigmoidal deviations. This model has been tested by Kalogeras and Brostow (2009) on various polymer mixtures and gave a very good fit, which supports the utility of fitting $\Delta H_{mix,E}$ to the Redlich-Kister equation.

In Figure 4.2.1, the experimental T_g values of the binary system of glucose and maltodextrin DE 6 are presented from Truong (2003).

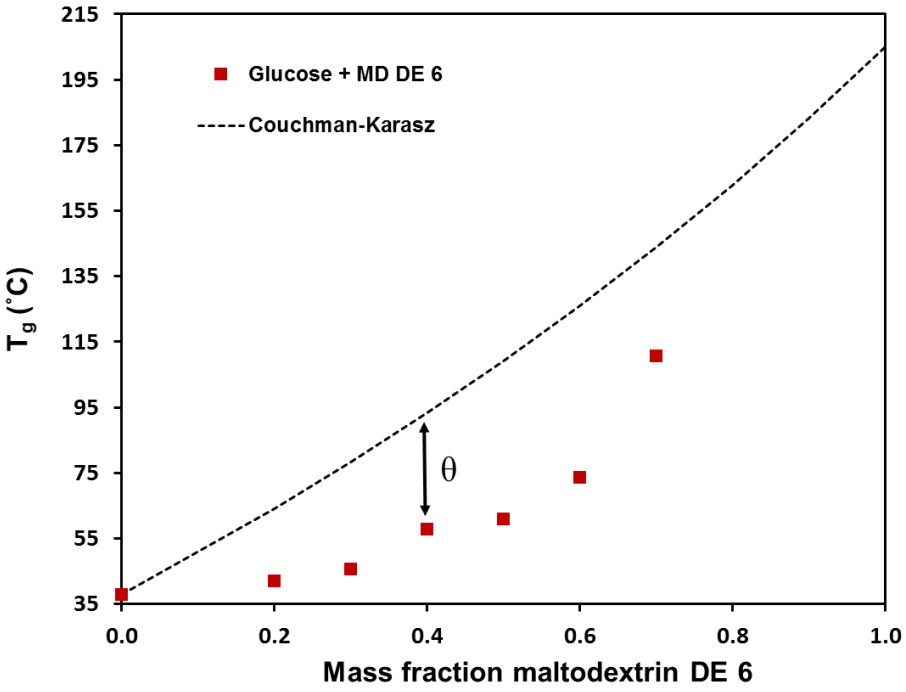


Figure 4.2.1. Binary system of glucose and maltodextrin DE 6. The experimental data are from (Truong, 2003).

The dashed line correlates to the Couchman-Karasz prediction, which overestimates the glass transition temperatures of the mixture. The underlying interaction ΔH_{mix} between glucose and maltodextrin DE 6 can be expressed in the form of the Redlich-Kister equation with n=1.

$$\Delta H_{mix,E} = x_i x_j [A_0 + A_1(x_i - x_j)] \quad (\mathrm{n} = 1)$$
$$\theta = \frac{\Delta H_{mix,E}}{x_1 \Delta C_{p,1} + \mathrm{x}_2 \Delta C_{p,2}} \tag{4.16}$$

For the binary glucose and maltodextrin DE 6 system equation (4.11) can be rewritten:

$$T_g = \frac{x_G \Delta C_{p,\mathrm{G}} T_{g,\mathrm{G}} + \mathrm{x}_2 \Delta C_{p,\mathrm{MD}} T_{g,\mathrm{MD}}}{x_1 \Delta C_{p,\mathrm{G}} + \mathrm{x}_2 \Delta C_{p,\mathrm{MD}}} - \theta \tag{4.17}$$

$$T_g = \frac{x_G \Delta C_{p,\mathrm{G}} T_{g,\mathrm{G}} + \mathrm{x}_2 \Delta C_{p,\mathrm{MD}} T_{g,\mathrm{MD}}}{x_1 \Delta C_{p,\mathrm{G}} + \mathrm{x}_2 \Delta C_{p,\mathrm{MD}}} - \frac{x_G x_{MD} [A_0 + A_1(x_G - x_{MD})]}{x_1 \Delta C_{p,\mathrm{G}} + \mathrm{x}_2 \Delta C_{p,\mathrm{MD}}} \tag{4.18}$$

Where the indices G and MD represent glucose and maltodextrin. The T_g values for glucose and maltodextrin have been taken from Truong (2003). Before moving forward to the prediction, it is important to discuss the influence of ΔC_p. Avaltroni et al. (2004) highlighted in his article that ΔC_p accounts for the arrangement of the hydrogen bonds of the molecules forming the glass. The more organised the molecular interactions in the glassy state are, the closer the resemblance it has to its crystalline state and the higher is ΔC_p. Therefore, ΔC_p should decrease for amorphous substances with increasing molecular weight. However, due to the kinetic nature of the glass, the measured ΔC_p can differ strongly, which makes it harder to compare different components. For polysaccharides, the higher polydispersity makes it difficult to correlate the molecular weight to ΔC_p, thus maltodextrins are often presented by their number average molecular weight M_n from a corresponding malt-oligomers instead of the molecular weight. Orford et al. (1989) correlated ΔC_p to the maltooligomers:

$$\Delta C_p = \Delta C_{p\infty} + \frac{b}{M_n} \tag{4.19}$$

Where $\Delta C_{p\infty}$=0.387 J·g^{-1}°C^{-1} and b=90.81 J·mol^{-1}°C^{-1}. The ΔC_p for maltodextrin DE 2 was 0.40 J·g^{-1}°C^{-1}, for maltodextrin DE 10 was 0.44 J·g^{-1}°C^{-1}and for DE 19 was 0.46 J·g^{-1}°C^{-1} and as an approximation in the range from DE 2-19 the average ΔC_p can be defined as 0.43 J·g^{-1}°C^{-1}. In order to keep the prediction consistent through the work, ΔC_p was set as a constant for each component (Table 4.2.1).

Table 4.2.1. ΔC_p for sugar, organic acid and polysaccharides from (Truong, 2003).

Material	**ΔC_p (J·g^{-1}°C^{-1})**
Sucrose	0.43
Fructose	0.62
Glucose	0.58
Citric acid	0.70
L-malic acid	0.82
Polysaccharides	0.43

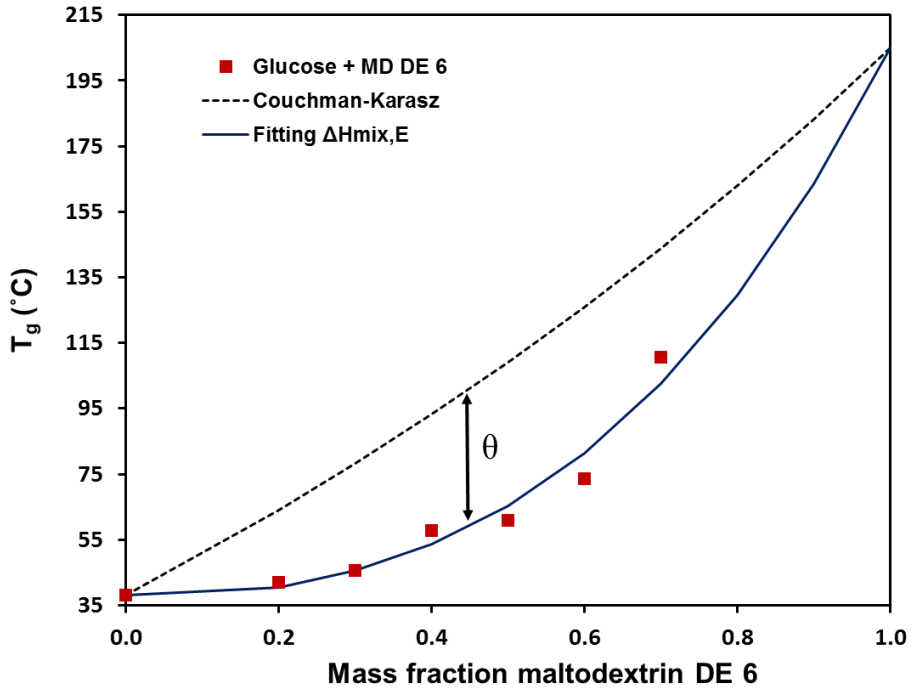


Figure 4.2.2. T_g of binary system of glucose and maltodextrin DE 6 with fitted θ. The experimental data are from (Truong, 2003).

With ΔC_p defined for various materials, the coefficients A_0 and A_1 for $\Delta H_{mix,E}$ can be fitted to the experimental data by minimizing the least square of error. The fitted coefficients are $A_0 = 88.32\, J \cdot g^{-1}$ and $A_1 = -12.07\, J \cdot g^{-1}$ from equation (4.18) and give a good presentation of the measured DSC T_g values with an R^2 of 0.99 (Figure 4.4.2).

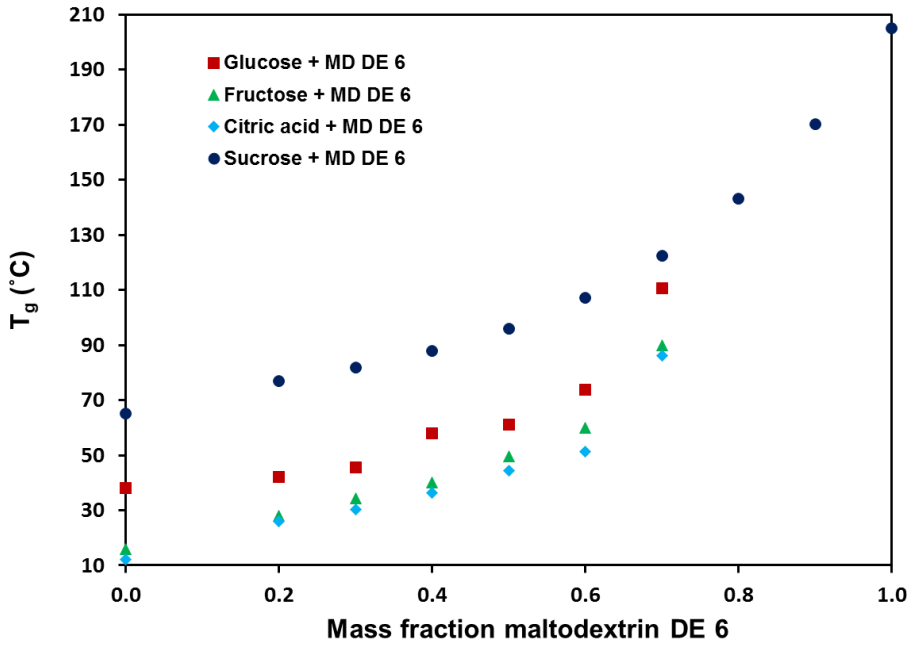


Figure 4.2.3. T_g of binary system of glucose, sucrose, fructose and citric acid with maltodextrin DE 6. The experimental data are from (Truong, 2003).

Besides the glucose and maltodextrin system, Truong (2003) studied the combination of citric acid, sucrose and fructose with maltodextrin DE 6. As can be seen in Figure 4.2.3, the glass transition temperature of each individual mixture steadily increases by small amounts until maltodextrin DE 6 makes up 70% of the total mixture. From this point the glass transition temperature of the sucrose and maltodextrin DE 6 steeply increases with each additional amount of maltodextrin. van der Sman (2013b) used a simple approach in his work to compare the glass transition temperatures of different binary mixtures by normalizing the individual T_g values.

$$T_{g,norm} = \frac{T_{g,data} - T_{g,1}}{T_{g,2} - T_{g,1}} \tag{4.20}$$

Where $T_{g,1}$ and $T_{g,2}$ are the glass transition temperatures of the pure solids. By applying this approach to the data of maltodextrin DE 6 mixtures, the normalized T_g values can be directly compared. Figure 4.2.4 shows the normalized T_g values of the data presented in Figure 4.2.3. From a first observation, it is noticeable how similar the overall trend of the different mixtures is. In the lower region, from the 0 to 0.7 weight fraction of maltodextrin DE 6, the T_g values of the binary systems increase with each 0.1 increment

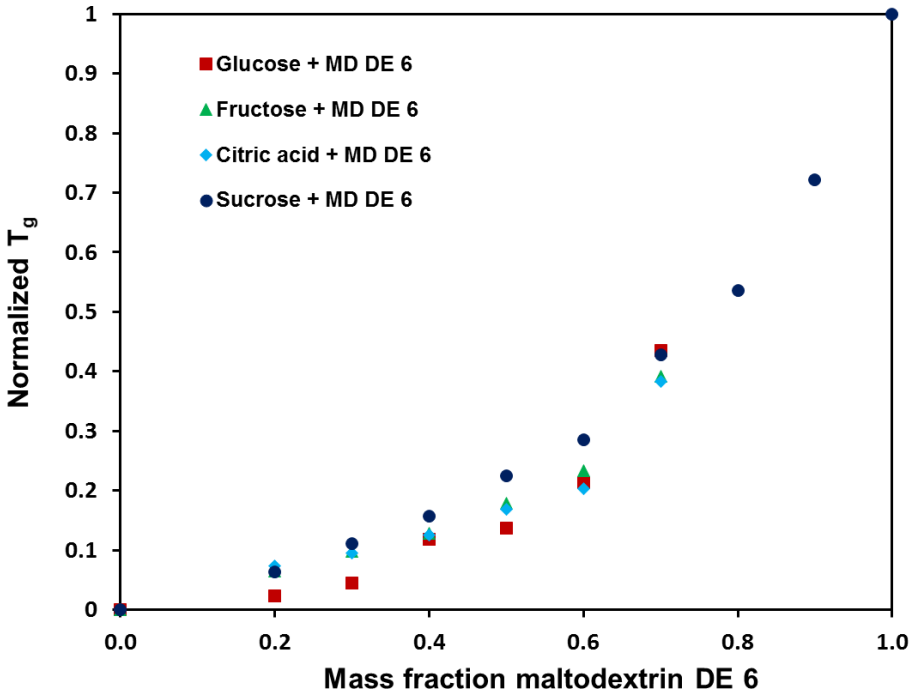


Figure 4.2.4. Replotted normalized T_g values of the binary maltodextrin DE 6 mixtures.

of maltodextrin weight fraction by about 4-6% of the T_g values of maltodextrin DE 6. At high weight fractions 0.7 to 1 of maltodextrin DE 6 in the system, the advance of the T_g values of the mixtures is in the range of 10-30%.

For the glucose system, the increase of the glass transition temperatures below a weight fraction of 0.4 of maltodextrin DE 6 seems to be much slower than for the other systems, however, the T_g values seem to catch up at higher amounts of maltodextrin DE 6 in the systems. The general tendency of the binary maltodextrin DE 6 systems raises the question, is it possible to use constant values for A_0 and A_1 to represent $\Delta H_{mix,E}$ for all datasets. Figure 4.2.5 shows the prediction of the normalized T_g values of each binary system using the corresponding fitted $\Delta H_{mix,E}$ using the individually fitted A_0 and A_1 value. As already demonstrated on the binary system glucose and maltodextrin DE 6, the new approach gives a very good description of the increase of the glass transition temperature. The same is true for the other binary blends with sucrose, citric acid and fructose (Figure 4.2.5).

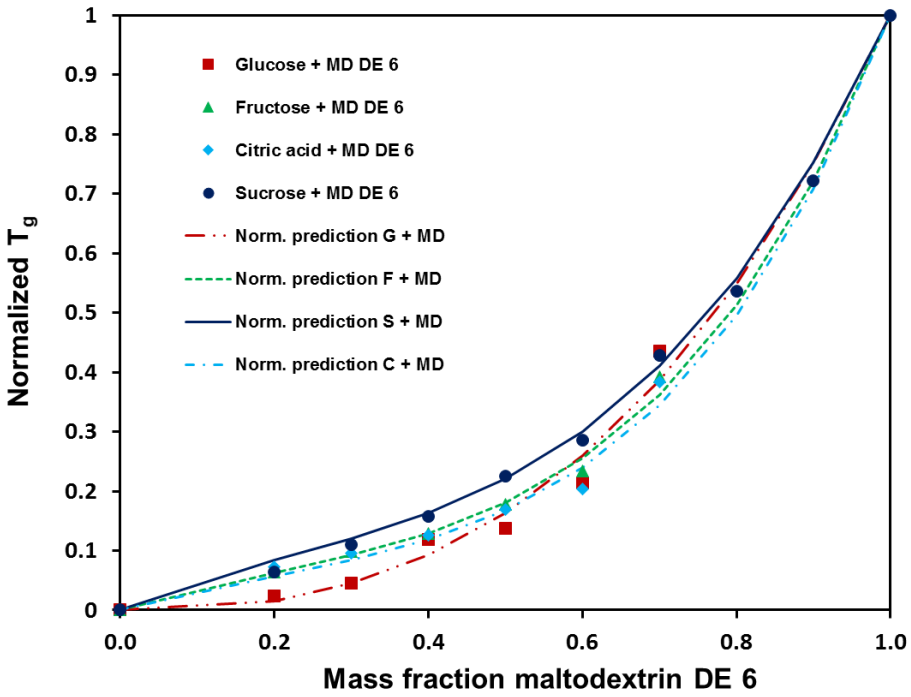


Figure 4.2.5. Representation of the binary maltodextrin DE 6 systems using the individual fitted A_0 and A_1 coefficients.

The coefficient A_0 and A_1 used to calculate $\Delta H_{mix,E}$ are listed in Table 4.2.2. As expected, due to the very similar trend of the increase in T_g, the coefficients for the binary systems with sucrose, fructose and citric acid have almost identical values for the coefficients. The values of glucose vary slightly, especially for A_1. This is due to the rapid increase in

T_g from 0.3 to 0.4. Since the other systems are so similar, in this work it is proposed to generalize the coefficients A_0 and A_1. Therefore the average values of the three systems are used. The aim of this approach is to describe the overall trend of low molecular weight components and polysaccharides as accurately as possible, but also in a simple manner. The effectiveness of this approach will demonstrate if the simplification is valid. The alternative is to use a weighted average of the coefficients that corresponds to the composition of the system under investigation.

Table 4.2.2. Coefficient of the Redlich-Kister equation of the normalized binary systems.

	Normalized		
Binary system	**$A_{0,norm}$ ($J \cdot g^{-1} °C^{-1}$)**	**$A_{1,norm}$ ($J \cdot g^{-1} °C^{-1}$)**	**R^2**
Fructose + MD DE 6	0.4759	-0.2623	0.998
Sucrose + MD DE 6	0.4958	-0.2849	0.999
Citric acid+ MD DE 6	0.4687	-0.2997	0.995
Glucose + MD DE 6	0.5289	-0.0723	0.992
Average (F/S/C)	0.4801	-0.2823	

From the averaged coefficients $A_{0,norm}$ and $A_{1,norm}$ the coefficient for the binary system can be calculated.

$$A_0 = A_{0,norm}(T_{g,2} - T_{g,1}) \tag{4.21}$$

$$A_1 = A_{1,norm}(T_{g,2} - T_{g,1}) \tag{4.22}$$

$T_{g,2}$ and $T_{g,1}$ are the T_g values of the pure components in a binary system, where $T_{g,2}$ represents in this case the $T_{g,2}$ of the polysaccharide maltodextrin DE 6 and the $T_{g,1}$ of the low molecular weight component. As expected, the overall prediction of the binary systems of maltodextrin DE 6 with sucrose, fructose and citric acid only show minor changes without any adjustments of the R^2 values. The prediction for the binary system glucose shows some deviation from the data with a slightly worse fit with a R^2 of 0.98. Due to the changes in the coefficient, the glass transition temperature of the binary glucose blend will be overestimated at very low maltodextrin DE 6 contents (Figure 4.2.6).

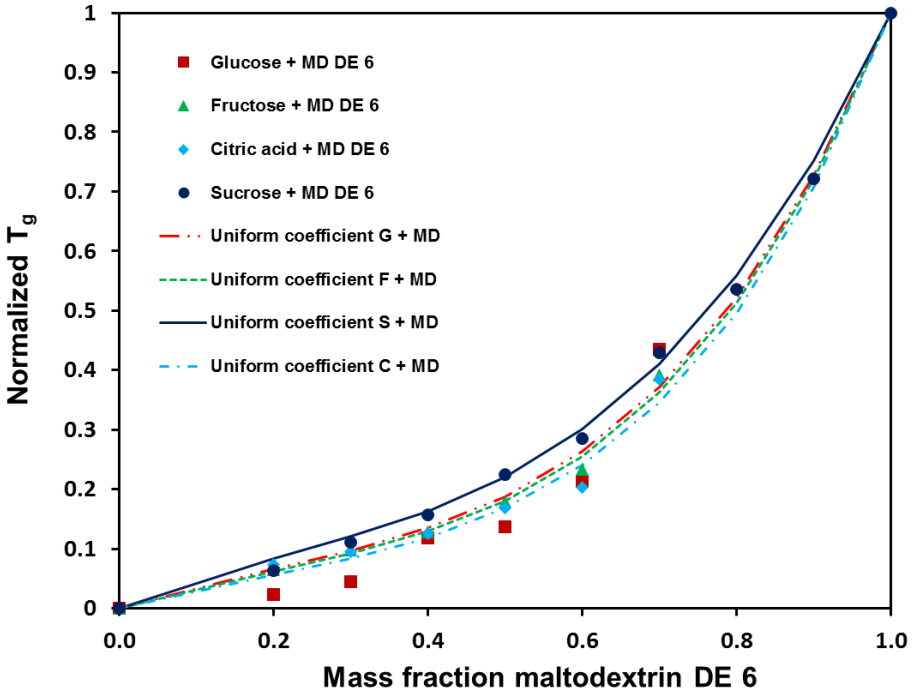


Figure 4.2.6. Prediction of binary system with Maltodextrin DE 6 using the average coefficients.

Until now only binary systems have been considered, however equation (4.11) can also be extended for multicomponent systems.

$$T_g = \frac{\sum_{i=1}^{n} x_i \Delta C_{p,\mathrm{i}} T_{g,i}}{\sum_{i=1}^{n} x_i \Delta C_{p,\mathrm{i}}} - \frac{\Delta H_{mix,E}}{\sum_{i=1}^{n} x_i \Delta C_{p,\mathrm{i}}} \tag{4.23}$$

The first part of the equation is the general extension of the Couchman-Karasz equation. The second term $\Delta H_{mix,E}$ is the deviation of the mixture of all low molecular weight components in relation to the polysaccharide in the system. Therefore the coefficient A_0 and A_1 will be defined as followed.

$$A = A_{norm,average}(T_{g,poly} - T_{g,mixture\ low}) \tag{4.24}$$

$T_{g,\ poly}$ is the T_g value of the pure polysaccharide and $T_{g,\mathrm{mixture\ low}}$ is the T_g value of the mixture of all low molecular weight components. $T_{g,\mathrm{mixture\ low}}$ is calculated with the extended Cochman-Karasz equation at zero polysaccharide content.

$$T_{g,mixtrure\ low} = \frac{\sum_{i=1}^{n} x_{i,low} \Delta C_{p,i\ low} T_{g,i\ low}}{\sum_{i=1}^{n} x_{i,low} \Delta C_{p,i\ low}} \tag{4.25}$$

4.2.1 Testing of the approach on literature data

In the literature, several binary systems of various combinations of low molecular weight components and polysaccharides have been studied. In order to validate the approach taken in this work, T_g data from binary systems of sucrose and various polysaccharide polymers have been collected and normalized to compare the trend between the systems (Figure 4.2.7). In the lower range of the polymer weight fractions, from 0 to 0.5, the increase of T_g is consistently almost identical for the various systems. At a weight fraction of 0.6 of polymer, the data seem to be scattered and the prediction is more at the lower end of the normalized values. Overall, the reasonable approach seems to be to estimate the trend of the sucrose and polymer blends.

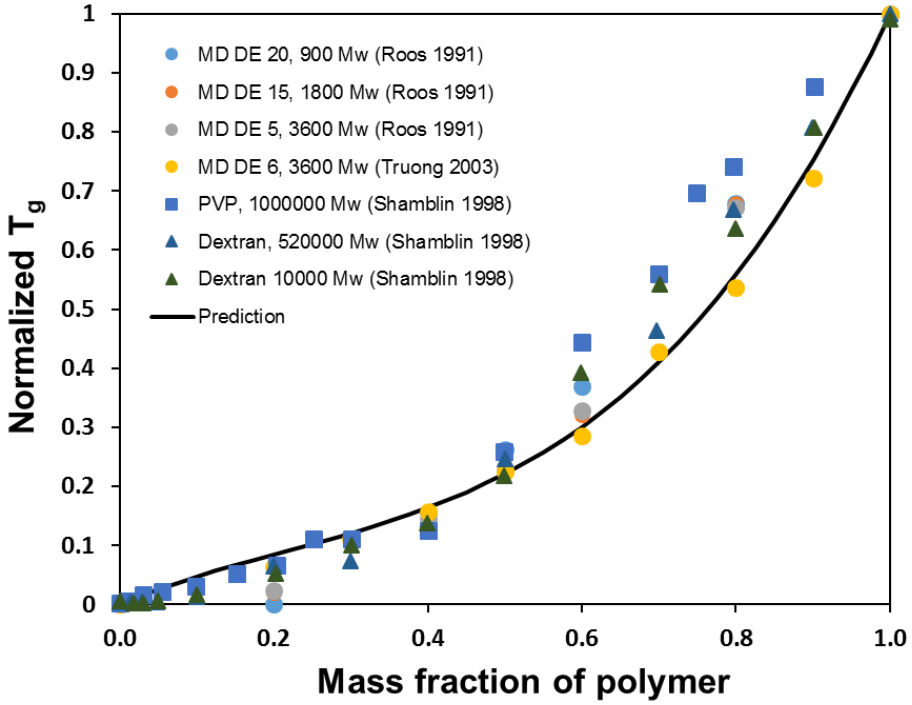


Figure 4.2.7. Normalized T_g value of binary mixtures of sucrose and polymer data from (Roos & Karel, 1991c; Shamblin & Zografi, 1998; Truong, 2003).

Fruit juices never consist of only one component, but rather are a mixture of various low molecular weight components, where sugars and organic acids contribute to the major solids in the juice (see Section 2.2). In order to transform the juices into a powder, usually a drying aid such as maltodextrin with varying DE values is utilized. In general, a fruit juice powder with a fixed amount of drying aid is produced and studied. However, Fongin et al. (2017) presented in their work the increase of the glass transition temperature of freeze dried mango pulp with incremental raising of maltodextrin DE 17-21 content. The chemical composition of mango pulp was not mentioned, therefore the sugar and organic acid solid composition of mango pulp from Jaya and Das (2009) was used. The mass

fraction of soluble solids was sucrose (45.7%), glucose (33.6%), fructose (18.6%) and citric acid (2.1%). The glass transition temperature of pure maltodextrin DE 17-19 was measured as 162.6˚C by Fongin et al. (2017). The ΔC_p and the T_g values of the pure components in Table 4.2.3 were used for all following predictions of the glass transition temperature of mixtures. Only the T_g values of the polysaccharides change depending on the study.

Table 4.2.3. T_g and ΔC_p values of pure components used for the prediction of fruit juice powders.

Material	ΔC_p ($J \cdot g^{-1} ^\circ C^{-1}$)	T_g (˚C)
Sucrose	0.43	68
Fructose	0.62	14.5
Glucose	0.58	38
Citric acid	0.70	14
L-malic acid	0.82	-14.5
Maltodextrin DE 17-19	0.43	162.6

The data points in Figure 4.2.8 represent the measured T_g values of the different mixtures of mango solids and maltodextrin DE 17-19. Similar to the systems described above, at the lower range of maltodextrin DE 17-19 the increases are slower and the T_g values start

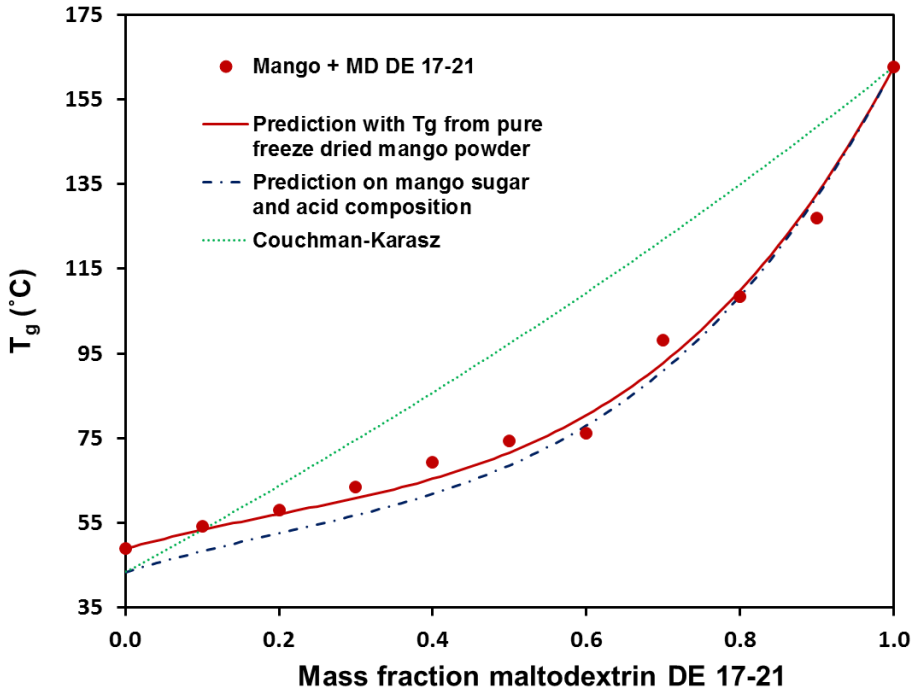


Figure 4.2.8. Prediction of T_g values of mango powder with various content of maltodextrin DE17-19. The experimental data is from (Fongin et al., 2017).

to rise up rapidly at a weight fraction of 0.7. For the model the values in Table 4.2.3 were used. The dashed line represents the prediction based on the chemical composition of the sugars, organic acid and maltodextrin DE 17-19. The predicted glass transition temperature of the pure mango powder is 43.4˚C instead of the measured 48.9˚C. The predicted values have an average error around 5.1˚C and a coefficient of determination (R^2) of 0.976, which is very good for a pure composition dependent prediction. This shows that the overall trend of the increase of the glass transition temperature of fruit juice powders with polysaccharides is consistent. The prediction can be further improved by using the T_g value of pure mango powder 48.9˚C as a starting value, which is presented by the continuous line in Figure 4.2.8. This predicted line is a better fit of the T_g data with an average error of 3.1˚C and R^2 of 0.991. As a comparison, the dotted line is the prediction of the extended version of the Couchman-Karasz equation. The overall prediction of the T_g values of the mixtures is not accurate and it fails to predict the mixing behaviour (average error of 16.69˚C and R^2 of 0.71).

4.3 Flory-Huggins Free Volume theory (FHVT)

In Chapter 2 the concept of sorption was discussed with the definition of the different types of sorption isotherms. The experimental data are commonly fitted to either the BET or GAB models to represent the sorption isotherm over a range of water activities. The BET and the GAB models are derived from the adsorption of gas molecules on surfaces. In Figure 4.3.1 on the left side the GAB model is shown. The idea behind the GAB model is that the adsorbed molecules form a monolayer on the surface (1 to 2) and once the monolayer completely covers the surface, the adsorbed molecules attach to themselves and form a multilayer (2 to 3). The GAB model gives a very good representation of the typical sigmoidal behaviour of the sorption isotherm of food systems. Ubbink et al. (2007) tried to connect the coefficients used in the GAB model to the conceptual ideas and the physical changes seen in amorphous carbohydrate mixtures. Therefore, the sorption behaviour of the binary blends with various ratios of maltose and a maltopolymer were studied. The coefficient M_0 is often defined as the moisture content at which the monolayer covers the complete surface. Ubbink et al. (2007) demonstrated that M_0 is directly linked to the anhydrous specific volume of the carbohydrate mixture matrix. With increasing maltose content, the specific volume of carbohydrate mixture decreases along with the value of M_o. This highlights the relevance of the molecular packing of the carbohydrate matrix on the sorption isotherm. The coefficient M_0 can be best interpreted

as the filling of available interstitial spaces and the interaction with available hydrogen bond sites in the carbohydrate matrix instead of the coverage of a monolayer on a surface.

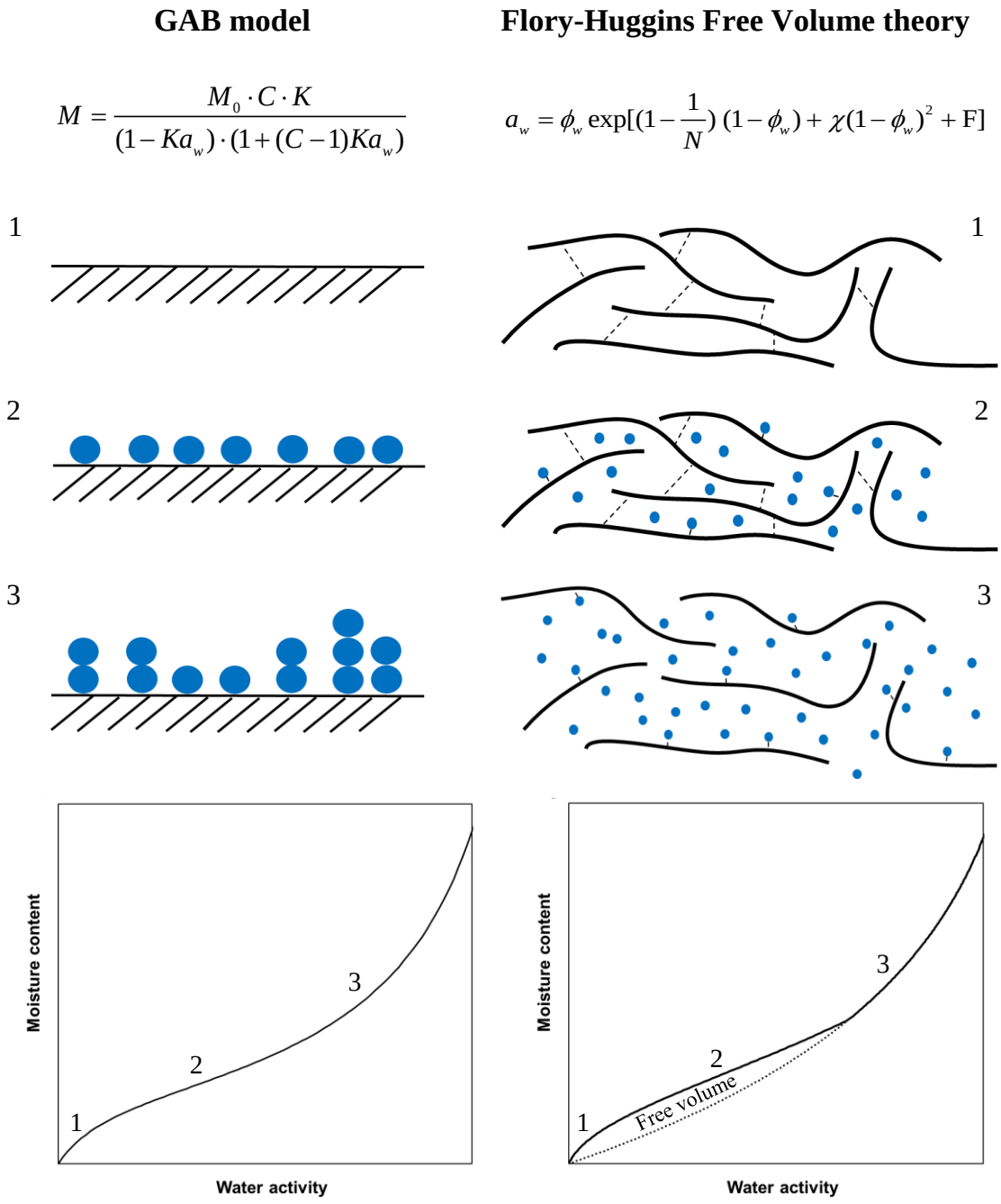


Figure 4.3.1. Concept of the GAB and Flory-Huggins Free Volume theory adapted from (Ubbink et al., 2007).

The parameter C cannot be directly related to any changes in the specific volume, the composition of the system or the molecular weight of the individual components. However the parameter K^{-1} is linked to the critical water activity at which T_g of the systems is identical to the storage temperature and the system transits from the glassy to

the rubbery state. Some of the parameters from the GAB model can be correlated to the physical properties of a carbohydrate matrix, however it does not account well to the physical changes in an amorphous matrix.

Other physical models describe the direct changes in the glassy and rubbery state. One of these models is the free volume model. The concept is that during the formation of a glassy matrix polymers due to the slower relaxation of the polymer chains, the molecular packing exhibits free interstitial spaces also known as free volume voids. The polymers are packed more loosely and connected via intermolecular interactions, as seen in Figure 4.3.1 on the right side 1. The water molecules are absorbed into the amorphous matrix, fill the free volume voids and interact with the polymer via hydrogen bonds (1-2). Townrow et al. (2010) studied the free volume voids of various maltose-maltopolymer blends by PALS. The results showed that the free volume voids are not big enough to account for all the water molecules absorbed into the glassy matrix. Even at moisture contents of below 4%, only a part of the water molecules fill up the voids, whereas most of the water molecules are dispersed in the solid matrix and bound to the carbohydrate molecules. Once the voids are filled, they further expand the voids and further loosen the molecular interaction between the polymer chains. At one point, the relaxation of the polymer is no longer restricted and the glass transition temperature of the systems is identical to the storage temperature. The system then transits into the rubbery state. Once the polymer is in the rubbery state, the sorption can be described solely by the Flory-Huggins solution model. The dashed line in the graph describes the sorption behaviour, if only the solution of the polymer and water are considered. The continuous line accounts for the free volume in the amorphous matrix and relates the packaging history to the glass transition temperature of polymer. The two lines intersect as soon as the system turns into the rubbery state and the system is described by the Flory-Huggins model.

The Flory-Huggins solution model coupled with the Ventras structural relaxation model has been applied successfully for binary, but also to more complex food systems (Jin et al., 2014; Ubbink et al., 2007; van der Sman, 2013a, 2016; Zhang & Zografi, 2000). The advantage of the Flory-Huggins Free Volume theory (FHVT) is the possibility to combine the occurring structural changes and interaction between solute and solvent. Furthermore, the FHVT model is not limited to fitting to existing data such as the BET and GAB models, but can be derived from the composition of the system. In the following the equations the Flory-Huggins Free Volume theory will be presented. First, the general

Flory-Huggins model will be displayed and then, the context of the absorption into the glassy matrix will be discussed.

4.3.1 Absorption into a material in the rubbery state

The rubbery state of a polymer mixture can be described as a Flory-Huggins solution, where the smaller and bigger polymers are arranged as point particles on a lattice structure. Considering a polymer and water system, in the case of high dilution the solution properties of the solution should be close to ideal. Therefore the entropy of the mixture can be written as:

$$-\frac{\Delta S_{mix}}{k_B} = n_w \ln x_w + n_s \ln x_s \tag{4.26}$$

x_w and x_p are the weight fractions of water and the solute and k_b is the Boltzmann constant. In the case of the solute being a polymer, the equation can be transformed into the characteristically Flory-Huggins expression.

$$-\frac{\Delta S_{mix}}{k_B} = n_w \ln \phi_w + n_p \ln \phi_p \tag{4.27}$$

Where ϕ_w and ϕ_p are the lattice volume fractions. In the Flory-Huggins model the enthalpy of interaction between the several molecular units are expressed as following, where χ is the Flory-Huggins interaction parameter for the solute and solvent.

$$\frac{\Delta H_{mix}}{k_B T} = \chi n_w \phi_p \tag{4.28}$$

From the total free energy of mixing $\Delta G_{mix} = \Delta H_{mix} - T\Delta S_{mix}$ the water activity can be acquired.

$$a_w = \phi_w \exp[(1-\frac{1}{N})(1-\phi_w) + \chi(1-\phi_w)^2] \tag{4.29}$$

N is the ratio of molar volume of the solute to the solvent; for polymers it becomes negligibly small. One important aspect of the Flory-Huggins model is the definition of the lattice units. Ubbink et al. (2007) stated for similar sized monomeric units the choice is not problematic, since the molecular size is comparable. However, for solute and solvent mixtures that exhibit very distinct unit sizes such as water and polymer, it does matter. This is especially true, if the lattice volume fraction is defined by the dependence

of the density and weight fraction of the components, since it is underestimating the mixing entropy of water due to the large size difference of the molecules. However, because of the reasonable results from van der Sman (2013a) and Jin et al. (2014), the approximation of the lattice volumes is derived from a simple ratio of the density and weight fraction of the components.

$$\phi_i = \frac{\frac{x_i}{\rho_i}}{\sum \frac{x_i}{\rho_i}} \tag{4.30}$$

ρ_i is the density and x_i is the weight fraction of component i. The other components can also be defined as an weight average in the system van der Sman (2013a).

$$\frac{1}{N_{eff}} = \frac{\sum_{i \neq w} \frac{\phi_i}{N_i}}{\sum_{i \neq w} \phi_i} \tag{4.31}$$

$$N_i = \frac{\frac{\rho_i}{M_{n,i}}}{\frac{\rho_{water}}{M_{\mathrm{n,water}}}} \tag{4.32}$$

Where N is the ratio of molar volume of solute to solvent.

$$\chi_{eff} = \frac{\sum_{i \neq w} \phi_i \chi_{i,w}}{\sum_{i \neq w} \phi_i} \tag{4.33}$$

Where $\chi_{i,w}$ is the FH interaction parameter of compound i. The research of van der Sman (2013a) and Jin et al. (2014) demonstrated the FH interaction parameter to be independent of temperature for sugar, polyol and polysaccharide. For lower carbohydrates with a

degree of polymerisation ≤ 2, the FH interaction parameter is a function of the number average molecular weight (Figure 4.3.2).

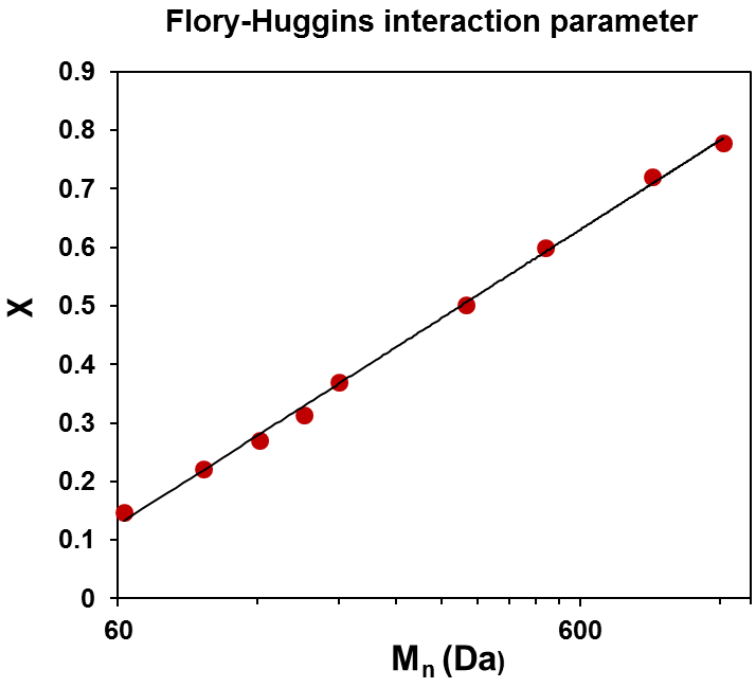


Figure 4.3.2. Flory-Huggins interaction χ parameter as a function of number average molecular weight. Representation of the data from van der Sman (2017).

The relation of the parameter and the molecular weight can be expressed as:

$$\chi_1 = 0.2188\ln(M_n) - 0.769 \tag{4.34}$$

The Flory-Huggins equation can be extended for multicomponent systems:

$$a_w = \phi_w \exp[(1-\frac{1}{N_s})\,\phi_s + (1-\frac{1}{N_p})\,\phi_p + \chi_{ws}\phi_s(1-\phi_w) + \chi_{wp}\phi_p(1-\phi_w) - \chi_{ps}\phi_p\phi_s]$$

(4.35)

For this model, the interaction parameter between the different solutes χ_{ps} is approximated to be zero due to the chemical compatibility of the different sugars and polysaccharides (Ubbink et al., 2007). Therefore, the expression can be simplified.

$$a_w = \phi_w \exp[(1-\frac{1}{N_{eff}})\,(1-\phi_w) + \chi_{eff}\,(1-\phi_w)^2] \tag{4.36}$$

With:

$$\phi_i = \frac{\frac{x_i}{\rho_i}}{\sum \frac{x_i}{\rho_i}} \qquad \frac{1}{N_{eff}} = \frac{\sum_{i \neq w} \frac{\phi_i}{N_i}}{\sum_{i \neq w} \phi_i} \qquad \chi_{eff} = \frac{\sum_{i \neq w} \phi_i \chi_{i,w}}{\sum_{i \neq w} \phi_i}$$

In very highly diluted regions a_w of 0.9 to 1, the Flory-Huggins model becomes invalid in this form, but the very high diluted regions are not relevant for our purpose of calculating the stability of powders, since the powders are liquefying at these high water activities.

4.3.2 Absorption into a glassy matrix

The Flory-Huggins solution model can only represent systems in the rubbery state. It is not capable of accounting for anomalous volumetric behaviour at low water activities. Once a polymer matrix transitions into the glassy state, the sorption mechanism will depend on the molecular packing and the history of the glass. The molecular packing of the polymers or carbohydrate systems in the glassy state can be represented by free volume voids, which can be occupied by small molecular weight components or water molecules at lower water activities. At higher water activities, the water molecules expand the voids and break the bond network in the system until the relaxation of the polymer is no longer restricted and it turns into the rubbery state (Kilburn et al., 2004; Ubbink, 2010). The free volume sorption model was first introduced by Vrentas and Vrentas (1991), who appended an additional term, F, to the solution model of Flory-Huggins. This approximation gave a good representation to the observed experimental data (Jin et al., 2014; Ubbink et al., 2007; Zhang & Zografi, 2000, 2001).

As long as the experimental temperature T lies below T_g of the system, the free volume term F is added to the solution model.

$$a_w = \phi_w \exp[(1 - \frac{1}{N})(1 - \phi_w) + \chi(1 - \phi_w)^2 + \mathrm{F}] \tag{4.37}$$

$$F = \frac{1}{RT} M_{n,w} x_s^{\,2} \Delta C_{p,s} \left(\frac{dT_{g,\mathrm{mix}}}{dx_w} \right) \left(\frac{T}{T_{g,mix}} - 1 \right) \tag{4.38}$$

Where $M_{n,w}$ is the molecular weight of water, x_s is the weight fraction of all solids, $T_{g,mix}$ the glass transition temperature of solid in K and water mixture, R the gas constant, $\Delta C_{p,s}$

the weight average of all pure solid specific heat capacities differences at T_g in J $g^{-1}K^{-1}$ and T the ambient temperature in K.

$$\frac{dT_{g,mix}}{dx_w} = \frac{\Delta C_{p,\mathrm{w}} \Delta C_{p,\mathrm{s}}\ x_s\ (T_{g,w} - T_{g,s})}{(\Delta C_{p,\mathrm{s}} x_s + \Delta C_{p,\mathrm{w}} x_w)^2} \tag{4.39}$$

Instead of using ΔC_p of water and the solid mixtures the plasticizing effect of water can be expressed in form of the k value of the Gordon-Taylor equation:

$$T_{g,mix} = \frac{x_s T_{g,\mathrm{s}} + k x_w T_{g,\mathrm{w}}}{x_s + k x_w} \tag{4.40}$$

$$\frac{dT_{g,mix}}{dx_w} = \frac{k\ x_s\ (T_{g,w} - T_{g,s})}{(x_s + k x_w)^2} \tag{4.41}$$

Roos (2006) presented the linear correlation of the anhydrous onset point T_g of a sugar system and the plasticizing expressed via the k value of the Gordon-Taylor:

$$k = 0.0293 \mathrm{T}_{g,\,anhydrous} + 3.61 \tag{4.42}$$

Truong (2003) continued to use this correlation in his work and adapted the equation to his experimental values.

$$k = 0.0211 \mathrm{T}_{g,\,anhydrous} + 3.0423 \tag{4.43}$$

Seventy-six different mixtures, with their corresponding k values, have been collected from the literature and plotted over the anhydrous T_g of the mixtures. From these data, a fitted equation has been derived which represents the correlation best fit in Figure 4.3.3. In the literature, the most common way to define the T_g values is by the midpoint and the extrapolated onset point. For the fitting of k value to the experimental data, T_g data from the midpoint and onset point have been used for binary water-solid systems. The difference between the midpoint and onset point is assumed to be minor due to the small transition width of these systems. The problem with the generalization of the k value for the solid-water systems is that the method of measuring the moisture content has a huge impact on the final k value. If the moisture content is measured, for example via a vacuum oven, the glass transition temperature of the solid-water system is related to the free mobile water phase. However, by using a Karl-Fisher titration, the total moisture content can be correlated to the glass transition temperatures of the system, therefore, for the same system, different k values can be estimated. Especially, in systems with a high T_g, which

have not passed into the rubbery state, the diffusion of water is more limited, explaining the deviation of k values for systems with higher T_g values.

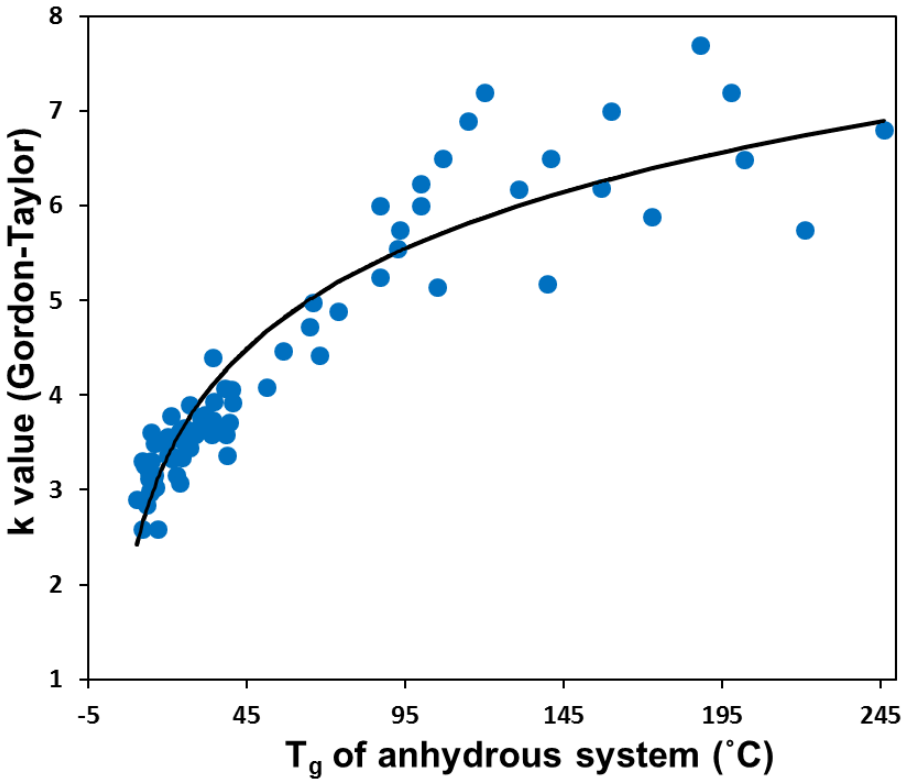


Figure 4.3.3. Data and prediction of the constant k value of the Gordon-Taylor equation for solid water systems from the literature (Orford et al., 1989; Roos & Karel, 1991a; Roussenova et al., 2014; Ruiz-Cabrera et al., 2016; Ruiz-Cabrera & Schmidt, 2015; Truong, 2003; Ubbink et al., 2007).

Also, if insoluble components are in the system, a different moisture content is correlated to the glass transition temperature, therefore only artificial systems with known compositions were collected. In this work the k value is expressed as:

$$k = 7.7 - 7.7 \ln\left(\left(\frac{T_{g,\infty}}{T_{g,\text{anhydrous}}}\right)^{B_k}\right)$$
$$T_{g,\infty} = 463.43°C \text{ and } B_k = 0.18 \qquad (4.44)$$
$$T_{g,\text{anhydrous}} \geq 10°C$$

Where $T_{g,\infty}$ is defined as the maximum T_g of the systems where the k value reaches its maximum of 7.7 and B_k is a constant. The equation does not consider systems with a negative glass transition temperature. These systems are irrelevant for fruit juice powders and the closer the actual glass transition temperature is to that of the T_g of water, the more ideal the mixing seems to become and can be approximated by equation (4.44).

4.4 Test on literature values

The mobility diagram introduced in Section 2.12 is a useful outline to demonstrate the stability of powders stored at different relative humidities. In this way, the relationship between the water activity and the glass transition temperature can be connected and allows one to determine the change from the glassy state into the rubbery state where the powder particle starts to become sticky, caking and, at higher relative humidities, turn into highly viscous syrup.

In the following, the idea is to be able to test if it is possible to predict the stability diagram of fruit juice powders from the literature on the basis of the chemical composition using the presented model for the glass transition temperature of mixtures and combining it with the FHVT model for the absorption of moisture. In the literature the main contribution of investigated fruit powders are fruit purees in combination with different drying aids. Besides the high portions of sugars and organic acids, purees contain other components such as dietary fibres and smaller amounts of protein and ash. In this approach the assumption is made that the main contributions to the glass transition temperature are the high sugar and organic acid content and therefore the absorption of moisture into the sugar- and acid-rich phase is the critical part of the stability of the powders. For the prediction of the Flory-Huggins Free Volume theory, the values of Table 4.4.1 are used to estimate the relationship of moisture content and water activity. The density data of the sugars and organic acids are used from Truong (2003) and the average measured density for maltodextrins with various dextrose equivalents was obtained from Takeiti et al. (2010).

Table 4.4.1. Density, number average molecular weight and interaction parameter χ used in the FHVT model (Duvallet et al., 1989; Takeiti et al., 2010; Truong, 2003).

Material	Density (kg/m^3)	M_n (g/mol)	χ
Sucrose	1526	342.30	0.5
Fructose	1653	180.16	0.37
Glucose	1551	180.16	0.37
Citric acid	1665	192.13	0.38
L-malic acid	1610	134.08	0.3
Maltodextrin DE 4-6	1300	3600	1.02
Maltodextrin DE 9-13	1300	1800	0.87
Maltodextrin DE 17-21	1300	1150	0.78
Gum arabic	1300	180000	1.02

4.4.1 Test of component with increasing molecular weight

Before the fruit powders can be discussed, the modification of the interaction parameter of the Flory-Huggins model has to be described in more detail. Originally, the Flory-Huggins interaction parameter was derived for synthetic polymers accounting for the Van der Waals forces occurring between polymers and between polymers and solvent. Biopolymers and carbohydrates interact via hydrogen bonds with the solvent. The Flory-Huggins model does not account for hydrogen bonds, but the interaction via hydrogen bonds can be simplified by a composition dependent interaction parameter shown by van der Sman (2017). The Flory-Huggins interaction parameter loses its original meaning and becomes a fitting parameter, which includes the interaction between solute and solvent. van der Sman (2017) found the interaction parameter to increase with the molecular weight of the solutes, as seen in Figure 4.3.2. In the study it is further proposed that the interaction parameter for polymers DP > 2 changes with the water volume fraction in the system:

$$\chi_{w,p} = 0.5 + (\chi - 0.5)\phi_p^2 \tag{4.45}$$

Where χ is derived from equation (4.34) and the ϕ_p is the volume fraction of the polymer. By testing the approach for various polymer and water blends, it could be observed that the absorbed moisture content at higher water activities was overestimated and thus the correlated glass transition temperature values, as illustrated in Figure 4.4.1. The

correlation of the interaction parameter with molecular weight can be interpreted as the deviation from ideal mixing of the solvent and solute. For smaller molecules such as monosaccharides, polyols and organic acids the dissimilarity in molecular size and the energetic difference of the molecules and water are relatively small and therefore the value of the interaction parameter is relatively low.

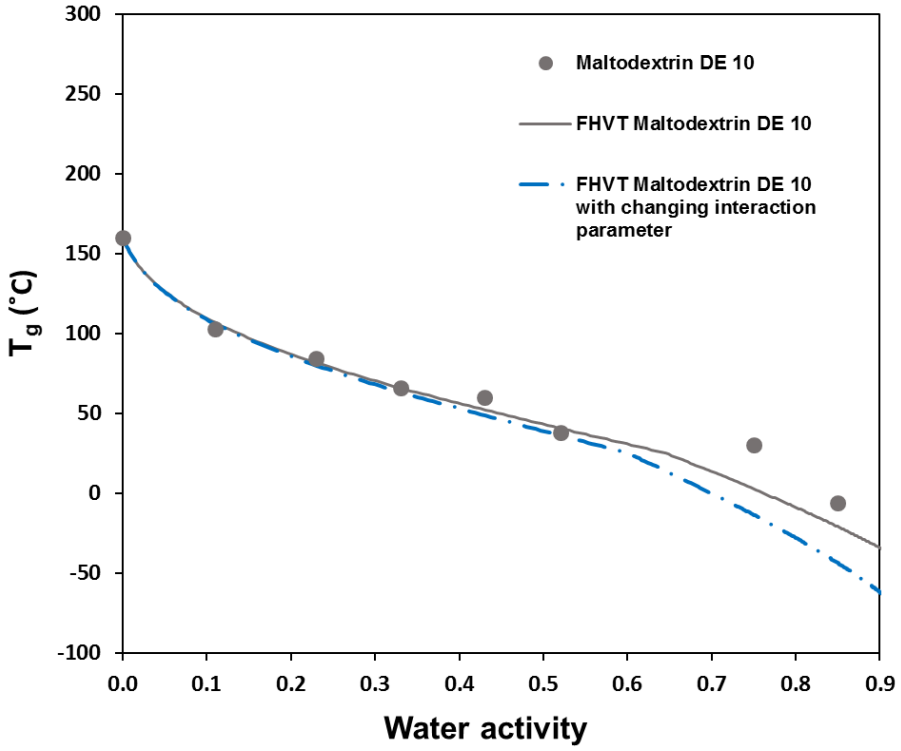
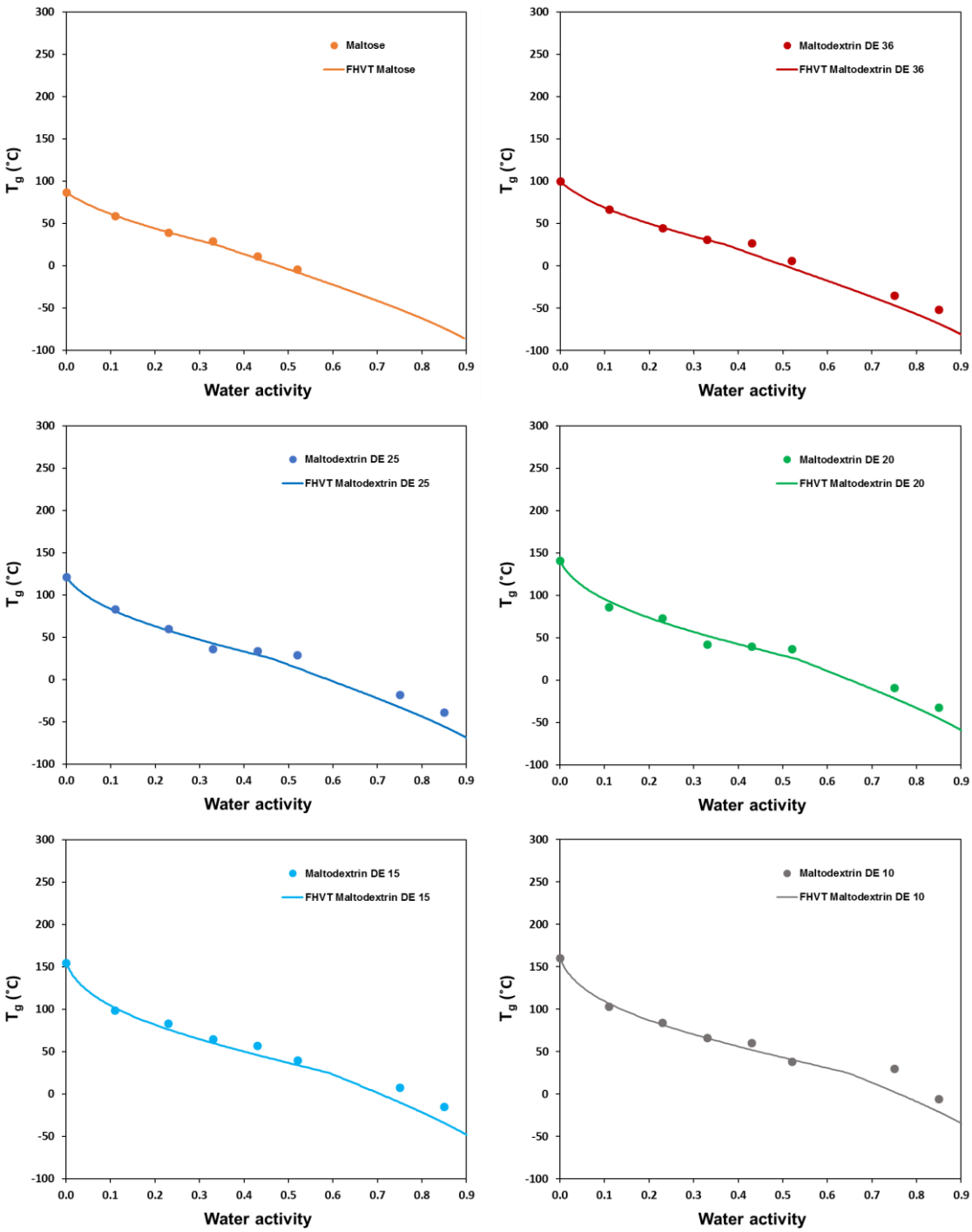


Figure 4.4.1. Prediction of the relation of the water activity and glass transition temperature for maltodextrin DE 10 using a fixed and changing interaction parameter. Experimental data from (Roos & Karel, 1991c).

For polymers, due to the difference in size and conformational configuration in comparison to water molecules, the interaction parameter is larger, accounting for enthalpy and entropy deviations from ideal mixing. These differences do not dissipate with the increase of the water molecules in the systems, therefore the interaction parameter is believed to be constant. The interaction parameter does not increase infinitely with the molecular weight, the exact relation between the interaction parameter and polymers with very high molecular weight are still not fully understood and further investigations are required in this field.


Maltose
FHVT Maltose
Maltodextrin DE 36
FHVT Maltodextrin DE 36
Maltodextrin DE 25
FHVT Maltodextrin DE 25
Maltodextrin DE 20
FHVT Maltodextrin DE 20
Maltodextrin DE 15
FHVT Maltodextrin DE 15
Maltodextrin DE 10
FHVT Maltodextrin DE 10
T_g (°C)
Water activity

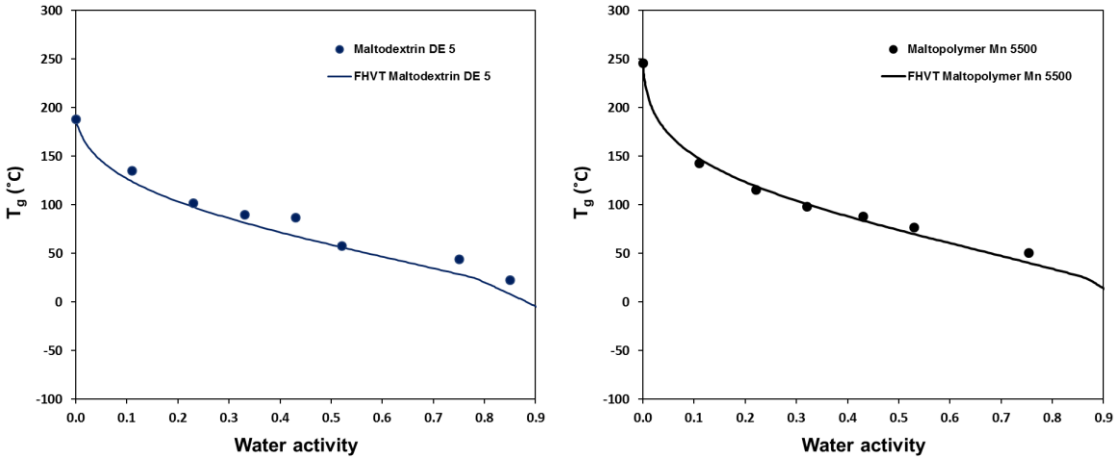


Figure 4.4.2. Prediction of the relation of the water activity and glass transition temperature for maltose and maltopolymers with increasing number average molecular weight. Data from (Roos & Karel, 1991c; Ubbink et al., 2007).

In this study, the interaction parameter was correlated to the number average molecular weight and it was approximated that polymers with a number average molecular weight higher than 3600 g/mol have the same value of the interaction parameter of 1.02.

Figure 4.4.2 shows the relation of the water activity and the glass transition temperature of various maltose and maltopolymers with increasing number average molecular weight. The prediction of the different systems demonstrates that the correlation of the interaction parameter and the number average molecular weight works well and the predicted values are a very good fit to the experimental data (Table 4.4.2).

Table 4.4.2. Number average molecular weight, Flory-Huggins interaction parameter and coefficent of determination of the prediction for maltose and maltopolymers.

Parameter	**Mal-tose**	**MD DE 36**	**MD DE 25**	**MD DE 20**	**MD DE 15**	**MD DE 10**	**MD DE 5**	**Malto-polymer**
M_n (g/mol)	342	500	720	900	1200	1800	3600	5500
T_g (˚C)	92	100	121	141	155	160	188	246
χ	0.50	0.59	0.67	0.72	0.78	0.87	1.02	1.02
R^2	0.99	0.97	0.96	0.97	0.96	0.95	0.95	0.99

4.4.2 Freeze dried grapefruit puree powders

Telis and Martínez-Navarrete (2009) studied the glass transition temperature and sorption isotherms of pure grapefruit puree powder and with three different drying aids maltodextrin DE 4-6, maltodextrin DE 16.5-19.5 and gum arabic. The drying aids were added until the ratio of the 1/1 of soluble solids to drying aids was reached. The main solubles in grapefruit were identified as sucrose, fructose, glucose and citric acid in mass ratios of 46, 21, 18, 15 respectively (Fabra et al., 2009).

In Table 4.4.3, the measured glass transition temperatures of the grapefruit powders at zero water activity are presented, as well as the corresponding predicted T_g values using the method. The estimates of the T_g values of the pure grapefruit and the grapefruit with maltodextrins are especially close to the experimental data. The fact that the grapefruit powders with the different maltodextrins are so close together underlines the fact that T_g of mixtures with polysaccharides below 50% of polymer in the system are mainly attributed to the low molecular weight components in the system. The blend of grapefruit and gum arabic falls slightly out of the trend with a higher T_g value of 73˚C. The T_g value of pure gum arabic was not given, therefore the value of 170˚C was assumed. The actual value could be much higher, dependent on the composition of the gum arabic.

Table 4.4.3. Predicted and measured glass transition temperatures of grapefruit powders (Telis & Martínez-Navarrete, 2009).

Material	T_g (˚C)	$T_{g,\,pred}$ (˚C)
Pure grapefruit	38.0	39
Grapefruit + MD DE 17-21	58.7	62
Grapefruit + MD DE 4-6	60.7	68
Grapefruit + Gum arabic	73.1	64

Once the glass transition temperature of the mixture is calculated, the FHVT model can be used to estimate the relation between the water activity and moisture content. In the following the moisture isotherms will not be compared, since the absorption into purees is not only a function of the soluble fraction, but also the insoluble parts. The glass transition temperature of the bulk system is believed to be only dependent on the amorphous fraction and therefore the measured sorption isotherm of the bulk system is not directly comparable. However, the overall trend of the measured and predicted sorption isotherm has to be similar. A detailed example of the prediction approach can be found in Appendix A.1 for the grapefruit and maltodextrin DE 4-6 powder.

In Figure 4.4.3, the glass transition temperatures of the grapefruit powders and the predicted values can be observed in relation to the corresponding water activities. The glass transition temperature of the pure grapefruit powder decreases steeply up to a water activity of 0.43, after that it seems that the decrease flattens out slightly and falls back at a water activity of 0.84. The predicted line for the pure grapefruit powder correlates very well with the experimental data, especially up to the water activity of 0.43. The estimated values are very close to the measured values with a R^2 of 0.97. It only falls short of describing the small curvature between a_w of 0.53 to 0.75.

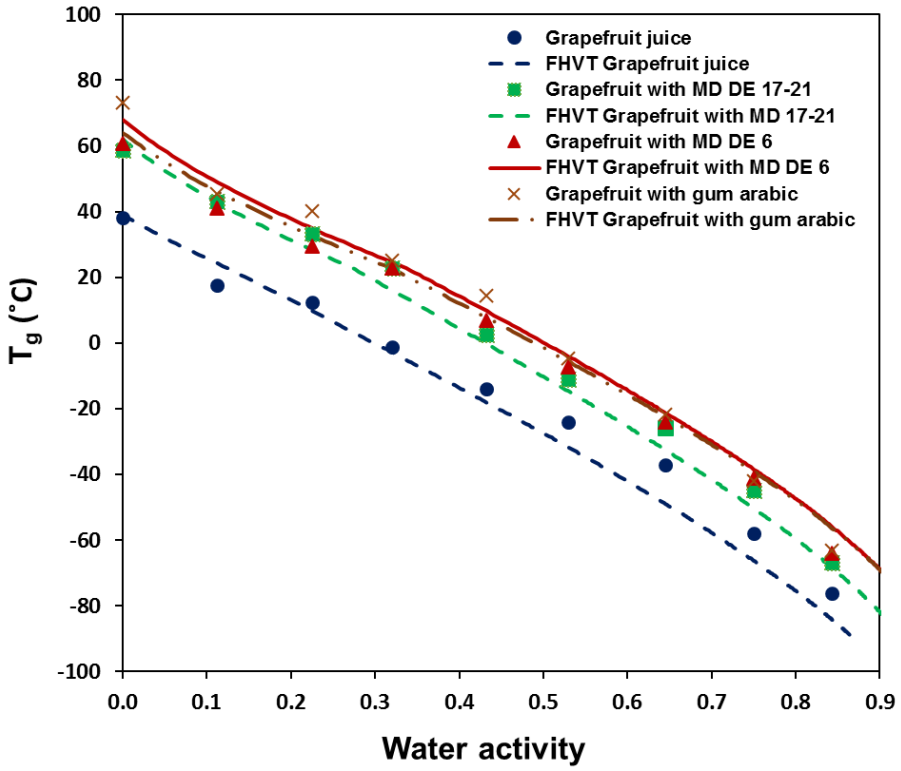


Figure 4.4.3. Prediction of the relation of the water activity and glass transition temperature for data of the grapefruit powders presented by (Telis & Martínez-Navarrete, 2009).

The same is the case for grapefruit powder with maltodextrin DE 4-7.07 and DE 17-21. The predicted values until 0.43 are very similar and deviate from a_w 0.53 to 0.75, whereas the predicted value for the system with maltodextrin DE 4-7.07 are marginally better with an R^2 of 0.99 and R^2 of 0.99 for the blend with maltodextrin DE 17-21. Also, the grapefruit powder with gum arabic shows a similar trend to powders containing maltodextrins, however the decrease in the glass transition temperature seems to be flatter than for the other systems. The predicted T_g value at a_w=0 is off by 9˚C to the measured value, therefore the predicted line starts at a lower glass transition temperature. If the

starting value of 64˚C is used the overall trend is well represented by the predicted line with an R^2 of 0.98.

4.4.3 Freeze dried mango puree powders

Fongin et al. (2017) studied the effect of various amounts of maltodextrin DE 17-21 on the glass transition temperature of mango powder. The prediction of the glass transition temperature has already been discussed in detail previously, therefore here it is only mentioned that for prediction of the stability curve, estimated T_g values from the pure solid composition were utilized. The overall prediction can be improved by adapting the T_g of the solid mixture to that of the pure mango powder, however the overall error is relatively small since the T_g values are not far apart. Furthermore, Fongin et al. (2017) investigated the effect of moisture on the glass transition temperature of several mango powders with various ratios of maltodextrin DE 17-21. The different ratios of maltodextrin in the powder as well as the predicted and measured glass transition temperatures are presented in Table 4.4.4.

Table 4.4.4. The predicted and measured $T_{g,solid}$ values used for the FHVT model Fongin et al. (2017).

Fraction of maltodextrin	T_g (˚C)	$T_{g,\,pred}$ (˚C)
0	48.9	43
0.2	58.1	53
0.4	69.4	62
0.6	76.1	78
0.8	108.5	109
1	162.6	-

Figure 4.4.4 shows the stability diagrams of the mango powders containing various fractions of maltodextrin DE 17-21 and the corresponding predicted values of the FHVT model. For pure mango powder the measured and predicted values follow a linear trend. For mango powders with various maltodextrin DE 17-21 fractions, the FHVT model in combination with the predicted glass transition temperatures follows the trend of the experimental data accurately with an R^2 above 0.95 (Table 4.4.5). Although some of the predicted T_g values of the solid mango mixtures differ slightly from the measured values,

the resulting error is minor, since the overall trend for the system with low glass transition temperature and polysaccharide fraction is quite similar.

Table 4.4.5. Coefficient of determination of the estimated stability curves of the various mango powders.

MD DE 17-21 fraction	**0**	**0.2**	**0.4**	**0.6**	**0.8**	**1**
R^2	0.95	0.98	0.98	0.99	0.99	0.99

The overall trend of decreasing T_g values with increasing water activity is almost linear for the pure mango powders up to a weight fraction of 0.4 maltodextrin with a small curvature at higher water activities. At a weight fraction of 0.6 maltodextrin DE 17-21, a stronger T_g depression from 0 water activity to 0.11 than from 0.11 to 0.22 can be observed. The greater the maltodextrin content the more pronounced the decrease of the glass transition temperature is from the solid mixtures to lower water activity levels.

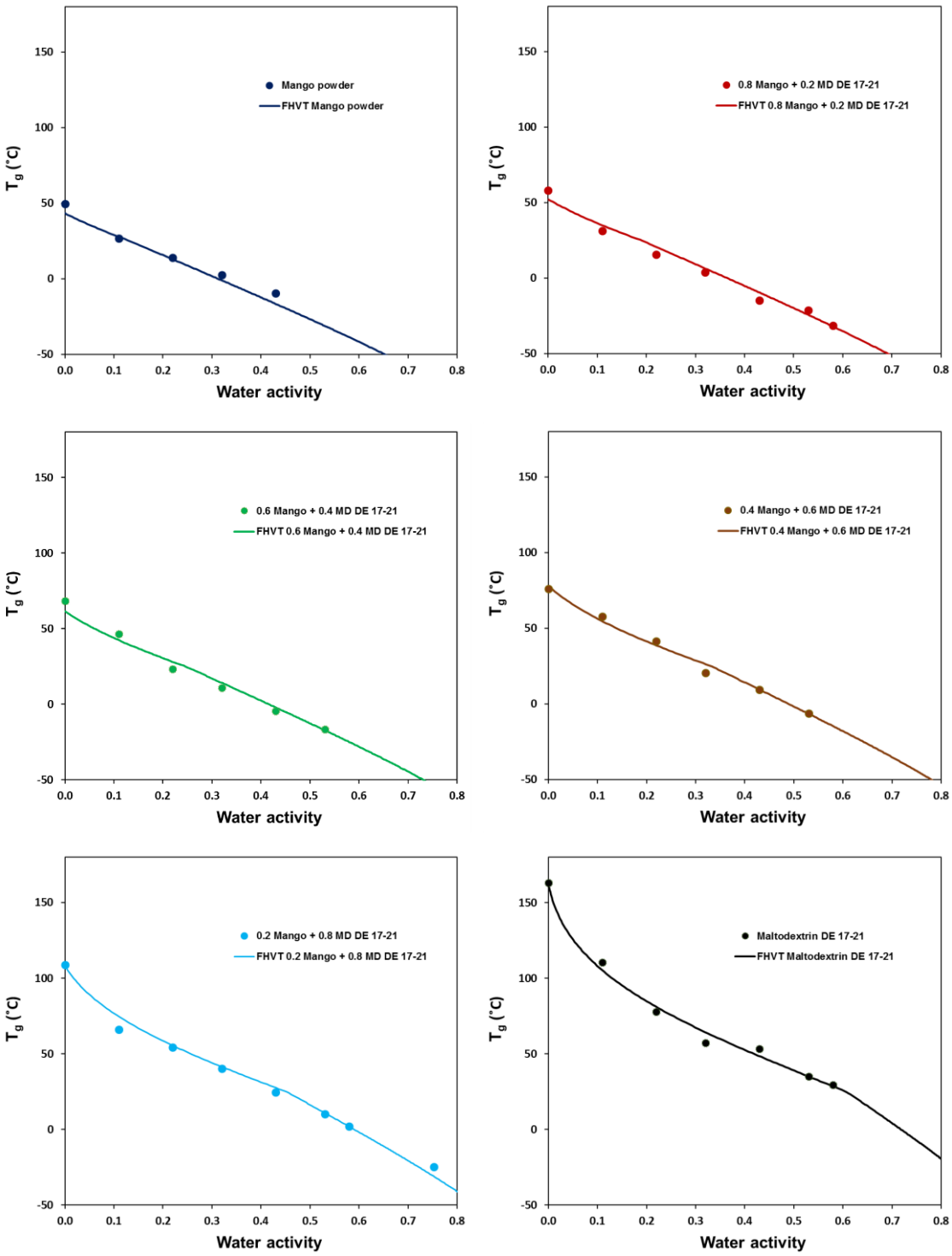


Figure 4.4.4. Prediction of the relation of the water activity and glass transition temperature for data of the mango powders with various maltodextrin DE 17-21 fractions presented by (Fongin et al., 2017).

The free volume model from Vrentas and Vrentas (1991) incorporates the existing free volume in the system, which correlates well to the overall glass transition temperature of the system.

The concept becomes clearer by comparing the different sorption isotherms of the low molecular weight components with the various maltodextrin DE 17-21 fractions (Figure 4.4.5). Considering the pure mango powder the solid glass transition temperature is ca. 48.9˚C and at a water activity of 0.11 it is ca. 26˚C, which is still above the storing temperature of 25˚C. Between a water activity of 0.11 and 0.22 there is enough moisture absorbed into the system that it transitions into the rubbery state, where the sorption can be described by the Flory-Huggins model.

As can be seen in Figure 4.4.5 A, the overall absorbed moisture of the pure mango powder surpasses the sorption level of the other powders. The sorption in the rubbery state is dependent on the interaction parameter of the solid mixtures with the moisture, as explained in Section 4.3.1, which becomes more marked at higher water activities (Figure 4.4.5 A). At lower water activities the absorbed moisture is quite similar for systems up to a weight fraction of 0.6 maltodextrin. This directly correlates to the described increase of the glass transition temperature of the mixtures. At lower polysaccharide contents the mobility of the solid matrix is defined by the low weight molecules (Kawai & Hagura, 2012), which also relates to the reduction of free volume of the mixture (Kilburn et al., 2004; Ubbink, 2010). The mango powder with a weight fraction of 0.8 maltodextrin DE 17-21 exhibits a much higher glass transition temperature than the other mixtures due to the very high content of maltodextrin DE 17-21. The free volume in the system is much greater, therefore the moisture can easily fill these voids, which is demonstrated by the higher moisture content at low water activities (Figure 4.4.5 B). Pure maltodextrin DE 17-21 has a much higher glass transition temperature and a less densely packed structure with more free void space.

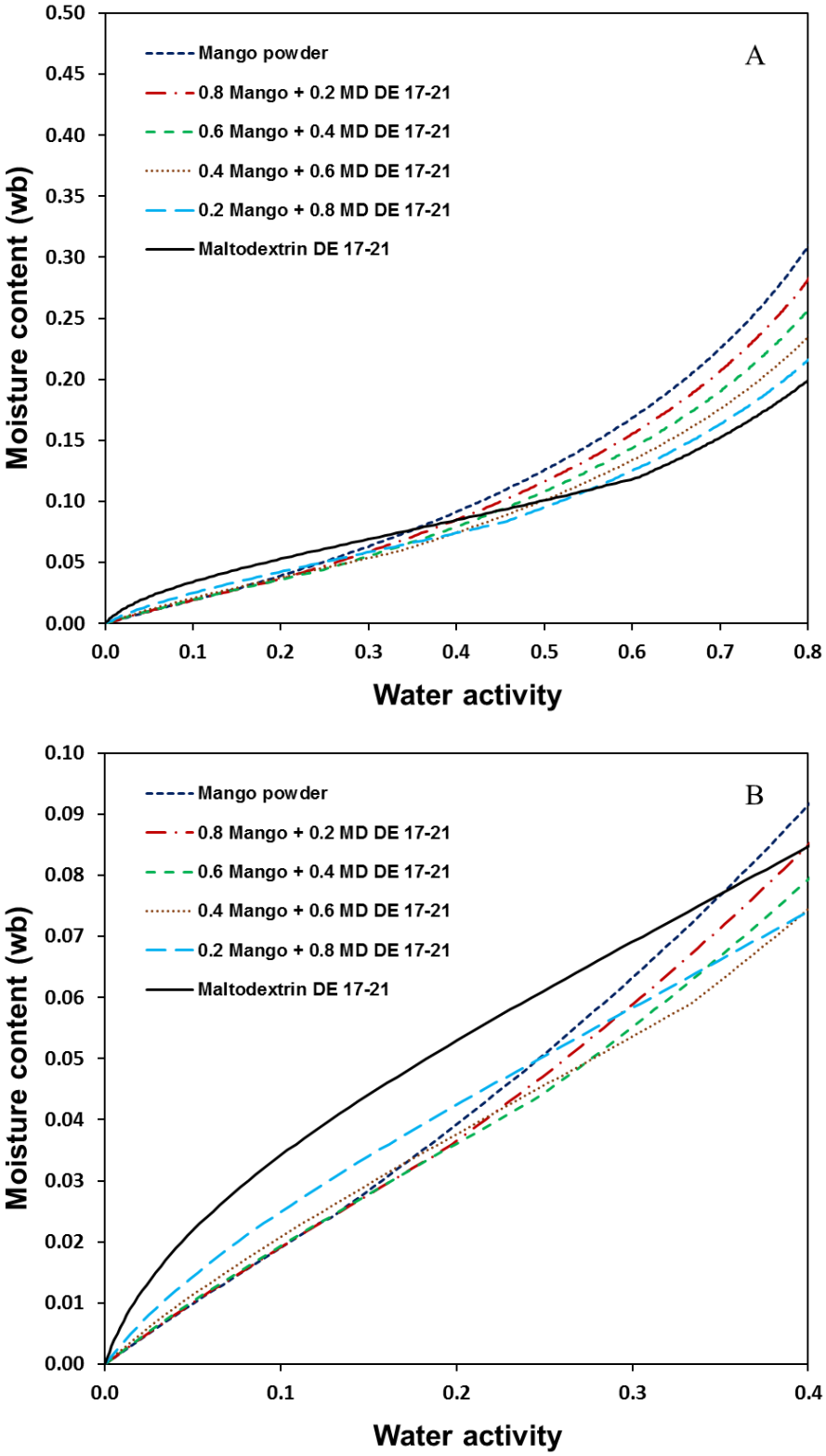


Figure 4.4.5. Sorption isotherms of mango soluble solids with various maltodextrin DE 17-21 fractions from A) 0 to 0.8 water activity and B) an enlargement at low water activity from 0 to 0.4.

Fongin et al. (2017) argues that the insoluble part of the mango pulp reduces the water holding capacity and therefore reduces the plasticizing effect of water on the T_g depression. This would imply that the insoluble and soluble parts directly influence the glass transition. However, these parts have to be observed separately from each other. The soluble fraction of the pulp forms an amorphous phase, which defines the glass transition temperature of the solid states. Crystallinity and fillers can have an effect on the glass transition temperature under certain parameters (see Section 2.6.4). Even under the circumstance of the crystalline regions inhibiting the mobility of the amorphous phase, the absorption of water into the amorphous phase has to be considered individually. A good comparison is spray dried skim milk powder, where the proteins are embedded in an amorphous lactose matrix. The glass transition temperature of the powder is related to the glass transition temperature of lactose. The T_g depression is dependent on the absorbed moisture content in the amorphous lactose matrix and can only be conditionally related to the overall moisture content of the powder.

4.4.4 Spray dried lemon juice powders

Paterson and Bröckel (2015) investigated the stability of a lemon juice powder plus maltodextrin DE 10 mixture produced by spray drying. The composition of the soluble solids in lemon juice was 17.19 g/L citric acid, 4.25 g/L L-malic acid, 6.85 g/L glucose and 8.04 g/L fructose. The maltodextrin DE 10 content was adjusted to reach a 1.5:1 ratio of maltodextrin DE 10 to soluble solids.

The glass transition temperature for the lemon juice plus maltodextrin DE 10 mixture could not be compared with an experimental value because the produced powder was not analysed at zero water activity. In one of the following studies in this thesis, it was found that the glass transition temperature of pure lemon juice powder was around 8˚C above the predicted value, therefore the effect of maltodextrin DE 10 for both theoretical systems was estimated. Maltodextrin De 10 has a T_g of 160˚C. At a T_g solid of 14˚C for lemon juice powder at the corresponding T_g value at 0.6 weight fraction of maltodextrin De 10 is 53˚C, at a T_g solid of 22˚C for lemon juice powder predicted T_g of the lemon juice powder plus 0.6 weight fraction maltodextrin DE 10 is 56˚C.

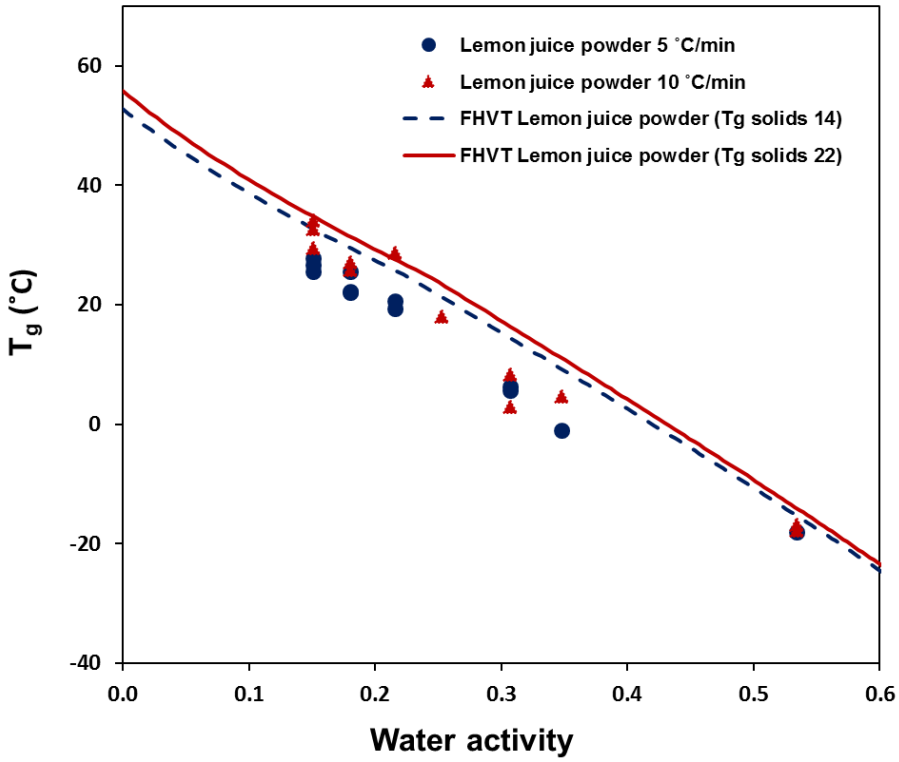


Figure 4.4.6. Predicted stability curves of spray dried lemon juice powder with 0.6 weight fraction of maltodextrin DE 10. The experimental data are from (Paterson & Bröckel, 2015).

As can be seen in Figure 4.4.6, the trend of the predicted stability curves is very similar to the experimental data obtained at the two heating rates of 5 ˚C/min and 10 ˚C/min. The prediction based only on the solid composition gives a better fit to the experimental data with a R^2 of 0.78 for data with 5 ˚C/min and 0.93 for 10 ˚C/min. The estimation using the T_g value of 56˚C at zero water activity as a starting value shows a stronger deviation from the data, the trend is correct, however the predicted values are shifted to slightly higher values. This results in a poorer fit of the experimental values with a R^2 of 0.65 for data with 5 ˚C/min and 0.89 for 10 ˚C/min. The approximation of the glass transition temperature of the pure lemon juice solids of 22˚C seems to be too high. There is also the case that the predicted values at zero water activity could be further apart from the real underlying glass transition temperature, however the overall trend of the system appears to be similar to the systems discussed previously.

4.4.5 Freeze dried strawberry puree powder

Mosquera et al. (2012) studied the critical water content for the storage of strawberry powder alone and in combination with the drying aids maltodextrin DE 16.5-19.5 and gum arabic. The composition of the soluble solids in strawberry was 1.1 g/100g citric acid, 0.6 g/l00g sucrose, 3.2 g/100g glucose and 3.5 g/100g fructose. The maltodextrin DE 16.5-19.5 content was adjusted to reach a 1:1 ratio of maltodextrin DE 16.5-19.5 to soluble solids. Similar to the previously discussed powders, the prediction model gives a good representation of the trend of the experimental data (Figure 4.4.7), the corresponding R^2 values are 0.95 for strawberry powder, 0.98 for strawberry with MD DE 16.5-19.5 powder and 0.95 for strawberry with gum arabic powder. From Figure 4.4.7, it can be

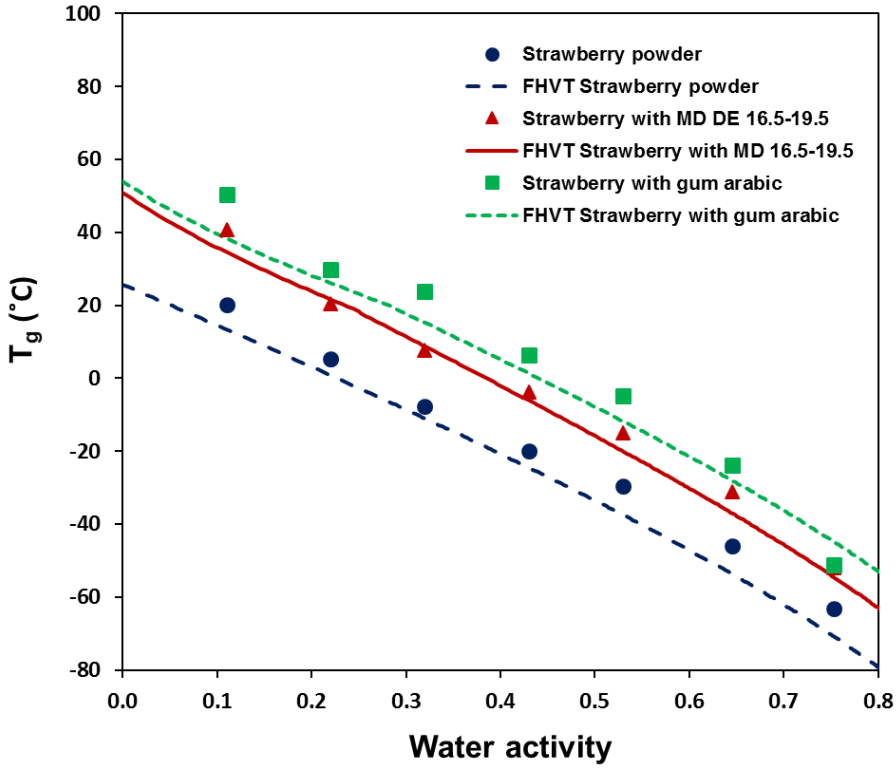


Figure 4.4.7. The relation of water activity and glass transition temperature of pure strawberry puree and in combination with maltodextrin DE 16.5-19.5 and gum arabic. The experimental data are from Mosquera et al. (2012).

observed that the prediction lines are much lower at a water activity of 0.11. This corresponds to the lower estimated glass transition of the solid mixture. The predicted T_g value of 26˚C at zero water activity from the sugar and organic acid composition for the pure strawberry powder is too low. On the other hand the presented T_g value of 68˚C for the solid strawberry puree, using the fitted Gordon-Taylor equation to approximate the T_g values of the solid mixtures, overestimates the real glass transition temperature. Since the

T_g value of the strawberry puree powder is already underestimated the predicted values for the mixture with maltodextrin DE 10 and gum arabic are also lower than the real underlying T_g values.

4.4.6 Deviation of the FHVT models

Not all powders from the literature can be accurately predicted using the FHVT model in combination with the T_g approach. Two studies showed spray dried powders, which exhibit a different sorption isotherm trend and therefore differ from the previous presented studies. Tonon et al. (2009) studied the relation of the water activity and the glass transition temperature for spray dried acai juice powders containing maltodextrin DE 10, DE 20 and gum arabic. The main soluble solids components were identified as glucose 1.11 g/100g, fructose 0.57 g/100g and citric acid 0.32 g/100g. The drying aid made up 75% of the soluble solids and drying mixture. The predicted glass transition temperatures are quite similar to the ones presented in the study (Table 4.4.6). At this high concentration of polysaccharide the effect on the soluble solids of the juice are relatively small, since the matrix of the system is dominated by the large polysaccharides.

Table 4.4.6. Predicted and presented glass transition temperatures of acai powders by Tonon et al. (2009).

Material	T_g (°C)	$T_{g,\,pred}$ (°C)
Acai + MD DE 20	79.1	82
Acai + MD DE 10	94	87
Acai + Gum arabic	88.3	89

Considering the prediction of the relation of water activity and glass transition temperature via the FHVT model (Figure 4.4.8), the overall trend of the experimental data differs markedly from the predicted values. The model strongly overestimates the moisture content at the different water activities and therefore the corresponding glass transition temperatures are lower. The overall fit is less accurate for each blend, with a R^2 of 0.76, 0.77 and 0.86 for the added drying aid MD DE 10, DE 20 and gum arabic respectively.

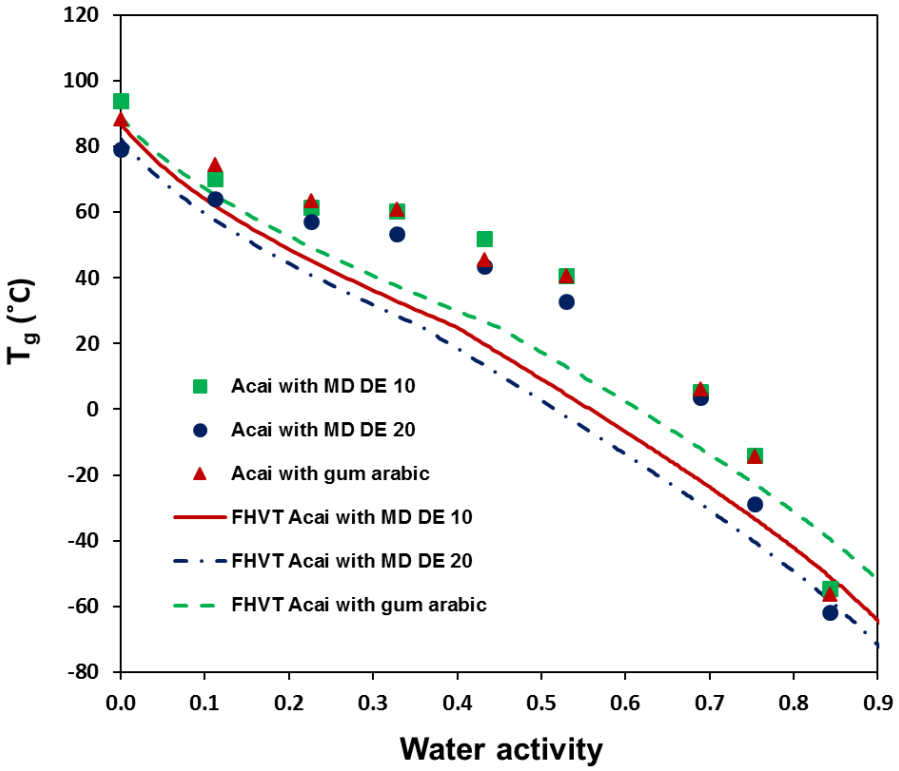


Figure 4.4.8. Prediction of the relation of the water activity and glass transition temperature for data of the acai powders with various drying aids presented by (Tonon et al., 2009).

For comparison reasons the mango powder and acai powder at similar maltodextrin contents are plotted in the same graph (Figure 4.4.9). Since the main component in both systems is maltodextrin DE 20 the overall behaviour of the systems should be very similar due to high polysaccharide contents of 80%. It can be observed, up to a water activity of 0.22, that the two systems show the same trend. For the acai powder, the T_g are almost constant between water activities of 0.22 and 0.43, which implies that the powder did absorb a minimal amount of moisture.

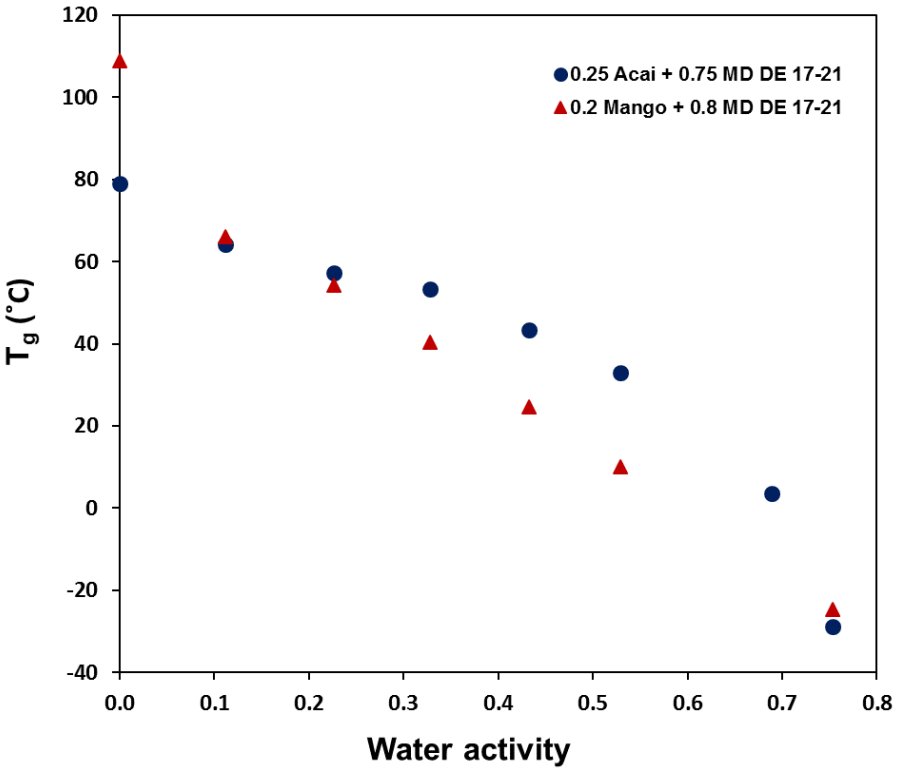


Figure 4.4.9. T_g values of mango powder and acai powder with similar maltodextrin DE 20 contents at various water activities.

This is not the case for the mango powder, where there is gradual increase in the moisture content and therefore a progressive depression in the T_g values of the powder. The fitted and predicted sorption isotherms for the mango powder and acai powder are illustrated in

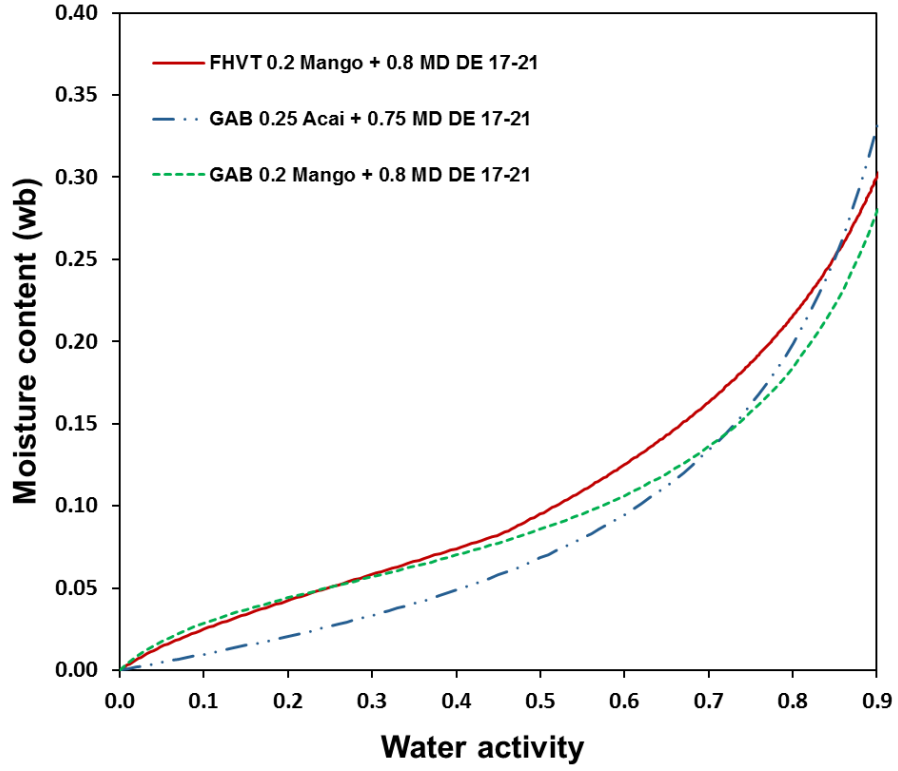


Figure 4.4.10. Modelled sorption isotherm of the mango and acai powders at high maltodextrin amounts using the GAB and FHVT models.

Figure 4.4.10, where the FHVT and GAB models show a direct increase of the moisture content in the mango powder. The acai powder does not follow the expected trend, but rather increases very slowly till it catches up with the other isotherms at higher water activities.

The question is whether this difference arises from the morphology difference between the spray and freeze dried powders. Viganó et al. (2012) studied the absorption of water into pineapple pulp with 50% (on solid basis) maltodextrin DE 20 using different drying techniques. In her study, the spray dried samples were more hydrophilic than the freeze dried samples, which would result in a faster decrease of the T_g values than for freeze dried samples. This would mean for the acai powders that the glass transition temperatures should be even lower than the ones for mango powder, if the above argument is valid.

A study by Islam et al. (2016) concentrated on spray dried orange juice powder with various additions of maltodextrin DE 10. The final powders had ratios of 50:50, 40:60 and 30:70 orange solids to maltodextrin DE 10. The main soluble solids in orange juice were identified as sucrose, glucose, fructose and citric acid in mass ratios of 45, 24, 21 and 10 respectively (Kelebek et al., 2009). The estimated T_g values of the powder mixtures are quite different from the presented values in the studies (Table 4.4.7). There are several possible reasons: the glass transition temperature of the pure orange juice solid mixtures may be higher than the estimated value, and the maltodextrin that has been used may have a higher T_g than that assumed. However, due to the high measured T_g values at water activities at 0.11, it can be assumed that the glass transition temperature values at zero water activity should be higher than the predicted values.

Table 4.4.7. Predicted and presented glass transition temperatures of orange powders from Islam et al. (2016).

Material	**T_g (˚C)**	**$T_{g,\,pred}$ (˚C)**
0.5 orange + 0.5 MD DE 10	71.9	65
0.4 orange + 0.6 MD DE 10	95	74
0.3 orange + 0.7 MD DE 10	103.8	88

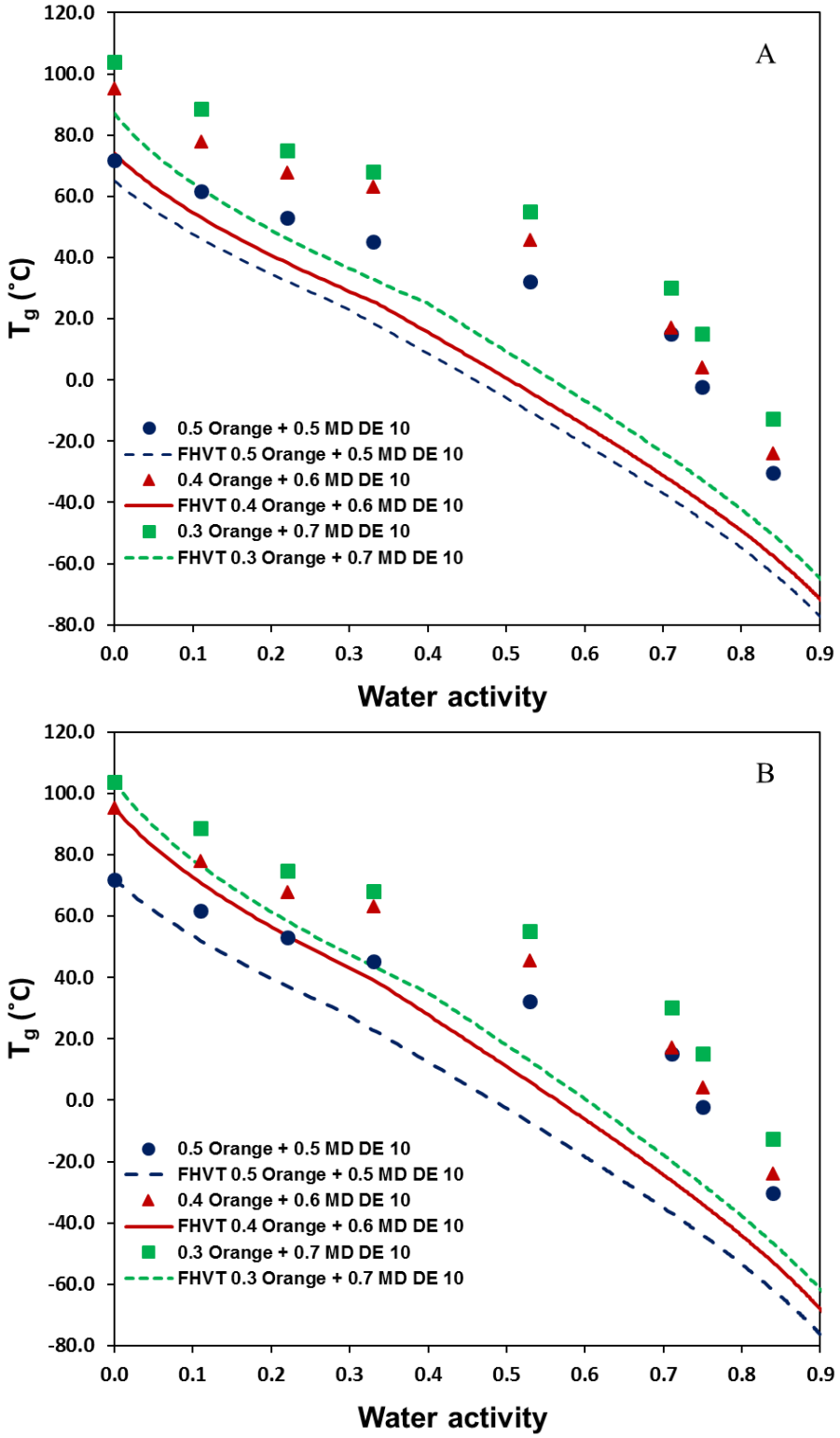


Figure 4.4.11. Prediction of the relation of the water activity and glass transition temperature for data of the orange juice powders with fractions of MD DE 10. In A, only the predicted values are used. In B, the T_g solid values of the mixture of powder from the study by Islam et al. (2016) are utilized.

Similar to the previous described system the experimental data follows a more fully curved line than the slight curvature of the FHVT model (Figure 4.4.11 (A)), which makes the overall prediction of the relation of water activity and glass transition temperature very difficult with an R^2 of 0.42 for the 40:60 ratio and 0 for the other two systems. Adjusting the T_g values of the solid mixture to the values presented only be improves the overall prediction slightly (Figure 4.4.11 (B)). The great difference in the sorption isotherms for the predicted orange juice powders in comparison to the measured sorption isotherm is similar to the example shown in Figure 4.4.10 and does not allow for an accurate fit to the experimental data.

4.5 Conclusion

In this chapter, a new model of predicting the glass transition temperature of low molecular weight mixtures with carbohydrate polymers was developed on the basis of the chemical composition. The modifications of the Couchman-Karasz equation allow to account for the negative deviation from linearity seen for the glass transition temperature of mixtures of low molecular weight components upon the addition of carbohydrate polymers. An adapted Flory-Huggins Free Volume Theory (FHVT) model was presented as an alternative approach for estimating the sorption isotherm of fruit juice powders on the basis of the chemical composition, instead of relying on the fitting of the BET or GAB models to the experimental data. The combination of the prediction model of the glass transition temperature of mixtures in the dry state and the FHVT model were applied to estimate the glass transition temperature at various water activities for fruit powders presented in the literature. This approach resulted in a very good representation of the trend of the glass transition temperature for the different system at various water activities. Some limitations were found in predicting the trend of T_g for some fruit powders due to discrepancies between the behaviour of the sorption isotherm found in the literature and estimated ones. However, the test of the approach on the literature data demonstrated that it is possible to predict the glass transition temperature of carbohydrate mixtures with only the chemical composition of the powders as an input criteria.

The next step is to validate the effect of polysaccharide on the T_g of the fruit juice solids and T_g values of fruit juice powders in general. Therefore six commercially produced fruit and vegetable juice concentrate freeze dried powders are investigated for their glass transition temperature in the following chapter.

5. Pure fruit juice powders

5.1 Introduction

In Chapter 4 it was mentioned that some of the predicted T_g values, on the basis of the sugar and organic acid profile for the pure fruit powders at zero water activity, deviated from the measured glass transition temperatures. For the grapefruit powder, the variance was only minor at 1˚C but for strawberry powder the difference was extreme at 40˚C. Not only was there a discrepancy between the predicted and the measured T_g values, but also the glass transition temperatures of the fruit powders differed strongly from each other. In order to get a better understanding, the glass transition temperature of the solid mixtures of juice powders freeze dried from six commercial locally produced juices from New Zealand were investigated. The six commercial juices were kiwifruit, blackcurrant, clear apple, cloudy apple and carrot in the form of concentrates; lemon juice, which was not concentrated. These juices were freeze dried at 10% (solids concentration) and the solid mixtures had their glass transition temperature at zero water activity measured by DSC. The juices were analysed for their sugar and organic acid profile, which was used to predict the glass transition temperature. The predicted values were compared with the measured ones. The freeze dried fruit juice powders were stored at 30˚C over water activities of 0.11, 0.23, 0.32 and 0.43 to identify the relation of the absorbed moisture content to the plasticizing effect of water on the glass transition temperature of the fruit powders.

5.2 Composition of fruit juices

In Section 2.2 the composition of fruits and commercial juices was discussed and the sugars sucrose, fructose and glucose and the organic acids citric acid and L-malic as well as the sugar alcohol sorbitol were attributed to be the main solids in commercial juices. Therefore, the sugar and organic acid profiles of the commercial juices were investigated to determine the ratios of each solid component in the juice. Table 5.2.1 presents the complete sugar and organic acid profile of the different commercial juices. For all the fruit juices the main sugar is fructose, which is typical, especially for apples, but also for blackcurrant and kiwifruit. Blackcurrant and lemon have a high amount of organic acids in the form of citric acid.

Table 5.2.1. Sugar and organic acid profile of the different fruit and vegetable juices.

Compound[a]	Black currant	Kiwi fruit	Clear apple	Cloudy apple	Lemon	Carrot
Brix	65.30	71.35	76.35	44.50	8.94	42.40
Total solids[b] (g/100g)	68.98 ± 0.63	74.12 ± 0.59	80.26 ± 1.98	42.10 ± 0.47	9.36 ± 0.49	42.44 ± 0.47
Fructose (g/100g)	18.67 ± 0.24	22.97 ± 0.74	37.98 ± 1.37	21.39 ± 0.17	1.88 ± 0.46	5.98 ± 0.86
Glucose (g/100g)	13.61 ± 0.30	20.89 ± 0.52	10.98 ± 0.88	8.05 ± 0.72	1.61 ± 0.32	7.25 ± 0.39
Sucrose (g/100g)	0.08 ± 0.17	1.60 ± 0.05	8.94 ± 0.35	4.44 ± 0.18	ND	18.25 ± 0.46
Sorbitol (g/100g)	ND	ND	10 ± 0.06	0.52 ± 0.16	ND	ND
Citric acid (g/100g)	18.17 ± 0.06	5.7 ± 0.53	ND	ND	4.56 ± 0.004	ND
L-malic acid (g/100g)	ND	1.99 ± 0.23	3.38 ± 0.08	2.19 ± 0.16	0.16 ± 0.05	1.03 ± 0.14
Total sugar and acid (g/100g)	50.53 ± 0.37	53.22 ± 2.07	62.72 ± 2.70	36.60 ± 0.88	8.22 ± 0.73	32.6 ± 1.83
Total sugar and acid/ total solid	0.73	0.72	0.78	0.86	0.87	0.77

a) Sugars and organic acids were analysed by HPLC method, average ± SD, n=2

b) Vacuum method 60˚C at 70 Pa for 3 h, average ± SD, n=3

c) ND=not detected

Table 5.2.2 presents the sugar and organic acid composition of the juices. For blackcurrant the composition is almost evenly spread between fructose, glucose and citric acid. Cloudy and clear apple contain mostly fructose (60%) and a much smaller content of organic acids in form of L-malic acid. As expected, lemon juice contains mainly citric acid, contributing to 56% of the total solid content. Carrot juice has the highest content of sucrose, around 56% of the total amount of solids.

Table 5.2.2. Distribution of the sugar and organic acid composition in the fruit and vegetable juices.

Compound	Black currant	Kiwi fruit	Clear apple	Cloudy apple	Lemon	Carrot
Fructose (%)	37	43	61	58	23	18
Glucose (%)	27	39	18	22	20	22
Sucrose (%)	-	-	14	12	-	56
Citric acid (%)	36	11	-	-	56	-
L-malic acid (%)	-	4	5	6	2	3
Sorbitol (%)	-	-	2	1	-	-

The distribution of the sugars and organic acid in the juices agree well with general compositions stated in the literature (Eisele & Drake, 2005; Ford, 2012; Heiberg et al., 1992). However, considering the total mass balance of the sugar and organic acid in the juices (Table 5.2.1) in comparison to the total solid content there is still a large discrepancy. For blackcurrant and kiwifruit the sugars and organic acids contribute around 72% of the total solid content, for clear apple and carrot around 77% and for lemon and cloudy apple the fraction is much higher at ca. 86%. These values might not be entirely accurate due to variance in the HPLC measurement and the total solid content. For the kiwifruit and blackcurrant juice, the difference is almost 30% between sugar and organic acids and the total solid content.

In this study the juices have not been studied for their protein, fat and dietary fibre content, but the chemical composition of commercial blackcurrant juice concentrate has been presented in the New Zealand food composition database (Research, 2019). The contribution of these components is relatively small with fats making only up 0.5 g/100g, proteins 0.3 g/100g and dietary fibres 3.1 g/100g of the total solid content. By adding these amounts to the sugar and organic compounds the whole composition represents roughly 80% of the total solid content, which leaves another 20% that is unknown. Willems and Low (2016) investigated the effect of the intensive enzyme treatment in commercial pear juice production on the cell wall polysaccharides in the juice. The study showed that the monosaccharide and oligosaccharide content from the hydrolysed pectins, starch and hemicellulose increases in the mashing stage and by further carbohydrase treatment. Other processing stages have shown to have little influence on the carbohydrate profile observed in the chromatographic results (Willems & Low, 2016).

The blackcurrant juice concentrate was analysed for the molecular weight of the residual carbohydrates in the juice concentrate using the method of Willems and Low (2016) (see Chapter 3). The sample was precipitated in alcohol to separate most of the monosaccharides from the higher molecular weight components. The prepared sample was analysed using Fast Liquid Protein Chromatography (FLPC) to identify the approximate molecular weight of the total carbohydrate content as well as the size of the pectin chains in the form of the galacturonic acid content. In Figure 5.2.1, the chromatogram of the FPLC analysis of the precipitated sample of blackcurrant juice concentrate and various dextran standards can be observed. The black line corresponds to

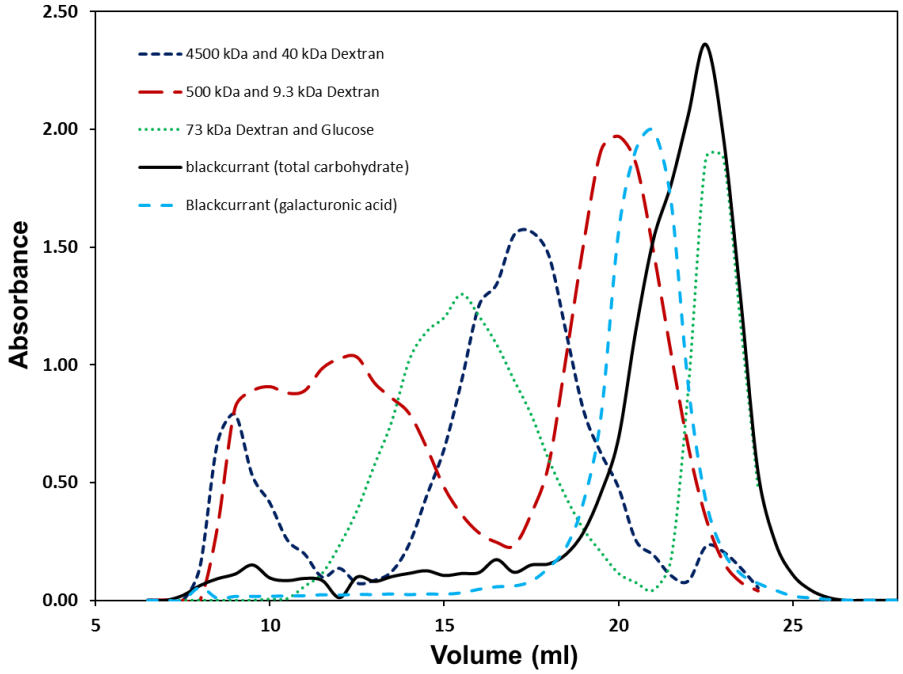


Figure 5.2.1. FLPC chromatogram of the total carbohydrate content and galacturonic acid in blackcurrant in combination of various dextran standards.

the total carbohydrate content in the sample and as it can be seen that the signal shows some correspondence to the higher molecular weight dextrans. The intensity of the total carbohydrate content starts to increase markedly at a volume of around 19 mL, at around the same volume that the 9.3-kDa dextran exhibits its maximum. Since the peaks of the components are relatively broad it is hard to allocate the molecular weight of the total carbohydrate to one of the standard peaks. However, it can be assumed that the majority of the total carbohydrates have a molecular weight below that of the 9.3-kDa dextran. The peak's maximum is reached at a volume of 22.5 mL, just below that of the maximum of glucose at 23 mL. This indicates that there might be still a great fraction of low molecular weight components in the precipitated sample in combination with mostly lower molecular weight polymers. If only the signal of the galacturonic acid is considered in

Figure 5.2.1 it can be seen that the residual pectin chains exhibit a lower degree of polymerisation (DP). The same would be expected for the other polysaccharides in the juice, but due to limitations of the FLPC column it was not possible to separate the monosaccharides from the polysaccharides with lower DP value in the total carbohydrate curve.

5.3 T_g of juice and vegetable powders at zero water activity

For better comparison purposes the glass transition temperature is defined as the midpoint of the transition in the DSC heat flow signal. Since the glass transition temperature is not technically occurring at one temperature but over a temperature range the extrapolated onset and offset point as well as the width of the transition are stated to give a more accurate characterization of the glass transition temperature.

The measured glass transition temperatures of fruit juice powders were much higher than expected. Table 5.3.1 shows the glass transition temperatures of various juice powders at zero water activity. Three powders have a T_g value above 20˚C, with 26.46˚C being the lowest for lemon juice powder then cloudy apple powder at 28.15˚C and clear apple powder at 29.63˚C. Surprisingly, blackcurrant and kiwi juice powders exhibit glass transition temperatures above 30˚C at 34.46˚C and 37.29˚C, respectively. Due to the high content of sucrose in carrot juice it was not unexpected to find the T_g value of carrot juice powder to be 50.53˚C, which is much higher than the T_g values of the other fruit juice powders.

Table 5.3.1. T_g of fruit and vegetable powders at zero water activity.

Juice	T_g mid (˚C)	Onset (˚C)	Offset (˚C)	Width (˚C)
Blackcurrant	34.5 ± 0.1	30.5 ± 0.6	38.4 ± 0.4	7.9 ± 0.9
Kiwifruit	37.3 ± 0.2	33.2 ± 0.3	41.4 ± 0.3	8.3 ± 0.5
Clear apple	29.6 ± 0.9	25.0 ± 1.3	34.4 ± 0.6	9.4 ± 0.7
Cloudy apple	28.2 ± 0.2	24.4 ± 0.3	32.2 ± 0.1	7.7 ± 0.4
Lemon	26.5 ± 0.2	22.8 ± 0.1	30.3 ± 0.2	7.6 ± 0.1
Carrot	50.5 ± 0.3	45.6 ± 0.4	55.7 ± 0.2	10.2 ± 0.2

Average ± SD, n=3

The predicted glass transition temperatures of the juice powders, on the basis of their sugar and organic acid composition, is shown in Table 5.3.2. As stated previously, the estimated values are much lower than the measured ones. The smallest difference between

the measured and predicted T_g values is 6˚C for carrot juice powder. The difference in the predicted versus measured glass transition temperatures for lemon, cloudy and clear apple juice powder are around 8˚C. The greatest mismatch can be found for the blackcurrant and kiwifruit powders with a difference of 14˚C. This further illustrates the disagreement of the predicted T_g values of the pure juice fruit powders discussed in Chapter 4. Seemingly, the T_g prediction on the basis of the sugar and organic composition underestimates the real glass transition temperatures of the juice powders. As previously mentioned, the sugar and organic acid content accounts for roughly 80% of the total solid fraction for blackcurrant and kiwifruit juice. Interestingly, these two juices have the lowest sugar and organic acid fraction of all the juices and at the same time exhibit the greatest difference between the predicted and measured T_g value. Considering the findings in Figure 5.2.1 it is very likely a polydisperse mixture of residuals polymers contribute to the higher glass transition temperatures observed in the DSC signals.

Table 5.3.2. Comparison of predicted and measured T_g values of pure juice powders at zero water activity.

Juice	T_g mid (˚C)	T_g pred (˚C)	ΔT_g (˚C)
Blackcurrant	34.5 ± 0.1	20	14
Kiwifruit	37.3 ± 0.2	23	14
Clear apple	29.6 ± 0.9	22	8
Cloudy apple	28.2 ± 0.2	20	8
Lemon	26.5 ± 0.2	18	8
Carrot	50.5 ± 0.3	45	6

Average ± SD, n=3

An additional study of three powders produced from commercial smoothie mixtures, which were made of various vegetable purees and different fruit juices, show the same trend. The predicted glass transition temperatures were roughly 10˚C below the measured T_g values, which indicates that this trend is likely to be observed for all different kinds of juices and purees.

5.3.1 Second glass transition temperature in fruit powders

The presence of other components than the sugars and organic acids becomes clearer when observing Figure 5.3.1. Figure 5.3.1 (A) shows the DSC heat flow signal for the six

different juice powders at zero water activity as a function of the temperature for the second heating cycle. The transition from the glassy state to the rubbery state is explicitly marked by the step change in the heat capacity and therefore the endothermic change in the heat flow signal. Typically, for a mixture of low molecular components, the measured width of the transition is around 10˚C, which makes it easily detectable. The heat flow curves of carrot and lemon juice powder pass through the transition and level off. This is not the case for the other juice powders; after the steep transition the signal levels off and then another clear transition can be observed. Figure 5.3.1 (B) illustrates the separate signal of the cloudy apple powder for both heating cycles. In both cycles the two transitions are explicitly visible. These separate transitions underline the fact that there are two different phases in the juice powders. Each phase relaxation occurs at different temperature ranges. Tedeschi et al. (2016) investigated the binary blend of sucrose and modified starch. In the study, two distinct transitions in the DSC heat flow signal were detected. It was stated that during the formation of the glassy matrix structure, two amorphous phases were created.

The first one, at the lower temperature, mostly consists of sucrose molecules with a few modified starch molecules embedded. For the second transition, the opposite is the case, with the starch molecules surrounded by a smaller amount of sucrose molecules, which act as a plasticizer on the glass transition temperature on the starch rich phase. The same concept is applicable to the juice powders. The transition at lower temperatures is associated with the amorphous phase rich in sugars and organic acids in combination with some other molecules, which increase the glass transition temperature of the phase. The transition at higher temperature is composed of a smaller fraction of the sugars and organic acids and a greater fraction of molecules with a higher glass transition temperature. The DSC heat flow signal cannot provide any quantitative information about the ratios of the two amorphous phases present in the system. The magnitude of the step change of the first transition in Figure 5.3.1 (B) is much greater than the step change of the second transition, therefore it is arguable that the phase rich in low molecular weight components is the predominant amorphous phase in the glassy matrix, which is to be expected as these components make up the greater percentage of the solid content.

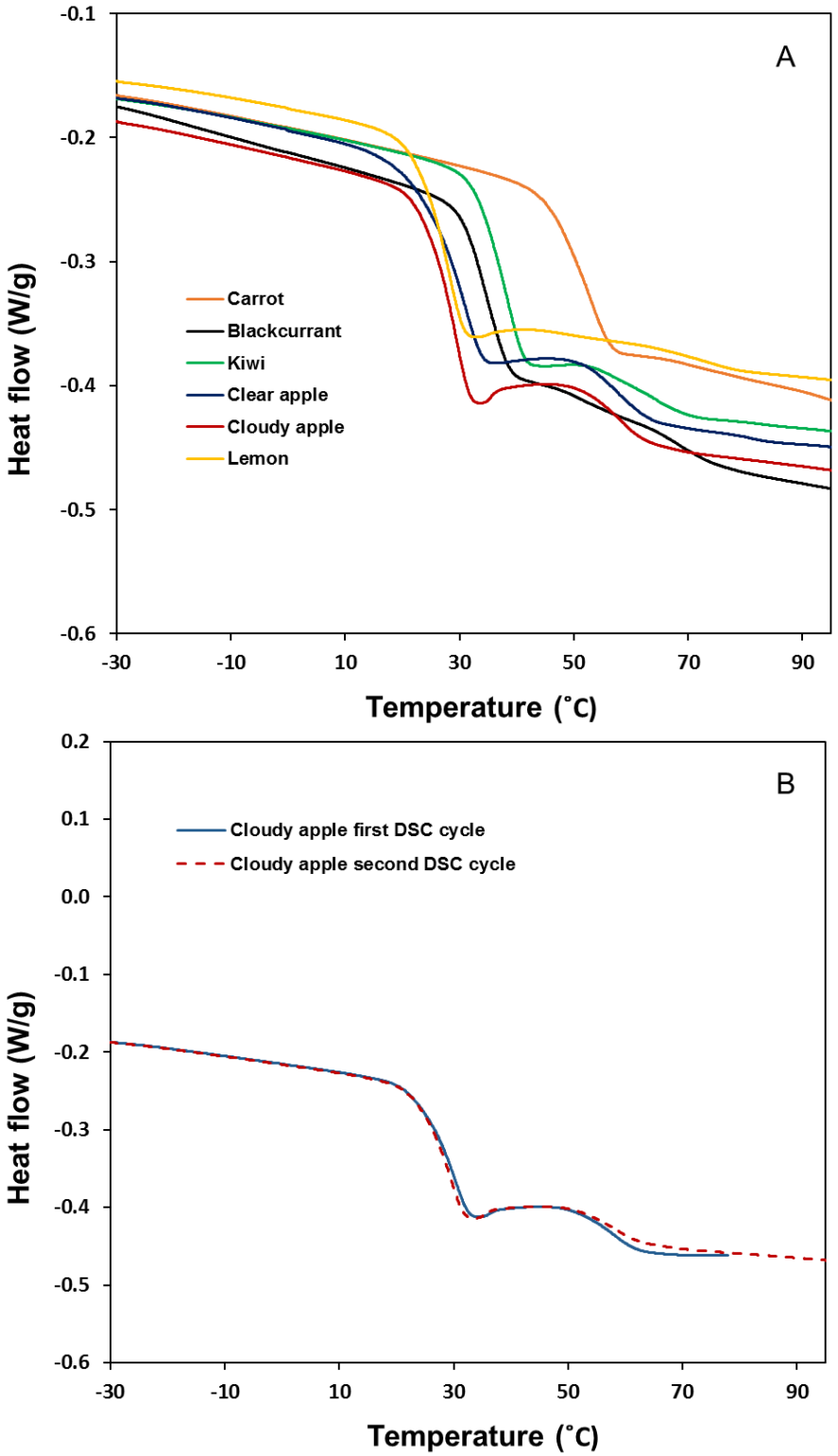


Figure 5.3.1. (A) The second cycle of the DSC heating curve of the various juice powders at zero water activity. (B) Both heating cycles of the DSC signal of cloudy apple juice powder.

Table 5.3.3. Second transition of the cloudy apple, clear apple, kiwifruit and blackcurrant juice powders detected in the second cycle of the DSC heating curve.

Juice	T_g mid (˚C)	Onset (˚C)	Offset (˚C)	Width (˚C)
Blackcurrant	61.7 ± 3.6	53.7 ± 3.9	68.5 ± 4.1	14.8 ± 0.4
Kiwifruit	63.9 ± 2.0	58.9 ± 3.7	69.5 ± 0.3	10.5 ± 3.6
Cloudy apple	57.7 ± 0.2	52.3 ± 0.1	63.0 ± 0.3	10.7 ± 0.3
Clear apple	57.6 ± 0.3	51.9\ ± 0.2	63.2 ± 0.5	11.3 ± 0.3

Average ± SD, n=3

The second glass transition temperatures of the juice powders are around 60˚C, with cloudy and clear apple being on the lower side (Table 5.3.3). This is expected, since their first glass transition temperatures were lower in the first place. Comparing the midpoints of the first and second glass transition temperatures, the second T_g values are roughly 25–29˚C higher than the T_g values of the first transition. It is noticeable that the width of the transition also slightly increases from around 8˚C to more than 10˚C.

5.4 Water activity and T_g of juice powders

Additionally to the glass transition temperature of the juice powder at zero water activity, the effect of moisture on the glass transition temperature was studied. The glass transition temperatures of the juice powders with water activities of 0.11, 0.22, 0.32 and 0.43 were measured. The study was not extended to higher water activities because the powders turn into a syrup at higher water activities and are far below their stability region. Furthermore, at a water activity of 0.43 a decrease in moisture content could be detected for the juice powders at the end of the second week storage time, which was accompanied by some crystal formation in the samples. Despite the small fractions of crystals in the samples it is assumed that the main amorphous fraction was not greatly influenced by the crystals. The T_g depression as a function of the moisture content was predicted using the approach described in Chapter 4 to validate the prediction method for juice powders.

5.4.1 Predicted sorption isotherms of the powders by the FHVT model

In order to relate the effect of water on the glass transition temperature the predicted sorption isotherm of the amorphous mixtures has to correspond to the overall trend of the moisture increase. Considering Figure 5.4.1 the overall trend of the sorption isotherms follows the increase of moisture content in the powders in relation to the various water activities. The predicted values are slightly higher than the measured values, especially at

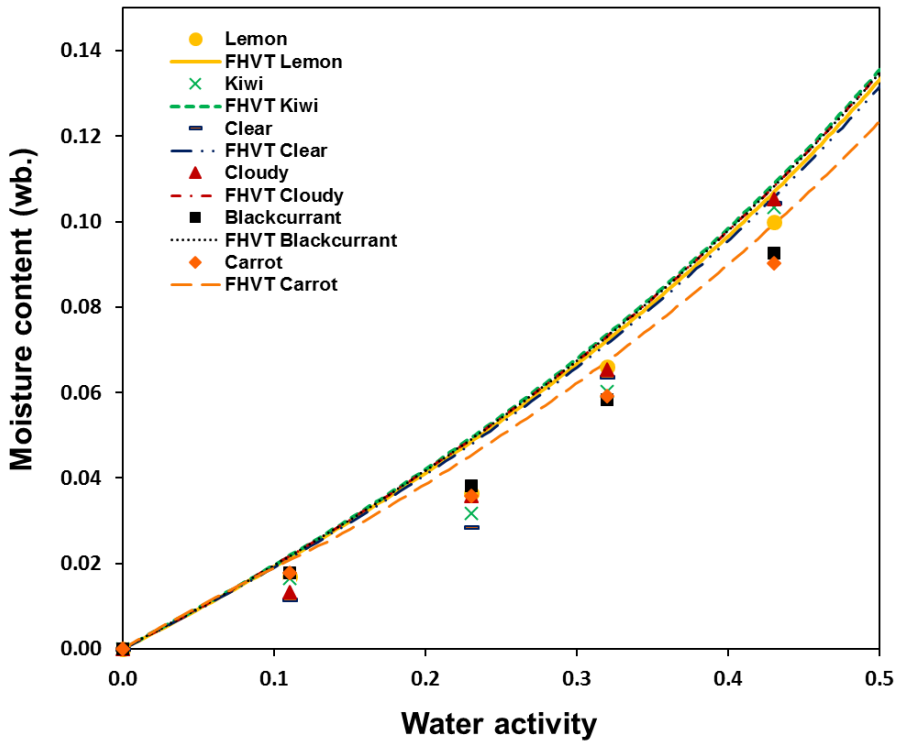


Figure 5.4.1. Moisture content of the six juice powders at different water activities and the predicted corresponding sorption isotherm using the FHVT model.

a water activity of 0.23, but the overall difference is reasonably small, which corresponds well to the similar behaviour for the juice powders. The carrot powder isotherms follow a slightly different path due to the high concentration of sucrose in the system, whereas the other juices have a greater proportion of very low molecular components such as monosaccharides and organic acids. The FHVT model allocates a similar interaction $\chi = 0.38$ with water to the low molecular weight components. Only small deviations are evident due to slight differences in their molecular weight. From the fact that the trend of the sorption isotherms is identical for the various juices powders, even though the distribution of the sugars and organic acids differ between the juices, it can be assumed that the low molecular weight component can be categorized into one group with a very similar interaction parameter. It is noticeable that the measured moisture content for clear apple juice powder is especially low at a water activity of 0.11 and 0.23 in comparison to the other samples. The estimated moisture content at the various water activities using the FHVT model can be related back to the glass transition temperature as presented for the pure fruit powders in the following section.

5.4.2 Blackcurrant juice powder

The physical modification of juice powders occurring with shifts in the moisture content become especially clear by correlating the changes of the T_g values in Table 5.4.1 with the visual alterations illustrated in Figure 5.4.2.

Table 5.4.1. Glass transition temperature of blackcurrant juice powder at different water activities.

Blackcurrant 1st transition

Water activity	T_g mid (˚C)	Onset (˚C)	Offset (˚C)	Width (˚C)
0	34.5 ± 0.1	30.5 ± 0.6	38.4 ± 0.4	7.9 ± 0.9
0.11	19.5 ± 0.9	13.7 ± 0.7	25.3 ± 1.3	11.7 ± 0.7
0.22	6.7 ± 0.5	1.3 ± 0.5	12.1 ± 0.5	10.9 ± 0.4
0.32	-7.3 ± 0.9	-12.0 ± 0.6	-2.5 ± 1.1	9.5 ± 0.5
0.43	-20.3 ± 0.4	-24.4 ± 1.7	-16.3 ± 0.3	8.1 ± 1.5

Average ± SD, n=3, storage temperature 30˚C

The T_g value of blackcurrant juice at a water activity of 0.11 was 19.47˚C, which is around 9˚C below the storage temperature of 30˚C. The powder particles had completely caked together and the powder lost its free flowing properties (Figure 5.4.2). The increase to a water activity of 0.22 and 0.33 leads to a further decrease of the glass transition to 6.68˚C and -7.29˚C respectively. At a water activity of 0.43 the glass transition temperature was -20.32˚C. The glass transition temperature decreases by 15˚C from 0 to 0.11 water activity, by 13˚C from 0.11 to 0.22 water activity, by 14˚C from 0.23 to 0.32 water activity and by 13˚C from 0.32 to 0.43 water activity. This linear decrease of the glass transition temperature is exactly what is expected from the results in Chapter 4.

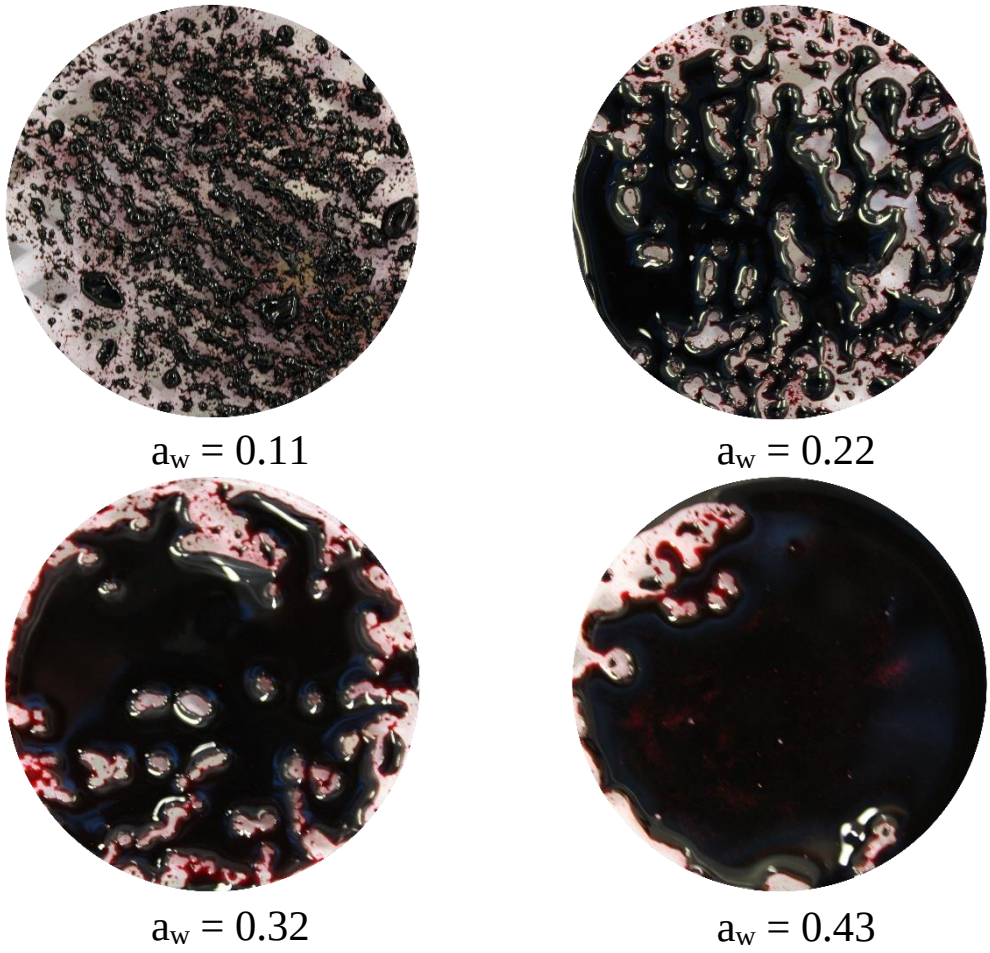


Figure 5.4.2. Visual changes in blackcurrant juice powder stored at 30˚C at different relative humidities.

In Figure 5.4.2 the visual changes are clearly visible. The separated powder particles are still visible at 0.11 water activity. At 0.22 water activity more particles are aggregated together and there is no distinct separation noticeable. With the increase of the water activity from 0.22 to 0.32 the mixture spreads further out and at 0.43 it forms one complete lump. The powders at a water activity of 0.23 and 0.32 look like a liquid, however they are very brittle, similar to a hard candy. As soon as the system has a water activity of 0.43 it loses its brittleness and becomes a highly viscous syrup.

The dashed line in Figure 5.4.3 represents the estimates based only on the sugar and organic acid composition. Since the predicted value of the blackcurrant powder at zero water activity is already off by 14˚C, it is not suprising that the predicted T_g values do not conform with the measured values in Figure 5.4.3. The difference between the predicted

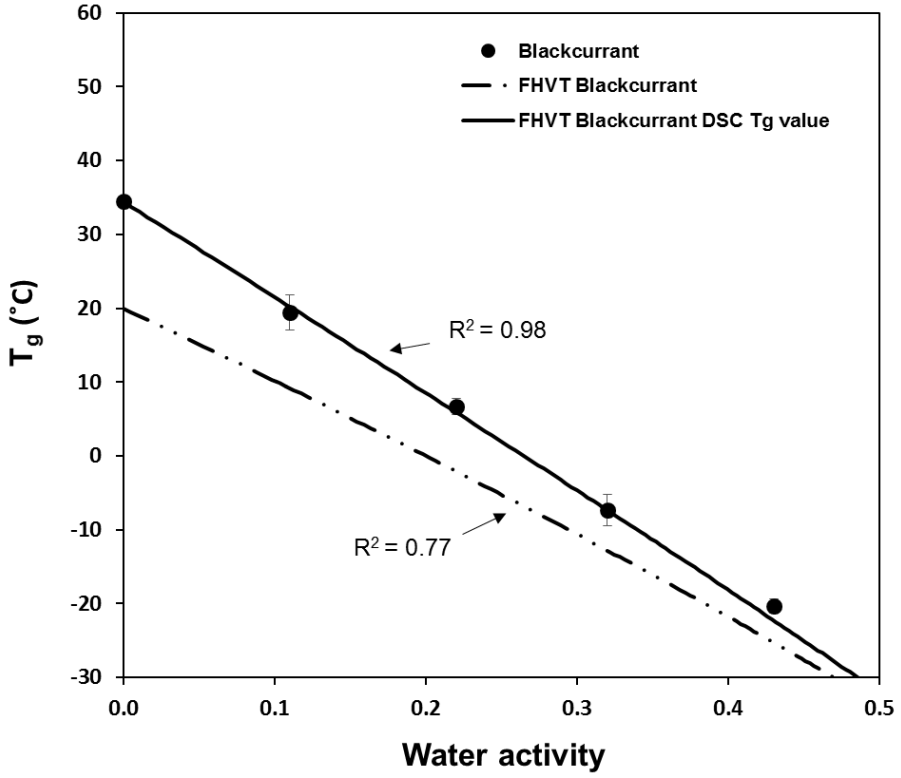


Figure 5.4.3. Prediction of the effect of water on the T_g depression of blackcurrant juice powder on the basis of the chemical composition and using the DSC value of blackcurrant juice powder at zero water activity. The error bars refer to the 95% confidence interval for n=3.

and measured T_g values becomes smaller at a water activity of 0.43, since the moisture content is already so high that the initial difference in the T_g values has a lower impact. The overall R^2 of the predicted values is 0.77. However, if the measured value at zero water activity is used to predict the trend for the blackcurrant powder, the estimated T_g values agree very well with the measured values with an R^2 of 0.98. This is almost certainly due to the correction linked to the unknown low molecular weight pectins or other carbohydrates shown to be present in Section 5.2.

5.4.3 Kiwifruit juice powder

The powder produced from kiwifruit concentrate shows a very similar trend regarding the T_g values at the various water activities to that seen for blackcurrant juice powder (Table 5.4.2). The T_g values are slightly higher than for the blackcurrant powder, because the glass transition temperature is 3˚C above the T_g value of the blackcurrant at zero water activity. This trend continues until a water activity of 0.43, where the T_g value of the kiwifruit concentrate powder is only 1˚C higher than the blackcurrant juice powder. The glass transition temperature decreases by 15˚C from 0 to 0.11 water activity, by 12˚C from 0.11 to 0.22 water activity, by 16˚C from 0.23 to 0.32 water activity and by 16˚C from 0.32 to 0.43 water activity. The T_g depression is marginally higher for the kiwifruit powder than for the blackcurrant powder observed from a 0.11 to 0.22 water activity.

Table 5.4.2. Glass transition temperature of kiwifruit juice powder at different water activities.

Kiwifruit 1st transition

Water activity	T_g mid (˚C)	Onset (˚C)	Offset (˚C)	Width (˚C)
0	37.3 ± 0.2	33.2 ± 0.3	41.4 ± 0.3	8.3 ± 0.5
0.11	21.9 ± 0.2	16.9 ± 0.2	27.0 ± 0.4	10.1 ± 0.4
0.22	10.4 ± 0.6	4.4 ± 0.2	16.4 ± 0.9	11.9 ± 0.8
0.32	-5.7 ± 0.7	-9.8 ± 0.6	-1.5 ± 0.8	8.3 ± 0.2
0.43	-21.2 ± 0.1	-24.7 ± 0.1	-17.7 ± 0.1	6.9 ± 0.2

Average ± SD, n=3, storage temperature 30˚C

The visual changes in kiwifruit powder (Figure 5.4.4) are also very similar to those seen for blackcurrant juice powder. The particles agglomerate at a water activity of 0.11, then spread out further at water activities of 0.22 and 0.32, until they turn into a complete syrup at a water activity of 0.43.

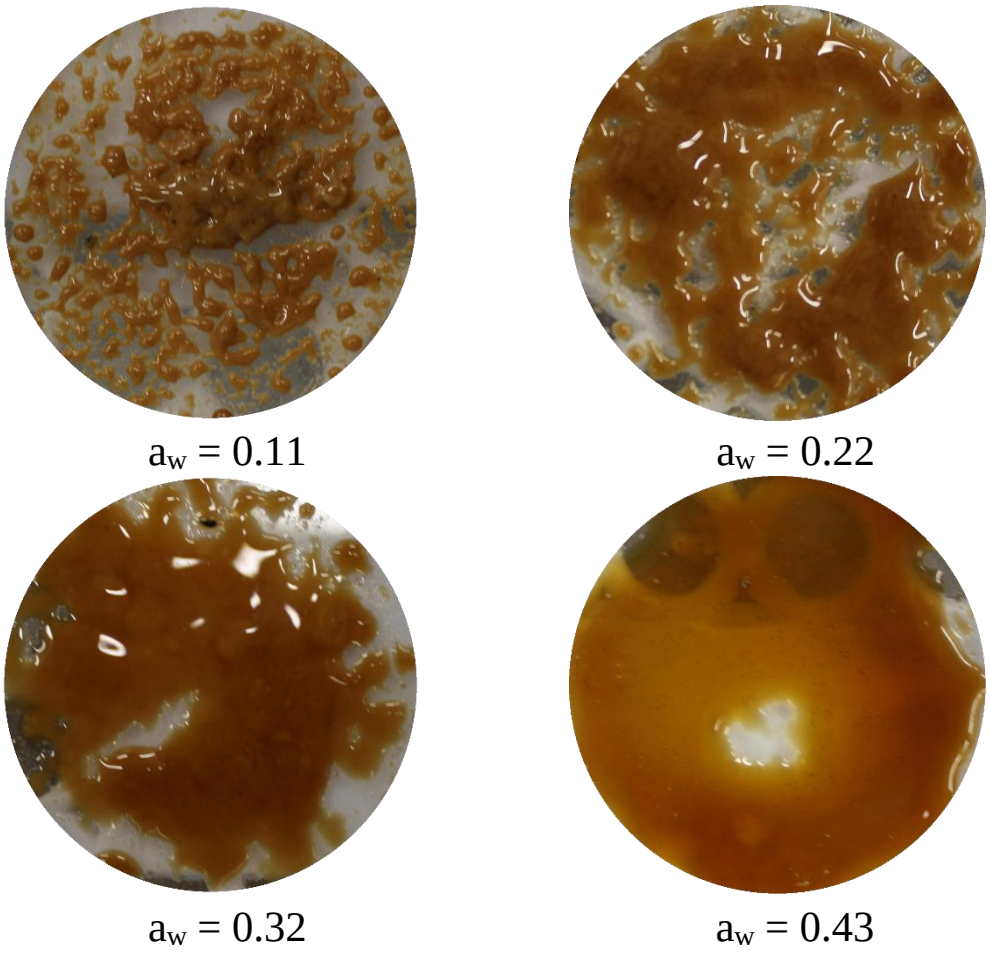


Figure 5.4.4. Visual changes in kiwifruit juice powder stored at 30˚C at different relative humidities.

As expected, the predicted values on the basis of the chemical composition are underestimating the impact of moisture content on the glass transition temperature of the kiwifruit concentrate powder due to the lower predicted T_g value at zero water activity. The overall prediction agrees slightly better than for the blackcurrant juice powder, with an R^2 of 0.84. When the measured T_g value of the kiwifruit juice powder is used, the prediction gives an almost perfect fit with an R^2 of 0.99. Only the measured T_g value at a water activity of 0.22 seems to be higher than the predicted value (Figure 5.4.5).

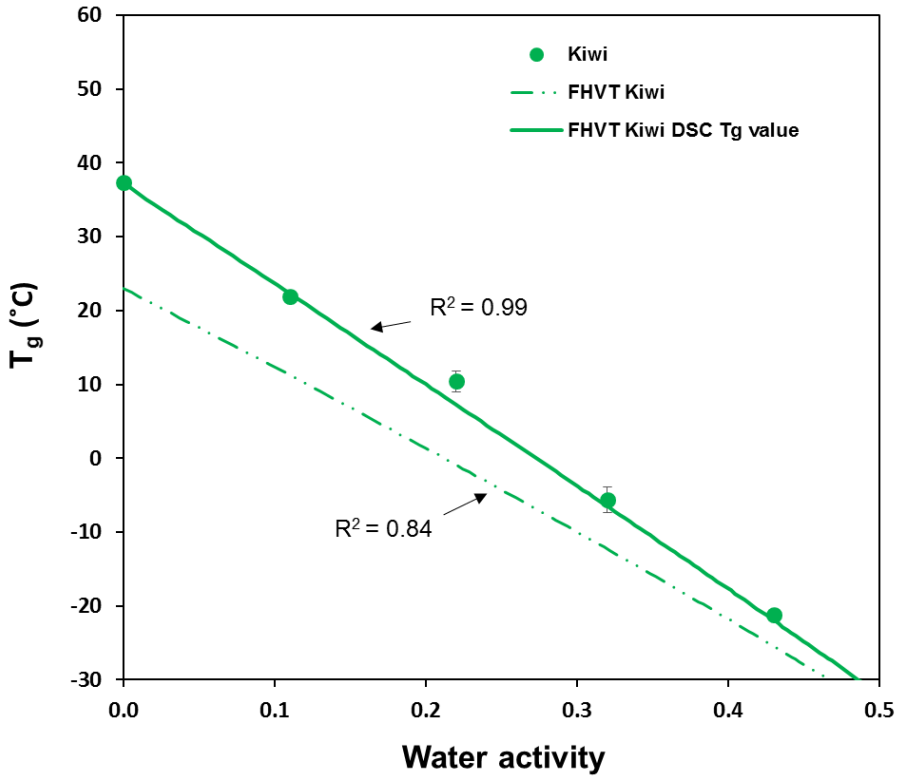


Figure 5.4.5 Prediction of the effect of water on the T_g depression of kiwifruit juice powder on basis of the chemical composition and using the DSC value of kiwifruit juice powder at zero water activity. The error bars refer to the 95% confidence interval for n=3.

5.4.4 Clear apple juice powder

The T_g values of the clear apple juice powder show a different T_g trend than the previously described powders. The glass transition temperature of the clear apple concentrate decreases by only 8˚C between 0 to 0.11 water activity (Table 5.4.3) which is a much smaller decrease than for the previously described powders. It decreases by 14˚C from 0.11 to 0.22 water activity, by 18˚C from 0.23 to 0.32 water activity and by 14˚C from 0.32 to 0.43 water activity. At the higher water activities the behaviour agrees well with the trend seen for the previous powders.

Table 5.4.3. Glass transition temperature of clear apple juice powder at different water activities.

Clear apple 1st transition

Water activity	T_g mid (˚C)	Onset (˚C)	Offset (˚C)	Width (˚C)
0	29.6 ± 1.0	25.0 ± 1.3	34.4 ± 0.6	9.4 ± 0.7
0.11	21.9 ± 0.9	16.8 ± 1.0	27.1 ± 0.8	10.3 ± 0.3
0.22	8.0 ± 1.8	0.9 ± 1.3	15.1 ± 2.4	14.1 ± 1.2
0.32	-10.1 ± 0.8	-13.9 ± 0.6	-6.3 ± 0.9	7.6 ± 0.3
0.43	-24.2 ± 0.4	-27.0 ± 0.3	-21.4 ± 0.6	5.7 ± 0.3

Average ± SD, n=3, storage temperature 30˚C

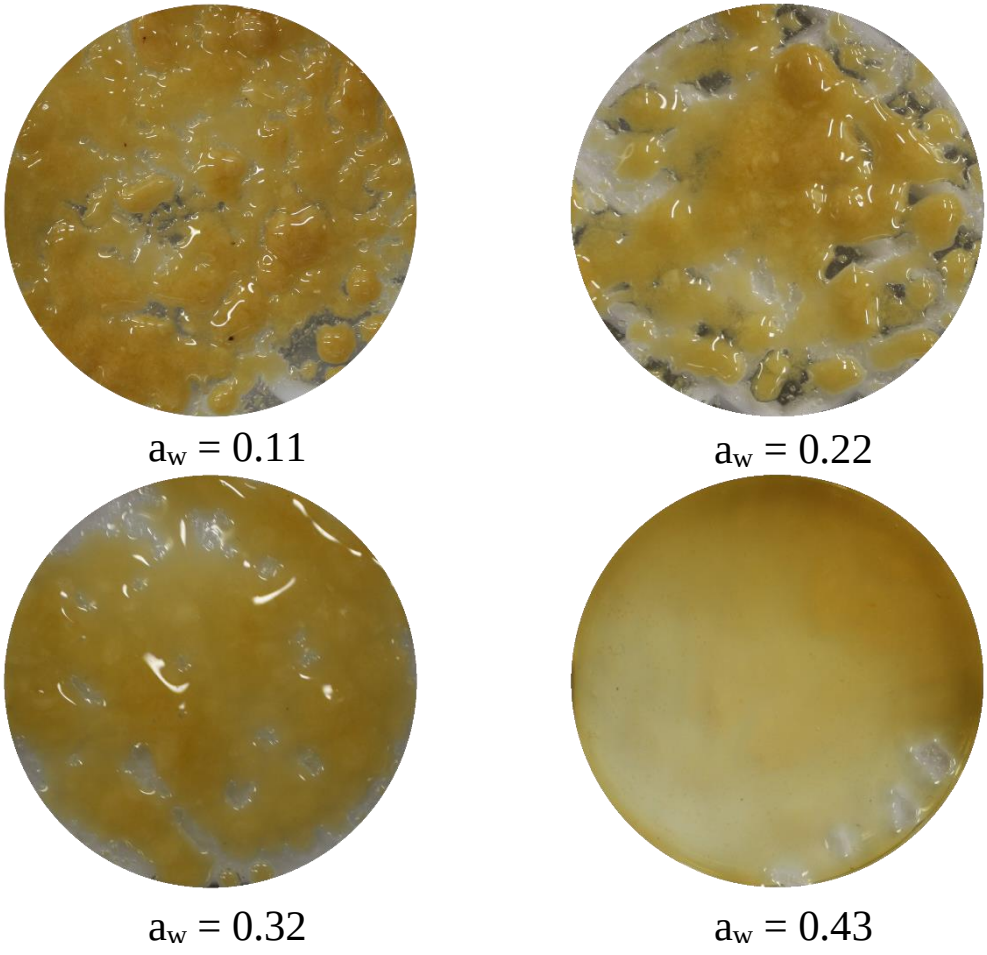


Figure 5.4.6. Visual changes of clear apple juice powder stored at 30˚C at different relative humidities.

The clear apple juice powder appears to be more liquefied at a water activity of 0.11 (Figure 5.4.6). It is harder to differentiate between the individual particles. At the other water activities the same visual changes as for the previous powders can be seen. The predicted values based on the sugar and organic acid composition match the measured values more closely for clear apple concentrate powder since the glass transition temperature of the predicted and measured powder at zero water activity are much closer as seen in (Table 5.4.3 and Figure 5.4.7) with an R^2 of 0.87. By using the measured value of clear apple concentrate powder the prediction can be improved to a fit of R^2 of 0.97. The overall fit is a bit lower than the other powders, this is due to the higher measured T_g values at a water activity of 0.11 and 0.22.

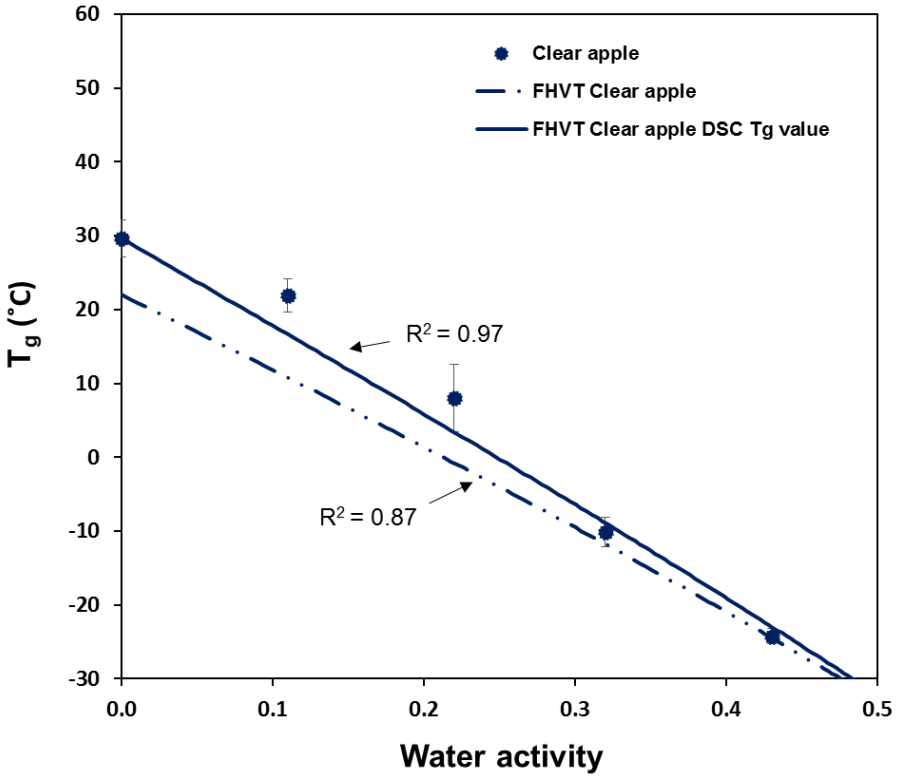


Figure 5.4.7 Prediction of the effect of water on the T_g depression of clear apple juice powder on the basis of the sugar and organic acid composition and using the DSC value of clear apple juice powder at zero water activity. The error bars refer to the 95% confidence interval for n=3.

5.4.5 Cloudy apple juice powder

The cloudy apple juice powder shows the same trend as the kiwifruit and blackcurrant powders. The observed decrease of 11˚C from 0 to 0.11 water activity from the original 28.15˚C to 16.99˚C for cloudy apple juice powder would have been expected for the clear apple juice concentrate powder as well, as it corresponds well to the linear trend seen for the other juice powders (Table 5.4.4). The T_g value drops by 14˚C from 0.11 to 0.22 water activity, by 13˚C from 0.22 to 0.32 water activity and by 14˚C from 0.32 to 0.43 water activity, which shows that the change in T_g between the various water activities is almost identical.

Table 5.4.4. Glass transition temperature of cloudy apple juice powder at different water activities.

Cloudy apple 1st transition

Water activity	T_g mid (˚C)	Onset (˚C)	Offset (˚C)	Width (˚C)
0	28.2 ± 0.2	24.4 ± 0.3	32.2 ± 0.1	7.7 ± 0.4
0.11	16.9 ± 0.5	11.2 ± 0.5	20.9 ± 2.4	9.8 ± 2.0
0.22	2.5 ± 1.0	-1.9 ± 0.8	7.2 ± 1.2	9.2 ± 0.4
0.32	-10.9 ± 0.3	-14.5 ± 0.4	-7.3 ± 0.1	7.1 ± 0.3
0.43	-24.7 ± 0.1	-27.3 ± 0.1	-22.1 ± 0.2	5.2 ± 0.2

Average ± SD, n=3, storage temperature 30˚C

The visual alterations are quite different from the previously discussed powders. It has to be noted that the other juices were clarified and do not contain any haze or other cloudy particles. The cloudy apple juice powder seemingly does not change physically from the water activity of 0.11 to 0.22 (Figure 5.4.8).

At these relative humidity levels the powder is already sticky and forms large agglomerates. At a water activity of 0.32 the bigger particles shrink together and at a water activity of 0.43 the powder turns into a syrup. Due to the cloudy particles the whole structure still keeps part of its structure and does not spread out like the powders of the clarified juices do.

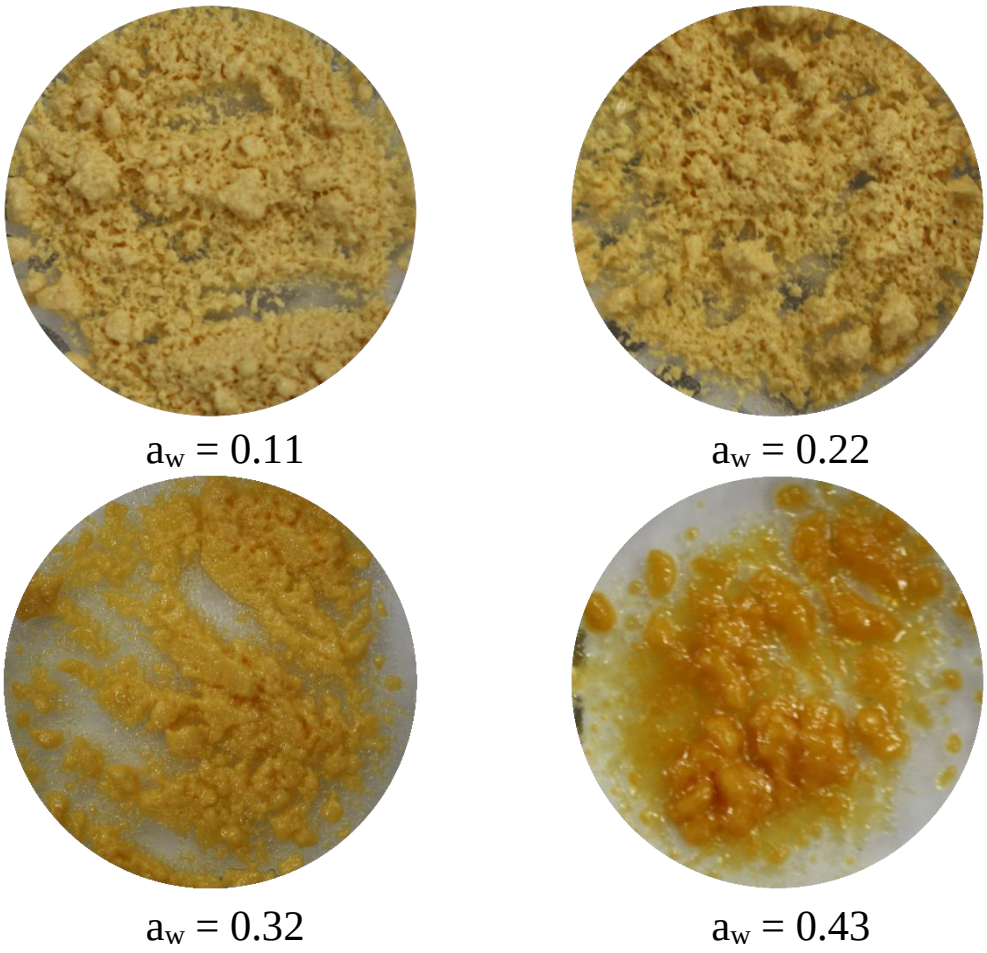


Figure 5.4.8. Visual changes in cloudy apple juice powder stored at 30˚C at different relative humidities.

As can be seen in Figure 5.4.9 both predictions show good agreement to the other experimental data, since the difference between the predicted and measured T_g value of clear concentrate powder at zero water activity is very similar and therefore the R^2 of the prediction on basis of composition is 0.91 and utilizing the measured T_g value is 0.99.

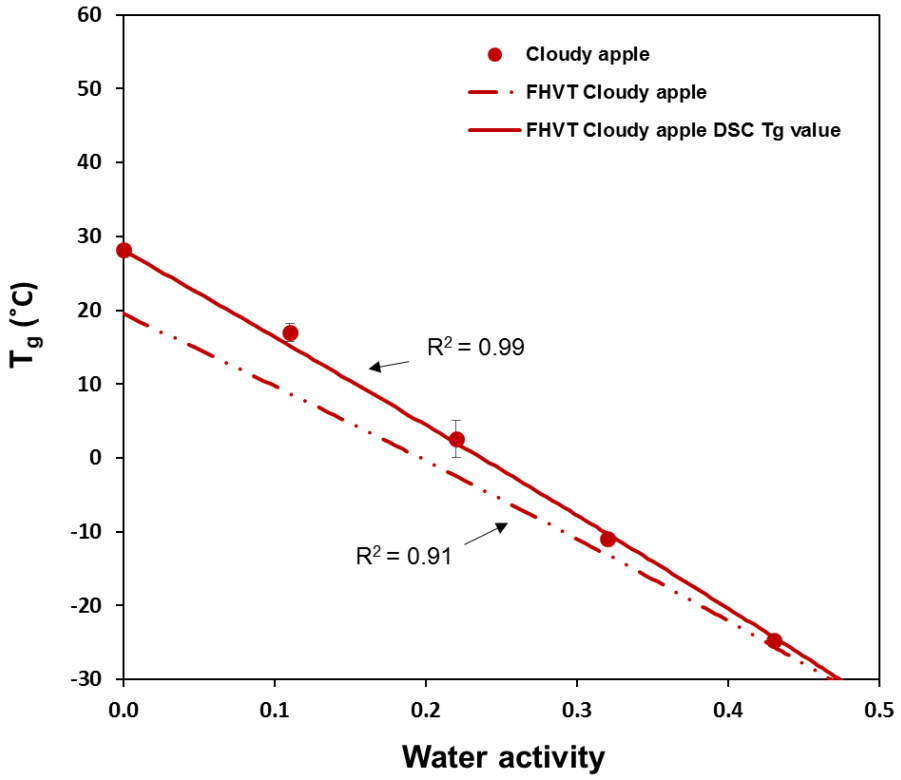


Figure 5.4.9. Prediction of the effect of water on the T_g depression of cloudy apple juice powder on the basis of the sugar and organic acid composition and using the DSC value of cloudy apple juice powder at zero water activity. The error bars refer to the 95% confidence interval for n=3.

5.4.6 Lemon juice powder

The lemon juice powder shows the lowest T_g values of all the fruit powders, since it exhibits the lowest glass transition temperature of 26.46˚C at zero water activity. The T_g decrease between the different water activities is very similar with a 14˚C decrease from 0 to 0.11, 11˚C from 0.11 to 0.22, 12˚C from 0.22 to 0.32 and 13˚C from 0.32 to 0.43 (Table 5.4.5). With these changes in the T_g values, the lemon juice powder behaves exactly as the other juice powders.

Table 5.4.5. Glass transition temperature of lemon juice powder at different water activities.

	Lemon			
Water activity	**T_g mid (˚C)**	**Onset (˚C)**	**Offset (˚C)**	**Width (˚C)**
0	26.5 ± 0.2	22.8 ± 0.1	30.3 ± 0.2	7.6 ± 0.1
0.11	12.2 ± 0.5	7.2 ± 0.6	17.2 ± 0.4	9.9 ± 0.3
0.22	0.7 ± 0.5	-4.2 ± 0.5	5.7 ± 0.6	9.9 ± 0.1
0.32	-10.9 ± 0.1	-14.9 ± 0.2	-6.7 ± 0.1	8.3 ± 0.2
0.43	-23.5 ± 0.1	-26.7 ± 0.2	-20.4 ± 0.1	6.3 ± 0.3

Average ± SD, n=3, storage temperature 30˚C

Similar to the cloudy apple juice powder, the lemon juice powder keeps the particle resemblance between a water activity of 0.11 and 0.22 (Figure 5.4.10). At a water activity of 0.32 it starts to agglomerate into bigger lumps and at a water activity of 0.43 the surface of lemon juice powder exhibits a damped look, which indicates the transition into a syrup.

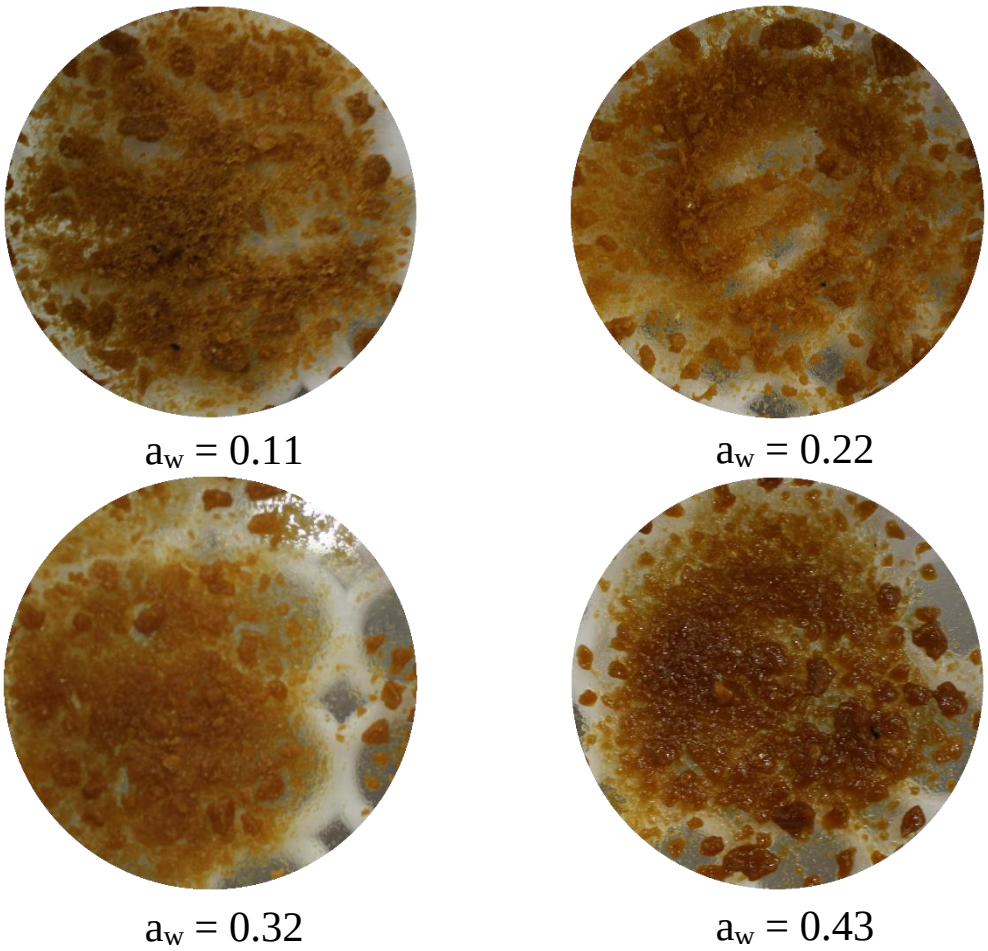


Figure 5.4.10. Visual changes in lemon juice powder stored at 30˚C at different humidities.

The prediction of the lemon juice powder is reasonable (Figure 5.4.11); even the estimates on the basis of the sugar and organic acid composition are in reasonable agreement with the experimental values, especially at the higher water activities of 0.32 and 0.43 with an overall R^2 of 0.84. The larger error arises again from the larger difference of 12˚C for the predicted and measured T_g values of the lemon juice powder. As soon as the measured T_g value is utilized in the prediction the R^2 reaches 0.99.

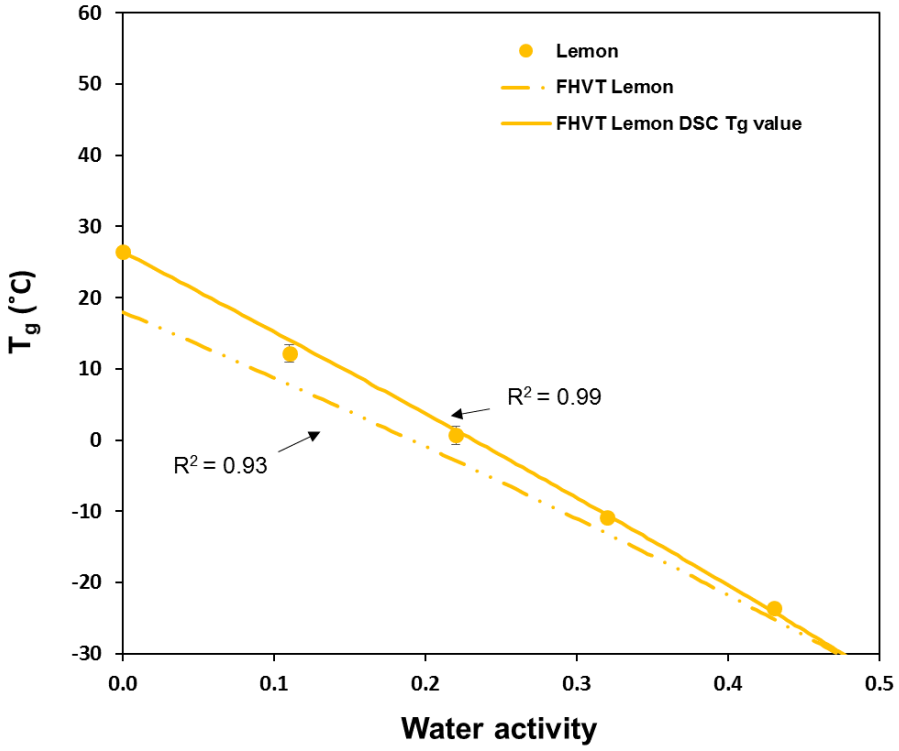


Figure 5.4.11. Prediction of the effect of water on the T_g depression of lemon juice powder on the basis of the sugar and organic acid composition and using the DSC value of clear apple concentrate powder at zero water activity. The error bars refer to the 95% confidence interval for n=3.

5.4.7 Carrot juice powder

Compared with the fruit powders, the vegetable carrot contains a much higher fraction of sucrose and lower amounts of organic acids, therefore the glass transition temperature of carrot juice powder is around 20˚C above the juice powders at zero water activity. Due to the higher glass transition temperature of the carrot powder it is expected from the previous work in Chapter 4 that the decrease in glass transition temperature from 0 to 0.11 water activity would be slightly larger than for the juice powders. This is confirmed from the T_g values of the carrot juice powder at different water activities (Table 5.4.6).

The decrease in T_g value is 20.06˚C from 0 to 0.11 water activity, which is even higher than expected, but it is also the T_g value with the highest uncertainty with a standard deviation of 1.53. The T_g drops by 12˚C from 0.11 to 0.22, 13˚C from 0.22 to 0.32 and 16˚C from 0.32 to 0.43. From the water activity of 0.22 the carrot powder follows the general trend that can be observed for all the other juice powders (Table 5.4.6).

Table 5.4.6. Glass transition temperature of carrot juice powder at different water activities.

	Carrot			
Water activity	**T_g mid (˚C)**	**Onset (˚C)**	**Offset (˚C)**	**Width (˚C)**
0	50.5 ± 0.3	45.6 ± 0.4	55.7 ± 0.2	10.2 ± 0.2
0.11	30.5 ± 1.5	25.1 ± 1.2	35.8 ± 1.9	10.7 ± 0.7
0.22	18.7 ± 0.3	12.5 ± 0.4	24.9 ± 0.2	12.4 ± 0.2
0.32	5.9 ± 0.9	0.4 ± 0.6	11.6 ± 1.2	11.1 ± 0.6
0.43	-10.6 ± 0.5	-15.3 ± 0.5	-5.8 ± 0.5	9.5 ± 0.4

Average ± SD, n=3, storage temperature 30˚C

Due to the overall higher glass transition temperature the powder is more stable at a water activity of 0.11 and did not fully pass over into the rubbery state, so the individual particles are still visible (Figure 5.4.12). At a water activity of 0.22 the powder is fully caked as the transition region is below the storage temperature of 30˚C. At higher moisture content levels there is noticeable colour change in the powder from a yellow colour to the typical orange associated with carrots. At higher water activities the powder loses its particle structure and forms lumps similar to the other clarified juice powders.

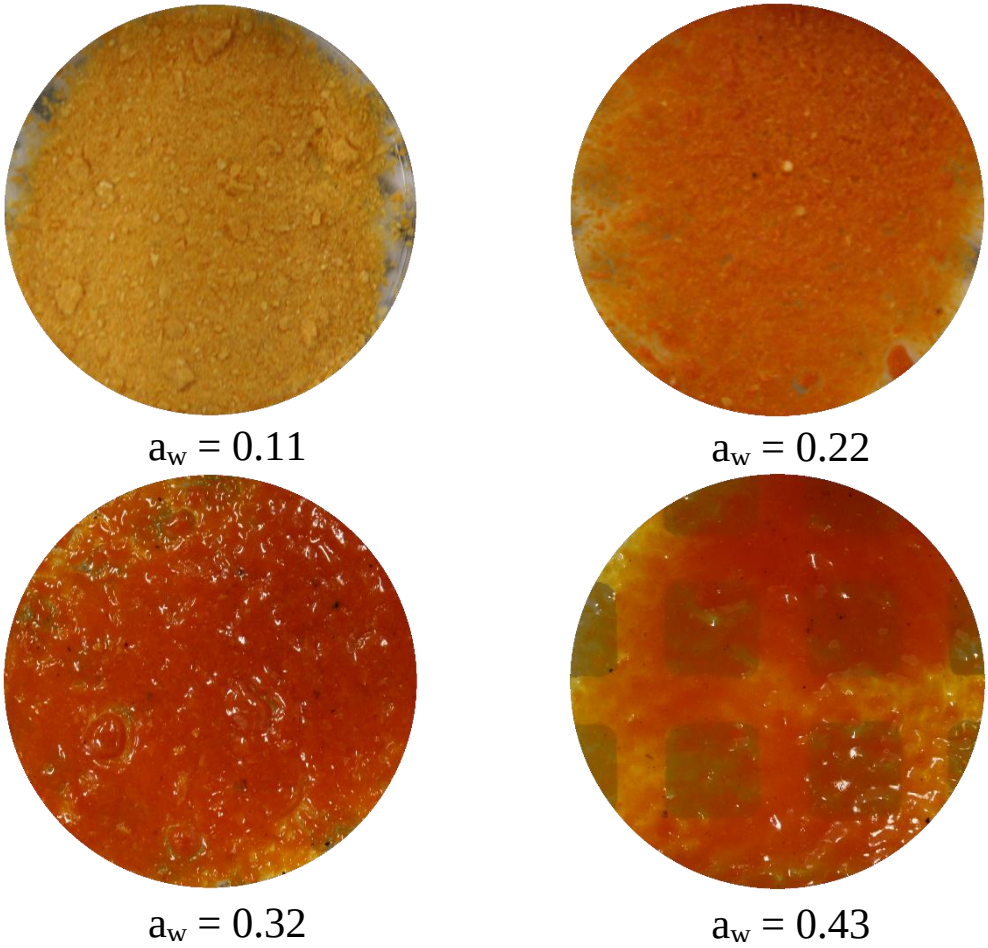


Figure 5.4.12. Visual changes in carrot juice powder stored at 30°C at different relative humidities.

The two predictions of the T_g values for the carrot juice powder agree with the experimental data with both R^2 values being above 0.9 (Figure 5.4.13). The estimated values on the basis of the sugar and organic acid composition are only slightly lower than the values using the measured glass transition temperature as a starting value for the prediction.

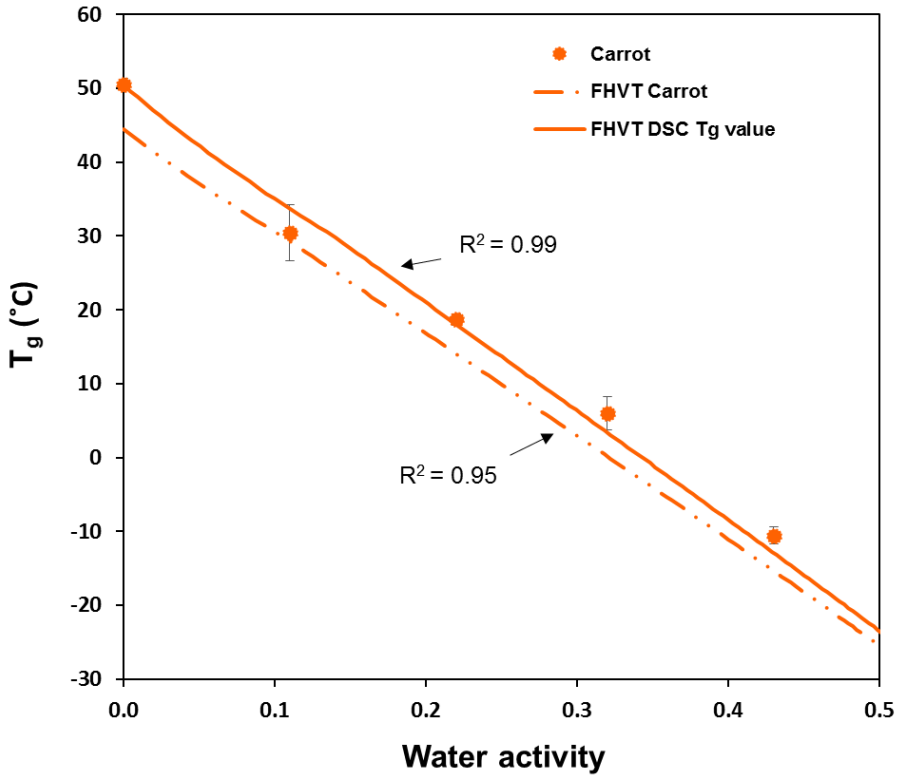


Figure 5.4.13. Prediction of the effect of water on the T_g depression of carrot juice powder on the basis of the sugar and organic acid composition and using the DSC value of clear apple concentrate powder at zero water activity. The error bars refer to the 95% confidence interval for n=3.

The study of the various pure fruit juice powders show that the measured and predicted T_g values differ slightly from each other. Carrot powder showed the lowest deviation (6˚C) from the measured T_g value, whereas the difference for blackcurrant and kiwifruit powder is around 14˚C. This shift to a higher glass transition temperature can be attributed to the presence of components such as breakdown products of mostly pectins and some other carbohydrates as explained previously. Throughout the description of the different powders and their T_g values at various water activities, it becomes clear that the accuracy of the prediction using the FHVT model is strongly dependent of the how close the estimated T_g value is to the measured T_g value at zero water activity. By considering the shift of the fruit juice powders to higher values, the overall prediction can be improved marginally. Interestingly, in the comparison of the cloudy to the clear apple juice, cloudy particles do not have any additional impact on the glass transition temperature. This could be due to the overall small amounts of cloudy particles in the juice, but it would be worthwhile to investigate whether insoluble components have an additional effect on the

glass transition temperature of fruit juice powders or other low molecular weight mixtures.

5.4.8 Second glass transition temperature

As mentioned in Section 5.3 the four fruit juice powders from blackcurrant, kiwifruit, clear apple and cloudy apple exhibit a second glass transition temperature. Furthermore, these transitions change depending on the moisture content in the sample. In Figure 5.4.14 the second glass transition temperatures of the four powders at the various water activities are presented. Considering Figure 5.4.14, it can be seen that the second transition of cloudy apple and clear apple juice powders follow almost the same trend over the different water activities. This is very likely due to the similar composition of the second amorphous phase, since the clear and cloudy apple only differs in a further clarification treatment. Similar to the first transition the values of the second transition for the clear apple powder are slightly higher than for the cloudy apple powder. Considering the cloudy apple juice powder the T_g decrease between the different water activities accounts for 6˚C from 0 to 0.11, 5˚C from 0.11 to 0.22, 5˚C from 0.22 to 0.32 and 6˚C from 0.32

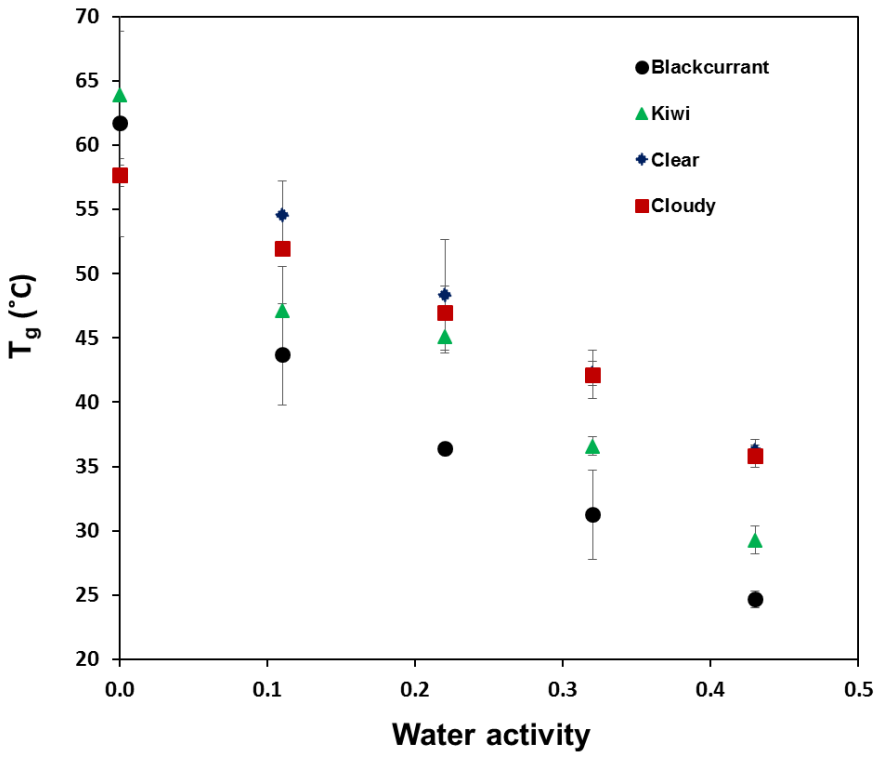


Figure 5.4.14. Second glass transition temperature of the blackcurrant, kiwi, clear apple and cloudy apple juice powders at different water activities. The error bars refer to the 95% confidence interval for n=3.

to 0.43. The overall depression of the second transition of the clear apple juice is lower in magnitude than it is the case for the first transition.

The kiwifruit and blackcurrant juice powders demonstrate a very different behaviour. Instead of a completely linear decrease of the second transition from 0 to 0.43 water activity, the value drops markedly by 18˚C and 17˚C from 0 to 0.11 water activity for blackcurrant and kiwifruit juice powder respectively. At higher water activities, these powders follow a similar trend with a continuous decrease of the transition values of about 7˚C from 0.11 to 0.22, 5˚C from 0.22 to 0.32 and 7˚C from 0.32 to 0.43. This difference could be related to different interaction with the water molecules at lower water activity, where the domain linked to the second transition observed for the kiwifruit and blackcurrant powders converts into a looser structure which exhibits a dynamic response at lower transitions and then the linear trend is shown by all powders at higher water activities

5.5 Conclusion

The study demonstrated that the plasticizing effect of water on the glass transition temperature of the juice powders follows a linear trend against water activity. The prediction of the mango powder and strawberry powder in the literature in Chapter 4 showed that low molecular weight mixtures exhibit a similar relation between the glass transition temperature and moisture content. The study of the juice powders here confirms the relationship for various kinds of juice with distinct sugar and organic acid profiles.

This study demonstrates that the prediction of the glass transition temperature of fruit powders at zero water activity is in all cases below the measured values. This is believed to be due to the combination of residual polysaccharides obtained during the juice production, which have an impact on the overall glass transition temperature of the juice solids. This is further supported by the observed second transition for certain juice powders. The comparison of the predicted and measured T_g value of the juice powders utilized in the FHVT model to account for the moisture content demonstrated that the accuracy of the prediction is highly dependent of the correctness of the chosen glass transition temperature of the juice powder at zero water activity. This is especially important for the prediction at water activities below 0.22, since the total moisture content is relatively low. At higher water activity, the difference of the glass transition

temperatures does not impact the predicted values as much as the two predicted lines are close together.

The study of the fruit juices provided a better understanding of the glass transition temperature and its relation to the moisture content in these systems. It also proved that the proposed prediction approach of Chapter 4 is applicable for predicting the T_g if fruit juice powders and their storage stability at various water activities.

The next step is to validate the effect of the polysaccharide on the glass transition temperature of the fruit juice solids. Therefore various mixtures of the polysaccharide maltodextrin DE 9-13 with the individual solid components in the blackcurrant juice and blackcurrant juice itself are investigated in the next chapter.

6. Blends with maltodextrin DE 9-13

6.1 Introduction

As demonstrated in the Chapter 5, fruit juices exhibit a low glass transition temperature, making it difficult to dry them. In Chapter 4, several examples were presented in which biopolymers in the form of polysaccharides have been utilized to increase the glass transition temperature of the fruit juice solids. It was also proposed that the effect on the glass transition temperature of mixtures of low molecular weight components with increasing contents of polysaccharides always follow a very similar trend. A new method to predict the glass transition temperature of low molecular mixtures and polysaccharides was derived and successfully tested against literature values. In order to validate the method further, the common polysaccharide maltodextrin DE 9-13 was combined with the low molecular weight components, citric acid, glucose and fructose, at various ratios (7:3, 1:1, 3:7). Furthermore a mixture of one third citric acid, one third fructose and one third glucose, to imitate the sugar and organic profile of blackcurrant juice as well as real blackcurrant juice, was mixed with the same ratios of maltodextrin DE 9-13. These systems were freeze dried at 30% (solids concentration) and the solids had their glass transition temperature at zero water activity measured via the DSC. The predicted values were compared with the measured values. The powders were further stored at 30˚C and equilibrated over various saturated salt solutions to achieve the water activities of 0.11, 0.23, 0.32 and 0.43. This allowed the plasticizing effect of water on the glass transition temperature to be measured. The measured T_g values were compared with the predicted values using the FHVT model.

6.2 Glass transition temperature of anhydrous powders

The glass transition temperature of the pure components used in the study was determined by either melt quenching or freeze drying. Since the samples of fructose and citric acid collapsed during the freeze drying step, the glass transition temperature was determined via melt quenching. Anhydrous fructose and citric acid crystals were heated over their melting peak (131.83˚C for fructose and 156.71˚C for citric acid), quenched and the transition in the second heating cycle was defined as the glass transition temperature. The heating and cooling rates were set constant at 10 ˚C/min. Glucose and maltodextrin DE 9-13 were freeze dried at 10% (solid concentration) and their glass transition temperatures

at zero water activity were measured via DSC. The T_g values of the pure components in Table 6.2.1 correspond well with the T_g values presented in Section 2.8.4 for low molecular weight components. The glass transition temperature of maltodextrin DE 9-13 of 175.33˚C is higher than that used in the calculations of in Chapter 3 (160˚C). Due to the nature of maltodextrin DE 9-13, being a hydrolysed product of starch, variations in the molecular size and therefore the glass transition temperature are to be expected.

Table 6.2.1. Glass transition temperature of pure components at zero water activity.

Juice	T_g mid (˚C)	Onset (˚C)	Offset (˚C)	Width (˚C)
Fructose	14.4 ± 0.4	10.9 ± 0.7	17.9 ± 0.8	7.1 ± 0.6
Glucose	38.3 ± 1.2	35.2 ± 1.5	41.5 ± 0.9	6.3 ± 0.6
Citric acid	14.3 ± 0.3	12.0 ± 0.4	16.9 ± 0.6	4.9 ± 0.8
MD DE 9-13	175.3 ± 6.8	169.7 ± 10.5	183.3 ± 6.9	13.6 ± 4.4

Average ± SD, n=3

As mentioned previously amorphous powders undergo an enthalpy recovery during the first heating cycle in the DSC due to enthalpy and volume relaxation taking placing in the glassy matrix during storage of the powders (Figure 6.2.1). It is common practice to heat

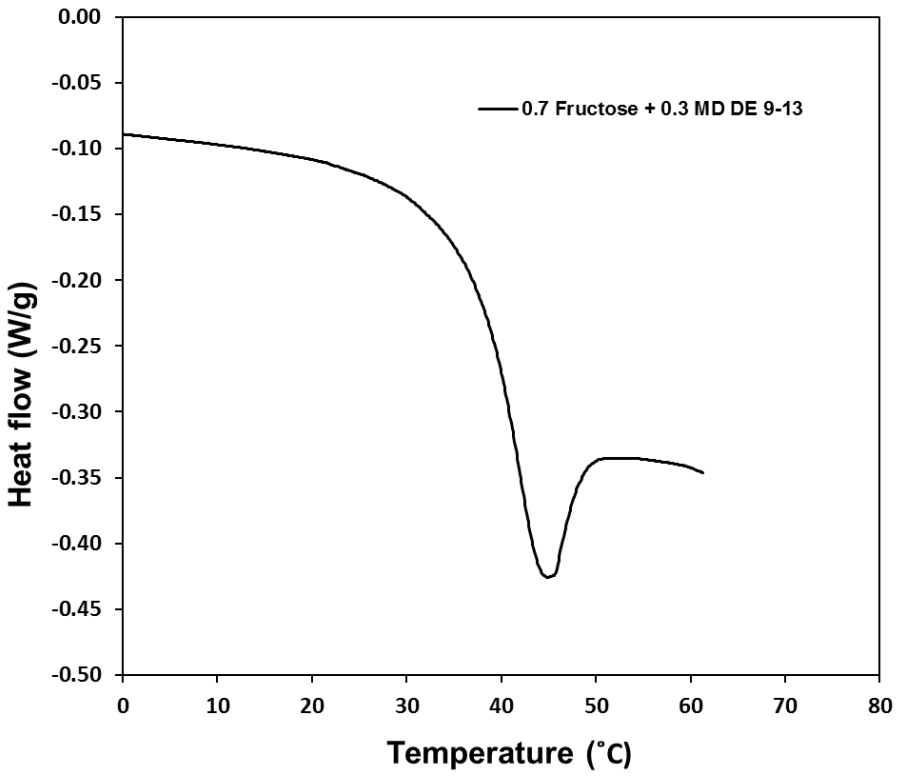


Figure 6.2.1. Enthalpy recovery peak of the powder containing 0.7 fructose and 0.3 maltodextrin DE 9-13.

the sample 20˚C above the observed enthalpy recovery peak and define the glass transition temperature as the transition midpoint or onset point in the second heating cycle. Some of the mixtures exhibited an enthalpy recovery at a higher temperature, therefore it was not clear if the final heating temperature would have an effect on the transition in the following heating cycle. Therefore, the impact of the final heating temperature on the glass transition temperature in the following heating cycle was tested by heating the samples to 70˚C, 100˚C and 130˚C. The heat flow signal for the powder containing 0.7 glucose and 0.3 maltodextrin DE 9-13 is shown in Figure 6.2.2. The

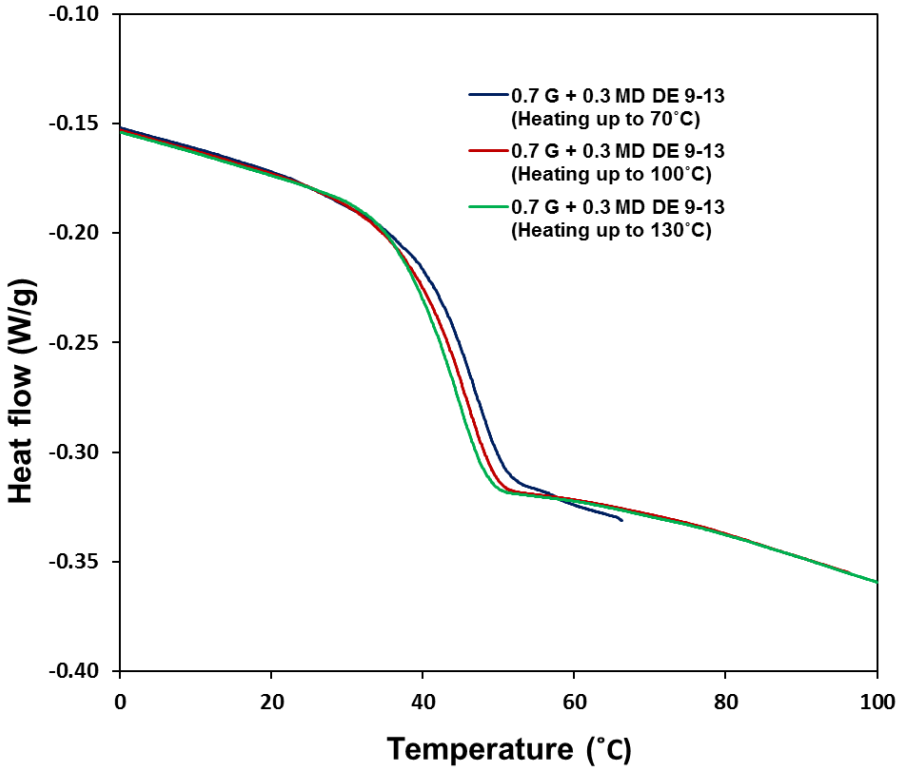


Figure 6.2.2. DSC thermogram of 0.7 glucose + 0.3 maltodextrin DE 9-13 with various final heating temperatures.

different lines represent the transitions following heating to 70˚C, 100˚C and 130˚C. As can be observed, the different final heating temperatures have only a minor effect on the transitions observed for the 0.7 glucose and 0.3 maltodextrin DE 9-13 blend (Table 6.2.2). The T_g value decreases by approximately 1.5˚C, which is reasonable as the molecules can rearrange themselves in the rubbery state and obtain a lower energy state on cooling.

Table 6.2.2. Effect of final heating temperature on the glass transition temperature of the 0.7 glucose and 0.3 maltodextrin DE 9-13 blend at zero water activity.

0.7 G + 0.3 MD DE 9-13

Final Temp.	T_g mid (˚C)	Onset (˚C)	Offset (˚C)
70˚C	45.9	40.8	51.0
100˚C	44.2	39.2	49.1
130˚C	42.8	49.3	48.1

Performing the same procedure for the blend of 0.7 fructose and 0.3 maltodextrin DE 9-13 resulted in a great change in the heat flow signal in Figure 6.2.3. The glass transition temperature of the blend after heating to 70˚C is around 30.92˚C. Heating the system an

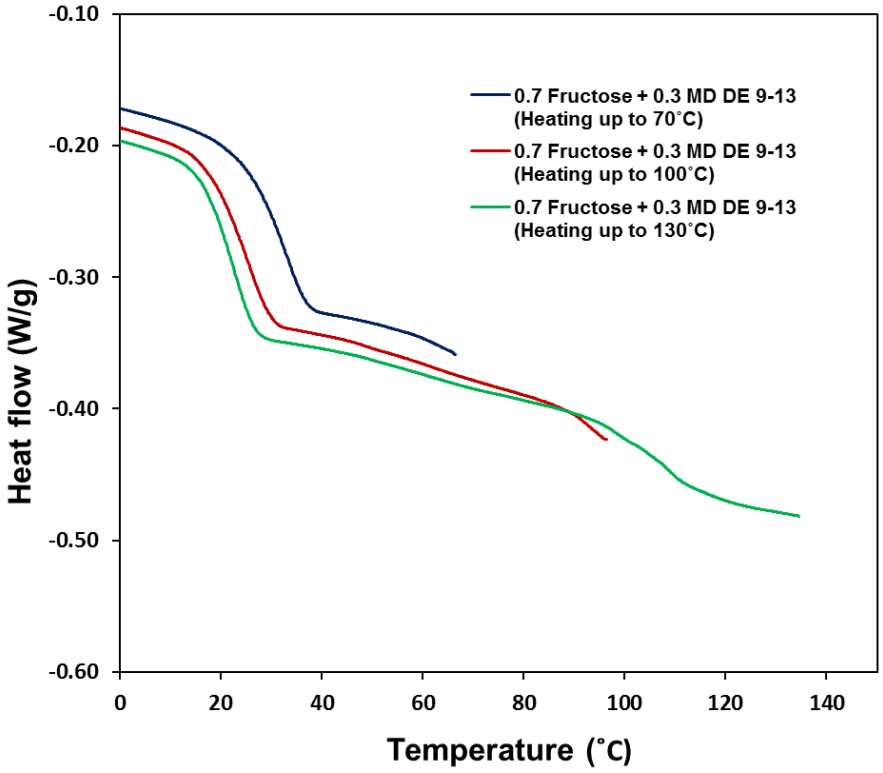


Figure 6.2.3. Heat flow signal of 0.7 fructose + 0.3 maltodextrin DE 9-13 with various final heating temperatures.

additional 30˚C to a final temperature of 100˚C results in a T_g drop of 7.44˚C to a T_g value of 23.48˚C (Table 6.2.3). A further increase in the final heating temperature to 130˚C has a smaller effect on the shift of the glass transition temperature. The heating temperature showed no effect on the colour of the sample, which excludes reactions taking place between the components. Interestingly, the heat flow signal after heating the sample to 130˚C showed that a second phase indicates that the increased final heating temperature

could produce a phase separation of the blend, resulting in a phase richer in maltodextrin DE 9-13 and another phase dominant in fructose molecules.

Table 6.2.3. Effect of final heating temperature on the glass transition temperature of the 0.7 fructose and 0.3 maltodextrin DE 9-13 blend at zero water activity.

0.7 F + 0.3 MD DE 9-13

Final Temp.	T_g mid (˚C)	Onset (˚C)	Offset (˚C)
70˚C	30.9	25.2	36.8
100˚C	23.5	18.2	28.9
130˚C	21.3	16.6	25.9

For the mixture of glucose, fructose and citric acid with maltodextrin DE 9-13, the effect of the final heating temperature was evident as well (Figure 6.2.4). The T_g value was originally at 35.84˚C after heating the sample to 70˚C and the T_g value dropped to 30.49˚C

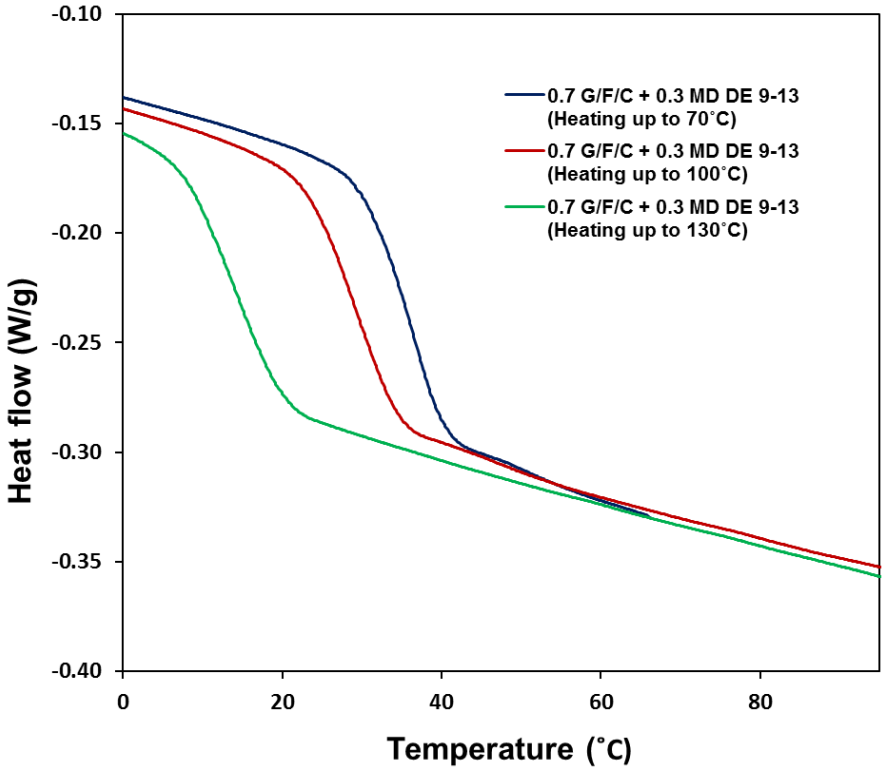


Figure 6.2.4. Heat flow signal of 0.7 G/F/C + 0.3 maltodextrin DE 9-13 with various final heating temperatures.

after further heating to 100˚C (Table 6.2.4). This is a shift of 5.35˚C, which is not as pronounced as for the fructose and maltodextrin DE 9-13 blend, but is much higher than the shift seen in the glucose and maltodextrin DE 9-13 system.

No signs of a phase separation are apparent, however the strong shift of the transition after heating the sample to 130˚C could be explained by some reactions of the sugars and organic acids, as evidenced by an observed slight colour change of the sample.

Table 6.2.4. Effect of final heating temperature on the glass transition temperature of the 0.7 G/F/C and 0.3 maltodextrin DE 9-13 blend at zero water activity.

0.7 G/F/C + 0.3 MD DE 9-13

Final Temp.	T_g mid (˚C)	Onset (˚C)	Offset (˚C)
70˚C	35.8	31.1	40.7
100˚C	30.5	24.6	36.4
130˚C	13.8	7.3	20.3

The combination of 0.7 citric acid and 0.3 maltodextrin DE 9-13 followed the same trend as the 0.7 glucose and 0.3 maltodextrin DE 9-13 blend and no strong shifts to lower transition temperatures can be observed. On the other hand, the blackcurrant powder with 0.7 blackcurrant and 0.3 maltodextrin DE 9-13 illustrates the same behaviour as the mixture of glucose, fructose and citric acid with maltodextrin DE 9-13 (data not shown). Similar to the blends high in low molecular weight components, the effect of the final heating temperature can be noticed in the powders with 0.5 weight fraction of maltodextrin DE 9-13 as well. For the systems with 0.7 weight fraction maltodextrin DE 9-13 it is impossible to stay below 100˚C, otherwise the enthalpy recovery cannot be removed completely from the sample. This study of the final heating temperatures regarding the different blends demonstrates that care has to be taken when choosing the appropriate final heating temperature, especially for the substances containing high fractions of fructose or combinations of sugars and organic acids. For the different powders the final heating temperature was set to 70˚C for powders with 0.3 and 0.5 weight fraction of maltodextrin DE 9-13 to avoid any shifts in the glass transition temperature.

6.2.1 Prediction of T_g values of the maltodextrin DE 9-13 blends

The glass transition temperatures of the different powders with various weight fractions of maltodextrin DE 9-13 (0.3, 0.5 and 0.7) are illustrated in Figure 6.2.5. The predicted T_g values are presented in Table 6.2.5 and the corresponding measured T_g values are shown in Table 6.2.6, which are in a very good agreement to the measured values as demonstrated in Figure 6.2.5.

Table 6.2.5. Predicted T_g values of the different components with various weight fractions of maltodextrin DE 9-13 at zero water activity.

	Prediction of T_g of powders at a_w=0 (˚C)				
MD fraction	**Glucose**	**Citric acid**	**Fructose**	**G/F/C**	**Blackcurrant**
0.3	51	27	29	35	48
0.5	64	41	44	49	61
0.7	89	70	73	77	87
R^2	0.98	0.97	0.95	0.99	0.99

The measured T_g values for the glucose and maltodextrin DE 9-13 blend are ca. 5˚C lower than the predicted T_g value for a weight fraction of maltodextrin DE 9-13 below 0.7. The T_g value at 0.7 weight fraction of maltodextrin DE 9-13 conforms with the predicted T_g value. This overestimation of the T_g was expected, since the prediction method is based on the average fitted coefficients A_0 and A_1, which have been shown to overestimate T_g values of the glucose and maltodextrin DE 6 blend as discussed in Section 4.2. Although, the predicted T_g values for the glucose and maltodextrin system are slightly overestimated, the overall trend of the effect of maltodextrin DE 9-13 on the T_g values is recognizable.

The predicted T_g values of the citric acid and maltodextrin DE 9-13 blend are in alignment with the T_g values for lower concentrations of maltodextrin DE 9-13 in the system.

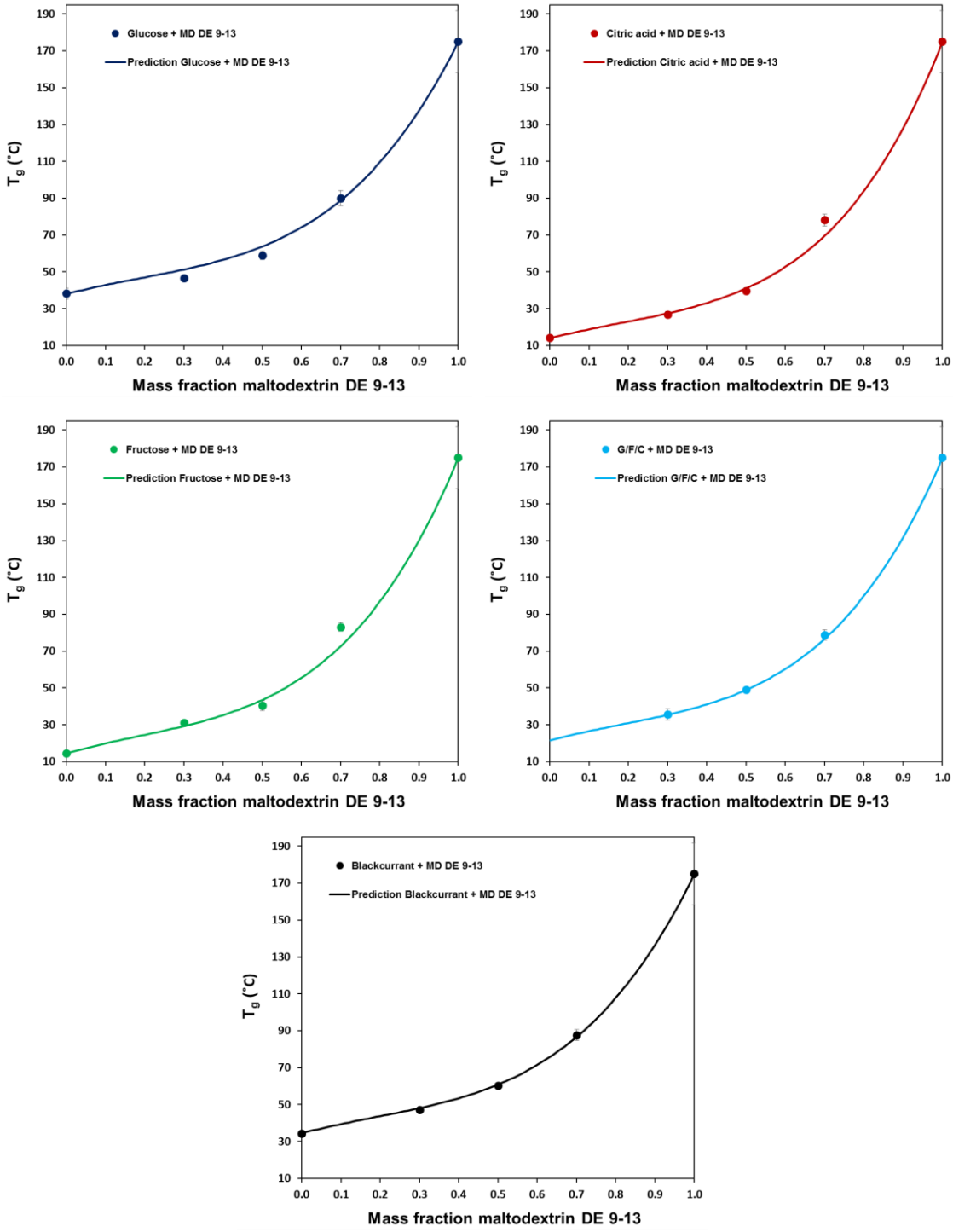


Figure 6.2.5. Predicted and measured T_g values of various blends with various ratios of maltodextrin DE 9-13 at zero water activity. The error bars refer to the 95% confidence interval for n=3.

The measured T_g value at 0.7 weight fraction of maltodextrin DE 9-13 is ca. 8˚C higher than the predicted values.

The same is true for the fructose and maltodextrin DE 9-13 mixture, i.e. the predicted T_g value at high concentrations of maltodextrin DE 9-13 has a difference between the measured and predicted T_g value of ca. 10˚C. The measured T_g values are more scattered for the fructose and maltodextrin DE 9-13 mixture than for the other blends, thus its obtained R^2 of 0.95 is the lowest for all the mixtures.

The multicomponent system of the mixture of glucose, fructose and citric acid (G/F/C) and blackcurrant juice with maltodextrin DE 9-13 shows the best agreement of the measured and predicted T_g values with a difference of ca. 1–2˚C. It appears that the small differences seen in blends of the individual components with maltodextrin DE 9-13 balance each other out in the multicomponent systems and the systems follows nearly perfectly the predicted T_g line.

The trend of the midpoint T_g values of the maltodextrin DE 9-13 blends has been discussed, but studying the values given in Table 6.2.6 a change in the width of the transition with increasing maltodextrin DE 9-13 concentration is noticeable. For the pure components the width of the transition is narrow, with a range of ca. 5 to 8˚C. An increase of weight fraction of maltodextrin DE 9-13 to 0.3 has only a minor effect on the width seen in the DSC heat flow signal, except for the blackcurrant juice, where the range is around 18˚C instead of the 10˚C as for the other systems. At 0.5 weight fraction the transition width is between 13˚C for the fructose and maltodextrin DE 9-13 and 24˚C of citric acid and maltodextrin DE 9-13. With an increase to 0.7 weight fraction of maltodextrin DE 9-13 in the various mixtures the width of the transition raises to between 43˚C and 53˚C.

Table 6.2.6. Measured T_g values of the different components with various ratios of maltodextrin DE 9-13 at zero water activity.

Fraction	T_g mid (˚C)	Onset (˚C)	Offset (˚C)	Width (˚C)
Glucose	38.2 ± 1.2	35.2 ± 1.5	41.5 ± 0.9	6.3 ± 0.6
0.7 G + 0.3 MD	46.8 ± 0.4	42.1 ± 0.3	51.5 ± 1.0	9.4 ± 1.2
0.5 G + 0.5 MD	58.9 ± 1.0	48.0 ± 0.6	69.8 ± 1.6	21.8 ± 1.3
0.3 G + 0.7 MD	90.0 ± 1.7	69.1 ± 1.8	111.1 ± 4.7	42.1 ± 6.2

Average ± SD, n=3

Fraction	T_g mid (˚C)	Onset (˚C)	Offset (˚C)	Width (˚C)
Citric acid	14.3 ± 0.3	12.0 ± 0.4	16.9 ± 0.6	4.9 ± 0.8
0.7 C + 0.3 MD	26.9 ± 0.7	21.7 ± 0.9	32.4 ± 0.7	10.7 ± 1.0
0.5 C + 0.5 MD	39.6 ± 0.7	27.6 ± 1.7	51.6 ± 0.6	24.0 ± 1.0
0.3 C + 0.7 MD	78.2 ± 1.3	55.0 ± 1.9	101.4 ± 3.1	46.4 ± 4.3

Average ± SD, n=3

Fraction	T_g mid (˚C)	Onset (˚C)	Offset (˚C)	Width (˚C)
Fructose	14.4 ± 0.4	10.9 ± 0.7	17.9 ± 0.8	7.1 ± 0.6
0.7 F + 0.3 MD	31.0 ± 0.5	25.6 ± 0.7	36.6 ± 0.3	10.9 ± 0.7
0.5 F + 0.5 MD	40.4 ± 1.1	33.8 ± 1.1	47.0 ± 0.5	13.2 ± 2.8
0.3 F + 0.7 MD	83.2 ± 1.0	59.4 ± 2.1	108.8 ± 0.3	49.4± 2.2

Average ± SD, n=3

Fraction	T_g mid (˚C)	Onset (˚C)	Offset (˚C)	Width (˚C)
0.7 G/F/C + 0.3MD	35.7 ± 1.2	30.7 ± 0.8	40.9 ± 1.7	10.3 ± 0.9
0.5 G/F/C + 0.5MD	49.1 ± 0.4	40.5 ± 0.3	57.7 ± 0.7	17.2 ± 0.7
0.3 G/F/C + 0.7MD	78.7 ± 1.1	54.8 ± 1.6	102.7 ± 4.0	47.9 ± 5.6

Average ± SD, n=3

Fraction	T_g mid (˚C)	Onset (˚C)	Offset (˚C)	Width (˚C)
Blackcurrant	34.5 ± 0.1	30.5 ± 0.6	38.4 ± 0.4	7.9 ± 1.0
0.7 BL + 0.3 MD	47.1 ± 0.3	38.1 ± 0.3	56.1 ± 0.5	18.0 ± 0.7
0.5 BL + 0.5 MD	60.2 ± 0.5	49.8 ± 1.9	70.6 ± 1.0	20.7 ± 2.9
0.3 BL + 0.7 MD	87.7 ± 1.2	60.9 ± 1.9	114.1 ± 1.0	53.2 ± 2.1

Average ± SD, n=3

The rapid increase of the width of the DSC signal becomes evident by Figure 6.2.6. At high concentrations of fructose the transition follows the sharp step change typically seen for all low molecular weight components (Table 6.2.6). With the increase of the concentration of maltodextrin DE 9-13 in the system the signal starts to become broader and at a weight fraction of 0.7 the transition covers a range of ca. 49.37˚C.

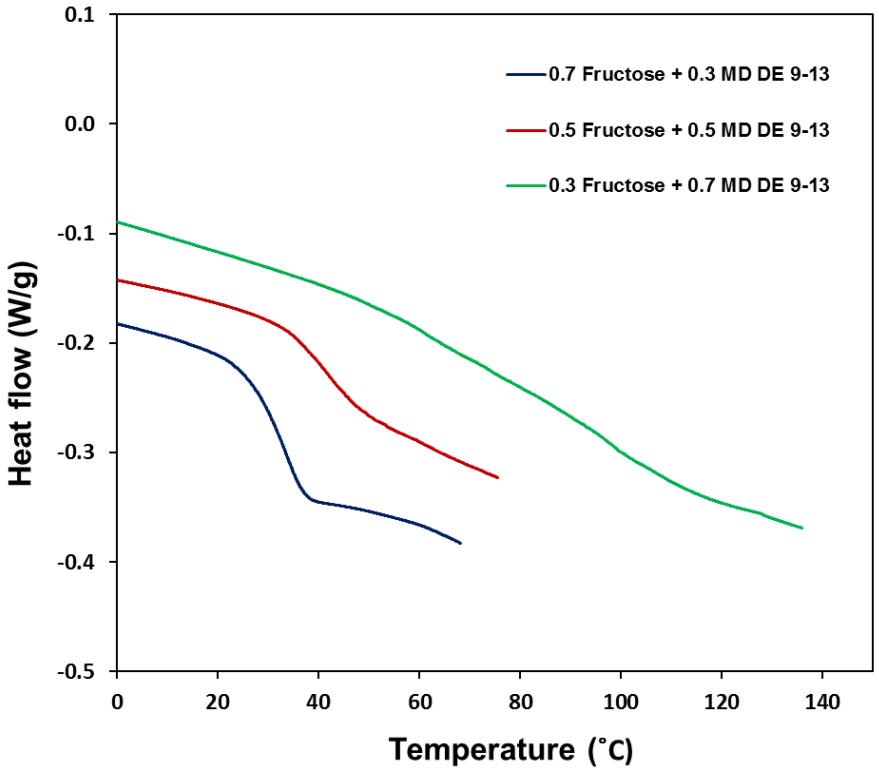


Figure 6.2.6. DSC heat flow signal of fructose and maltodextrin DE 9-13 blends with various ratios.

This broad signal leads to a great gap between the measured onset and midpoint for the glass transition temperature. Figure 6.2.7 illustrates the different onset, offset and midpoint T_g values for the various fructose and maltodextrin DE 9-13 blends. The solid line represents the predicted T_g values for the midpoint of the different mixtures. It can

be observed that the width of the gap between the onset and end points is smaller up to a weight fraction of 0.7.

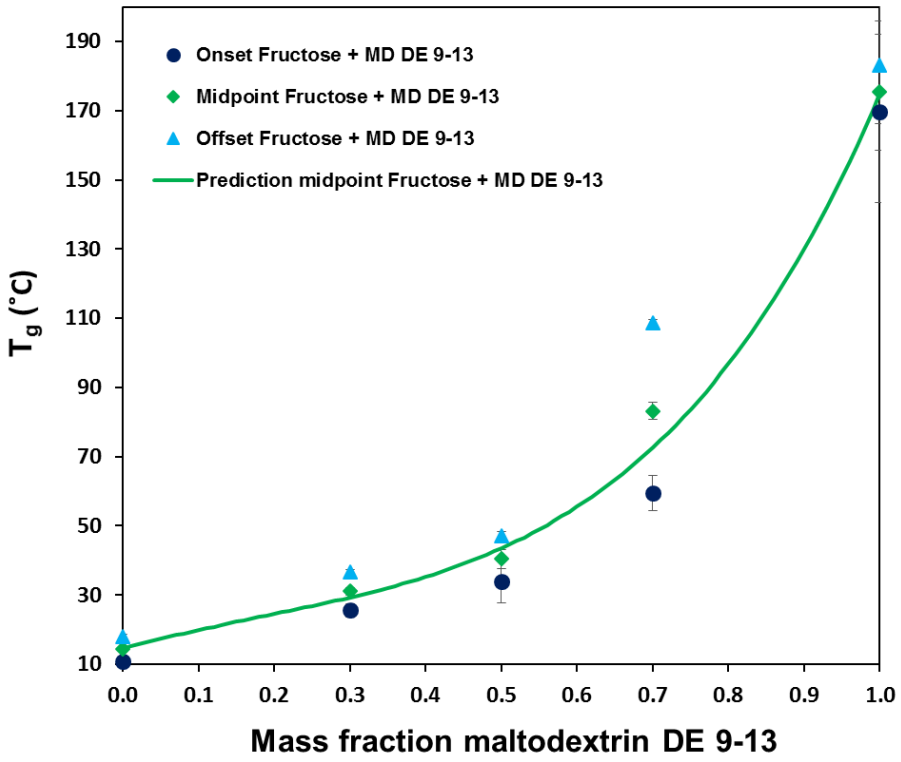


Figure 6.2.7. Onset, offset and midpoint T_g data for the fructose and maltodextrin DE 9-13 blends at zero water activity. The error bars refer to the 95% confidence interval for n=3.

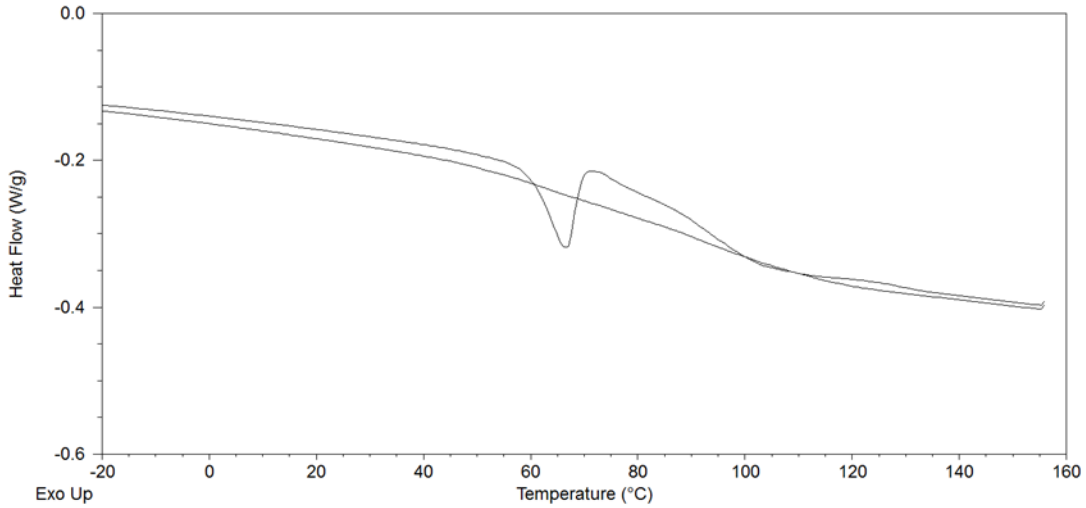
6.2.2 Dynamic heterogeneity in maltodextrin DE 9-13 blends

In Section 2.6.1, the two studies by Icoz et al. (2005) and Kawai and Hagura (2012) are discussed in detail. Both studies show the effect of mixing components with different molecular weights on the DSC heat flow signal. Icoz et al. (2005) demonstrated when mixing two dextrans with molecular weights of 970 Da and 2000 kDa that the DSC signal of the blend resembled the DSC signal of the 970-Da dextran, but broadened out as the concentration of the 2000 kDa dextran increased. The DSC heat flow signal of a mixture containing an 80% concentration of the 2000 kDa dextran was similar to the signal for pure 2000 kDa dextran. Kawai and Hagura (2012) investigated the change of the DSC heat flow signal of glucose blends with increasing concentrations of dextran. The study also showed a widening of the glass transition temperature with increasing concentration of dextrin in the system. As already stated in Section 2.5.1, a single glass transition temperature in a DSC thermogram is not a reliable indicator for complete homogeneity. Because of self-association of polymers and the dynamic fluctuation of various length

scales, the blend components exhibit different dynamic environments that may result in different temperature dependences of their relaxation rates. This dynamic heterogeneity can be observed as a wide glass transition temperature range, a broad distribution of the relaxation modes and two separated glass transition temperatures.

For instance, the polymer blend PMMA + PVPh appears to be completely homogeneous when analysed at a domain-size scale around ~20–30 nm by DSC and a single glass transition is determined for all blend compositions. With lower scaling of the domain-size to 1–15 nm by DMA the blend is heterogeneous (Barrat et al., 2010).

As stated above, dynamic heterogeneity is linked to the different relaxation behaviours and rates of the phases for each component in the mixture, even if the substances are completely miscible on a molecular level. Kawai and Hagura (2012) and Bosma et al. (1988) highlighted different relaxation behaviours of the various domains by annealing the samples below T_g. Each domain exhibits a different position and magnitude of the enthalpy recovery, which can be observed after reheating of the sample. Longer annealing times feature a more pronounced enthalpy recovery peak, but, as proven by Kawai and Hagura (2012), an annealing time of 16 h is sufficient to indicate the difference in relaxation rates of the various domains. The fructose and maltodextrin DE 9-13 sample, with a ratio of 3:7, was removed of their thermal history, annealed at different temperatures of 30˚C, 50˚C and 90˚C for 16 h and afterwards reheated to determine the enthalpy recovery peaks. Figure 6.2.8 displays the broad heat flow signal of the 0.3 fructose and 0.7 maltodextrin DE 9-13 blend, as well as the determined onset, midpoint and offset point of the transition.



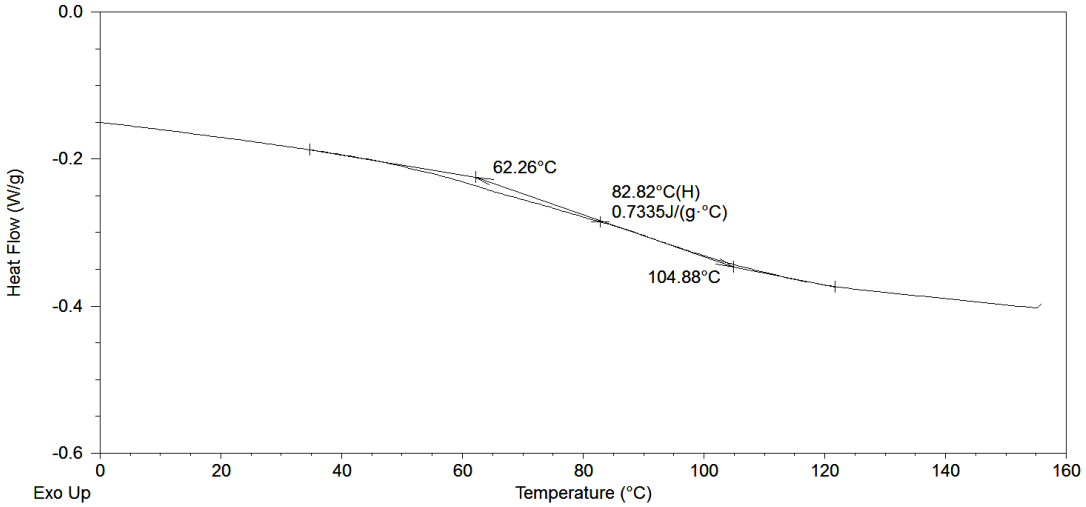
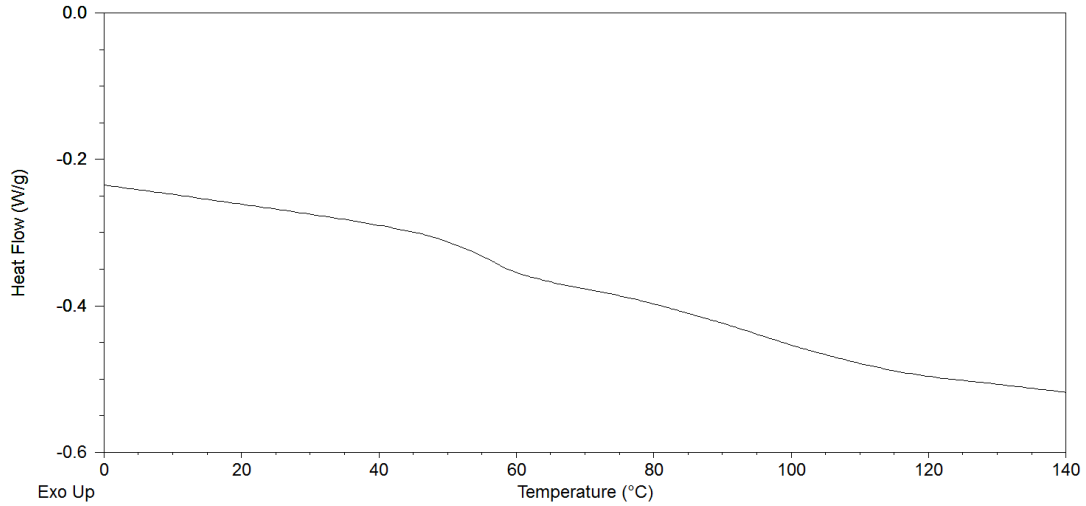


Figure 6.2.8. DSC thermogram after removal of their thermal history of 0.3 fructose and 0.7 maltodextrin DE 9-13.

After annealing the sample at 30˚C a small transition around 54˚C can be detected (Figure 6.2.9). Since the annealing temperature is relatively low for the onset temperature of 62˚C, the observed relaxation of the molecules is limited and only a small fraction of the mixture shows a relaxation response. This response can be associated to the domain rich in the smaller fructose molecules, since the low molecular weight components display a faster response rate at lower temperatures.



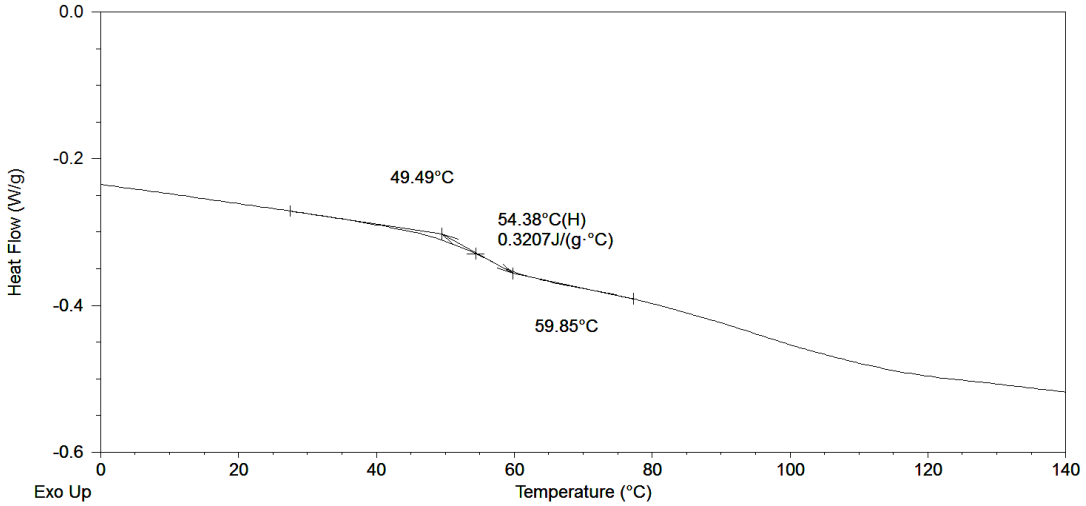


Figure 6.2.9. DSC thermogram after annealing at 30˚C for 16 h of the 0.3 fructose and 0.7 maltodextrin DE 9-13 blend.

Annealing at a temperature of 50˚C for 16 h results in a quite different DSC signal (Figure 6.2.10). Two distinct transitions are detected in the DSC thermogram. Correctly, the two transitions are the responses of the enthalpy relaxation of the different domains during the annealing step. With a longer annealing time the first transition would take the form of the sharp drop of the enthalpy recovery seen in Figure 6.2.8. However, if the two enthalpy recovery peaks would be considered as individual relaxation steps, the first transition would be around 68.95˚C, which is close to the peak maximum observed for the enthalpy recovery in Figure 6.2.8. Icoz et al. (2005) and Kawai and Hagura (2012) stated that the response at lower temperatures is related to the local domain rich in low molecular weight components as seen by the red dots for fructose molecules in Figure 6.2.11.

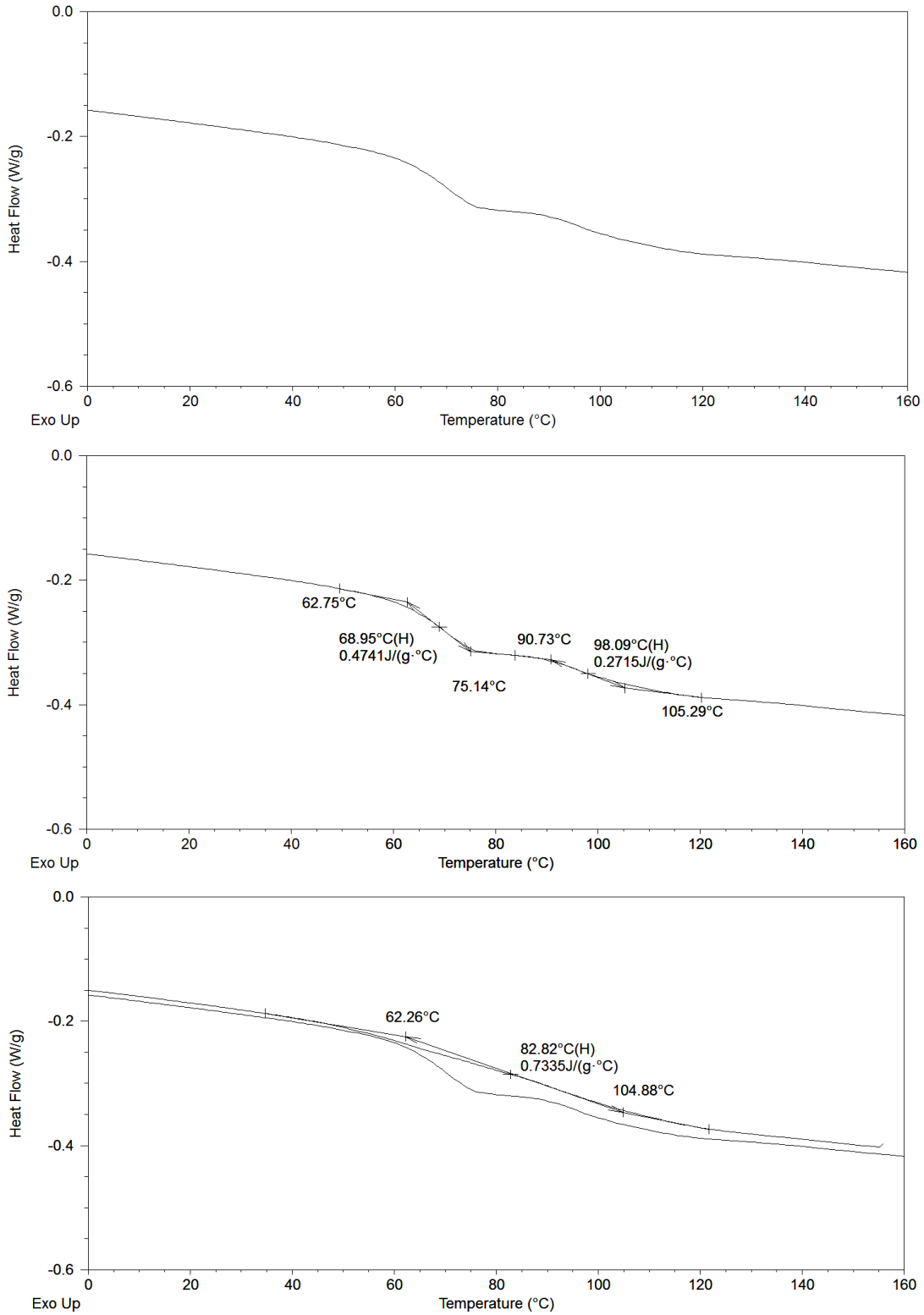


Figure 6.2.10. DSC thermogram after annealing at 50˚C for 16h of the 0.3 fructose and 0.7 maltodextrin DE 9-13 blend.

The transition related to relaxation of the domain at higher temperature is around 98.09˚C and corresponds to the relaxation behaviour of the domain of the higher molecular weight component, maltodextrin DE 9-13, in combination with the smaller fraction of fructose molecules (Figure 6.2.11). Interestingly, the onset of the first transition is around 62.75˚C,

which is similar to the onset point of the broad transition at 62.26˚C. The same is true for the offset point of the second transition, where the offset is at 105.29˚C and for the broad transition is at 104.88˚C. Additionally, if the average of the two midpoints of the

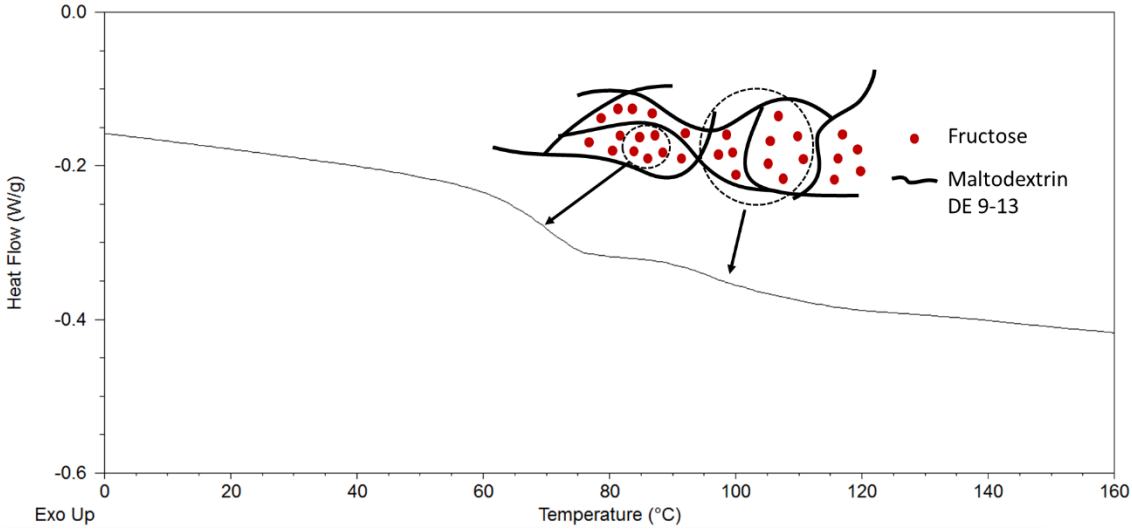


Figure 6.2.11. DSC thermogram of 0.3 fructose and 0.7 maltodextrin DE 9-13 in combination with the different relaxation response of the different domains in the blend after annealing at 50˚C for 16h.

transitions is considered, which is around 83.52˚C, this comes very close to the measured T_g value of 82.28˚C. It could be a coincidence that the annealing time and the proposed glass transition temperatures of the relaxation steps of the two domains corresponded so well to the overall glass transition temperature of the mixture. More annealing studies would have to be done to prove the idea of the partly developed enthalpy recovery peaks as an indicator of the glass transition temperature of the different domains. The problem with the idea is that the aging kinetics do not have to correlate to the glass transition temperatures of the individual components as shown by Bosma et al. (1988) with the two polymers polyvinylchloride (PVC) and poly(isopropyl methacrylate) (PiPMA). Although the glass transition temperatures of both polymers are almost identical, the aging kinetics are quite different, resulting in distinct enthalpy recovery peaks.

Annealing the sample at a temperature of 90˚C and therefore above the relaxation temperature of the first domain, the first enthalpy recovery peak is absent in the DSC thermogram and only the second peak is visible (Figure 6.2.12).

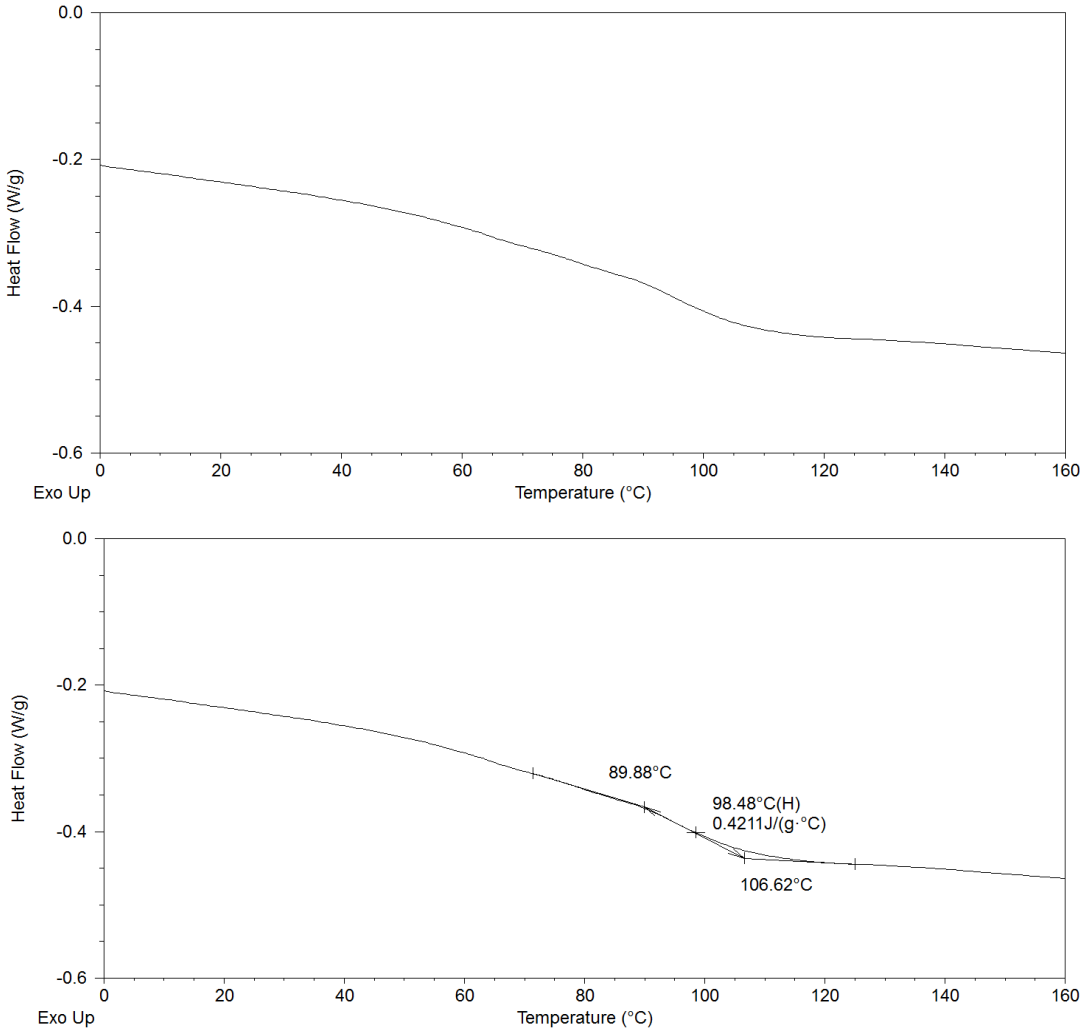


Figure 6.2.12. DSC thermogram after annealing at 90˚C for 16 h of the 0.3 fructose and 0.7 maltodextrin DE 9-13 blend. The bottom graph includes the characterization of the enthalpy peak.

Comparing the different enthalpy recoveries of the different fructose and maltodextrin DE 9-13 systems from the first run in the DSC thermogram in Figure 6.2.13 it becomes obvious that the sharp enthalpy recovery peak can be associated with the fructose molecules. With increasing concentration of maltodextrin DE 9-13 in the mixture the magnitude of the enthalpy peak decreases and at a weight fraction of 0.7 an additional bend in the heat flow signal after the first peak can be observed. Due to the long aging time even at much lower annealing temperatures, the two transitions seen in Figure 6.2.10 compress together and form the shape seen in Figure 6.2.13.

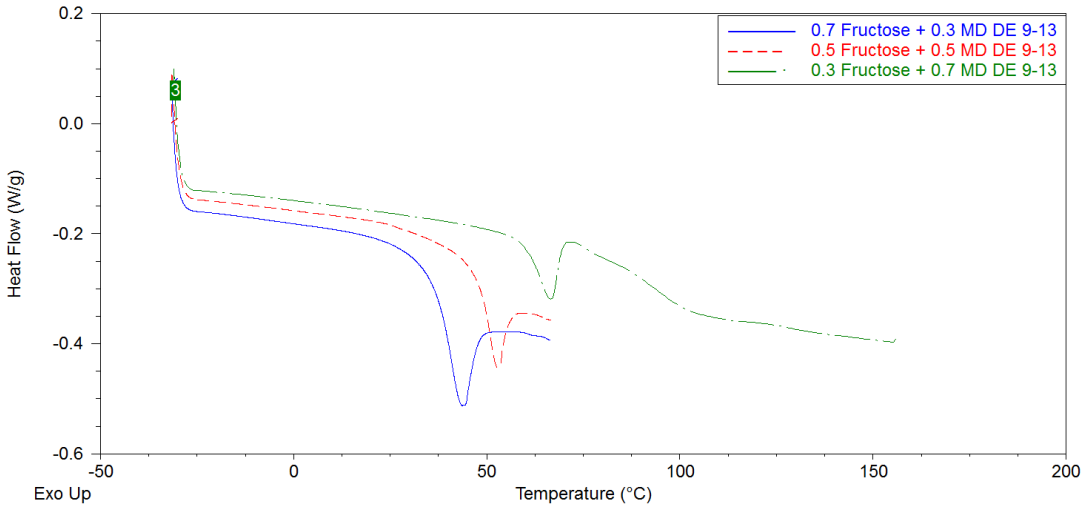


Figure 6.2.13. DSC thermogram of the thermal history of various fructose and maltodextrin DE 9-13 blends after the first heating cycle at zero water activity.

It is possible to illustrate the dynamic heterogeneity for the fructose and maltodextrin mixture. It is assumed the difference in dynamic response rate of the two domains is due to the great difference in molecular weight between the fructose molecules and the maltodextrin DE 9-13 molecules. The same effect should be visible for all mixtures, where, due to the difference in molecular size, the domains exhibit distinct dynamic environments. In order to test the theory further, the blackcurrant juice and maltodextrin DE 9-13 blend in a ratio of 3:7 was annealed at 50˚C for 16 h and reheated to analyse the enthalpy recoveries. As expected, the same aging behaviour could be observed (Figure 6.2.14) as for the 0.3 fructose and 0.7 maltodextrin DE 9-13 blend in Figure 6.2.10. The average T_g value of the two proposed transitions seen in Figure 6.2.14 at 69.75˚C and 102.38˚C is around 86˚C, which again agrees well with the measured glass transition temperature of the broad transition. In the future DMA measurements with a higher sensitivity should be conducted to examine if the different local dynamic responses can be directly detected in addition to the corresponding temperature range. Instead of going through the more complicated annealing step, the various thermal histories of the different blackcurrant juice and maltodextrin blends can give an idea of the relaxation behaviour of the system. As previously discussed for the fructose and maltodextrin DE 9-13 blends, in the blackcurrant and maltodextrin DE 9-13 blends only one enthalpy recovery peak can be detected for lower concentrations of maltodextrin DE 9-13. At a weight fraction of 0.7 the same enthalpy recovery shape can be detected as for the fructose and maltodextrin DE 9-13 blend.

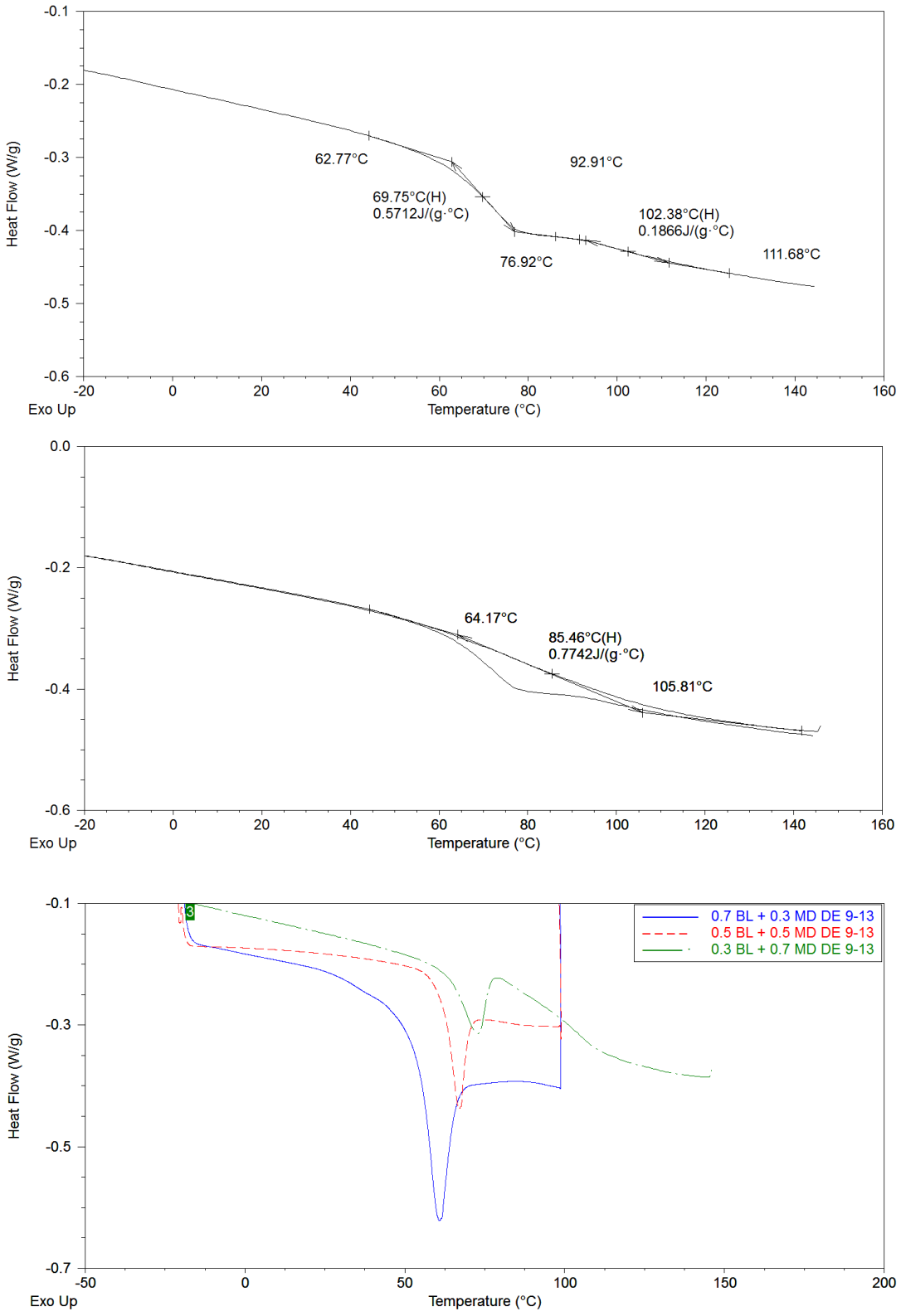


Figure 6.2.14. DSC thermogram after annealing at 50˚C for 16 h of the 0.3 blackcurrant juice and 0.7 maltodextrin DE 9-13 blend shown in the first two graphs. The bottom graph shows the thermal history of various blackcurrant juice and maltodextrin DE 9-13 blends after the first heating cycle.

6.3 Water activity and T_g of powders

Previously the glass transition temperature of the different powder mixtures and their anomalies were discussed at zero water activity. In this part the effect of water on the glass transition temperature of the presented powder mixtures is reviewed. Therefore the glass transition temperature of the powders with water activities of 0.11, 0.22, 0.32 and 0.43 were measured as was done for the pure fruit juice powders. Similar to the study of the fruit juice powders, the FHVT model is used to predict the sorption behaviour of the system and to correlate it back to the glass transition temperature of the mixture at the corresponding water activity. Two distinct initial T_g values of the powder mixture are used for the FHVT prediction. The first initial T_g value is the measured T_g value of the mixture and the other one is the estimated T_g value discussed in the Section 6.1.1. In the following only the midpoint T_g values are discussed; a more detailed representation of glass transition temperature of the mixture can be found in Appendix A.2.

6.3.1 Glucose and maltodextrin DE 9-13 powder

The glass transition temperatures of the different glucose and maltodextrin DE 9-13 mixtures at various water activities are displayed in Table 6.3.1. Comparing the change of the T_g values of the different blends from zero to 0.11 water activity, it becomes noticeable that with increasing concentration of maltodextrin DE 9-13 in the mixture the drop of the T_g value becomes greater. At 0.3 weight fraction of maltodextrin in the powder the T_g value drops by 18.59˚C. The drop increases to 28.14˚C with a further increase of the maltodextrin DE 9-13 weight fraction to 0.5 and reaches a change of 38.42˚C at 0.7 weight fraction.

Table 6.3.1. Glass transition temperature of glucose and maltodextrin DE 9-13 at different water activities.

	Midpoint T_g (˚C)		
Water activity	**0.7 G + 0.3 MD**	**0.5 G + 0.5 MD**	**0.3 G + 0.7 MD**
0	46.8 ± 0.4	58.9 ± 1.0	90.0 ± 1.7
0.11	28.2 ± 0.4	30.8 ± 0.4	51.6 ± 1.6
0.22	15.4 ± 0.4	18.7 ± 0.4	40.3 ± 0.2
0.32	5.0 ± 1.0	10.3 ± 1.9	29.1 ± 1.3
0.43	-14.3 ± 0.2	-5.9 ± 1.6	12.7 ± 0.9
R^2 (T_g value)	0.97	0.85	0.89
R^2	0.85	0.67	0.90

Average ± SD, n=3, storage temperature 30˚C

This trend aligns with the findings presented in Chapter 4, where the systems with a higher glass transition temperature usually exhibit higher moisture contents at lower water activities. Also, the effect of the moisture content on the T_g depression, as seen in Figure 6.3.1, is more pronounced, which is related to the difference in the glass transition

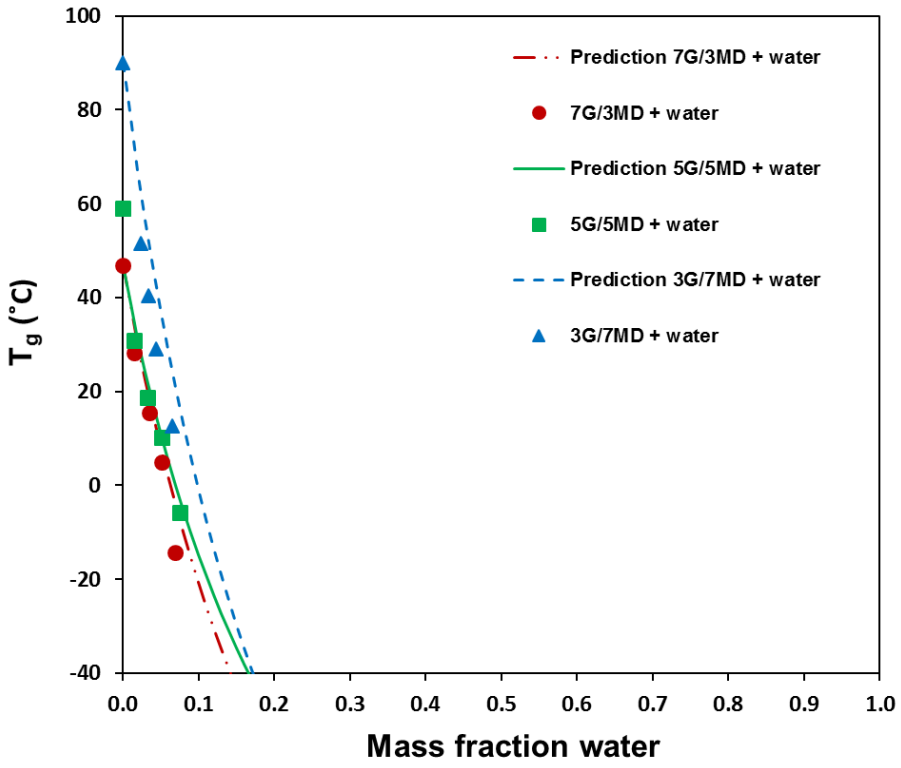


Figure 6.3.1. Effect of the moisture content on the glass transition temperature of the various glucose and maltodextrin DE 9-13 blends.

temperature of the solid mixture and water. The typical trend for solvent and polymer mixture was presented in more detail in Section 4.2.

In Figure 6.3.2 the measured and predicted T_g values of the different glucose and maltodextrin DE 9-13 blends as a function of water activities are illustrated. The two predicted lines reproduce the trend seen for the measured T_g values of the 0.7 glucose and 0.3 maltodextrin DE 9-13 system accurately. As mentioned in Chapter 5, the model overestimates the glass transition temperature of the glucose and maltodextrin DE 9-13

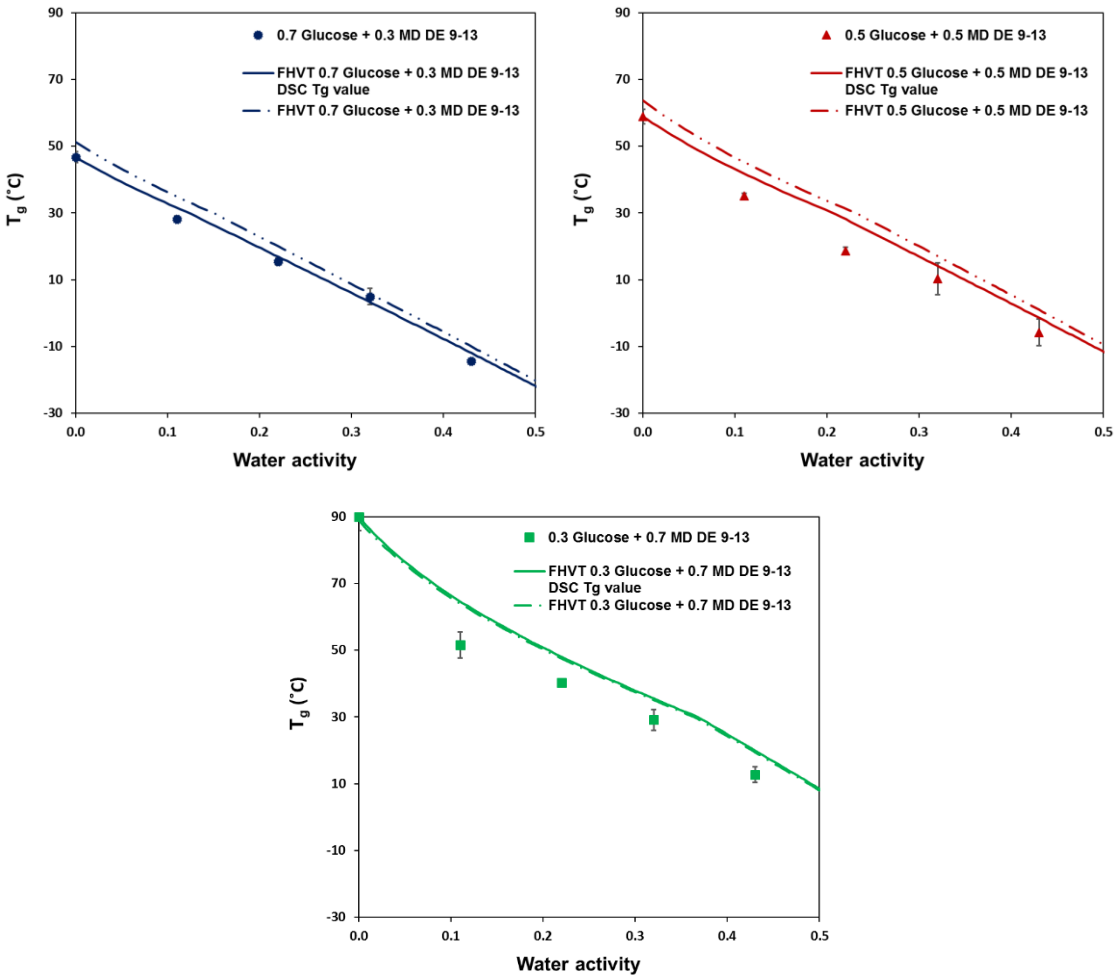


Figure 6.3.2. Prediction of the effect of water on the T_g depression of glucose and maltodextrin DE 9-13 using the measured and estimated T_g value for the FHVT model. The error bars refer to the 95% confidence interval for n=3.

blend at lower maltodextrin DE 9-13 contents. Therefore the predicted line using the estimated T_g value is slightly overestimating the T_g values at the various water activities with an R^2 of 0.85. If the measured T_g value at zero water activity is used in the FHVT model then the R^2 value improves to 0.95 (Table 6.3.1).

The predicted T_g values of the 0.5 glucose and 0.5 maltodedxtrin DE 9-13 blend are considerably higher than the measured T_g values. Once more the estimated T_g values of the blend at zero water activity are overestimated leading to higher predicted glass transition temperature at the various water activities. The overall R^2 is 0.85 using the measured T_g value at zero water activity in the FHVT model and 0.67 for the estimated T_g value, which is not an accurate representation of the experimental data. The fit of the predicted value and measured value is in better agreement for the higher content 0.7 of maltodextrin DE 9-13 in the system with almost identical R^2 values of 0.90 and 0.89 for the two sets of predicted T_g values due to the conformance of the measured and estimated T_g value at zero water activity. Despite the better fit of the predicted T_g values to the experimental data, the predicted T_g values are overestimating the glass transition temperature of the measured T_g values slightly.

It is possible to predict the relationship between the glass transition temperature of the different glucose and maltodextrin DE 9-13 blends at the various water activities, but it has to be stated that the agreement of the predicted and measured T_g values for the glucose and maltodextrin DE 9-13 blends is not as good as for the fruit juice powders in Chapter 5. The T_g depression of the glucose and maltodextrin DE 9-13 between zero to 0.11 water activity is much higher than the FHVT model predicts.

6.3.2 Citric acid and maltodextrin DE 9-13 powder

The citric acid and maltodextrin DE 9-13 blend with a ratio of 7:3 could not be investigated due to rapid crystal formation of the citric acid molecules. For the other systems no crystal formation could be detected in the three week storage time. The difference between the T_g values at zero and 0.11 water activity is not as distinctive as for the glucose and maltodextrin DE 9-13 blends. It only accounts for a decrease of 15.78˚C for 0.5 maltodextrin DE 9-13 and 26.01˚C for 0.7 maltodextrin De 9-13 in the system Table 6.3.2.

Table 6.3.2. Glass transition temperature of citric acid and maltodextrin DE 9-13 at different water activities.

	Midpoint T_g (˚C)	
Water activity	**0.5 C + 0.5 MD**	**0.3 C + 0.7 MD**
0	39.6 ± 0.7	78.2 ± 1.3
0.11	23.9 ± 1.4	52.2 ± 1.1
0.22	14.0 ± 2.4	42.1 ± 0.7
0.32	5.8 ± 2.0	33.7 ± 0.8
0.43	-6.0 ± 0.9	18.0 ± 2.2
R^2 (DSC T_g value)	0.95	0.98
R^2	0.90	0.90

Average ± SD, n=3, storage temperature 30˚C

The prediction of the measured T_g values for both systems is in a good agreement for both citric acid and maltodextrin DE 9-13 blends (Figure 6.3.3). As expected, the 0.5 citric acid and 0.5 maltodextrin DE 9-13 blend T_g values follow an almost straight line over the various water activities. For the 0.3 citric acid and 0.7 maltodextrin DE 9-13 blend the predicted T_g values of the FHVT model, utilizing the estimated T_g values of the blend at zero water activity, are underestimating the measured values slightly due to the difference found between the measured and estimated T_g value at zero water activity. Nevertheless the R^2 with the estimated T_g values are both around 0.90, and R^2 using the measured T_g values are 0.95 and 0.98, which is a good representation of the experimental data (Table 6.3.2).

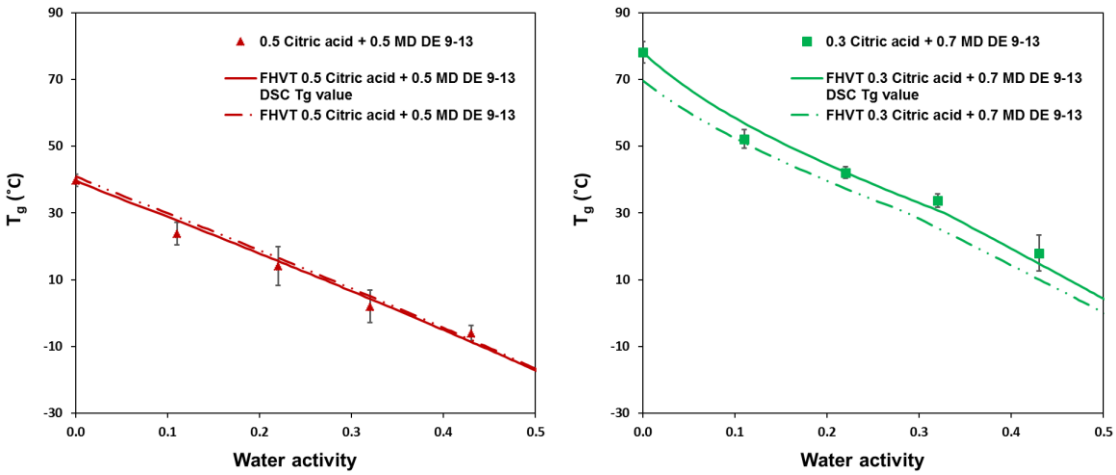


Figure 6.3.3. Prediction of the effect of water on the T_g depression of citric acid and maltodextrin DE 9-13 using the measured and estimated T_g value for the FHVT model. The error bars refer to the 95% confidence interval for n=3.

6.3.3 Fructose and maltodextrin DE 9-13 powder

The mixtures of fructose and maltodextrin DE 9-13 exhibit similar trends as the blends of citric acid or glucose with maltodextrin DE 9-13. The T_g depression of the fructose and maltodextrin DE 9-13 from zero to 0.11 water activity increases with the maltodextrin DE 9-13 content from 12.37˚C at 0.3 weight fraction of maltodextrin DE 9-13 to 16.84˚C at 0.5 and finally to 37.36˚C at 0.7 weight fraction of maltodextrin De 9-13 Table 6.3.3.

Table 6.3.3. Glass transition temperature of fructose and maltodextrin DE 9-13 at different water activities.

	Midpoint T_g (˚C)		
Water activity	**0.7 F + 0.3 MD**	**0.5 F + 0.5 MD**	**0.3 F + 0.7 MD**
0	31.0 ± 0.5	40.4 ± 1.1	83.2 ± 1.0
0.11	18.6 ± 1.9	23.6 ± 0.7	45.8 ± 1.6
0.22	6.4 ± 0.2	15.2 ± 0.4	36.3 ± 0.6
0.32	-3.0 ± 0.6	4.7 ± 0.1	31.1 ± 0.4
0.43	-20.9 ± 0.6	-13.2 ± 1.9	8.5 ± 0.7
R^2 (DSC T_g value)	0.95	0.93	0.85
R^2	0.94	0.81	0.92

Average ± SD, n=3, storage temperature 30˚C

The trend of the 0.7 fructose and 0.3 maltodextrin DE 9-13 blend follows the same behaviour as the glucose blend and other low molecular mixtures such as the fruit juice powders (Figure 6.3.4). Both predictions conform with the measured T_g values and have an R^2 of 0.95 and 0.94 (Table 6.3.3). As seen in Figure 6.3.4, the estimated T_g value at zero water activity is off by ca. 3.61˚C from the measured value, which results in an over prediction of the T_g values at various water activities and an R^2 of 0.81 instead of 0.93 for the FHVT model prediction using the measured T_g value. Interestingly, the 0.3 fructose and 0.7 maltodextrin DE 9-13 blend shows a different behaviour. The FHVT prediction using the measured T_g value overestimates the trend of the fructose and maltodextrin DE 9-13 blend across the different water activities with an R^2 of 0.85 and the prediction utilizing the estimated T_g value shows a much better fit to experimental data with an R^2 of 0.92. It could be that the measured T_g value of 83.16˚C associated with the broad transition is too high and the true underlying T_g value is closer to the predicted T_g value.

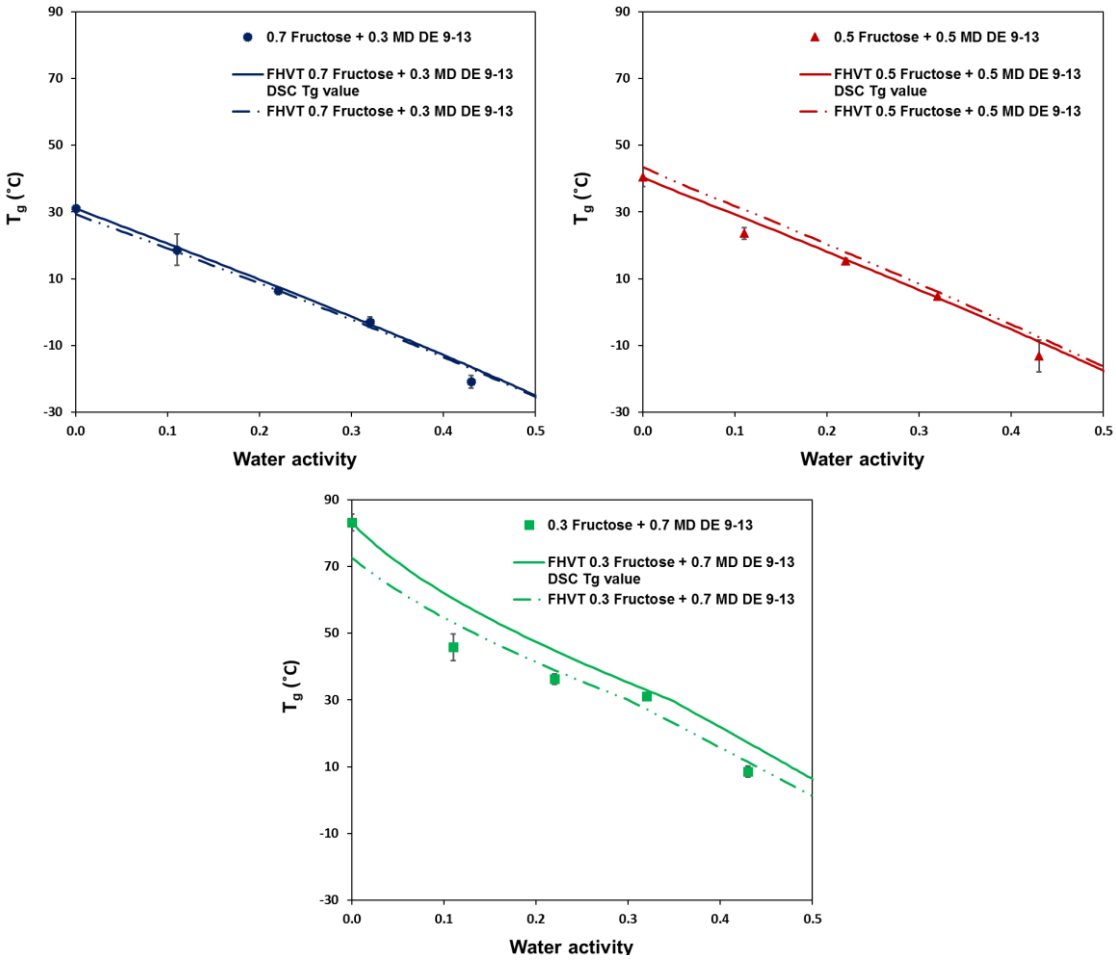


Figure 6.3.4. Prediction of the effect of water on the T_g depression of fructose and maltodextrin DE 9-13 using the measured and estimated T_g value for the FHVT model. The error bars refer to the 95% confidence interval for n=3.

6.3.4 G/F/C and maltodextrin DE 9-13 powder

The mixtures of one third glucose, one third fructose and one third citric acid with various ratios of maltodextrin DE 9-13 exhibit decreases in T_g value from zero to 0.11 water activity of 14.54˚C, 17.63˚C and 27.52˚C with increasing maltodextrin DE 9-13 concentration (Table 6.3.4).

Table 6.3.4. Glass transition temperature of G/F/C and maltodextrin DE 9-13 at different water activities.

	Midpoint T_g (˚C)		
Water activity	**0.7 G/F/C + 0.3 MD**	**0.5 G/F/C + 0.5 MD**	**0.3 G/F/C + 0.7 MD**
0	35.7 ± 1.2	49.1 ± 0.4	78.7 ± 1.1
0.11	21.2 ± 0.5	31.5 ± 0.1	51.2 ± 1.5
0.22	10.2 ± 0.7	23.1 ± 0.8	39.4 ± 0.9
0.32	-0.4 ± 2.2	10.1 ± 0.2	31.6 ± 0.7
0.43	-14.2 ± 1.0	-4.5 ± 1.2	16.0 ± 1.0
R^2 (DSC T_g value)	0.99	0.98	0.98
R^2	0.99	0.98	0.98

Average ± SD, n=3, storage temperature 30˚C

As described in Chapter 5, the prediction of the glass transition temperature of multicomponent systems at zero water activity shows the best agreement with experimental data, therefore the predicted T_g values by the FHVT model are almost identical. For all systems the match of the measured and predicted T_g values is in a good agreement (Figure 6.3.5). Not only does the predicted line represent the overall trend at the various water activities, but it is also in accordance with the measured T_g value, giving an overall R^2 between of 0.98 and 0.99 for the various systems (Table 6.3.4).

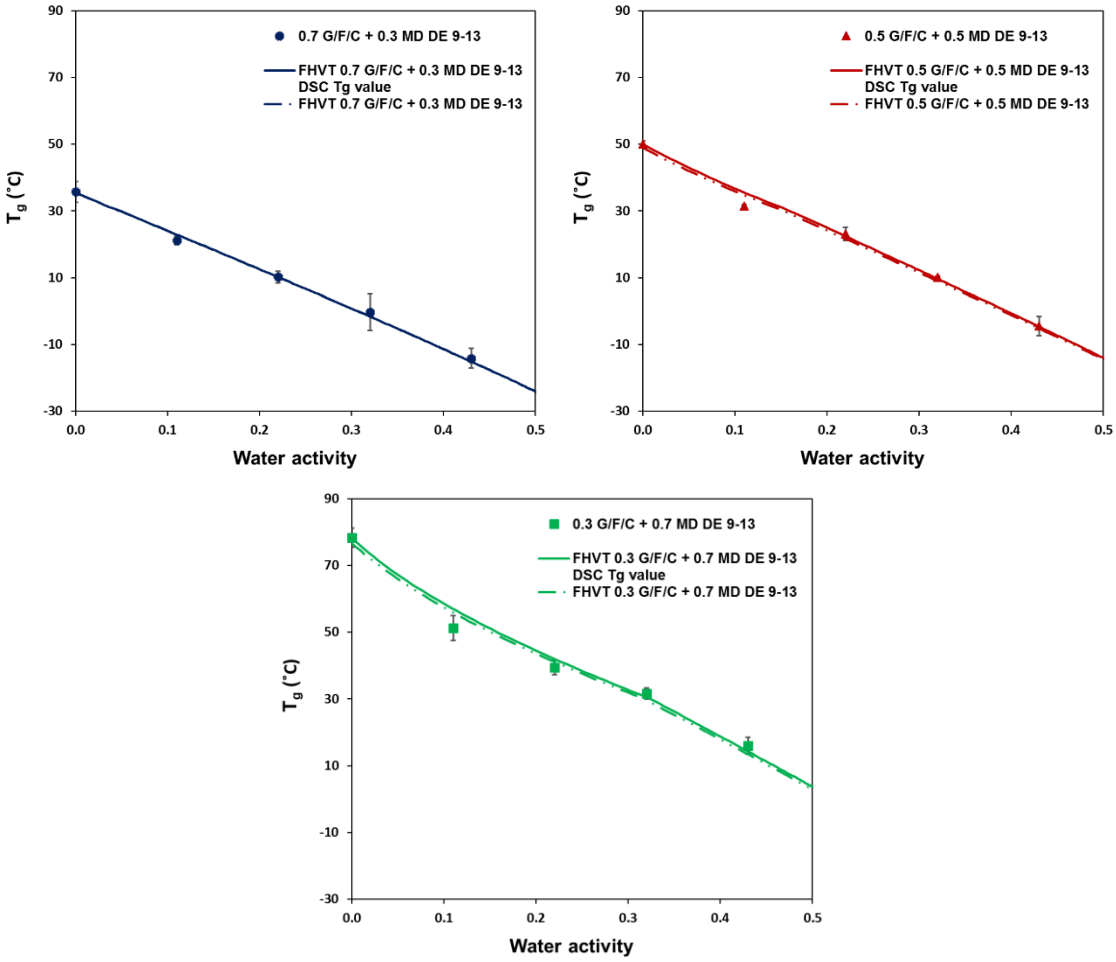


Figure 6.3.5. Prediction of the effect of water on the T_g depression of one third glucose, one third fructose and one third citric acid with maltodextrin DE 9-13 using the measured and estimated T_g value for the FHVT model. The error bars refer to the 95% confidence interval for n=3.

6.3.5 Blackcurrant and maltodextrin DE 9-13 powder

The blackcurrant and maltodextrin DE 9-13 blends show the same trend as the multicomponent system of glucose, fructose and citric with maltodextrin DE 9-13. The T_g values drop moderately by 17.35˚C, 19.84˚C and 32.83˚C from zero to 0.11 water activity with increasing maltodextrin DE 9-13 content Table 6.3.5.

Table 6.3.5. Glass transition temperature of blackcurrant juice and maltodextrin DE 9-13 at different water activities.

	Midpoint T_g (˚C)		
Water activity	**0.7 BL + 0.3 MD**	**0.5 BL + 0.5 MD**	**0.3 BL + 0.7 MD**
0	47.1 ± 0.3	60.2 ± 0.5	87.7 ± 1.2
0.11	29.8 ± 0.9	40.4 ± 0.2	54.9 ± 1.0
0.22	16.5 ± 0.5	29.3 ± 0.2	46.1 ± 0.9
0.32	6.1 ± 1.3	12.1 ± 0.4	36.8 ± 0.7
0.43	-10.2 ± 1.3	-0.7 ± 0.4	20.5 ± 2.3
R^2 (DSC T_g value)	0.98	0.98	0.94
R^2	0.96	0.96	0.94

Average ± SD, n=3, storage temperature 30˚C

In Figure 6.3.6 the measured and predicted T_g values of pure blackcurrant powder are presented as a function of water activity. The trend of the pure blackcurrant powder is added to compare the changes of the T_g depression over the various water activities seen with the increasing maltodextrin DE 9-13 content. At 0.3 weight fraction the T_g decreases relatively linearly as observed for the other studied systems and the literature data in Chapter 4. Increasing to 0.5 weight fraction results in a small dip at 0.11 water activity following the almost straight line. Both FHVT model predictions agree very well with the experimental data with only a minor difference in the R^2 for both systems. The R^2 of the measured T_g at zero water activity is 0.98 and using the estimated T_g values in the FHVT model the R^2 is slightly lower at 0.96. The 0.3 blackcurrant and 0.7 maltodextrin DE 9-13 blend exhibits the same drop in the glass transition temperature from 0 to 0.11 water activity as the previous described powders. Both predictions of the FHVT model for the blend are almost identical due to the good agreement of measured and estimated T_g value at zero water activity.

The predicted trend follows the measured T_g values well with small deviations between the T_g values at 0.11 water activity, therefore the R^2 is slightly lower than for the other blends at 0.94 for both FHVT model predictions.

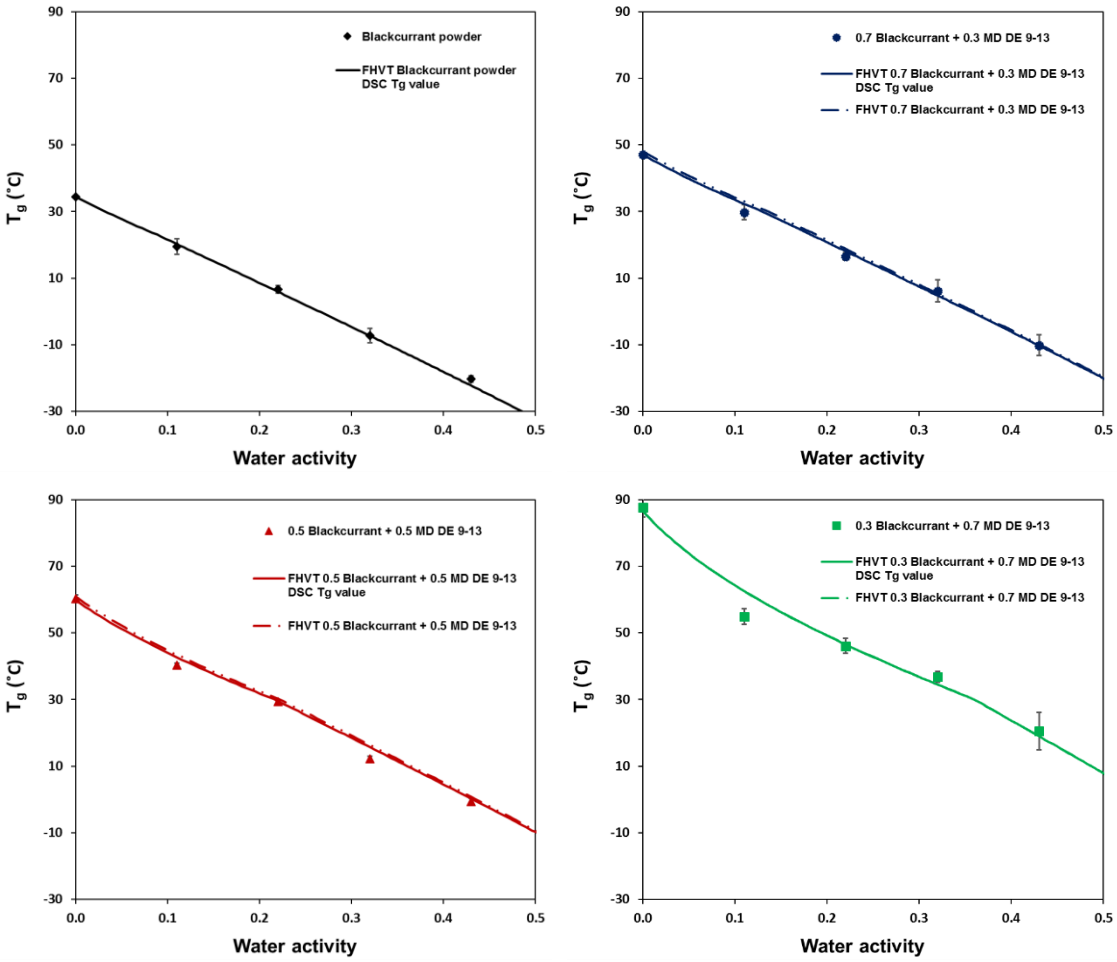


Figure 6.3.6. Prediction of the effect of water on the T_g depression of blackcurrant juice with maltodextrin DE 9-13 using the measured and estimated T_g value for the FHVT model. The error bars refer to the 95% confidence interval for n=3.

Additionally, the relationship of the water activity and the T_g value of the pure maltodextrin DE 9-13 was studied at the same water activities. The results of the sample at 0.32 water activity was inconsistent, which is evident in the greater error bars in Figure 6.3.7. The prediction of the T_g values of maltodextrin DE 9-13 corresponds well to the trend presented in Section 4.4.1 for the predictions of the T_g depression of maltodextrins with various dextrose equivalents, with an R^2 of 0.99.

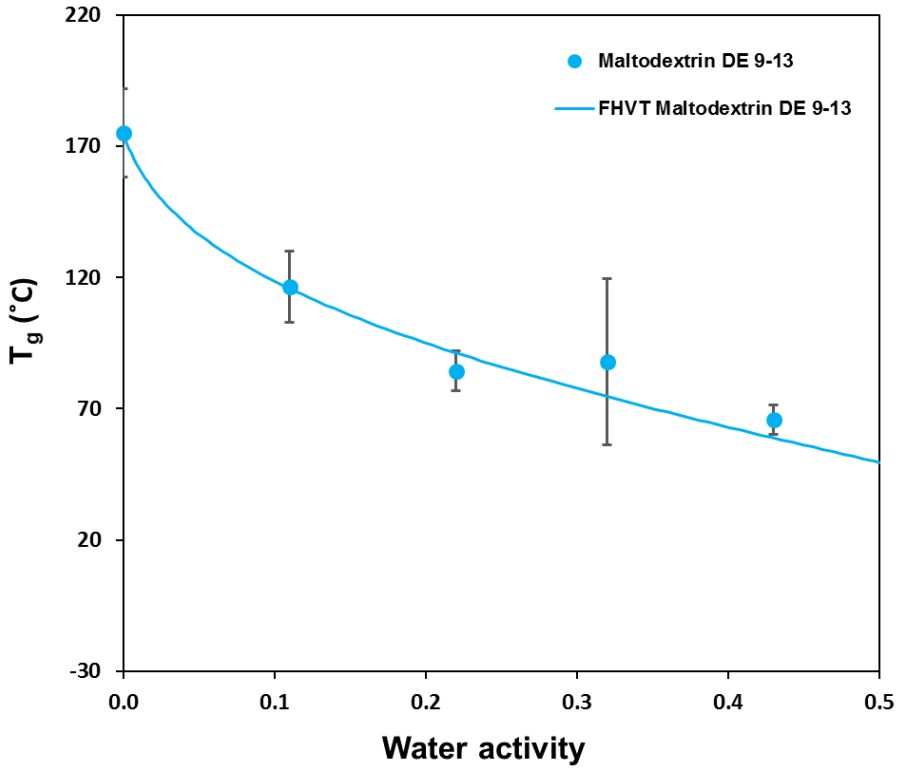


Figure 6.3.7. Prediction of the effect of water on the T_g depression of maltodextrin DE 9-13 using the measured T_g value for the FHVT model. The error bars refer to the 95% confidence interval for n=3.

6.4 Phase separation at low water activities

Throughout the study of the different maltodextrin DE 9-13 blends the steep drop in T_g from zero to 0.11 water activity is noticeable. During the discussion of the glucose and maltodextrin DE 9-13, the reason for the increase in the magnitude of the drop in T_g with higher maltodextrin DE 9-13 content is due to the higher moisture contents and the effect of solvents on the glass transition of solutes. This only provides an explanation for the difference seen for the different compositions, but it does not explain the steep drop in the first place.

By comparing the DSC thermograms of the various blends at all water activities, it is noticeable that blends at 0.11 water activity exhibit a second transition at higher temperatures (Figure 6.4.1). The magnitude of the transition becomes smaller with increasingly higher concentration of maltodextrin DE 9-13 in the system. Considering the glucose and maltodextrin DE 9-13 blends, the glass transition of the blend with 0.3 weight

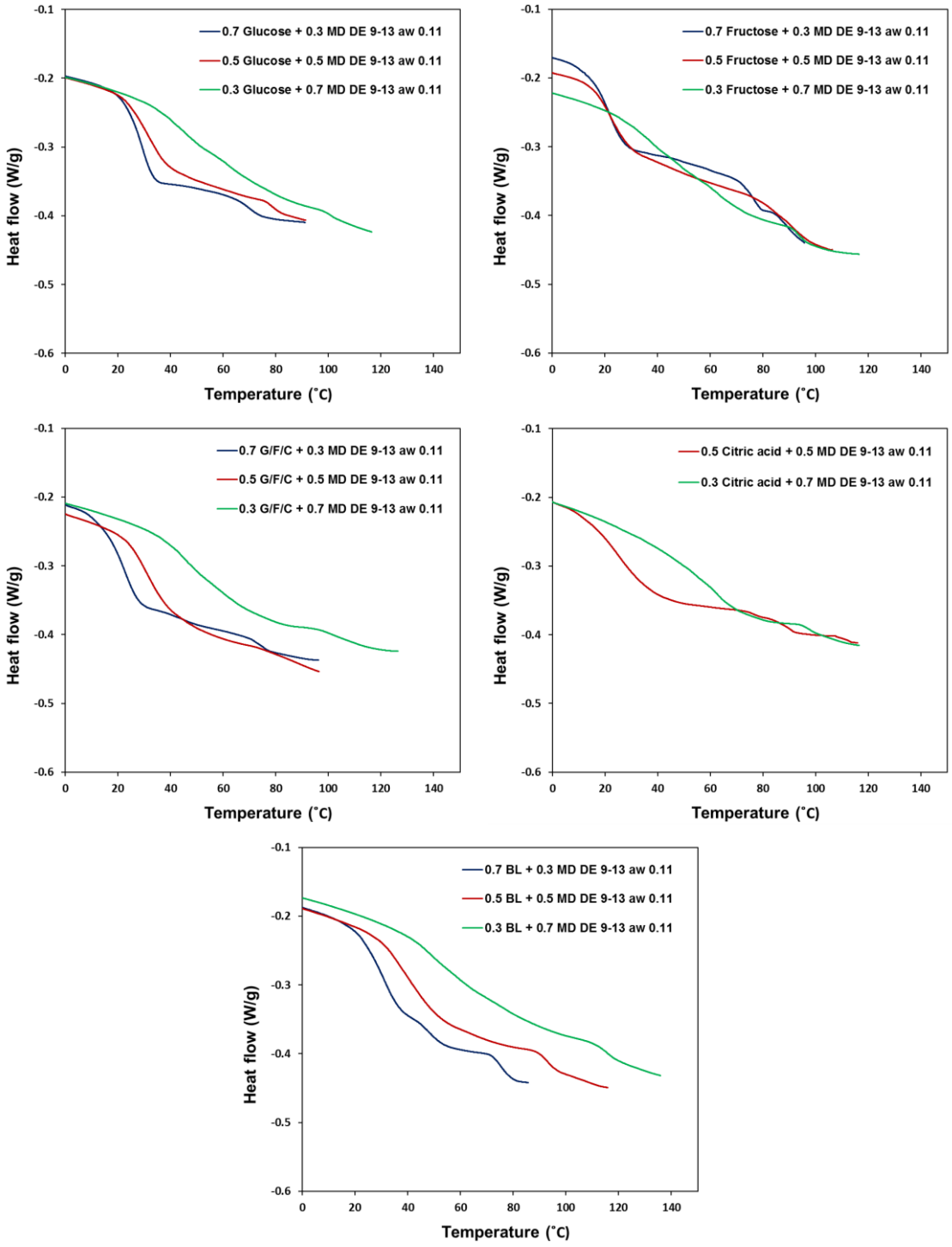


Figure 6.4.1. DSC thermogram of the different maltodextrin DE 9-13 blends at 0.11 water activity.

fraction of maltodextrin in the system is around 70.41˚C. The T_g value increases to 79.29˚C for 0.5 and 101.95˚C for 0.7 weight fraction of maltodextrin DE 9-13 in the system. The fructose, citric acid, and mixture of glucose, fructose and citric acid blends with maltodextrin DE 9-13 show the same behaviour as the glucose and maltodextrin DE

9-13 blend. Only the blackcurrant mixture, with a weight fraction of 0.3 maltodextrin DE 9-13 in the system, shows an anomaly around 45˚C, since between the main transition and the transition at the higher temperature there is another small transition (Figure 6.4.1). This transition may be attributable to the second transition observed for the pure blackcurrant powder in Chapter 4, which shows an individual relaxation step. At higher concentrations of maltodextrin DE 9-13 in the system the concentration of the responsible components reached such a low concentration level that the relaxation is not visible in the DSC thermogram.

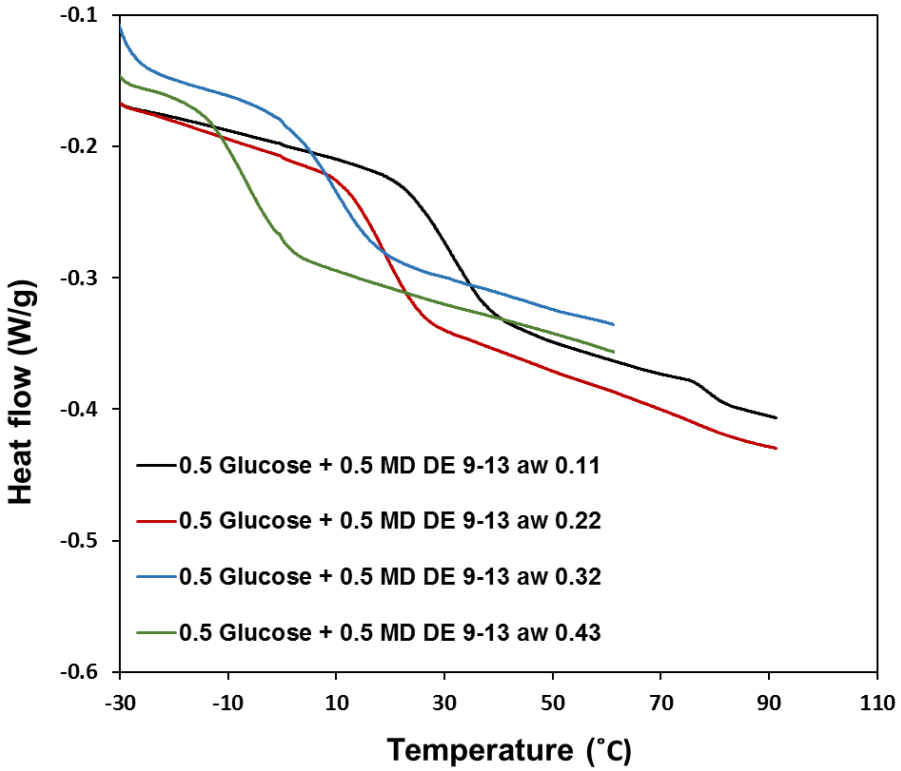


Figure 6.4.2. DSC thermogram of 0.5 glucose and 0.5 maltodextrin DE 9-13 blend at various water activities.

Interestingly, the transition apparent at higher temperatures is only clearly present in the DSC thermogram for the blends at a water activity of 0.11. In Figure 6.4.2, the DSC thermograms of the 0.5 glucose and 0.5 maltodextrin DE 9-13 mixture for water activities of 0.11, 0.22, 0.32 and 0.43 are displayed. Only the line representing the mixture at 0.11 water activity exhibits a clearly visible transition at a higher temperature. The fact that the second transition is only clearly represented at 0.11 water activity could be related back to the water content in the sample. Roussenova et al. (2014) studied the effect of the water content of mixtures of maltooligomer and glycerol on the hydrogen bond network. It was stated that at a water content of 3–5% the hydrogen bond network increases as the water molecules interact with the carbohydrate and glycerol via hydrogen bonds, whereas

at the same time the hydrogen network between glycerol and maltooligomer gets weaker. At low water contents of 3–5% the water molecules are dispersed throughout the matrix and initially interact with hydrogen sites of the other components, whereas at higher water contents the overall bond network becomes looser due to favoured water-water molecules interactions. This phenomenon could explain the existence of the visible second transition. The low water content at 0.11 water activity results in a decrease of the hydrogen bonds network between the low molecular components and the polysaccharide maltodextrin DE 9-13 as water molecules displace the attachment to the available hydrogen bond sites.

Local domains, richer in polysaccharide, could be affected more by the water molecules resulting in a phase separation and therefore giving a different response to the relaxation behaviour observed in the DSC thermogram. The decrease in the overall hydrogen bond network at higher water contents indicates that the water molecules are attracted to available hydrogen bond sites and this favours water-water molecule interactions. This suggests that at higher water contents the local difference in water molecules becomes relatively low, since the water molecules can configure themselves more freely in the matrix. This could be an explanation as to why a second transition is not visible at higher water activities, but future work has to be done to validate this explanation.

6.5 Conclusion

The study of the different low molecular weight components with maltodextrin DE 9-13 blends demonstrates the complexity of an apparently simple mixture. The effect of the final heating temperature on the observed transition in DSC thermograms illustrates the importance of the heating conditions on the glass transition temperature of the mixtures, with fructose being especially affected. The trends of glass transition temperatures of the various components with maltodextrin DE 9-13 content are well predicted using the approach presented in Chapter 5. Slight differences between the measured and estimated T_g values are evident at a weight fraction of 0.7 maltodextrin DE 9-13 in the system. These differences are related to the broad transitions of the mixtures present in the DSC thermograms. The widening of the transition is linked to the dynamic heterogeneous relaxation behaviour of the domains in the mixture. The distinct relaxation rates of the domains can be demonstrated by studying the enthalpy recovery of the different domains via annealing or the thermal history of stored samples. The relation of the glass transition temperature at different water activities for the different maltodextrin DE 9-13 blends

follows the same trend as the system described in Chapter 4, which highlights the common behaviour of low molecular weight and polysaccharide mixtures. The FHVT model gives a good representation of the measured T_g values at various water activities, whereas the multicomponent systems show a better alignment with the measured T_g values than the individual components themselves. The FHVT model falls short of describing the strong decrease in T_g from zero to 0.11 water activity. It is proposed that the large decrease in the T_g values is because the effect of water as a strong plasticizer, due to the local phase separation, results in a shift of the main transition to slightly lower temperatures and a second transition is visible at higher temperatures.

In this chapter, the mixing of low molecular weight components and the polysaccharide maltodextrin DE 9-13 have been described in detail. The following chapter will discuss the effect of two different polysaccharides, highly soluble inulin and resistant maltodextrin, and their mixtures on the glass transition temperature of glucose. Furthermore, alternative drying aids such as salts and their impact on the glass transition temperature are discussed.

7. Polysaccharide and salt mixtures

7.1 Introduction

The preceding study and review of the literature of low molecular weight components and their mixtures with biopolymers showed a similar trend to that seen for the mixture in Chapter 6 regarding the change in glass transition temperature with increasing biopolymer content. Thus it is possible to predict how the glass transition temperature of mixtures of low molecular weight components and polymers will behave. Most of the literature are focused on the polysaccharide maltodextrin with different dextrose equivalents, since it is a commonly utilized food ingredient. In this chapter, the impact of the addition of various polysaccharides with distinct molecular structures on the glass transition temperature of the monosaccharide glucose is discussed. Furthermore, the scope of the mixing of low molecular weight components with polysaccharides is extended by adding two and three polysaccharides together to the monosaccharide glucose.

The trend of the mixture of the low molecular weight component glucose should be identical, whether one polysaccharide or several additional polysaccharides are added, as long as no unexpected interactions between the polysaccharides take place. In order to validate this hypothesis, glucose was mixed with the following polysaccharides: highly soluble inulin (Orafti© HIS), digestive resistant maltodextrin (Fibersol©-2) and maltodextrin DE 9-13 at various ratios (0:1, 7:3, 1:1, 3:7, 2:8, 1:9 and 1:0). Moreover, a blend of the polysaccharides was created by mixing two polysaccharides together at a ratio of 1:1 such that blended combinations of inulin plus digestive resistant maltodextrin, inulin plus maltodextrin DE 9-13 and digestive resistant maltodextrin plus maltodextrin DE 9-13 were created. These blends were combined with glucose at the same ratios (0:1, 7:3, 1:1, 3:7, 2:8, 1:9 and 1:0). Finally, a combination of all three polysaccharides was produced in a 1:1:1 ratio of inulin, digestive resistant maltodextrin and maltodextrin DE 9-13 and mixed with glucose with the identical ratios as the other blends. The addition of a biopolymer with a high glass transition temperature is the most common method of increasing the glass transition temperature in a system.

Besides biopolymers, specific salts showed promising results in raising the glass transition temperature of blends with low molecular weight components. Therefore, the food safe salts disodium carbonate, trisodium citrate and trisodium phosphate were

chosen and added to glucose at the ratios 1:99, 1:19, 1:9 and 2:8, which equals 1, 5, 10 and 20%, respectively, to study the impact on the glass transition temperature. All systems were freeze dried at 10% (solids concentration) and the solid mixtures were tested for their glass transition temperatures at zero water activity via the DSC. The T_g values of the biopolymer mixtures were predicted and compared to the measured T_g values.

7.2 Polysaccharides

The three polysaccharides were analysed for their molecular weight distribution by the method stated in Chapter 3 to relate molecular weight to the observed glass transition temperature of the polysaccharide.

Inulin is a linear polysaccharide composed of D-fructose units joined by β- 2,1 bonds; the starting block is usually a glucose molecule linked by an α- 1,2 bond to a fructose molecule as found in sucrose (Figure 7.2.1). Inulin usually contains 11 to 65 repeating units of D-fructose. It is commonly extracted from chicory and belongs to the class of dietary fibres that are not digested in the small intestine (Niness, 1999). The molecular weight distribution of the highly soluble inulin can be seen in Figure 7.2.1. The blue line corresponds to the refractive index signal of the solids in the solution, whereas the red line refers to the size of the molecules. The refractive index peaks display a relatively narrow distribution, with a small leading peak. The main peak is eluted at about 68 min and contributes to roughly 80% of the total concentration; it has a M_w of 0.8 kDa and a M_n of 0.7 kDa. The leading peak contributes about 20% of the solids with a higher molecular weight of 3.3 kDa and a M_n of 2.7 kDa. As expected, the polydispersity of inulin is relatively narrow at around 1.16 and the glass transition temperature at 92.6˚C is clearly visible over a small temperature range (Figure 7.2.1). The overall molecular weight of 0.8 kDa is surprisingly low and corresponds to roughly five repeating units.

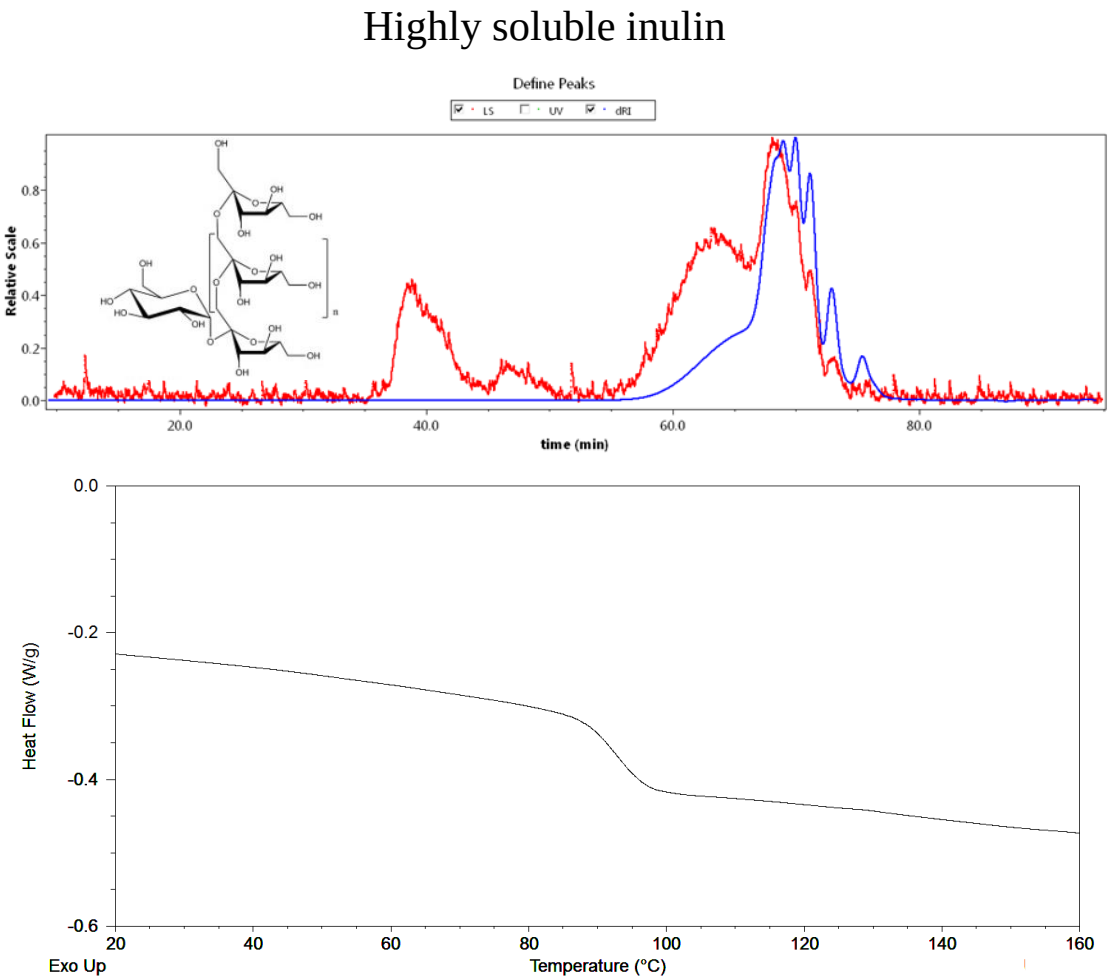


Figure 7.2.1. Molecular structure and chromatogram of inulin, as well as the representation of the observed transition of pure inulin in the DSC thermogram.

Digestive resistant maltodextrin is also a dietary fibre. It is industrially produced from starch by utilizing acid, enzyme and heat treatment to randomly rearrange the glucose units to form α- or β- 1,2, 1,3 and 1,4 bonds between them (Figure 7.2.2) (Hashizume & Okuma, 2009). The digestive resistant maltodextrin features a proportionally narrow refractive index peak as seen in Figure 7.2.2. The peak is broader than the peak for soluble inulin, with a minor bend at the beginning. The slightly broader peak contributes to 97% of the total concentration with an Mw of 3 kDa and a M_n of 1.9 kDa. The bend at the beginning of the peak only contributes to 3% of the solids with a M_w of 16.9 kDa and a M_n of 15.6 kDa, which results in a total M_w of 3.6 kDa and a M_n of 2.0 kDa. Due to the narrow peak, the polydispersity of digestive resistant maltodextrin is similar to that of inulin with a value of 1.78. This aligns with the findings of the average number and average molecular weight of various maltodextrins by Takeiti et al. (2010) . Also the

transition of the pure digestive resistant maltodextrin is marked by a clear step change seen in the DSC thermogram (Figure 7.2.2).

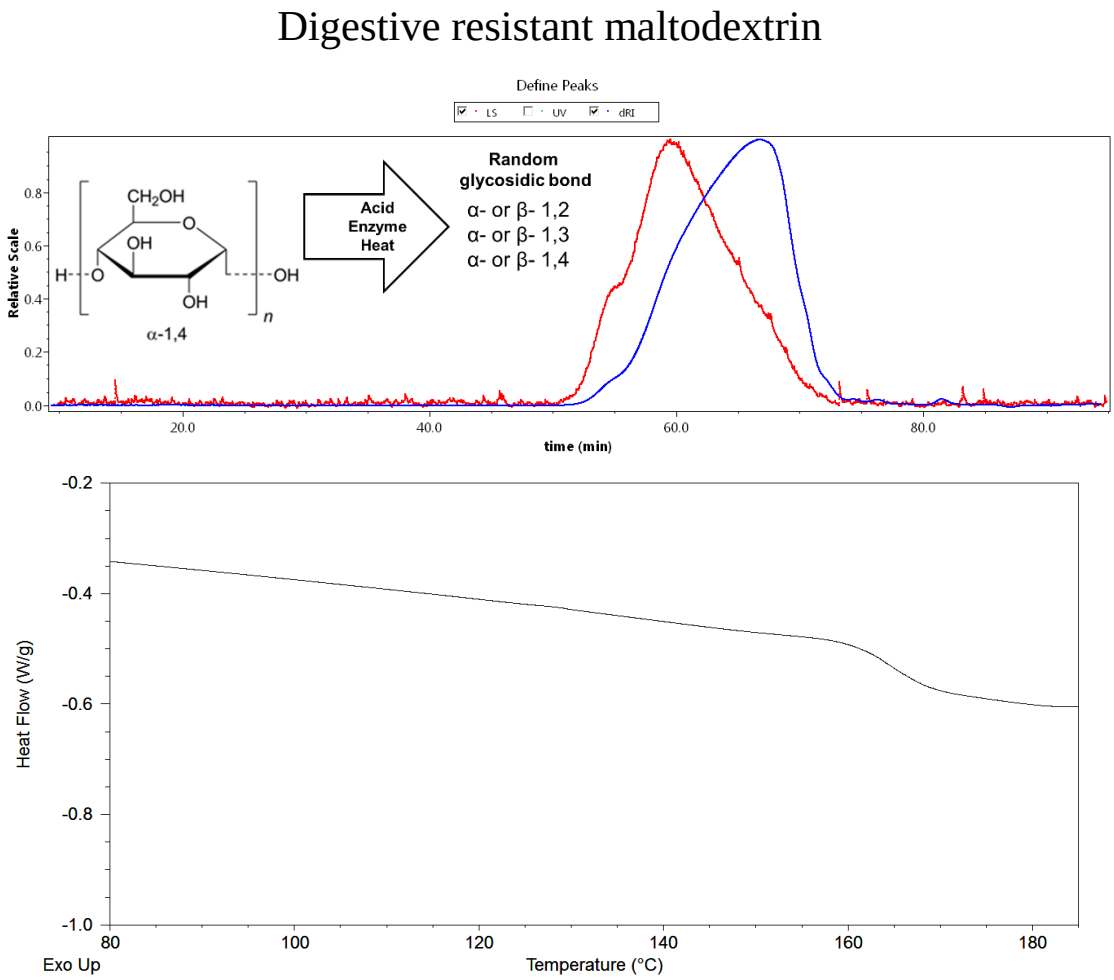


Figure 7.2.2. Molecular structure and chromatogram of digestive resistant maltodextrin, as well as the representation of the observed transition of pure digestive resistant maltodextrin in the DSC thermogram

The polysaccharide maltodextrin DE 9-13 is produced by a partial hydrolysis of starch (Takeiti et al., 2010). Unlike the previous polysaccharides, maltodextrin DE 9-13 exhibits two distinct peaks, which can be detected in the chromatogram seen in Figure 7.2.3. The first slightly broader and smaller peak is associated with a mixture of larger molecules with an average molecular weight of 101 kDa and a number average molecular weight of 44.1 kDa. This fraction contributes roughly 40% of the total solids of maltodextrin DE 9-13. The second peak is much narrower and makes up about 60% of the total concentration; the M_w of 3.4 kDa and the M_n of 1.9 kDa matches more the molar mass of digestive resistant maltodextrin. Considering the total average of both peaks, the molecular weight of 45.5 kDa and the number average of 3 kDa, with a polydispersity of 14.99, is much

higher than it would be expected for a maltodextrin and is higher than presented by Takeiti et al. (2010). In the study of Takeiti et al. (2010) the chromatogram of maltodextrin illustrates the first peak to be much closer to the second peak, resembling more the chromatograms of digestive resistant maltodextrin and highly soluble inulin. The greater portion of higher molecular components suggests that the hydrolysis of the starch has not been achieved evenly throughout the system. This high polydispersity could also be the reason for the indistinct transition observed in the DSC thermogram of maltodextrin DE 9-13 (Figure 7.2.3).

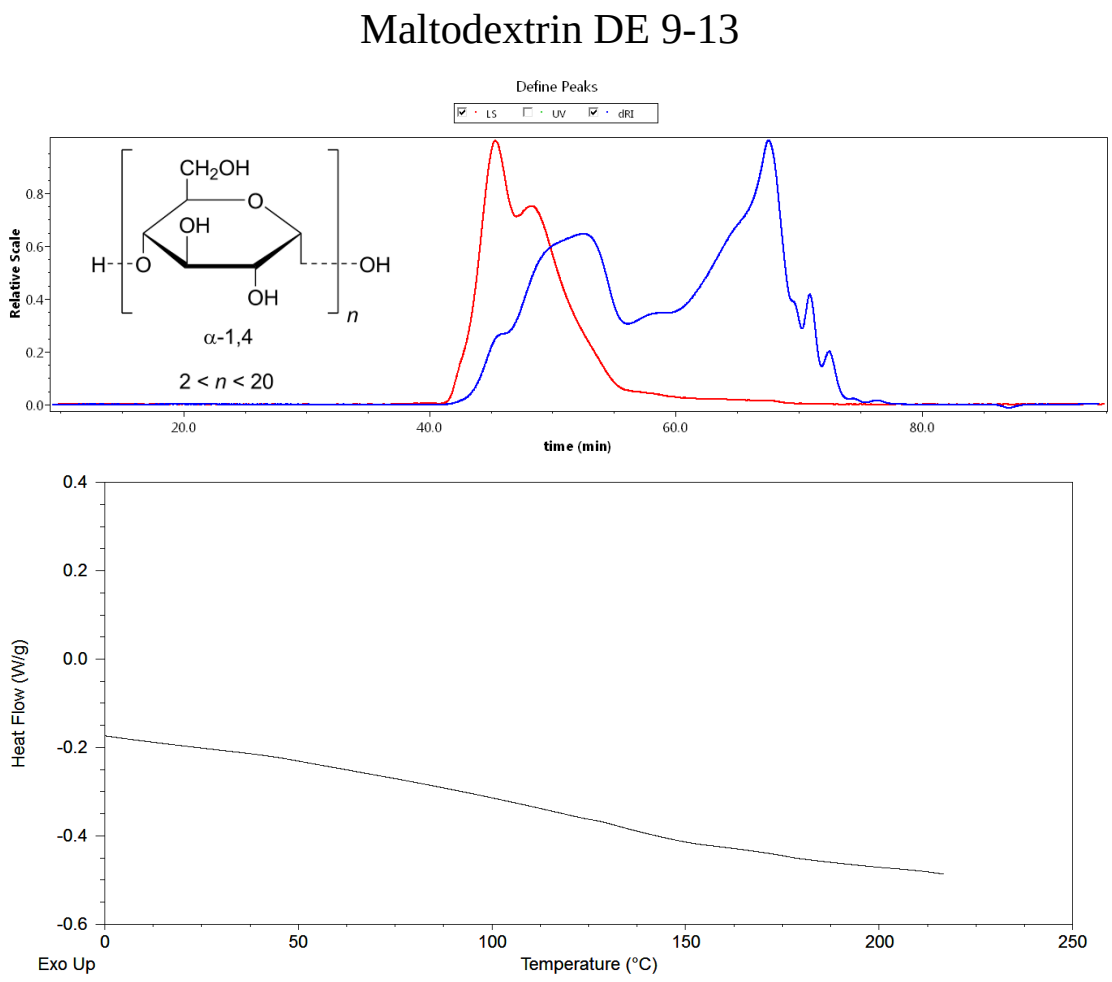


Figure 7.2.3. Molecular structure and chromatogram of maltodextrin DE 9-13, as well as the representation of the observed transition of pure maltodextrin DE 9-13 in the DSC thermogram

7.2.1 Glucose with one polymer

The three polysaccharides were added to the monosaccharide glucose to investigate the effect of different polysaccharide ratios on the glass transition temperature of the mixtures at zero water activity. The T_g values of the mixtures were predicted by using the equation (4.18); the coefficients of A_0 and A_1 were adjusted by using the difference between the glass transition temperature of pure glucose and the polysaccharides.

$$A = A_{norm}(T_{g,2} - T_{g,1}) \tag{4.19}$$

All the mixtures of glucose and the polysaccharides show the same trend as typically seen in solvent and solute systems in Chapters 4 and 6. The prediction of the inulin blend slightly underestimates the glass transition temperature of the mixtures, which could be an indicator that the mixture of glucose and the lower molecular weight inulin follows a slightly different behaviour due to the smaller difference between the molecular weight of the inulin and glucose molecules. Nevertheless, the overall trend of the measured glass transition temperatures agrees well with the predicted T_g values with an R^2 of 0.97 as seen in Figure 7.2.4. The blend of glucose and maltodextrin DE 9-13 has been already discussed in Chapter 6, but the additional systems with higher maltodextrin DE 9-13 fractions demonstrate the good prediction of the binary glass transition temperature with an R^2 of 0.99.

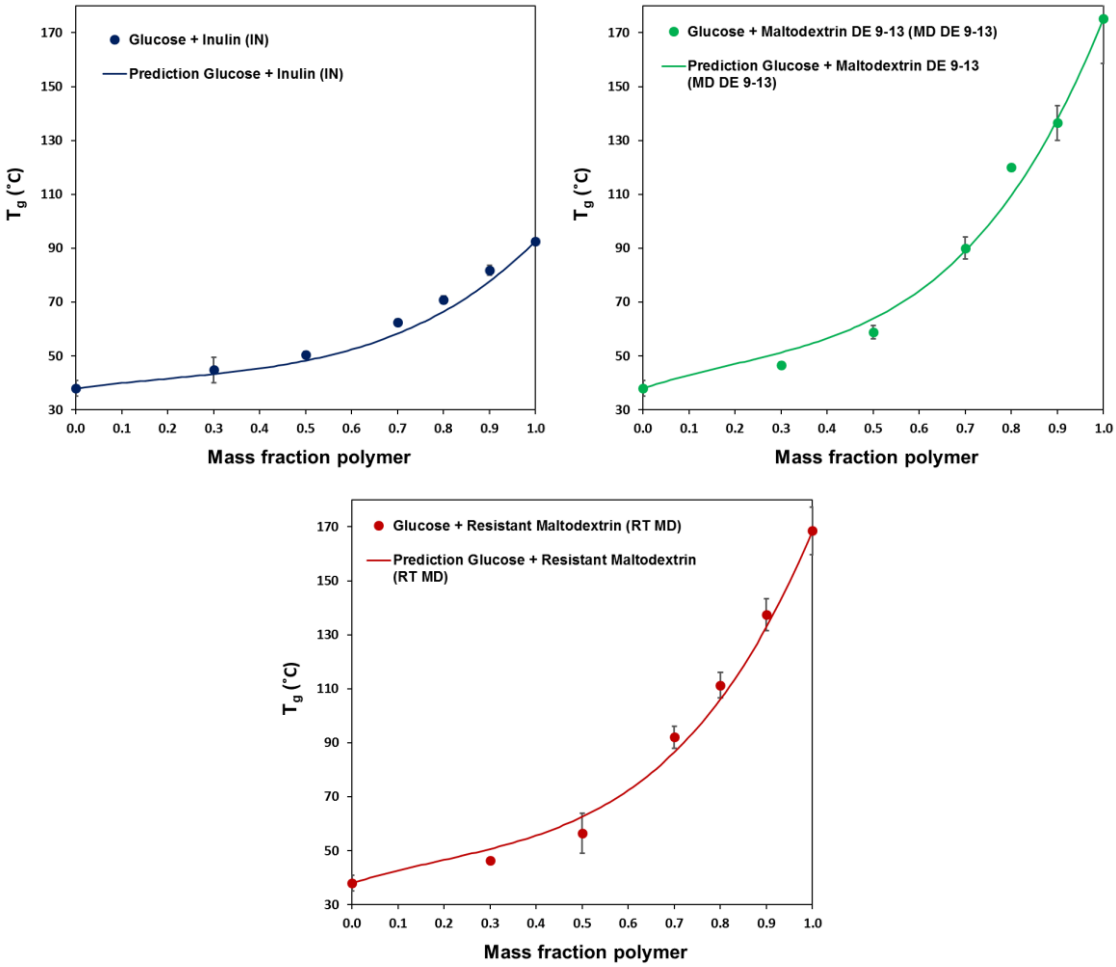


Figure 7.2.4. Representation of the measured and predicted T_g values of the binary blend of glucose and various polysaccharides at zero water activity. The error bars refer to the 95% confidence interval for n=3.

The blend of glucose and digestive resistant maltodextrin corresponds to a similar trend observed for the maltodextrin DE 9-13 mixture, with an R^2 of 0.99, which is due to the similar glass transition temperature and the similar molecular weight of digestive resistant maltodextrin and maltodextrin DE 9-13.

In Chapter 6, the changes in the thermal history for the blends of fructose or blackcurrant with maltodextrin DE 9-13 at higher contents were described. Interestingly, the same differences can be detected for the glucose and inulin blend, as seen in Figure 7.2.5. The width at 0.3 glucose and 0.7 inulin is 12.97°C, which is not nearly as broad as for all the maltodextrin DE 9-13 blends in Chapter 6. However, the thermal history is also displaying two distinct enthalpy recovery peaks, which could be an indicator that dynamic heterogeneity might be a very common phenomenon, whereby molecules of different sizes form a glassy matrix. In the future, molecules with increasing molecular size should

be mixed together to determine the necessary molecular size difference at which dynamic heterogeneity becomes noticeable.

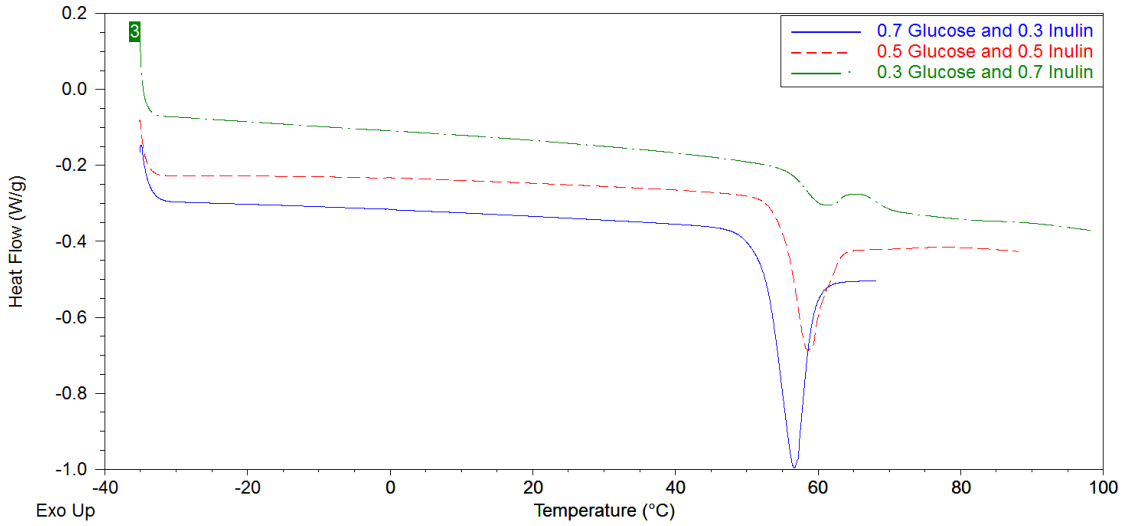


Figure 7.2.5. DSC thermogram of the thermal history of various glucose and inulin blends.

7.2.2 Glucose with two polymers

The addition of a blend of two polysaccharides at zero water activity instead of only one has the same effect as blends containing glucose plus one polymer on the glass transition temperature of the mixtures, as illustrated in Figure 7.2.6. Considering the mixture of maltodextrin DE 9-13 and inulin at the ratio of 1:1 with glucose, the T_g value is around 108.4˚C. The left graph displays the prediction using the measured T_g value, whereas the right graph shows the prediction using the estimated T_g value for the pure polysaccharide blends. The estimated T_g value is around 111˚C and thus very close to the measured T_g value. The predicted T_g values represent the trend of the glass transition temperature with the various polysaccharide fractions well. At higher polysaccharide contents the measured T_g values are deviating to higher temperatures, which is not accounted for in the prediction. The model using the estimated T_g value of the polysaccharide blend shows a slightly better agreement, since it assumes a higher T_g value and therefore matches the T_g values at higher polysaccharide contents better, with an R^2 of 0.96 instead of 0.95 using the measured T_g value. The combination of digestive resistant maltodextrin and inulin plus glucose deviates more strongly from the predicted T_g values than is the case for the maltodextrin DE 9-13 and inulin mixture. At a weight fraction of 0.5 of the polysaccharide blend the measured T_g values are higher than the predicted T_g values, which results in a poor R^2 of 0.86. This is mainly due to the low glass transition temperature of the measured 1/1 digestive resistant maltodextrin and inulin mixture of

95.86˚C. The measured T_g value is proportionally low compared with the maltodextrin DE 9-13 and inulin blend at 108.4˚C. It should be closer

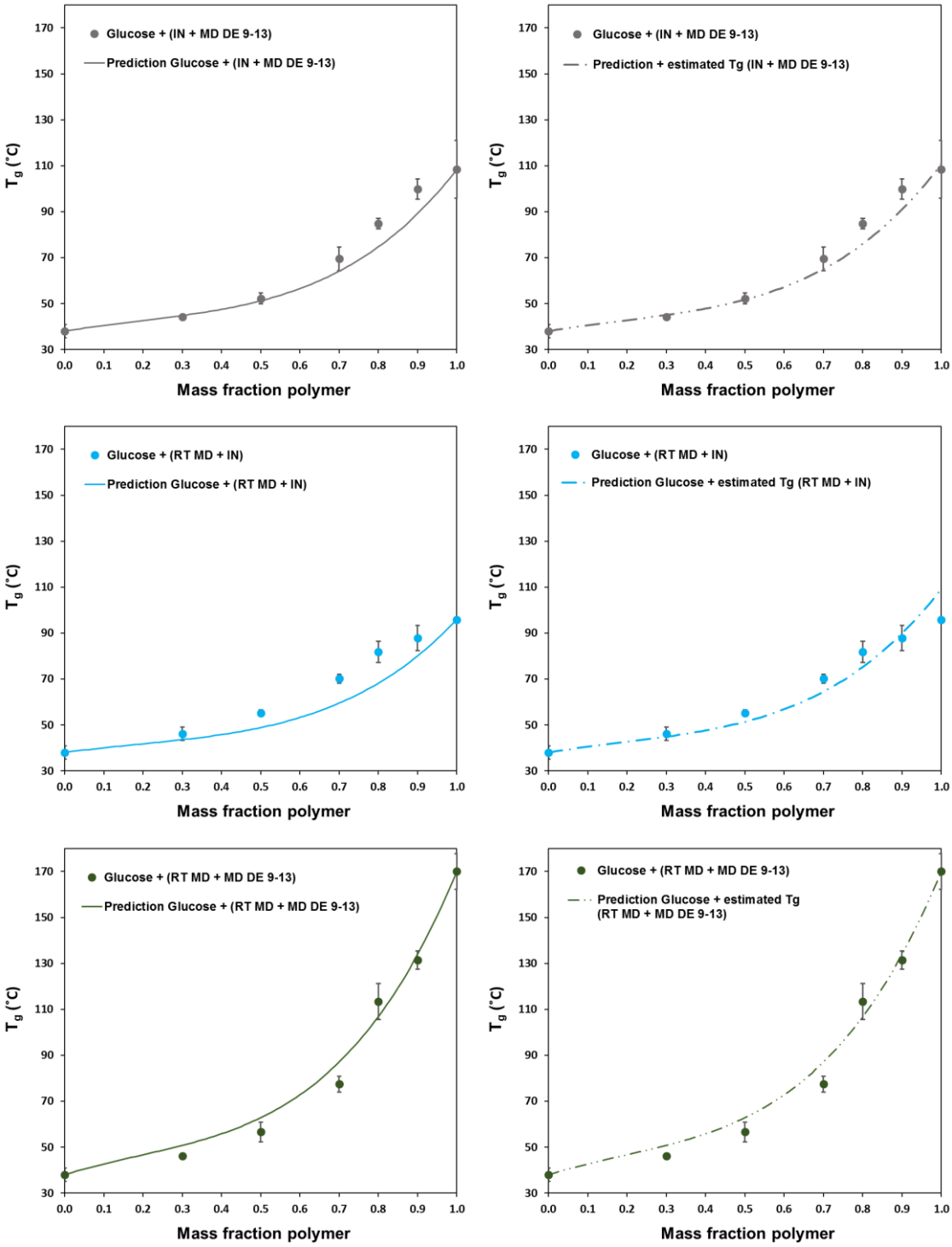


Figure 7.2.6. Representation of the measured (left) and predicted (right) T_g values of glucose and various polysaccharides blends at zero water activity. The error bars refer to the 95% confidence interval for n=3.

to the T_g value of 108.4˚C, since the glass transition temperature of pure digestive resistant maltodextrin is very close to the T_g value of pure maltodextrin DE 9-13 at

175.33˚C. By using the estimated T_g value of the blend of digestive resistant maltodextrin and inulin of 109.37˚C, the predicted T_g values follow the trend of the measured T_g values more closely with an R^2 of 0.97. The measured glass transition temperature of the blend of 1/1 digestive resistant maltodextrin to maltodextrin DE 9-13 is around 170.02˚C, which looks reasonable with the T_g values of pure maltodextrin DE 9-13 being around 175.33˚C and pure digestive resistant maltodextrin at 168.48˚C. Therefore it is not surprising that the addition of the blend of two polysaccharides has the same effect on the glass transition temperature of the glucose mixtures as additions of individual polysaccharides. The only notable difference is the divergent T_g value at 0.7 weight fraction of the polysaccharide mixture, which is around 77.46˚C, whereas for the one polysaccharide mixture the T_g value is around 90˚C. At higher or lower polysaccharide blend contents the T_g values are almost identical to the one polysaccharide systems in Section 7.2.1. The difference between the two different T_g predictions is minor: the measured and predicted T_g values are roughly 170.02˚C and 170˚C respectively with an R^2 of 0.99.

7.2.3 Glucose with three polymers

The investigation of the addition of two polysaccharides blends with glucose demonstrated that the glass transition temperature still follows the same trend as defined for one polysaccharide systems at zero water activity. In order to verify if mixtures of higher order correspond to the same pattern, three polysaccharides were mixed in equal proportions and the blend added to glucose to study the T_g values with increasing polysaccharide contents. In Figure 7.2.7 it can be observed that the behaviour of the systems with the three polysaccharide blend is identical to the previously described blends. Only the T_g value at 0.7 weight fraction of the polysaccharide blend in the system displays a shift from the pathway of T_g values with increasing polysaccharide contents. The shift of the T_g value at 0.7 weight fraction of the polysaccharide could be related to the observation fact stated by Icoz et al. (2005) and explained in Section 2.6.1, namely that as the weight fraction of the higher molecular weight component exceeds 0.7, the DSC heat flow signal of the mixture shifts to that of the component with the higher molecular weight. Since the weight fraction of 0.7 is at the outer limit of where the shift takes place, it could explain the deviations observed for the transitions at these polysaccharide fractions. The prediction using the measured T_g value of the polysaccharide mixture agrees well with the observed overall trend, with the one exception at 0.7 weight fraction, with an R^2 of 0.96.

The estimation of the glass transition temperature of the three polysaccharide mixture is not as straightforward as for the two polysaccharide systems. A weight average of the various

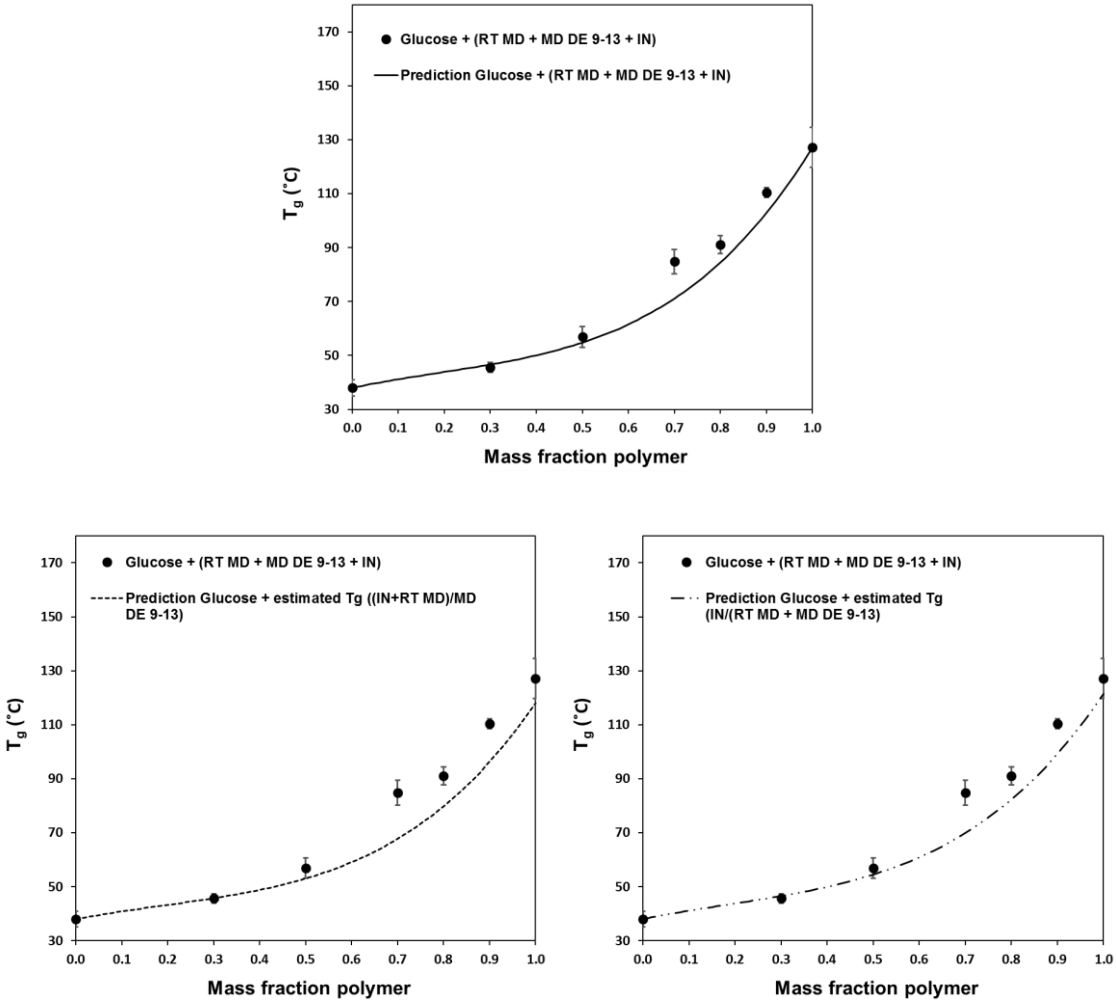


Figure 7.2.7. Representation of the measured (top) and predicted (bottom) T_g values of glucose and 1/1/1 inulin, digestive resistant maltodextrin and maltodextrin DE 9-13 a various ratios at zero water activity. The error bars refer to the 95% confidence interval for n=3.

T_g values of the polysaccharides is not appropriate, since it overestimates the glass transition temperature at 145.47˚C for the mixture. The polysaccharide mixtures follow the same principals as the mixtures of low molecular weight components with polymers. The problem that arises is that the multicomponent mixture is projected onto a binary system making it necessary to define a sequence of the mixing calculation, which manipulates the end results. In other words, the order in which the calculation is made affects the final result. In the left bottom graph, first the glass transition temperature of the mixture of digestive resistant maltodextrin with inulin is estimated. Then the T_g value of the binary system, at 109˚C, is set in relation to the glass transition temperature of pure

maltodextrin DE 9-13, resulting in a T_g value for the mixture of 118˚C. The other approach would be to calculate the glass transition temperature of digestive resistant maltodextrin and maltodedxtrin DE 9-13 first, at170˚C, and then set the estimated T_g value in relation to the T_g value of inulin, which gives a final T_g value of 121˚C for the polysaccharide mixture. The difference is not significant, but due to the distinct sequence the T_g values are slightly shifted resulting in a poorer agreement for the lower estimated T_g value (R^2 of 0.90) than for the higher estimated T_g value (R^2 of 0.94) (Figure 7.2.7).

7.3 Salts

The influence of salts on glass transition temperature was investigated because previous studies have indicated a positive impact of salts on the glass transition temperature of low molecular weight components. Kets et al. (2004) studied the effect of adding trisodium citrate to sucrose on the glass transition temperature of these mixtures. It was reported that at a weight fraction of 0.3 trisodium citrate in the mixture and zero moisture content, the glass transition temperature of the mixture was around 105˚C, whereas low moisture contents in the sample resulted in separation into two domains, one with a lower and the other with a higher T_g value. By investigating the OH stretching band of sucrose and trisodium citrate via FTIR and comparing it with that from pure sucrose, a shift to higher wavenumber could be detected. This indicates that the total hydrogen bond network becomes stronger on the addition of trisodium citrate to the solid matrix. Elmonsef Omar and Roos (2007) studied the glass transition temperature of lactose with small additions of various salts. The analysis of the different mixtures demonstrated that a salt consisting of monovalent ions such as sodium- and potassium chloride decreased the glass transition temperature. A study by Farahnaky et al. (2009) highlighted that the addition of sodium chloride to starch also reduced the glass transition temperature of the system. On the other hand, the addition of salts such as divalent magnesium- and calcium chloride increased on the glass transition temperature of the mixture.

Based on the different studies it is hypothesized that salts containing divalent ions act as a plasticizer by attaching to one of the hydroxyl groups (Figure 7.3.1) and therefore inhibiting the local dipole-dipole interactions between the molecules in the systems. Salts containing two sodium ions, such as disodium carbonate, can form two ion-dipole interactions with the hydroxyl groups of two separate molecules. This suggests that these salts act as a connector between low molecular weight components such as sugars (Figure 7.3.1). In carbohydrates the most common interaction between the sugar molecules are

dipole-dipole interactions in the form of hydrogen bonds. The strength of the hydrogen bonds is much weaker than the ion-dipole interactions, which occur between for example the hydroxyl group and the sodium atom (Israelachvili, 2011). This could imply that the salts and the other low molecular weight components form a more rigid structure and more energy is needed to break up the bonds for translational motion to take place, which could explain the higher glass transition temperature of mixtures with salts.

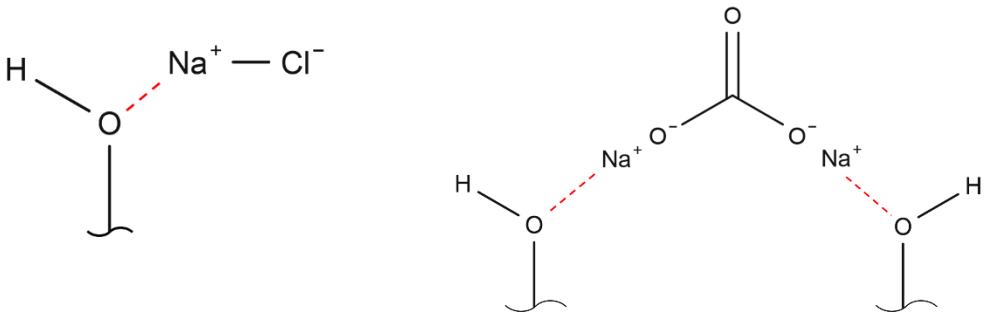
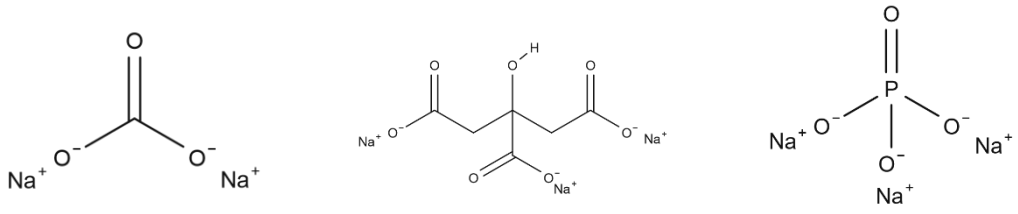


Figure 7.3.1. Outlined mechanism of monovalent salts in their interaction with other molecules in comparison to monovalent salts.

As discussed above, monovalent salts are not suitable to increase the glass transition temperature of the monosaccharide glucose. Therefore, the three multivalent salts in Figure 7.3.2 were chosen and their influence on the glass transition temperature with glucose was tested at zero water activity.



Disodium carbonate	Trisodium citrate	Trisodium phosphate
M_w=105.99 g/mol	M_w=258.06 g/mol	M_w=163.94 g/mol

Figure 7.3.2. Molecular structures and weights of disodium carbonate, trisodium citrate and trisodium phosphate.

In all three cases the addition has a direct effect on the glass transition temperature (Figure 7.3.3). The effects of disodium carbonate and trisodium citrate follow a similar trend. With increasing salt content the glass transition temperature of the mixtures increases strongly up to 0.1 weight fraction of salts in the systems. From this point on the increase

of the T_g value starts to flatten out and reaches T_g values of around 60˚C at 20% salt content. The mixture of glucose and trisodium phosphate behaves differently. In this case the glass transition temperature increases linearly with increasing content of trisodium phosphate in the system. At 0.1 weight fraction of trisodium phosphate the T_g value is at ca. 66.65˚C, surpassing the T_g value of the glucose blends with disodium carbonate and trisodium citrate at 0.1 weight fraction. With further increase to 0.2 weight fraction of trisodium phosphate in the mixture, the T_g value of the mixture rises to ca. 94.11˚C. Temperatures above 110˚C resulted in a reaction taking place, which makes an investigation of systems with higher salt contents not feasible.

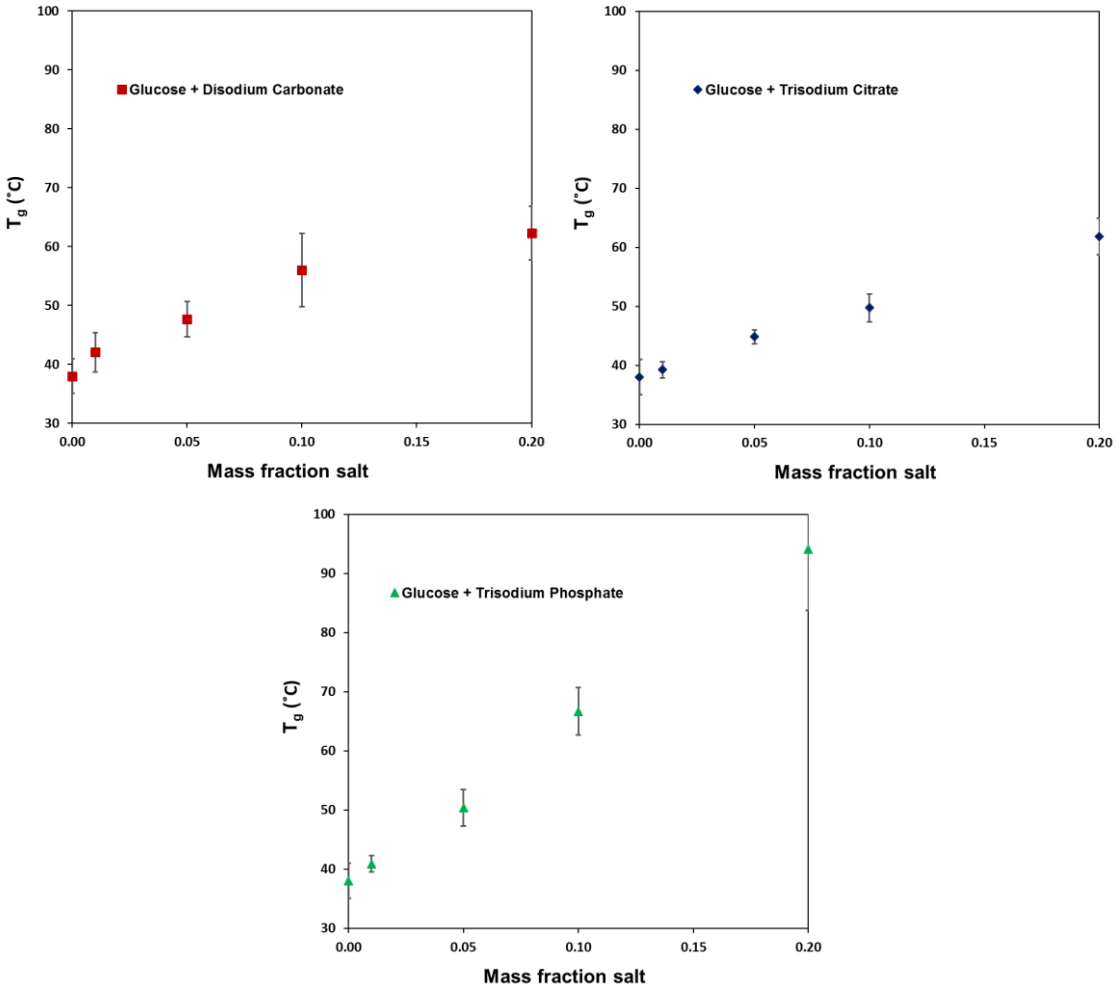


Figure 7.3.3. Measured T_g values of glucose with various salt blends at zero water activity. The error bars refer to the 95% confidence interval for n=3.

The great difference between the addition of a polysaccharide or a salt to increase the glass transition temperature of glucose is the observed effect of small fractions of salt on the T_g values. In Figure 7.3.4 the different salt blends are plotted against the glucose and maltodextrin DE 9-13 blends. Between a weight fraction of 0.3 and 0.5 maltodextrin DE 9-13 in the system, the impact of maltodextrin DE 9-13 on the glass transition temperature is very low. Even at a weight fraction of 0.5 the T_g value is at ca. 58.91˚C, which is still below the T_g values of glucose blends containing disodium carbonate and trisodium citrate at 0.2 weight fraction. In order to reach the T_g value of the glucose blend with trisodium phosphate at 0.4 weight fraction (90˚C), the glucose and maltodextrin DE 9-13 blend has to contain about 70% maltodextrin DE 9-13 (Figure 7.3.4).

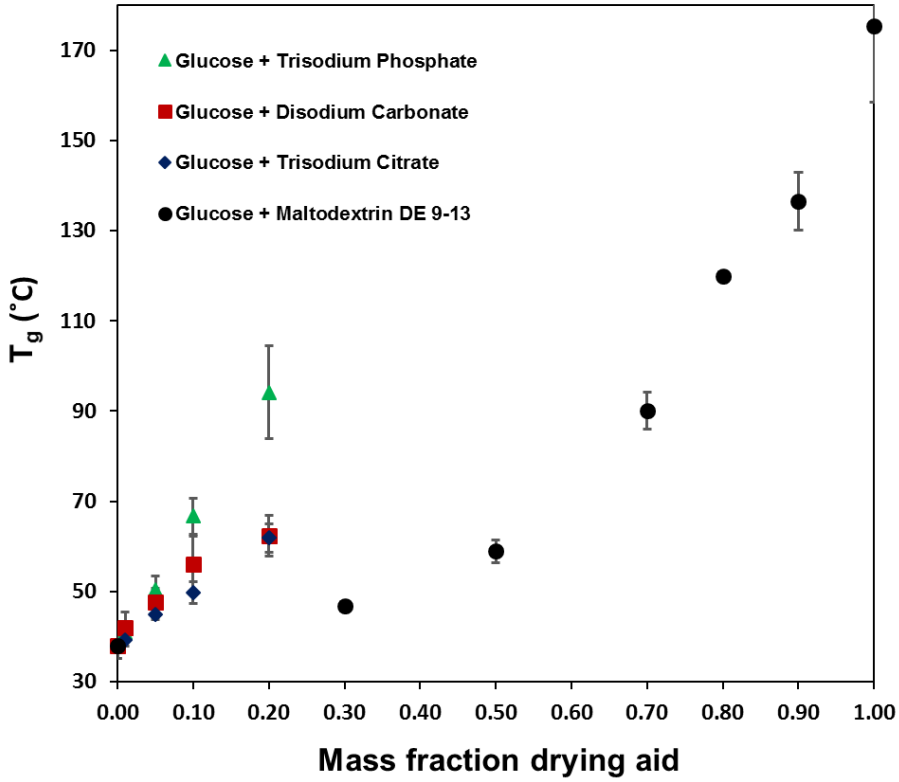


Figure 7.3.4. Comparison of the effect of salt and polysaccharide addition on the T_g values of mixture with glucose at zero water activity. The error bars refer to the 95% confidence interval for n=3.

This observed difference between the polysaccharides and salts could be related back to the molecular structure (Figure 7.3.5). As already previously explained in Chapter 6, if a polymer is introduced to a mixture of low molecular weight components at lower concentration, the low molecular weight components will interact with the polymer, but the whole molecular mobility is mainly determined by the smaller molecules. At higher concentrations of the polymer there are enough polymer molecules to restrict the mobility

of the smaller molecules and the whole structure becomes more rigid. Salts on the other hand have roughly the same molecular weight as low molecular weight component such as glucose. Therefore, even at smaller concentrations, more salt molecules are introduced into the mixture and the salts can act as a connector between the molecules, forming a denser molecular structure (Figure 7.3.5). This could be one possible explanation for the observed difference in the glass transition temperature between the addition of salts and polysaccharides to the monosaccharide glucose. In the future, additional FTIR and NMR studies could be used to further verify this explanation of the different mixing behaviour.

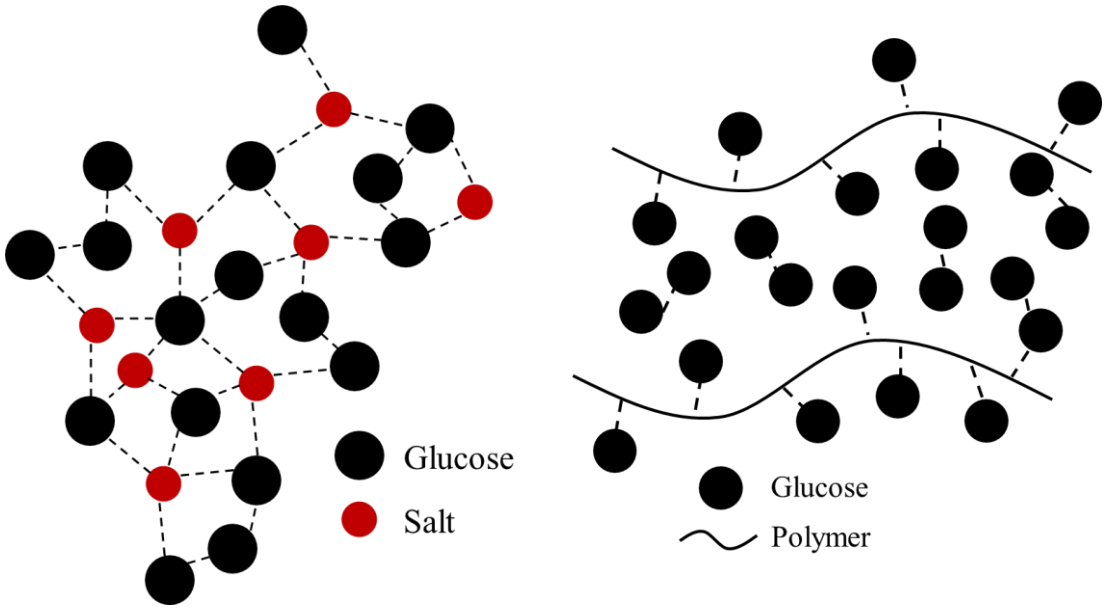


Figure 7.3.5. Schematic drawing of the possible different mechanisms by which salts and polysaccharides affect the molecular structure of mixtures containing low molecular components such as glucose.

7.4 Conclusion

The examination of the impact of various polysaccharides and their combinations on the glass transition temperature of glucose blends demonstrates well that the overall mixing behaviour of low molecular weight components and polysaccharides is similar, regardless of the polysaccharide in the system. By combining various polysaccharides the final glass transition temperature of the blend changes, but the overall trend of the T_g values can still be predicted once the glass transition temperature of the polysaccharide mixture is known. The study further shows that even by predicting the T_g values only on the basis of the T_g values of the pure components the agreement between the measured and predicted T_g

value is very good. This highlights the possibility to use a prediction approach based on the chemical composition to estimate the T_g values of mixtures.

The investigation of the various salts reveals another method to increase the T_g values of low molecular weight components as an alternative to the addition of polymers with a high glass transition temperature. Salts raise the glass transition temperature of glucose at lower concentrations than polysaccharides and it becomes obvious the mechanisms by which salts and polysaccharides raise of the glass transition temperature are quite distinct. The results of the salts suggest new opportunities for more studies to characterize the potential of small quantity of salts in formulations to modify the T_g value of mixtures.

After gaining enough confidence in the accuracy of the prediction method, the predictive approach is used to estimate reasonable spray drying conditions for a blackcurrant and maltodextrin DE 9-13 blend without relying on a trial and error approach. These results are discussed in the following chapter.

8. Case study of spray drying fruit juice

8.1 Introduction

The previous chapters demonstrate the feasibility of providing a good estimation of the glass transition temperature of mixtures on the basis of their chemical composition. Furthermore, it has been shown that the FHVT model is a useful tool to predict the relationship of the moisture content to the glass transition temperature at various water activities. By having a valuable method of identifying the glass transition temperature of different compositions and operating conditions, the risk of potential related stability issues such as caking during storage, as well as collapse and stickiness during processing can be prevented or minimized. The company (Frezzor Inc.) approached our group and requested a spray dried blackcurrant powder for their product. In order to successfully spray dry fruit juices, effective quantities reasonable amounts of drying aids and operating conditions are usually found by trial and error. In this study the goal was to avoid the trial and error approach by using a predictive method to define the necessary parameters. Therefore, the presented prediction approach was used to define an acceptable ratio of maltodextrin DE 9-13 to blackcurrant juice concentrate solids (11/9) to raise the glass transition temperature of the powder to make spray drying viable. A mass and energy balance of a spray dryer allows the operating range to be found without the particle surface exceeding $T\text{-}T_g$=25˚C. In this chapter the procedure for finding reasonable drying aid content and operating conditions for the successful spray drying of a blackcurrant juice and maltodextrin DE 9-13 blend is presented in greater detail.

8.2 Determination of the operational conditions range

As mentioned in Chapter 2, in spray drying the instant stickiness of the particles to the chamber wall or to other particles can result in product and quality loss or, in the worst case scenario, blockage of the spray dryer. The stickiness of the particles is attributed to their surface properties, especially the viscosity. Once the viscosity on the particle's surface is reduced from about 10^{12} Pa·s to 10^{7} Pa·s, liquid bridges can be formed between contiguous particles (Bhandari & Roos, 2017), which results in agglomeration of the particles. The decrease in viscosity is attributed to the components at the surface transitioning from the glassy to the rubbery state. The temperature above T_g at which the critical viscosity is surpassed is called the sticky point temperature (T_s). Paterson et al.

(2007) studied the particle stickiness of six dairy powders using a particle gun. The particles of the various powders were shot at stainless steel disks and the amount of deposition on the plate was measured. It was assumed that the particle surface equilibrates to the relative humidity of the transporting air before it comes in contact with the steel disk. It could be demonstrated that the temperature and relative humidity conditions at which the particles start to stick to the plate can be expressed by the difference of $T-T_g$=sticky point temperature. The limits for the difference of $T-T_g$ are strongly dependent on the composition at the surface of the particle. The disaccharide, lactose started to adhere to the plate surface at $T-T_g$=22.8˚C similar to the sticky point temperatures of 25˚C measured by Brooks (2000) and 26.2˚C measured by Chatterjee (2004). The difference of $T-T_g$ of skim milk and whole milk powders were between 33˚C and 40˚C, indicating that additional components such as proteins and fats have an effect on the elastic properties of the particle surface, which shifts the $T-T_g$ difference to higher limits. The impact of proteins on the particle morphology has been already been explained in greater detail in Section 2.9. Murti (2006) studied the sticky point of skim milk powder with a particle gun similar to that previously described, but also changed the air velocity from 5 to 35 m/s and the impact angle. It could be demonstrated that the $T-T_g$ increases linearly with velocity. This is related to the greater momentum of the particles such that the cohesive and adherence forces have to be greater to allow the particle to stick. For simplicity reasons, it was assumed that the velocity of particles was constant around 20 m/s and the $T-T_g$ values could be related to the values presented for lactose previously.

In the case of the solids mixtures of fruit juices, the main components that contribute to the T_g of the powder are the sugars and organic acids, which resemble the molecular structure and thermoplastic behaviour of lactose. Therefore it was assumed that the maximum of $T-T_g$=25˚C should not be surpassed to avoid stickiness occurring in the spray dryer. In this work, it was not possible to clarify if the drying aid maltodextrin DE 9-13, besides raising the glass transition temperature of the mixture, had an impact on shifting $T-T_g$ to higher values by modifying the viscosity at the particle surface. Unlike for proteins, it is assumed that the polysaccharide maltodextrin DE 9-13 is evenly distributed in the bulk of the particle and is not accumulated on the surface as stated by Fang and Bhandari (2012). Therefore it is assumed that the T_g value at the surface is identical to the measured bulk glass transition temperature. With this assumption, the glass transition temperature of the blackcurrant juice and maltodextrin DE 9-13 blend can be predicted using equation (4.23) and plotted as shown in Chapter 6 (Figure 8.2.1). It

was decided that a weight fraction of 0.55 maltodextrin DE 9-13 in relation to the solids in the blackcurrant juice should provide a sufficiently high glass transition temperature of 67˚C to successfully spray dry the mixture.

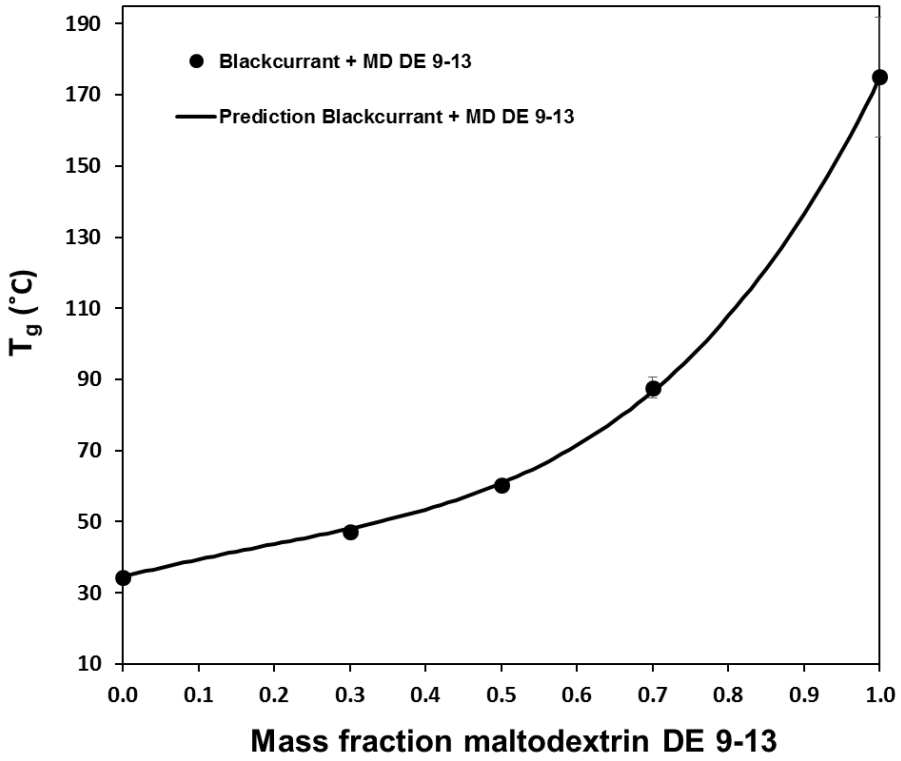


Figure 8.2.1. Prediction of blackcurrant juice and maltodextrin DE 9-13 blend with various ratios at zero water activity, as presented in Chapter 5.

The next step required is to determine reasonable operating conditions to avoid stickiness in the spray dryer. Paterson and Bröckel (2015) presented a procedure for finding an operational range by considering the mass and energy balance of the spray dryer. With the known solid concentration and flow rate of the feed, the air flow, evaporation rate, inlet air temperature, inlet temperature and heat losses, the final outlet temperature and relative humidity at the bottom of the spray dryer can be estimated. The approach was used for the GEA Niro Minor pilot scale spray dryer and the prediction showed a good agreement with the experimental results for milk powder. Zuo et al. (2004) calculated the spray drying conditions of skim milk for various feed flows and inlet temperatures with the corresponding outlet temperatures and relative humidities. If it is assumed that the surface of the particle reaches equilibrium with the surrounding relative humidity at the bottom of the spray dryer, the glass transition temperature at the surface can be estimated as a function of the relative humidity. The difference of the determined outlet temperatures and the predicted T_g values at the surface of the particles can be plotted over

the outlet temperatures for the various feed flow configurations. In the case of the blackcurrant juice and maltodextrin DE 9-13 mixture, the outlet and relative humidities were estimated for feed flows of 0.8, 0.9, 1.2 and 1.5 kg/h with inlet temperatures from 80˚C to 180˚C with an increment of 10˚C. The relation of the glass transition temperature and the relative humidity was determined by the FHVT model as explained in depth in the previous chapters.

In the case of this study, Table 8.2.1 gives a clearer description of the approach for the feed flow set to 0.9 kg/h. With all the important additional dryer properties such as air flow, evaporation etc. with the mass and energy balance, the outlet temperature and the corresponding relative humidity are estimated for a 0.9 kg/h feed flow with a fixed 40% solids concentration of the blackcurrant juice and maltodextrin DE 9-13 blend.

Table 8.2.1. Estimation of the outlet temperature glass transition temperatures at different inlet temperatures at a fixed feed flow and composition of blackcurrant and maltodextrin DE 9-13.

0.9 kg/h feed flow

40% solid concentration (0.45 BL + 0.55 MD DE 9-13)

T_{inlet} (˚C)	$T_{outlet,\ pred}$ (˚C)	$RH_{,pred}$ (%)	$T_{g,pred}$ at $RH_{,pred}$ (˚C)	$T_{outlet} - T_{g,pred}$
70	42	29	23	18
80	49	20	34	14.5
90	56	14.5	42	14
100	62	11	47	15
110	68	8	50	17.5
120	73	7	53	20
130	78	5	55	23
140	82	4.5	57	26
150	86	4	57	30
160	90	3.5	59	34
180	95	3	60	35

The glass transition temperature at the surface of the particle for the 0.45 blackcurrant and 0.55 maltodextrin DE 9-13 blend was predicted in relation to the corresponding relative humidity and subtracted from the outlet temperature to obtain $T\text{-}T_g$.

The $T\text{-}T_g$ values can be obtained for other feed flows and the difference of $T\text{-}T_g$ can be plotted over the outlet temperature as seen in Figure 8.2.2.

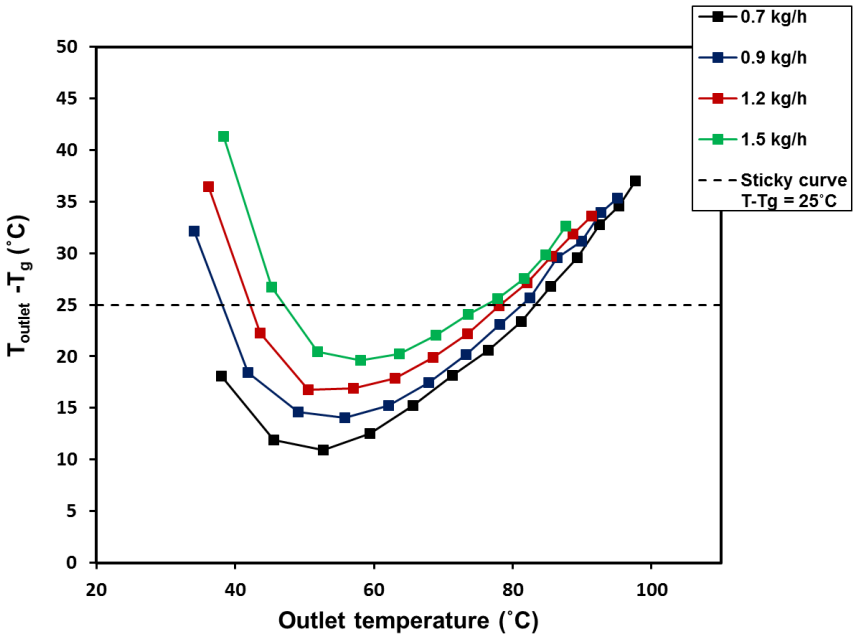


Figure 8.2.2. $T\text{-}T_g$ values as a function of the estimated outlet temperatures for 0.45 blackcurrant and 0.55 maltodextrin DE 9-13 blend estimated at various feed flows.

The points presented for $T\text{-}T_g$ in Figure 8.2.2 imply that there would be an optimum outlet temperature to operate the spray dryer with an outlet temperature around 55˚C for the different feed flows. However, this would mean the inlet temperature would be around 100-110˚C, which is too low for the conventional pilot scale spray dryer to provide a rapid evaporation of the water to form a solid particle. A feed flow of higher than 1 kg/h was not recommended for the pilot scale spray dryer due to possible blockage of the filter system, therefore the feed flow was targeted around 0.9 kg/h. Figure 8.2.3 displays the different operation regions. As mentioned, an outlet temperature below 60˚C is not realistic for this conventional spray dryer (blue area) and working at conditions above $T\text{-}T_g$=25˚C the powder would start to stick to the chamber wall, as shown by the red line for drying of pure blackcurrant juice (grey area). An outlet temperature from 60˚C to 80˚C provides a range where a free flowing powder can be produced, avoiding any stickiness issues (yellow area).

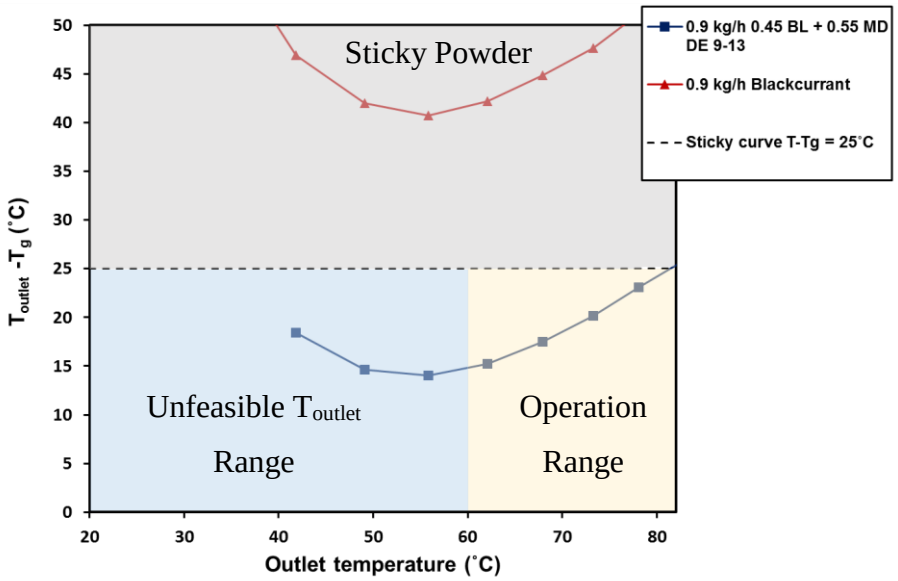


Figure 8.2.3. Characterization of the operating regions regarding the outlet temperature and T-T_g.

The final operational conditions of the spray dryer can be seen in Figure 8.2.4. An outlet temperatrure of 65˚C was kept by adjusting the inlet temperature around 120˚C and the feed flow around 0.87 kg/h. This results in a T-T_g≈20˚C, which gave a reasonable safety margain from the assumed maximum permitted T-T_g=25˚C and made for a successful production of a free flowing powder on the first tray (Figure 8.2.4). The client was very satisfied with the powder as an ingredient for their product.

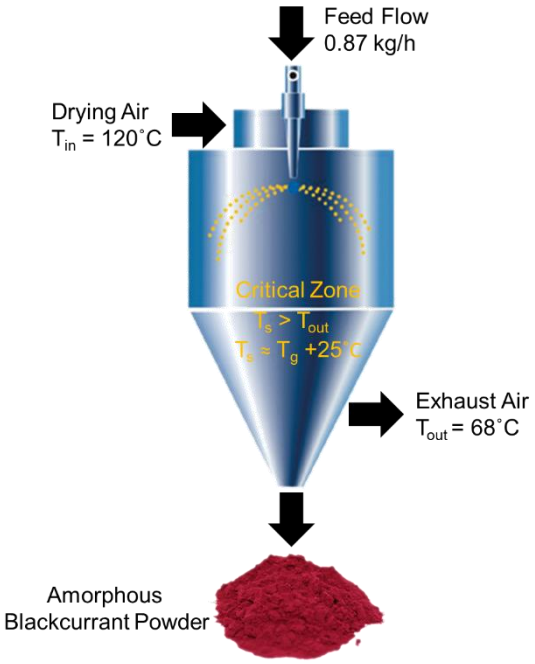


Figure 8.2.4. Final operating conditions during spray drying.

After successfully spray drying the blackcurrant and maltodextrin DE 9-13 blend, the powder was studied via DSC at various water activities of 0, 0.11, 0.22 and 0.32 in order to confirm the powder exhibited the same T_g relation at low water activities as the previous described freeze dried maltodextrin DE 9-13 blends. The relation between the glass transition temperature and the water activities follows the same trend as described

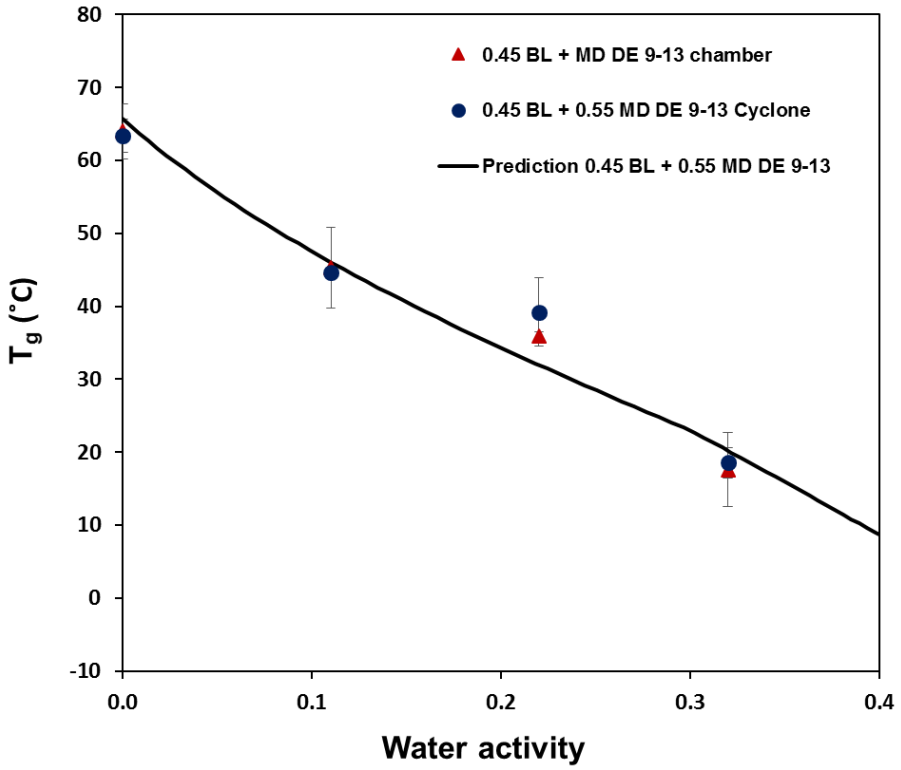


Figure 8.2.5. Prediction of the effect of water on the T_g depression of 0.45 blackcurrant and 0.55 maltodextrin DE 9-13 using the estimated T_g value for the FHVT model. The error bars refer to the 95% confidence interval for n=3

for the powders in Chapter 6 with an R^2 of 0.98 and 0.94 for the powder recovered from the chamber and cyclone respectively (Figure 8.2.5). The measured glass transition temperatures at 0.22 water activity for both powders are the only T_g values that deviate slightly from the predicted T_g values.

The chosen ratio of blackcurrant juice solids to maltodextrin DE 9-13 proved sufficient to allow spray drying of the mixture, but it would be interesting to know how the different ratios of maltodextrin DE 9-13 would affect the T-T_g trends. In Figure 8.2.6, the theoretical T-T_g values at a feed flow of 0.9 kg/h for the discussed blackcurrant juice and maltodextrin DE 9-13 blend with the ratios 0, 3/7, 1/1, 7/3 are displayed.

As discussed previously, it is not feasible to dry the pure concentrated blackcurrant juice due to the low glass transition temperature of the solids mixture. An increase to a weight fraction of 0.3 maltodextrin DE 9-13 in the blend results in a shift of the T-T_g values to just above the defined sticky line. As expected, at a weight fraction of 0.5 maltodextrin DE 9-13 the blend would be sprayable, and the minimum requirement of maltodextrin DE 9-13 could be found between a weight fraction of 0.3 and 0.5 under the present defined conditions. An increase of the maltodextrin DE 9-13 to a weight fraction of 0.7 results in a mixture that more closely resembles maltodextrin DE 9-13 and no stability issues at any operation range should be encountered.

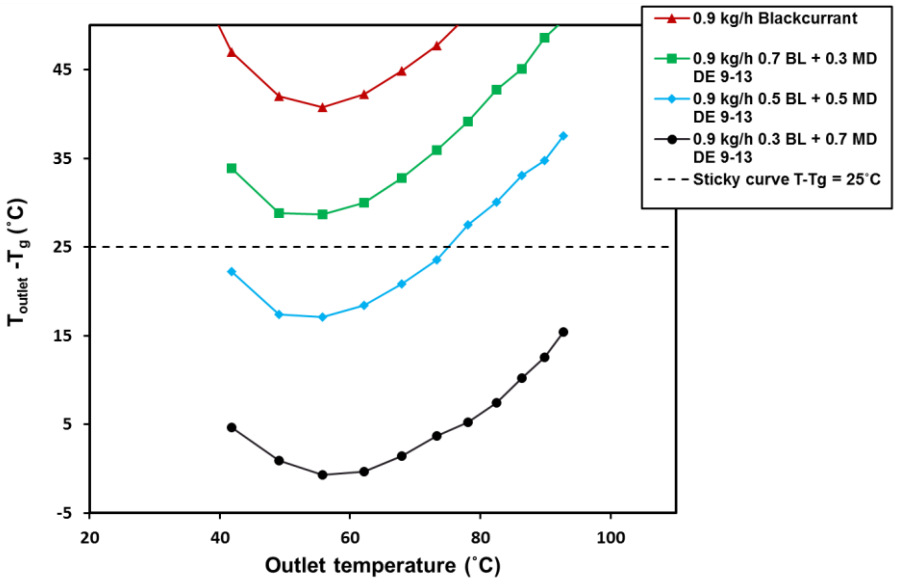


Figure 8.2.6. T-T_g values as a function of the estimated outlet temperatures for blackcurrant and various blends with maltodextrin DE 9-13 at a fixed feed flows of 0.9kg/h.

Throughout the study, it was assumed that the maximum for T-T_g=25˚C was set as a fixed value, since it agrees well with the findings for the disaccharide lactose. However, as disccused previously, the assumption that instant stickness occurs at T-T_g=25˚C for different ratios of maltodextrin DE 9-13 has not been verfied. In the previous chapter, the effect of additional polysaccharides on the glass transition temperature has been documented, but it is not clear if T-T_g also shifts to higher values with the increase of the polysaccharide content. In future studies some of the presented polysacchride mixtures should be tested for their sticky point via the particle gun and correlated back to the measured glass transition temperatures. This would give more insight into the relation of the glass transition temperature and the sticky point for polysaccharide mixtures. Furthermore, the use of polysaccharides with various molecular weights would be

recommanded in order to investigate if $T-T_g$ can be directly linked to the molecular weight of the components due to the increase of the visoelasticity of the mixture. With that knowledge a new set of spray drying trials could be done to find the absolute minimum requirement of maltodextrin DE 9-13 content to produce a free flowing powder.

8.3 Conclusion

The presented study highlights a possible approach to define reasonable operating conditions to spray dry a fruit juice on the basis of the chemical composition of the product and the aligned thermoelastic properties in combination with a general mass and energy balance of a spray dryer. The objective of this method is to provide the operator with a first draft of a reasonable operating range to avoid stickiness when formulating a new formulation. This allows the operator to directly rule out specific mixtures that cannot be succesfully spray dried. Once the operating conditions are chosen, other spray dryer criteria have to be taken into account to guarantuee a succesful spray dry trial such as particle size and distribution and drying rate. By combining the fundamental processes occuring during spray drying it would be possible to find the optimum operating conditions and maximise the spray drying output.

9. Conclusions and future work

9.1 Conclusions

The goal was to provide accurate prediction capability for T_g from fruit and vegetable powder composition and water activity. By knowing the glass transition temperature of solid mixtures, the stability related issues, such as stickiness in the spray dryer, can be minimized. The relationship between the sticky point and the glass transition temperature allows the determination of acceptable dryer operating conditions.

In this work a new method of predicting the glass transition temperature of low molecular weight mixture of carbohydrates was developed on the basis of their chemical composition. An adapted Flory-Huggins Free Volume Theory (FHVT) was presented as an alternative approach for estimating the sorption isotherm of fruit juice powders on the basis of the chemical composition, instead of relying on the fitting of the BET or GAB models to experimental data. The combination of the prediction method, the glass transition temperature and the FHVT model were applied to estimate the glass transition temperature at various water activities for fruit powders presented in the literature. The trend in glass transition temperature was very well represented by this approach, with the chemical composition of the powders being the only necessary input criteria.

Some fruit juice powders made without drying aids reported in the literature showed a disagreement between the measured and predicted T_g values at zero water activity. Therefore, six commercial fruit juices were converted into a powder and studied for their glass transition temperature at zero water activity. It was shown that the measured T_g values of the powders at zero water activity were around 6 to 8˚C higher than the predicted values. A study of the chemical composition suggested that the breakdown products of residual soluble polysaccharides increase the glass transition temperature and were responsible for a second glass transition temperature visible in the DSC thermogram.

The addition of maltodextrin DE 9-13 to various low molecular weight components exhibited a similar overall trend in increasing the glass transition temperature, which was well predicted by the model. Deviation between the measured and predicted T_g values at higher contents of polysaccharides can be attributed to the widening of the transition, which is linked to the dynamic heterogeneous relaxation behaviour of the different domains in the mixture. The distinct relaxation rates of the domains could be demonstrated by studying the enthalpy recovery of the different domains via annealing

or the thermal history of stored samples. The relation between the glass transition temperature at different water activities for the different maltodextrin DE 9-13 blends followed by a similar increase in T_g, which highlights the common behaviour of low molecular weight and polysaccharide mixtures observed in this work.

The examination of the impact of various polysaccharides and their combinations on the glass transition temperature of glucose blends demonstrated that the overall mixing behaviour of low molecular weight components and polysaccharides is similar, regardless of the polysaccharide in the system. It could be demonstrated that salts can be used as alternative drying aids as they raise the glass transition temperature at zero water activity at much lower concentrations than is the case for polysaccharides. The mechanisms of the raising of the glass transition temperature by salts and polysaccharides are quite distinct. Salts have a similar molecular weight and size as glucose and it is assumed that due to stronger ion-dipole interactions between the salt and sugar molecules a denser solid matrix is obtained, which increases the overall glass transition temperature of the mixture.

Finally, the prediction method could be used to formulate new recipes for fruit juice powders to control the glass transition temperature of the solids mixtures. By combining the knowledge about the glass transition temperature with the mechanisms for stickiness occurring above a critical $T\text{-}T_g$ level, drying can be optimized without relying on a trial and error method. This approach was successfully demonstrated for a blackcurrant and maltodextrin DE 9-13 blend produced for a commercial client in a pilot scale spray dryer.

9.2 Future work

This work provided more insight on the glass transition temperature of mixtures of sugars and fruit acids, but during the study, new questions were raised. The following aspects are recommended for future studies.

The focus of this work was to further characterize the effect of soluble components and their mixtures on the glass transition temperature. Insoluble components such as cellulose and other residual parts from the cell wall of fruits and their impact on the glass transition temperature were not further investigated. The T_g values of the cloudy and clear apple juice powders at zero water activity did not show any significant difference, indicating that the cloudy particles did not have an impact on the glass transition temperature. However, in commercial juice concentrates the quantity of insoluble components is relatively low in comparison to purees. This leaves the question as to whether higher concentrations of the cell wall materials in the mixtures would show an effect on T_g. In Section 2.6.3 and 2.6.4 the concept of the formation of "rigid amorphous phases" at the interface of crystalline regions or fillers is discussed, where the cell wall material could be categorized as an additional filler to the amorphous solid matrix of sugars and organic acids in the juice. These fillers or crystalline regions can lead to an increase of the glass transition temperature if the molecules are bound to the interface. The other case can be true as well such that the whole molecular structure becomes looser and molecular mobility increases resulting in a decrease in the glass transition temperature. It would be recommended to do a composition study by only mixing a monosaccharide such as glucose with a purely insoluble component such as cellulose, which still promotes the formation of bonds at the interface, and investigate the impact on the glass transition temperature. The study could be further expanded to consider the whole insoluble components of the cell wall material in fruits to fully understand the effect of different components on the glass transition temperature in these natural mixtures.

The Flory-Huggins Free Volume theory used in this thesis is based on the concept that the molecular packing of the different low and higher molecular weight component mixtures is independent of the drying technique. This is due to the similar time scales in the formation of the glassy state, which is evident in similar T_g values. Therefore, the absorption behaviour of powders should be similar for powders produced by spray drying or freeze drying, as long as no physical changes occurred during drying, which could affect the absorption behaviour such as stickiness or collapsing. However, studies

presented in the literature regarding powders produced by different drying techniques, as mentioned in Chapter 4, show different absorption trends in the sorption isotherms, which would indicate a different stability of the powders. It would be recommended to investigate the absorption behaviour of powders produced from pure components, in order to minimize any formulation variation, with different drying techniques. The T_g values of the powders at the various water activities could be linked back to any differences in the stability of these powders.

In Chapter 8, the critical $T\text{-}T_g$ limit is defined as a constant value based on the findings of the sticky point for lactose as reported in the literature. This is an assumption, which has be further validated. It would be interesting to study if the sticky point would be constant for mixtures of low molecular weight components with polysaccharides at various ratios. Therefore, the freeze dried powders in Chapter 6 could be used and further studied in the particle gun to observe if the critical $T\text{-}T_g$ limit is shifted to higher levels. This would give a better understanding of the relation between the glass transition temperature and the optimum operating temperature for low molecular mixtures such as fruit juices with polysaccharides.

Appendices

A.1 Example calculation of grapefruit powder

In the following, the prediction approach is explained for one example in a more detailed manner. All predictions in this work were done using this procedure.

The calculation of the glass transition temperature and the sorption isotherm predictions for grapefruit with maltodextrin DE 4-6 will be presented. The fraction of the individual components, the change in heat capacity and the glass transition temperature used for the prediction can be found in Table A.1.1.

Table A.1.1. Solid fraction of grapefruit powder with maltodextrin DE 4-6 and the change of heat capacity as well as T_g values of the individual components.

Material	**Solid fraction**	**ΔC_p ($J \cdot g^{-1} °C^{-1}$)**	**T_g (°C)**
Sucrose	0.23	0.43	68
Fructose	0.105	0.62	14.5
Glucose	0.09	0.58	38
Citric acid	0.075	0.70	14
Maltodextrin DE 4-6	0.5	0.43	188

First the glass transition temperature of the fruit juice solids is calculated from equation (0.1) with the values of Table A.1.1 and without the $\Delta H_{mix,E}$ term.

$$T_g = \frac{\sum_{i=1}^{n} x_i \Delta C_{p,\mathrm{i}} T_{g,i}}{\sum_{i=1}^{n} x_i \Delta C_{p,\mathrm{i}}} \tag{0.1}$$

$$T_{g,\,juice\,solids} = \frac{x_S \Delta C_{p,\mathrm{S}} T_{g,\mathrm{S}} + x_F \Delta C_{p,\mathrm{F}} T_{g,\mathrm{F}} + x_G \Delta C_{p,\mathrm{G}} T_{g,\mathrm{G}} + x_C \Delta C_{p,\mathrm{C}} T_{g,\mathrm{C}}}{x_S \Delta C_{p,\mathrm{S}} + x_F \Delta C_{p,\mathrm{F}} + x_G \Delta C_{p,\mathrm{G}} + x_C \Delta C_{p,\mathrm{C}}}$$

$$T_{g,\,juice\,solids} = 39°C$$

With the calculated glass transition temperature of the grapefruit solids the coefficients A_0 and A_1 from equation (0.2) can be calculated for the mixtures of maltodextrin DE 4-6.

$$\begin{aligned} A &= A_{norm,average}(T_{g,poly} - T_{g,mixture\,low}) \\ A_0 &= 0.4801 \cdot (188 - 39) = 72 \\ A_1 &= -0.2823 \cdot (188 - 39) = -42 \end{aligned} \tag{0.2}$$

The coefficients A_0 and A_1 are then implemented in equation (0.3) and $\Delta H_{mix,E}$ changes can be calculated accordingly to the weight fraction of the fruit solids as well as the amounts of maltodextrin DE 4-6 in the system.

$$\begin{aligned} \Delta H_{mix.E} &= x_i x_j [A_0 + A_1(x_i - x_j)] \quad (\mathrm{n} = 1) \\ \Delta H_{mix.E} &= (1 - x_{MD\,DE\,6}) x_{MD\,DE\,6} \cdot [72 - 42((1 - x_{MD\,DE\,6}) - x_{MD\,DE\,6})] \end{aligned} \tag{0.3}$$

$\Delta H_{mix,E}$ can be inserted into equation (0.4) to calculate the final glass transition temperature of the mixture.

$$T_g = \frac{\sum_{i=1}^{n} x_i \Delta C_{p,\mathrm{i}} T_{g,i}}{\sum_{i=1}^{n} x_i \Delta C_{p,\mathrm{i}}} - \frac{\Delta H_{mix,E}}{\sum_{i=1}^{n} x_i \Delta C_{p,\mathrm{i}}} \tag{0.4}$$

$$T_{g,solids} = \frac{(1 - x_{MD\,DE\,6)}) \Delta C_{p,\,fruit\,solids} T_{g,\,fruit\,solids} + x_{MD\,DE\,6)} \Delta C_{p,MD\,DE\,6} T_{g,MD\,DE\,6}}{(1 - x_{MD\,DE\,6)}) \Delta C_{p,\,fruit\,solids} + x_{MD\,DE\,6)} \Delta C_{p,MD\,DE\,6}}$$
$$- \frac{(1 - x_{MD\,DE\,6}) x_{MD\,DE\,6} \cdot [A_0 - A_1((1 - x_{MD\,DE\,6}) - x_{MD\,DE\,6})]}{(1 - x_{MD\,DE\,6)}) \Delta C_{p,\,fruit\,solids} + x_{MD\,DE\,6)} \Delta C_{p,MD\,DE\,6}}$$

$$T_{g,solids} = 68°C$$

With

$$\Delta C_{p,\,fruit\,solids} = x_S \Delta C_{p,\mathrm{S}} + x_F \Delta C_{p,\mathrm{F}} + x_G \Delta C_{p,\mathrm{G}} + x_C \Delta C_{p,\mathrm{C}}$$

Once the glass transition temperature of the mixture is estimated the sorption isotherm can be calculated. The trend of the sorption isotherm is predicted by the Flory-Huggins Free Volume theory equation with the values of Table A.1.2.

Table A.1.2 Density, number average molecular weight and Flory-Huggins interaction parameter of individual components in the grapefruit powder with maltodextrin DE 4-6.

Material	**Density (kg/m^3)**	**M_n (g/mol)**	χ
water	1.000	18.015	-
Sucrose	1.526	342.30	0.5
Fructose	1.653	180.16	0.37
Glucose	1.551	180.16	0.37
Citric acid	1.665	192.13	0.38
Maltodextrin DE 4-6	1.300	3600	1.02

The complete Flory-Huggins Free Volume model equation (0.5) is written as.

$$a_w = \phi_w \exp[(1-\frac{1}{N})\,(1-\phi_w) + \chi(1-\phi_w)^2 + \mathrm{F}] \tag{0.5}$$

In order to calculate the sorption isotherm the different parameters first have to be estimated. Starting with the volume fraction of water ϕ_w and the other components as described in equation (0.6).

$$\phi_i = \frac{\frac{x_i}{\rho_i}}{\sum \frac{x_i}{\rho_i}} \tag{0.6}$$

$$\phi_w = \frac{\frac{x_{water}}{\rho_{water}}}{\frac{x_{water}}{\rho_{water}} + \frac{x_S}{\rho_S} + \frac{x_F}{\rho_F} + \frac{x_G}{\rho_G} + \frac{x_C}{\rho_C} + \frac{x_{MD\,DE\,6}}{\rho_{MD\,DE\,6}}}$$

The changing volume fraction of sucrose, glucose, fructose, citric acid and maltodextrin DE 4-6 are derived in the same manner. Next the parameter N, which relates the difference in the size of the water molecule to the solid mixture, can be calculated from equation (0.7).

$$\frac{1}{N_{eff}} = \frac{\sum_{i \neq w} \frac{\phi_i}{N_i}}{\sum_{i \neq w} \phi_i} \tag{0.7}$$

$$N_i = \frac{\frac{\rho_i}{M_{n,i}}}{\frac{\rho_{water}}{M_{\mathrm{n,water}}}}$$

$$\frac{1}{N_{eff}} = \frac{\frac{\phi_S}{N_S} + \frac{\phi_F}{N_F} + \frac{\phi_G}{N_G} + \frac{\phi_C}{N_C} + \frac{\phi_{MD\,DE\,6}}{N_{MD\,DE\,6}}}{\phi_S + \phi_G + \phi_F + \phi_C + \phi_{MD\,DE\,6}}$$

$$\frac{1}{N_{eff}} = 0.058$$

The interaction parameter χ can be calculated from equation (0.8).

$$\chi_{eff} = \frac{\sum_{i \neq w} \phi_i \chi_{i,w}}{\sum_{i \neq w} \phi_i} \tag{0.8}$$

$$\chi_{eff} = \frac{\phi_S \chi_{\mathrm{S},w} + \phi_F \chi_{\mathrm{F},w} + \phi_G \chi_{\mathrm{G},w} + \phi_{citric} \chi_{\mathrm{C},w} + \phi_{MD\,DE\,6} \chi_{MD\,DE\,6,w}}{\phi_S + \phi_F + \phi_G + \phi_C + \phi_{MD\,DE\,6}}$$

$$\chi_{eff} = 0.75$$

The last step is to calculate the free volume term F in the equation. The free volume term is presented in equation (0.9).

$$F = \frac{1}{RT} M_w x_s^{\,2} \Delta C_{p,s} \left(\frac{dT_{g,\mathrm{mix}}}{dx_w} \right) \left(\frac{T}{T_{g,mix}} - 1 \right) \tag{0.9}$$

R=8.314 $J \cdot K^{-1}$ mol^{-1} is the real gas constant, x_s is the total solid fraction, $\Delta C_{p,s}$ =0.4837 $J \cdot K^{-1} mol^{-1}$ ($\sum_{i=1}^{n} x_i \Delta C_{p,\mathrm{i}}$) is the total change of heat capacity of the solid mixture calculated from the weight fraction of the components and T is the storage temperature 296 K . The glass transition temperature of the mixture of the powder with the increasing water

content of $T_{g,mix}$ is calculated by the Gordon-Taylor equation with k value estimated by equation (0.10) and $T_{g,mix}$ is defined in Kelvin.

$$T_{g,mix} = \frac{x_s T_{g,\text{solid}} - k x_w T_{g,\text{w}}}{x_s + k x_w} \tag{0.10}$$

With

$$k = 7.7 - 7.7 \ln\left(\left(\frac{463.43}{68}\right)^{0.18}\right) = 5.12$$

The derivative of $T_{g,mix}$ with respect to water fraction can be estimated by equation (0.11)

$$\frac{dT_{g,mix}}{dx_w} = \frac{k\, x_s\, (T_{g,w} - T_{g,solid})}{(x_s + k x_w)^2} \tag{0.11}$$

Where x_s and x_w is the weight fraction of the water and solid and $T_{g,solid}$ (68˚C). The free volume term disappears from the Flory-Huggins as soon as $T_{g,mix}$=T. Since the FHVT model is based on the total composition of the system the water activity is predicted from the moisture content in the samples. Finally, the predicted $T_{g,mix}$ values can be plotted over the estimated water activities to show the stability of the powders.

A.2 Glass transition temperature of MD DE 9-13 blends at various water activities

As previously mentioned, the glass transition temperature is defined as one data point out of convenience, but in order to fully describe the transition the endpoint and width have to be stated as well. Tables containing the full description of the transitions for all systems, which have been not presented in the main Section, are listed below.

A.2.1 Second transition in fruit juice powders

Blackcurrant 2nd transition

Water activity	T_g mid (˚C)	Onset (˚C)	Offset (˚C)	Width (˚C)
0	61.7 ± 3.6	53.7 ± 3.9	68.5 ± 4.1	14.8 ± 0.4
0.11	43.7 ± 1.6	39.3 ± 2.2	48.1 ± 2.5	8.8 ± 1.2
0.22	36.4 ± 0.1	31.8 ± 0.3	41.0 ± 0.3	9.9 ± 0.6
0.32	31.3 ± 1.4	24.4 ± 0.4	38.2 ± 2.4	13.9 ± 2.1
0.43	24.7 ± 0.3	20.4 ± 0.2	28.9 ± 0.5	8.6 ± 0.5

Average ± SD, n=3, storage temperature 30˚C

Kiwifruit 2nd transition

Water activity	T_g mid (˚C)	Onset (˚C)	Offset (˚C)	Width (˚C)
0	63.9 ± 2.0	59.0 ± 3.7	69.5 ± 0.3	10.5 ± 3.6
0.11	47.4 ± 1.4	43.1 ± 1.7	51.7 ± 1.2	8.7 ± 0.6
0.22	45.1 ± 0.5	39.8 ± 0.2	50.5 ± 1.1	10.7 ± 1.1
0.32	36.6 ± 0.3	30.7 ± 0.2	42.5 ± 1.0	11.9 ± 1.1
0.43	29.3 ± 0.4	21.3 ± 0.8	37.5 ± 1.1	16.2 ± 1.3

Average ± SD, n=3, storage temperature 30˚C

Clear apple 2nd transition

Water activity	T_g mid (˚C)	Onset (˚C)	Offset (˚C)	Width (˚C)
0	57.6 ± 0.3	51.9 ± 0.2	63.2 ± 0.5	11.3 ± 0.3
0.11	54.5 ± 1.1	47.3 ± 0.6	61.9 ± 1.9	14.6 ± 1.7
0.22	48.3 ± 1.7	41.0 ± 2.4	56.1 ± 1.7	15.1 ± 0.7
0.32	42.3 ± 0.4	34.9 ± 0.5	50.4 ± 0.4	15.5 ± 0.5
0.43	36.3 ± 0.3	26.7 ± 0.2	45.9 ± 0.7	19.2 ± 0.8

Average ± SD, n=3, storage temperature 30˚C

Cloudy apple 2nd transition

Water activity	T_g mid (˚C)	Onset (˚C)	Offset (˚C)	Width (˚C)
0	57.7 ± 0.2	52.3 ± 0.1	63.0 ± 0.3	10.7 ± 0.3
0.11	52.0 ± 0.2	45.1 ± 0.9	58.9 ± 1.1	13.8 ± 2.0
0.22	46.9 ± 0.8	40.4 ± 0.6	53.5 ± 1.0	13.1 ± 0.5
0.32	42.2 ± 0.8	34.6 ± 0.8	50.5 ± 0.4	16.0 ± 0.4
0.43	35.8 ± 0.4	27.6 ± 0.6	44.2 ± 0.4	16.6 ± 0.7

Average ± SD, n=3, storage temperature 30˚C

A.2.2 Glucose and maltodextrin DE 9-13 blends at various a_w

0.7 Glucose + 0.3 MD DE 9-13

Water activity	T_g mid (˚C)	Onset (˚C)	Offset (˚C)	Width (˚C)
0	46.8 ± 0.4	42.1 ± 0.3	51.5 ± 1.0	9.4 ± 1.2
0.11	28.2 ± 0.4	23.2 ± 0.5	33.2 ± 0.3	10.0 ± 0.2
0.22	15.4 ± 0.4	9.8 ± 0.2	20.7 ± 0.6	10.9 ± 0.8
0.32	5.0 ± 1.0	-1.8 ± 0.8	11.0 ± 1.1	12.8 ± 2.3
0.43	-14.3 ± 0.2	-19.0 ± 0.5	-9.7 ± 0.8	9.3 ± 1.2

Average ± SD, n=3, storage temperature 30˚C

0.5 Glucose + 0.5 MD DE 9-13

Water activity	T_g mid (˚C)	Onset (˚C)	Offset (˚C)	Width (˚C)
0	58.9 ± 1.0	48.0 ± 0.6	69.8 ± 1.6	21.8 ± 1.3
0.11	30.8 ± 0.4	23.2 ± 1.1	38.4 ± 0.7	15.2 ± 1.6
0.22	18.7 ± 0.4	12.6 ± 0.8	24.8 ± 0.7	12.2 ± 1.2
0.32	10.3 ± 1.9	2.0 ± 0.8	18.5 ± 3.2	16.5 ± 2.6
0.43	-5.9 ± 1.6	-13.0 ± 1.5	1.2 ± 1.8	14.2 ± 0.4

Average ± SD, n=3, storage temperature 30˚C

0.3 Glucose + 0.7 MD DE 9-13

Water activity	T_g mid (˚C)	Onset (˚C)	Offset (˚C)	Width (˚C)
0	90.0 ± 1.7	69.1 ± 1.8	111.1 ± 4.7	42.1 ± 6.2
0.11	51.6 ± 1.6	32.1 ± 0.4	70.7 ± 2.5	38.7 ± 2.4
0.22	40.3 ± 0.2	22.3 ± 0.5	57.8 ± 1.0	35.5 ± 1.4
0.32	29.1 ± 1.3	12.4 ± 0.9	44.8 ± 1.2	32.5 ± 0.3
0.43	12.7 ± 0.9	-2.1 ± 1.5	27.3 ± 3.2	29.4 ± 4.7

Average ± SD, n=3, storage temperature 30˚C

A.2.3 Citric acid and maltodextrin DE 9-13 blends at various a_w

0.5 Citric acid + 0.5 MD DE 9-13

Water activity	T_g mid (˚C)	Onset (˚C)	Offset (˚C)	Width (˚C)
0	39.6 ± 0.7	27.6 ± 1.7	51.6 ± 0.6	24.0 ± 1.0
0.11	23.9 ± 1.4	12.0 ± 1.4	35.7 ± 1.8	23.7 ± 1.5
0.22	14.0 ± 2.4	3.0 ± 2.3	25.1 ± 2.4	22.1 ± 0.1
0.32	5.8 ± 2.0	-5.1 ± 2.1	16.6 ± 2.1	21.7 ± 0.8
0.43	-6.0 ± 0.9	-16.4 ± 0.9	4.4 ± 1.0	20.8 ± 0.1

Average ± SD, n=3, storage temperature 30˚C

0.3 Citric acid + 0.7 MD DE 9-13

Water activity	T_g mid (˚C)	Onset (˚C)	Offset (˚C)	Width (˚C)
0	78.2 ± 1.3	55.0 ± 1.9	101.4 ± 3.1	46.4 ± 4.3
0.11	52.2 ± 1.1	39.1 ± 2.8	67.4 ± 0.2	28.3 ± 3.0
0.22	42.1 ± 0.7	27.4 ± 1.0	57.4 ± 1.7	30.0 ± 2.5
0.32	33.7 ± 0.8	18.2 ± 2.3	50.2 ± 2.2	31.9 ± 4.2
0.43	18.0 ± 2.2	1.9 ± 2.6	34.5 ± 1.7	32.6 ± 1.5

Average ± SD, n=3, storage temperature 30˚C

A.2.4 Fructose and maltodextrin DE 9-13 blends at various a_w

0.7 Fructose + 0.3 MD DE 9-13

Water activity	T_g mid (˚C)	Onset (˚C)	Offset (˚C)	Width (˚C)
0	31.0 ± 0.5	25.6 ± 0.8	36.6 ± 0.3	10.9 ± 0.7
0.11	18.6 ± 1.9	12.6 ± 1.6	24.7 ± 2.1	12.1 ± 0.6
0.22	6.4 ± 0.2	1.2 ± 0.1	11.7 ± 10.7	10.7 ± 0.3
0.32	-3.0 ± 0.6	-8.5 ± 1.0	2.7 ± 0.5	11.3 ± 0.5
0.43	-20.9 ± 0.6	-24.4 ± 0.4	-17.3 ± 0.5	7.1 ± 0.3

Average ± SD, n=3, storage temperature 30˚C

0.5 Fructose + 0.5 MD DE 9-13

Water activity	T_g mid (˚C)	Onset (˚C)	Offset (˚C)	Width (˚C)
0	40.4 ± 1.1	33.8 ± 1.1	47.0 ± 0.5	13.2 ± 2.8
0.11	23.6 ± 0.7	14.5 ± 0.4	32.3 ± 1.4	17.8 ± 1.5
0.22	6.4 ± 0.2	1.2 ± 0.1	11.7 ± 10.7	10.7 ± 0.3
0.32	-3.0 ± 0.6	-8.5 ± 1.0	2.71 ± 0.5	11.3 ± 0.5
0.43	-20.9 ± 0.6	-24.4 ± 0.4	-17.3 ± 0.5	7.1 ± 0.3

Average ± SD, n=3, storage temperature 30˚C

0.3 Fructose + 0.7 MD DE 9-13

Water activity	T_g mid (˚C)	Onset (˚C)	Offset (˚C)	Width (˚C)
0	83.2 ± 1.0	59.4 ± 2.1	108.8 ± 0.3	49.4± 2.2
0.11	45.8 ± 1.6	26.9 ± 0.2	63.7 ± 2.9	36.8 ± 2.8
0.22	36.3 ± 0.6	19.3 ± 1.9	52.8 ± 2.2	33.5 ± 3.8
0.32	31.1 ± 0.4	15.1 ± 1.1	47.9 ± 0.6	32.8 ± 1.6
0.43	8.5 ± 0.7	-6.5 ± 0.8	22.00 ± 2.5	28.5 ± 3.1

Average ± SD, n=3, storage temperature 30˚C

A.2.5 G/F/C and maltodextrin DE 9-13 blends at various a_w

0.7 G/F/C + 0.3 MD DE 9-13

Water activity	T_g mid (˚C)	Onset (˚C)	Offset (˚C)	Width (˚C)
0	35.7 ± 1.2	30.7 ± 0.8	41.0 ± 1.7	10.3 ± 0.9
0.11	21.2 ± 0.5	14.3 ± 1.6	28.1 ± 0.6	13.8 ± 0.1
0.22	10.2 ± 0.7	3.7 ± 0.4	16.7 ± 1.0	13. ± 0.8
0.32	-0.4 ± 2.2	-7.2 ± 1.2	6.5 ± 3.2	13.8 ± 2.4
0.43	-14.2 ± 1.0	-19.3 ± 0.4	-9.1 ± 1.0	10.2 ± 0.6

Average ± SD, n=3, storage temperature 30˚C

0.5 G/F/C + 0.5 MD DE 9-13

Water activity	T_g mid (˚C)	Onset (˚C)	Offset (˚C)	Width (˚C)
0	49.1 ± 0.4	40.5 ± 0.3	57.7 ± 0.7	17.2 ± 0.7
0.11	31.5 ± 0.1	22.8 ± 0.7	40.3 ± 0.7	17.5 ± 1.3
0.22	23.1 ± 0.8	12.3 ± 1.1	34.0 ± 0.9	21.7 ± 1.1
0.32	10.1 ± 0.2	1.7 ± 0.1	18.6 ± 0.3	17.0 ± 0.2
0.43	-4.5 ± 1.2	-12.6 ± 0.7	3.6 ± 1.6	16.2 ± 0.9

Average ± SD, n=3, storage temperature 30˚C

0.3 G/F/C + 0.7 MD DE 9-13

Water activity	T_g mid (˚C)	Onset (˚C)	Offset (˚C)	Width (˚C)
0	78.7 ± 1.1	54.8 ± 1.6	102.7 ± 4.0	47.9 ± 5.6
0.11	51.2 ± 1.5	35.0 ± 1.5	66.9 ± 1.4	31.9 ± 1.5
0.22	39.4 ± 0.9	23.2 ± 2.0	55.4 ± 0.3	32.2 ± 2.2
0.32	31.6 ± 0.7	14.7 ± 1.0	47.6 ± 2.7	32.9 ± 3.7
0.43	16.0 ± 1.0	-1.4 ± 0.6	33.0 ± 1.3	34.3 ± 1.0

Average ± SD, n=3, storage temperature 30˚C

A.2.6 Blackcurrant and maltodextrin DE 9-13 blends at various a_w

0.7 BL + 0.3 MD DE 9-13

Water activity	T_g mid (˚C)	Onset (˚C)	Offset (˚C)	Width (˚C)
0	47.1 ± 0.3	38.1 ± 0.3	56.1 ± 0.5	18.0 ± 0.7
0.11	29.8 ± 0.9	22.5 ± 0.2	37.0 ± 1.9	14.5 ± 2.0
0.22	16.5 ± 0.5	9.5 ± 0.4	23.5 ± 0.4	14.0 ± 0.1
0.32	6.2 ± 1.3	-0.1 ± 0.9	12.4 ± 2.0	12.6 ± 1.5
0.43	-10.2 ± 1.3	-16.4 ± 1.1	-3.9 ± 1.4	12.5 ± 0.3

Average ± SD, n=3, storage temperature 30˚C

0.5 BL + 0.5 MD DE 9-13

Water activity	T_g mid (˚C)	Onset (˚C)	Offset (˚C)	Width (˚C)
0	60.2 ± 0.5	49.8 ± 1.9	70.6 ± 1.0	20.7 ± 2.9
0.11	40.4 ± 0.2	30.9 ± 1.1	49.8 ± 0.7	18.8 ± 1.8
0.22	29.3 ± 0.2	18.4 ± 1.0	40.0 ± 1.3	21.6 ± 2.3
0.32	12.1 ± 0.4	3.3 ± 0.7	20.9 ± 0.5	17.6 ± 1.0
0.43	-0.7 ± 0.4	-9.1 ± 0.8	7.6 ± 1.0	16.7 ± 1.6

Average ± SD, n=3, storage temperature 30˚C

0.3 BL + 0.7 MD DE 9-13

Water activity	T_g mid (˚C)	Onset (˚C)	Offset (˚C)	Width (˚C)
0	87.7 ± 1.2	60.9 ± 2.0	114.1 ± 1.0	53.2 ± 2.1
0.11	54.9 ± 1.0	40.3 ± 0.4	68.8 ± 2.4	28.5 ± 2.8
0.22	46.1 ± 0.9	28.7 ± 0.3	63.5 ± 1.6	34.8 ± 1.3
0.32	36.8 ± 0.7	16.3 ± 0.2	57.4 ± 2.1	41.2 ± 2.3
0.43	20.5 ± 2.3	3.9 ± 1.0	36.2 ± 3.7	32.4 ± 3.7

Average ± SD, n=3, storage temperature 30˚C

A.2.7 Glucose and one polysaccharide

Glucose + MD DE 9-13

Fraction MD	T_g mid (˚C)	Onset (˚C)	Offset (˚C)	Width (˚C)
0.3	46.8 ± 0.4	42.1 ± 0.3	51.5 ± 1.0	9.4 ± 1.2
0.5	58.9 ± 1.0	48.0 ± 0.6	69.8 ± 1.6	21.8 ± 1.3
0.7	90.0 ± 1.7	69.1 ± 1.8	111.1 ± 4.7	42.1 ± 6.2
0.8	120.0 ± 0.3	97.3 ± 3.3	144.4 ± 4.7	47.1 ± 8.0
0.9	136.5 ± 2.6	127.3 ± 4.2	145.4 ± 3.8	18.1 ± 6.3
1	175.3 ± 6.8	169.7 ± 10.5	183.3 ± 6.9	13.6 ± 4.4

Average ± SD, n=3

Glucose + IN

Fraction MD	T_g mid (˚C)	Onset (˚C)	Offset (˚C)	Width (˚C)
0.3	44.8 ± 1.9	41.0 ± 1.6	48.6 ± 2.2	7.6 ± 0.5
0.5	50.5 ± 0.5	46.1 ± 0.6	54.9 ± 0.4	8.8 ± 0.3
0.7	62.5 ± 0.5	56.0 ± 0.4	69.0 ± 1.2	13.0 ± 1.5
0.8	70.3 ± 0.6	64.4 ± 0.7	76.3 ± 0.6	11.9 ± 0.5
0.9	80.8 ± 0.8	74.9 ± 1.3	86.8 ± 0.4	11.9 ± 0.9
1	92.6 ± 0.2	87.6 ± 0.4	97.6 ± 0.2	10.1 ± 0.5

Average ± SD, n=3

Glucose + RT MD

Fraction MD	T_g mid (˚C)	Onset (˚C)	Offset (˚C)	Width (˚C)
0.3	46.3 ± 0.3	42.2 ± 0.3	50.7 ± 0.4	8.6 ± 0.3
0.5	56.5 ± 3.0	50.9 ± 2.1	62.2 ± 3.9	11.3 ± 2.1
0.7	92.0 ± 1.6	80.4 ± 1.6	103.9 ± 1.7	23.5 ± 1.7
0.8	111.3 ± 1.9	99.5 ± 0.8	123.3 ± 2.7	23.8 ± 1.9
0.9	137.4 ± 2.4	125.6 ± 2.6	149.2 ± 5.9	23.5 ± 7.8
1	168.5 ± 3.6	164.8 ± 3.6	170.3 ± 1.7	5.6 ± 2.2

Average ± SD, n=3

A.2.8 Glucose and various polysaccharides

Glucose + IN/MD DE 9-13

Fraction MD	T_g mid (˚C)	Onset (˚C)	Offset (˚C)	Width (˚C)
0.3	44.2 ± 0.3	40.8 ± 0.1	47.7 ± 0.7	6.9 ± 0.7
0.5	52.3 ± 1.0	47.0 ± 1.2	57.6 ± 0.7	10.6 ± 0.6
0.7	69.6 ± 2.1	57.4 ± 1.3	81.7 ± 2.9	24.3 ± 1.5
0.8	84.9 ± 0.9	73.3 ± 1.5	96.5 ± 3.3	23.1 ± 4.7
0.9	99.9 ± 1.8	89.4 ± 0.1	110.4 ± 3.7	21.0 ± 3.8
1	108.4 ± 5.1	93.6 ± 8.1	122.8 ± 6.2	29.2 ± 10.5

Average ± SD, n=3

Glucose + RT MD/IN

Fraction MD	T_g mid (˚C)	Onset (˚C)	Offset (˚C)	Width (˚C)
0.3	46.2 ± 1.2	42.5 ± 1.4	47.7 ± 0.7	6.9 ± 0.7
0.5	52.3 ± 1.0	47.0 ± 1.2	57.6 ± 0.7	10.6 ± 0.6
0.7	69.6 ± 2.1	57.4 ± 1.3	81.7 ± 2.9	24.3 ± 1.5
0.8	84.9 ± 0.9	73.3 ± 1.5	96.5 ± 3.3	23.1 ± 4.7
0.9	99.9 ± 1.8	89.4 ± 0.1	110.4 ± 3.7	21.0 ± 3.8
1	108.4 ± 5.1	93.6 ± 8.1	122.8 ± 6.2	29.2 ± 10.5

Average ± SD, n=3

Glucose + RT MD/MD DE 9-13

Fraction MD	T_g mid (˚C)	Onset (˚C)	Offset (˚C)	Width (˚C)
0.3	46.2 ± 0.2	42.31 ± 0.2	50.1 ± 0.4	7.8 ± 0.4
0.5	56.7 ± 1.7	49.7 ± 0.3	63.6 ± 3.2	13.9 ± 3.0
0.7	77.5 ± 1.4	68.2 ± 0.7	86.6 ± 2.5	18.5 ± 2.4
0.8	112.4 ± 3.2	99.1 ± 2.7	127.9 ± 8.8	28.8 ± 11.5
0.9	131.5 ± 1.6	121.6 ± 4.3	142.2 ± 1.5	20.5 ± 5.8
1	170.0 ± 3.1	165.9 ± 1.4	174.1 ± 4.8	8.2 ± 3.5

Average ± SD, n=3

Glucose + MD DE 9-13/RT MD/IN

Fraction MD	T_g mid (˚C)	Onset (˚C)	Offset (˚C)	Width (˚C)
0.3	45.6 ± 0.7	41.6 ± 0.3	49.7 ± 1.2	8.0 ± 1.0
0.5	56.9 ± 1.5	49.9 ± 1.4	63.9 ± 1.8	14.0 ± 0.5
0.7	84.8 ± 1.8	67.9 ± 3.8	102.9 ± 1.4	35.1 ± 4.3
0.8	91.0 ± 1.3	80.8 ± 1.8	101.3 ± 1.0	20.4 ± 1.4
0.9	110.4 ± 0.8	98.2 ± 1.5	122.7 ± 1.0	24.5 ± 2.
1	127.2 ± 3.0	117.3 ± 7.5	137.0 ± 2.1	19.7 ± 9.1

Average ± SD, n=3

A.2.9 Glucose and salts

Glucose + Disodium carbonate

Fraction Salts	T_g mid (˚C)	Onset (˚C)	Offset (˚C)	Width (˚C)
0.01	42.0 ± 1.4	38.8± 1.6	45.6 ± 1.0	6.8 ± 0.6
0.05	47.7 ± 1.2	42.9 ± 1.5	52.6 ± 1.0	9.7 ± 0.5
0.1	56.0 ± 2.5	48.17 ± 4.0	66.5 ± 2.2	18.3 ± 5.9
0.2	62.3 ± 1.8	52.5 ± 6.6	67.9 ± 11.0	15.4 ± 4.9

Average ± SD, n=3

Glucose + Trisodium citrate

Fraction Salts	T_g mid (˚C)	Onset (˚C)	Offset (˚C)	Width (˚C)
0.01	39.2 ± 0.6	36.1 ± 0.8	42.9 ± 0.4	6.8 ± 0.5
0.05	44.8 ± 0.5	40.7 ± 0.6	49.1 ± 0.4	8.4 ± 0.2
0.1	49.7 ± 1.0	44.0 ± 1.2	55.9 ± 0.5	11.8 ± 0.7
0.2	61.9 ± 1.2	55.8 ± 1.9	68.2 ± 0.5	12.4 ± 1.6

Average ± SD, n=3

Glucose + Trisodium phosphate

Fraction Salts	T_g mid (˚C)	Onset (˚C)	Offset (˚C)	Width (˚C)
0.01	40.9 ± 0.5	37.3 ± 0.7	44.6 ± 0.3	7.3 ± 0.6
0.05	50.4 ± 1.3	45.0 ± 1.6	55.8 ± 0.9	10.7 ± 1.0
0.1	66.7 ± 1.6	60.4 ± 1.5	73.0 ± 1.8	12.5 ± 0.6
0.2	94.1 ± 4.2	89.7 ± 4.4	99.0 ± 3.6	9.3 ± 0.8

Average ± SD, n=3

A.2.10 Moisture content of powders at various a_w

	Fruit juice powder		
	Moisture content (g/100g solids)		
Water activity	**Lemon**	**Kiwifruit**	**Blackcurrant**
0.11	1.71 ± 0.06	1.67 ± 0.11	1.82 ± 0.05
0.22	3.77 ± 0.02	3.27 ± 0.06	3.96 ± 0.06
0.32	7.07 ± 0.07	6.40 ± 0.15	6.19 ± 0.06
0.43	11.10 ± 0.04	11.54 ± 0.12	10.21 ± 0.08

Average ± SD, n=3, storage temperature 30˚C

	Fruit juice powder		
	Moisture content (g/100g solids)		
Water activity	**Clear apple**	**Cloudy apple**	**Carrot**
0.11	1.16± 0.21	1.35 ± 0.09	1.80 ± 0.18
0.22	2.94 ± 0.41	3.72 ± 0.09	3.70 ± 0.07
0.32	6.79 ± 0.08	6.98 ± 0.13	6.28 ± 0.12
0.43	11.66 ± 0.13	11.76 ± 0.14	9.93 ± 0.09

Average ± SD, n=3, storage temperature 30˚C

	Glucose + Maltodextrin DE 9-13		
	Moisture content (g/100g solids)		
Water activity	**0.7 G + 0.3 MD**	**0.5 G + 0.5 MD**	**0.3 G + 0.7 MD**
0.11	1.46 ± 0.12	1.53 ± 0.06	2.40 ± 0.07
0.22	3.59 ± 0.33	3.31 ± 0.03	3.53 ± 0.21
0.32	5.39 ± 0.16	5.44 ± 0.05	4.56 ± 0.12
0.43	7.49 ± 0.18	8.15 ± 0.08	7.03 ± 0.24

Average ± SD, n=3, storage temperature 30˚C

Fructose + Maltodextrin DE 9-13

	Moisture content (g/100g solids)		
Water activity	**0.7 F + 0.3 MD**	**0.5 F + 0.5 MD**	**0.3 F + 0.7 MD**
0.11	1.43 ± 0.06	1.35 ± 0.05	1.99 ± 0.12
0.22	3.26 ± 0.13	3.49 ± 0.58	2.94 ± 0.10
0.32	5.09 ± 0.04	5.12 ± 0.07	4.22 ± 0.24
0.43	10.05 ± 0.04	7.87 ± 0.36	7.13 ± 0.27

Average ± SD, n=3, storage temperature 30˚C

G/F/C + Maltodextrin DE 9-13

	Moisture content (g/100g solids)		
Water activity	**0.7 G/F/C + 0.3 MD**	**0.5 G/F/C + 0.5 MD**	**0.3 G/F/C + 0.7 MD**
0.11	1.57 ± 0.02	0.97 ± 0.45	1.88 ± 0.08
0.22	3.11 ± 0.01	2.91 ± 0.01	2.86 ± 0.04
0.32	4.84 ± 0.21	4.83 ± 0.02	4.14 ± 0.14
0.43	8.92 ± 0.38	7.39 ± 0.13	6.64 ± 0.03

Average ± SD, n=3, storage temperature 30˚C

Citric acid + Maltodextrin DE 9-13

	Moisture content (g/100g solids)	
Water activity	**0.5 G/F/C + 0.5 MD**	**0.3 G/F/C + 0.7 MD**
0.11	1.35 ± 0.05	1.99 ± 0.12
0.22	3.49 ± 0.58	2.94 ± 0.10
0.32	5.12 ± 0.07	4.22 ± 0.24
0.43	7.87 ± 0.36	7.13 ± 0.27

Average ± SD, n=3, storage temperature 30˚C

Blackcurrant + Maltodextrin DE 9-13

	Moisture content (g/100g solids)		
Water activity	**0.7 BL + 0.3 MD**	**0.5 BL + 0.5 MD**	**0.3 BL + 0.7 MD**
0.11	1.43 ± 0.06	1.35 ± 0.05	1.99 ± 0.12
0.22	3.26 ± 0.13	3.49 ± 0.58	2.94 ± 0.10
0.32	5.09 ± 0.04	5.12 ± 0.07	4.22 ± 0.24
0.43	10.05 ± 0.04	7.87 ± 0.36	7.13 ± 0.27

Average ± SD, n=3, storage temperature 30˚C

References

Adhikari, B., & Bhandari, B. R. (2008). Glass-Transition Based Approach in Drying of Foods *Advances in Food Dehydration* (pp. 37-62): CRC Press.

Adhikari, B., Howes, T., Bhandari, B. R., & Troung, V. (2003). Surface Stickiness of Drops of Carbohydrate and Organic Acid Solutions During Convective Drying: Experiments and Modeling. *Drying Technology, 21*(5), 839-873.

Adhikari, B., Howes, T., Bhandari, B. R., & Troung, V. (2004). Effect of addition of maltodextrin on drying kinetics and stickiness of sugar and acid-rich foods during convective drying: experiments and modelling. *Journal of Food Engineering, 62*(1), 53-68.

Adhikari, B., Howes, T., Bhandari, B. R., & Truong, V. (2002). Surface stickiness of low molecular weight sugars and maltodextrin during drying. *Food Industry Journal, 5*(2), 112-124.

Adhikari, B., T.Howes, D.Lecomte, & B.R., B. (2005). A glass transition temperature approach for the prediction of the surface stickiness of a drying droplet during spray drying. *Powder Technology, 149*, 168-179.

Agrawal, S., Paterson, T., Jones, J., McLeod, J., & Bronlund, J. (2016). A mathematical model based parametric sensitivity analysis of an evaporative crystallizer for lactose monohydrate. *Food and Bioproducts Processing, 97*, 1-11.

Alves, N. M., Mano, J. F., Balaguer, E., Meseguer Dueñas, J. M., & Gómez Ribelles, J. L. (2002). Glass transition and structural relaxation in semi-crystalline poly(ethylene terephthalate): a DSC study. *Polymer, 43*(15), 4111-4122.

Arvanitoyannis, I., Blanshard, J. M. V., Izzard, M. J., Lillford, P. J., & Ablett, S. (1993). Calorimetric study of the glass transition occurring in aqueous glucose: Fructose solutions. *Journal of the Science of Food and Agriculture, 63*(2), 177-188.

Askadaskii, A. A., Popova, M., Matseevich, T. A., & Kurskaya, E. (2014). The influence of the degree of crystallinity on the glass transition temperature of polymers *Advanced Materials Research, 864-867*, 751-754.

Askadskii, A. A. (2003). *Computational material science of polymers*: Cambridge International Science Publishing.

Askadskii, A. A., Matseevich, T. A., & Markov, V. A. (2016a). Determination of glass-transition temperatures of polymers: A modified computational scheme. [journal article]. *Polymer Science Series A, 58*(4), 506-516.

Askadskii, A. A., Matseevich, T. A., & Markov, V. A. (2016b). Modified calculation scheme for evaluation and prediction of glass transition temperatures of polymers. *Doklady Physical Chemistry, 466*(1), 12-14.

Avaltroni, F., Bouquerand, P. E., & Normand, V. (2004). Maltodextrin molecular weight distribution influence on the glass transition temperature and viscosity in aqueous solutions. *Carbohydrate Polymers, 58*(3), 323-334.

Barrat, J.-L., Baschnagel, J., & Lyulin, A. (2010). Molecular dynamics simulations of glassy polymers. [10.1039/B927044B]. *Soft Matter, 6*(15), 3430-3446.

BeMiller, J. N., & Whistler, R. L. (1996). Carbohydrates. In O. R. Fennema (Ed.), *Food Chemistry* (Vol. 3rd edition, pp. 157-224): Marcel Dekker.

Benczdi, D., Tomka, I., & Escher, F. (1998). Thermodynamics of Amorphous StarchWater Systems. 1. Volume Fluctuations. *Macromolecules, 31*(9), 3055-3061.

Berlin, E., Anderson, B. A., & Pallansch, M. J. (1973). Water Sorption by Dried Dairy Products Stabilized with Carboxymethyl Cellulose. *Journal of Dairy Science, 56*(6), 685-689.

Berüter, J. (1985). Sugar Accumulation and Changes in the Activities of Related Enzymes during Development of the Apple Fruit. *Journal of Plant Physiology, 121*(4), 331-341.

Bhandari, B., & Roos, Y. H. (2017). Introduction to Non-Equilibrium States and Glass Transitions—The Fundamentals Applied to Foods Systems. In B. Bhandari & Y. H. Roos (Eds.), *Non-Equilibrium States and Glass Transitions in Foods* (pp. xxxiii-l).

Bhandari, B. R., Datta, N., Crooks, R., Howes, T., & Rigby, S. (1997). A semi-empirical approach to optimise the quantity of drying aids required to spray dry sugar-rich foods. *Drying Technology, 15*(10), 2509-2525.

Bhandari, B. R., Datta, N., & Howes, T. (1997). Problems Associated With Spray Drying Of Sugar-Rich Foods. *Drying Technology, 15*(2), 671-684.

Bhandari, B. R., & Hartel, R. W. (2005). Phase Transitions During Food Powder Production and Powder Stability *Encapsulated and Powdered Foods* (pp. 261-292): CRC Press.

Bhandari, B. R., & Howes, T. (1999). Implication of glass transition for the drying and stability of dried foods. *Journal of Food Engineering, 40*(1-2), 71-79.

Biliaderis, C. G. (1991). The structure and interactions of starch with food constituents. *Canadian Journal of Physiology and Pharmacology*(69), 60-78.

Biroli, G., & Bouchaud, J.-P. (2012). The Random First-Order Transition Theory of Glasses: A Critical Assessment *Structural Glasses and Supercooled Liquids* (pp. 31-113).

Blanchard, L.-P., Hesse, J., & Malhotra, S. L. (1974). Effect of Molecular Weight on Glass Transition by Differential Scanning Calorimetry. *Canadian Journal of Chemistry, 52*(18), 3170-3175.

Blumenkrantz, N., & Asboe-Hansen, G. (1973). New method for quantitative determination of uronic acids. *Analytical Biochemistry, 54*(2), 484-489.

Boonyai, P., Bhandari, B., & Howes, T. (2004). Stickiness measurement techniques for food powders: A review. *Powder Technology, 145*, 34-46.

Bosma, M., Ten Brinke, G., & Ellis, T. S. (1988). Polymer-polymer miscibility and enthalpy relaxations. *Macromolecules, 21*(5), 1465-1470.

Boyer, R. F. (1975). Glassy transitions in semicrystalline polymers. *Journal of Polymer Science: Polymer Symposia, 50*(1), 189-242.

Brekner, M.-J., Schneider, H. A., & Cantow, H.-J. (1988). Approach to the composition dependence of the glass transition temperature of compatible polymer blends and the effect of local chain orientation. *Die Makromolekulare Chemie, 189*(9), 2085-2097.

Brennan, J. G., Herrera, J., & Jowitt, R. (1971). A study of some of the factors affecting the spray drying of concentrated orange juice, on a laboratory scale. *Journal of Food Technology, 6*, 295-307.

Brinke, G. T., Karasz F. E., & Ellis T. S. (1983). Depression of glass transition temperatures of polymer networks by diluents. *Macromolecules, 16*(2), 244-249.

Brooks, G. F. (2000). *The sticking and crystallisation of amorphous lactose.* (M.E.), Massey University, Palmerston North, New Zealand.

Brostow, W., Chiu, R., Kalogeras, I. M., & Vassilikou-Dova, A. (2008). Prediction of glass transition temperatures: Binary blends and copolymers. *Materials Letters, 62*(17–18), 3152-3155.

Busin, L., Buisson, P., & Bimbenet, J.-J. (1996). Notion of glass transition applied to the spray drying of carbohydrate solutions. *Sciences des Aliments, 16*, 443-459.

Camacho-Zuñiga, C., & Ruiz-Treviño, F. A. (2003). A New Group Contribution Scheme To Estimate the Glass Transition Temperature for Polymers and Diluents. *Industrial & Engineering Chemistry Research, 42*(7), 1530-1534.

Cassano, A., Drioli, E., Galaverna, G., Marchelli, R., Di Silvestro, G., & Cagnasso, P. (2003). Clarification and concentration of citrus and carrot juices by integrated membrane processes. *Journal of Food Engineering, 57*(2), 153-163.

Ceci, L., & Lozano, J. E. (1998). Determination of enzymatic activities of commercial pectinases for the clarification of apple juice. *Food Chemistry, 61*(1–2), 237-241.

Champion, D., Le Meste, M., & Simatos, D. (2000). Towards an improved understanding of glass transition and relaxations in foods: molecular mobility in the glass transition range. *Trends in Food Science & Technology, 11*(2), 41-55.

Chatterjee, R. (2004). *Characterising stickiness of dairy powders.* (M.E.), Massey University, Palmerston North, New Zealand.

Chen, T., Fowler, A., & Toner, M. (2000). Literature Review: Supplemented Phase Diagram of the Trehalose–Water Binary Mixture. *Cryobiology, 40*(3), 277-282.

Cheng, S. Z. D., & Jin, S. (2002). Chapter 5 - Crystallization and melting of metastable crystalline polymers. In Z. D. C. Stephen (Ed.), *Handbook of Thermal Analysis and Calorimetry* (Vol. Volume 3, pp. 167-195).

Cheuyglintase, K., & Morison, K. R. (2010). Carrot Fiber as a Carrier in Spray Drying of Fructose *Water Properties in Food, Health, Pharmaceutical and Biological Systems: ISOPOW 10* (pp. 191-197).

Chinachoti, P., & Steinberg, M. P. (1986). Moisture Hysteresis is Due to Amorphous Sugar. *Journnal of Food Science, 51*(2), 453-455.

Chirife, J., & Buera, M. P. (1995). A critical review of some non-equilibrium situations and glass transitions on water activity values of foods in the microbiological growth range. *Journal of Food Engineering, 25*(4), 531-552.

Couchman, P. R., & Karasz, F. E. (1978). A classical thermodynamic discussion of the effect of composition on glass-transition temperatures. *Macromolecules, 11*(1), 117-119.

Cowie, J. M. G., Garay, M. T., Lath, D., & McEwen, L. J. (1989). Formation of polymer-polymer complexes and blends in the system poly(acrylic acid)-poly(vinyl methyl ether). *British Polymer Journal, 21*(1), 81-85.

Davtyan, S. P., Tonoyan, A. O., Varderesyan, A. Z., & Müller, S. C. (2014). Frontal copolymerization in the presence of nano-particles. *European Polymer Journal, 57*, 182-186.

Di Gioia, L., & Guilbert, S. (1999). Corn Protein-Based Thermoplastic Resins: Effect of Some Polar and Amphiphilic Plasticizers. *Journal of Agricultural and Food Chemistry, 47*(3), 1254-1261.

Di Marzio, E. A. (1990). The glass temperature of polymer blends. *Polymer, 31*(12), 2294-2298.

Dietrich, H., Steden, E. K., Patz, C. D., Will, F., Rheinberger, A., & Hopf, I. (2007). Increase of sorbitol in pear and apple juice by water stress, a consquence of climate change? *Food Processing*(6), 348-356.

Djemour, A., Sanctuary, R., & Baller, J. (2015). Mobility restrictions and glass transition behaviour of an epoxy resin under confinement. *Soft Matter, 11*(13), 2683-2690.

Dolinsky, A., Maletskaya, K., & Snezhkin, Y. (2000). Fruit and vegetable powders production technology on the bases of spray and convective methods. *Drying Technology, 18*(3), 747-758.

Downton, G. E., Flores-Luna, J. L., & King, C. J. (1982). Mechanism of stickiness in hygroscopic, amorphous powders. *Industrial and Engineering Chemistry Fundamentals, 21*, 447-451.

Duvallet, S., Fenyo, J. C., & Vandevelde, M. C. (1989). Meaning of molecular weight measurements of gum arabic. *Polymer Bulletin, 21*(5), 517-521.

Ehrenfest, P. (1933). Phasenumwandlungen im üblichen und erweiterten Sinn, classifiziert nach den entsprechenden Singularitäten des thermodynamischen Potentiales. *Proceedings Koninklijke Akademie van Wetenschappen, 36*, 153-157.

Eisele, T. A., & Drake, S. R. (2005). The partial compositional characteristics of apple juice from 175 apple varieties. *Journal of Food Composition and Analysis, 18*(2–3), 213-221.

Elkins, E. R., Matthys, A., Lyon, R., & Huang, C. J. (1996). Characterization of Commercially Produced Apple Juice Concentrate. *Journal of Food Composition and Analysis, 9*(1), 43-56.

Elmonsef Omar, A. M., & Roos, Y. H. (2007). Water sorption and time-dependent crystallization behaviour of freeze-dried lactose–salt mixtures. *LWT - Food Science and Technology, 40*(3), 520-528.

Fabra, M. J., Talens, P., Moraga, G., & Martínez-Navarrete, N. (2009). Sorption isotherm and state diagram of grapefruit as a tool to improve product processing and stability. *Journal of Food Engineering, 93*(1), 52-58.

Fang, Z., & Bhandari, B. (2012). Comparing the efficiency of protein and maltodextrin on spray drying of bayberry juice. *Food Research International, 48*(2), 478-483.

Fang, Z., Wang, R., & Bhandari, B. (2013). Effects of Type and Concentration of Proteins on the Recovery of Spray-Dried Sucrose Powder. *Drying Technology, 31*(13-14), 1643-1652.

Farahnaky, A., Farhat, I. A., Mitchell, J. R., & Hill, S. E. (2009). The effect of sodium chloride on the glass transition of potato and cassava starches at low moisture contents. *Food Hydrocolloids, 23*(6), 1483-1487.

Finegold, L., Franks, F., & Haltey, R. H. M. (1989). Glass/rubber transitions and heat capacities of binary sugar blends. [10.1039/F19898502945]. *Journal of the Chemical Society, Faraday Transactions 1: Physical Chemistry in Condensed Phases, 85*(9), 2945-2951.

Fongin, S., Kawai, K., Harnkarnsujarit, N., & Hagura, Y. (2017). Effects of water and maltodextrin on the glass transition temperature of freeze-dried mango pulp and an empirical model to predict plasticizing effect of water on dried fruits. *Journal of Food Engineering, 210*, 91-97.

Ford, C. M. (2012). The Biochemistry of Organic Acids in the Grape. In H. Geros, M. Chaves & S. Delrot (Eds.), *The Biochemistry of the Grape Berries* (pp. 67-88).

Foster, K. D. (2002). *The Prediction of Sticking in Diary Powders* (PhD), Massey University, Massey University.

Fox, T. G. (1956). Influence of diluent and copolymer composition on the glass temperature of copolymers. *Bull. Am. Phys. Soc*(1).

Fox, T. G., & Flory, P. J. (1950). Second-order transition temperature and related properties of polystyrene. I. Influence of molecular weight. *J. Appli. Phys., 21*, 581-591.

Fukuoka, E., Makita, M., & Yamamura, S. (1989). Glassy State of Pharmaceuticals. III. : Thermal Properties and Stability of Glassy Pharmaceuticals and Their Binary Glass Systems. *Chemical & Pharmaceutical bulletin, 37*(4), 1047-1050.

Gernigon, G., Baillon, F., Espitalier, F., Le Floch-Fouéré, C., Schuck, P., & Jeantet, R. (2013). Effects of the addition of various minerals, proteins and salts of organic acids on the principal steps of α-lactose monohydrate crystallisation. *International Diary Journal 30*(2), 88-95.

Gordon, M., & Taylor, J. S. (1952). Ideal copolymers and the second-order transitions of synthetic rubbers. I. Non-crystalline copolymers. *Journal of Applied Chemistry, 2*, 493-500.

Griffith, J. H., & Rånby, B. G. (1960). Dilatometric measurements on poly(4-methyl-1-pentene) glass and melt transition temperatures, crystallization rates, and unusual density behavior. *Journal of Polymer Science, 44*(144), 369-381.

Gunko, S., Verbych, S., Bryk, M., & Hilal, N. (2006). Concentration of apple juice using direct contact membrane distillation. *Desalination, 190*(1), 117-124.

Gutzow, I. S., Schmelzer, J. W. P., Mazurin, O., Priven, A., Todorova, S., & Petroff, B. (2011). Basic Properties and the Nature of Glasses: An Overview *Glasses and the Glass Transition* (pp. 9-89): Wiley-VCH Verlag GmbH & Co. KGaA.

Hancock, B. C., & Zografi, G. (1994). The Relationship Between the Glass Transition Temperature and the Water Content of Amorphous Pharmaceutical Solids. [journal article]. *Pharmaceutical Research, 11*(4), 471-477.

Hartmann, M., & Palzer, S. (2011). Caking of amorphous powders — Material aspects, modelling and applications. *Powder Technology, 206*(1–2), 112-121. d

Hashizume, C., & Okuma, K. (2009). Fibersol-2 Resistant Maltodextrin: Functional Dietry Fiber Ingredient. In S. Sungsoo Cho & P. Samuel (Eds.), *Fiber Ingredients: Food Applications and Health Benefits* (pp. 480): CRC Press.

Hatakeyama, T., & Quinn, F. X. (1999). *Thermal Analysis Fundamentals and Applications to Polymer Science* (2 ed.): John Wiley & Sons

Heiberg, N., Måge, F., & Haffner, K. (1992). Chemical Composition of Ten Blackcurrant (Ribes nigrum L.) Cultivars. *Acta Agriculturae Scandinavica, Section B — Soil & Plant Science, 42*(4), 251-254.

Heiss, R., & Eichner, K. (1971). Die Haltbarkeit von Lebensmitteln mit niedrigen und mittleren Wassergehalten. *Chemie, Mikrobiologie, Technologie der Lebensmittel, 1*, 7.

Hillert, M. (2008). *Phase equilibria, phase diagrams and phase transformations : their thermodynamic basis*. Cambridge: Cambridge University Press

Hitac-Hightech. (1995). DSC measurements of polystrene: the effects of molecular weight on glass transition. (68).

Hoseney, R. C., Zeleznak, K. J., & Lai, C. S. (1986). Wheat gluten, a glassy polymer. *Cereal Chem, 63*, 2.

Hurtta, M., Pitkänen, I., & Knuutinen, J. (2004). Melting behaviour of d-sucrose, d-glucose and d-fructose. *Carbohydrate Research, 339*(13), 2267-2273.

Hwang, C.-A., Holste, J. C., Hall, K. R., & Ali Mansoori, G. (1991). A simple relation to predict or to correlate the excess functions of multicomponent mixtures. *Fluid Phase Equilibria, 62*(3), 173-189.

Icoz, D. Z., Moraru, C. I., & Kokini, J. L. (2005). Polymer–polymer interactions in dextran systems using thermal analysis. *Carbohydrate Polymers, 62*(2), 120-129.

Iglesias, H. A., Chirife, J., & Lombardi, J. L. (1975). Water sorption isotherms in sugar beet root. *International Journal of Food Science & Technology, 10*(3), 299-308.

Immergut, E. H., & Mark, H. F. (1965). Principles of Plasticization *Plasticization and Plasticizer Processes* (Vol. 48, pp. 1-26)

Islam, M. Z., Kitamura, Y., Yamano, Y., & Kitamura, M. (2016). Effect of vacuum spray drying on the physicochemical properties, water sorption and glass transition phenomenon of orange juice powder. *Journal of Food Engineering, 169*, 131-140.

Israelachvili, J. N. (2011). 4 - Interactions Involving Polar Molecules. In J. N. Israelachvili (Ed.), *Intermolecular and Surface Forces (Third Edition)* (pp. 71-90).

Izard, M. J., Ablett, S., Lillford, P. J., Hill, V. L., & Groves, I. E. (1996). A Modulated Differential Scanning Calorimetric study. *Journal of thermal analysis, 47*(5), 1407-1418.

Jasim, A. (2010). Thermal Phase Transitions in Food *Mathematical Modeling of Food Processing* (pp. 225-250): CRC Press.

Jaya, S., & Das, H. (2009). Glass Transition and Sticky Point Temperatures and Stability/Mobility Diagram of Fruit Powders. [journal article]. *Food and Bioprocess Technology, 2*(1), 89-95.

Jenckel, E., & Heusch, R. (1953). Die Erniedrigung der Einfriertemperatur organischer Gläser durch Lösungsmittel. *Kolloid-Zeitschrift, 130*(2), 89-105.

Jeong-Ah, S., Jiyoung, O., Kim, H. K., Hwang, Y.-H., Yang, Y. S., & Kim, S. J. (2005). Study of Glass Transition Temperatures in Sugar Mixtures. *Journal of the Korean Physical Society, 46*(3), 606-609.

Jiang, B., Liu, Y., Bhandari, B., & Zhou, W. (2008). Impact of Caramelization on the Glass Transition Temperature of Several Caramelized Sugars. Part I: Chemical Analyses. *Journal of Agricultural and Food Chemistry, 56*(13), 5138-5147.

Jin, X., van der Sman, R. G. M., van Maanen, J. F. C., van Deventer, H. C., van Straten, G., Boom, R. M., & van Boxtel, A. J. B. (2014). Moisture Sorption Isotherms of Broccoli Interpreted with the Flory-Huggins Free Volume Theory. [journal article]. *Food Biophysics, 9*(1), 1-9.

Jose, C. S., Asp, N. G., Burvall, A., & Dahlqvist, A. (1977). Water Sorption in Lactose Hydrolyzed Dry Milk. *Journal of Dairy Science, 60*(10), 1539-1543.

Jung, S. S., Lee, Y. B., & Jeon, B. S. (2014). Measurement of the Loss Factor and the Young's Modulus in Structural Steel by Using a Laser Beam Reflection Method Measurement of the Loss Factor and the Young's Modulus in Structural Steel. *Journal of the Korean Physical Society, 65*(7), 1024-1027.

Kalichevsky, M. T., Jaroszkiewicz, E. M., Ablett, S., Blanshard, J. M. V., & Lillford, P. J. (1992). The glass transition of amylopectin measured by DSC, DMTA and NMR. *Carbohydrate Polymers, 18*(2), 77-88.

Kalogeras, I. M. (2016). Glass-Transition Phenomena in Polymer Blends *Encyclopedia of Polymer Blends* (pp. 1-134): Wiley-VCH Verlag GmbH & Co. KGaA.

Kalogeras, I. M., & Brostow, W. (2009). Glass transition temperatures in binary polymer blends. *Journal of Polymer Science Part B: Polymer Physics, 47*(1), 80-95.

Kanig, G. (1963). Zur Theorie der Glastemperatur von Polymerhomologen, Copolymeren und weichgemachten Polymeren. *Kolloid-Zeitschrift und Zeitschrift für Polymere, 190*(1), 1-16.

Kawai, K., & Hagura, Y. (2012). Discontinuous and heterogeneous glass transition behavior of carbohydrate polymer–plasticizer systems. *Carbohydrate Polymers, 89*(3), 836-841.

Kefford, J. F., & Chandler, B. V. (1970). The chemical constituents of citrus fruits *Academic Press*, 169-211.

Kelebek, H., Selli, S., Canbas, A., & Cabaroglu, T. (2009). HPLC determination of organic acids, sugars, phenolic compositions and antioxidant capacity of orange juice and orange wine made from a Turkish cv. Kozan. *Microchemical Journal, 91*(2), 187-192.

Kelley, F. N., & Bueche, F. (1961). Viscosity and glass temperature relations for polymer-diluent systems. *Journal of Polymer Science, 50*(154), 549-556.

Kern Sears, J., & Darby, J. R. (1982). The Technology Of Plasticizers *Journal of Polymer Science: Polymer Letters Edition, 20*(8), 459-459.

Kets, E. P. W., Ijpelaar, P. J., Hoekstra, F. A., & Vromans, H. (2004). Citrate increases glass transition temperature of vitrified sucrose preparations. *Cryobiology, 48*(1), 46-54.

Khalloufi, S., El-Maslouhi, Y., & Ratti, C. (2000). Mathematical Model for Prediction of Glass Transition Temperature of Fruit Powders. *Journal of Food Science, 65*(5), 842-848.

Kilburn, D., Claude, J., Mezzenga, R., Dlubek, G., Alam, A., & Ubbink, J. (2004). *J. Phys. Chem. B, 108*, 12436.

Kim, Y. J., Suzuki, T., Hagiwara, T., Yamaji, I., & Takai, R. (2001). Enthalpy relaxation and glass to rubber transition of amorphous potato starch formed by ball-milling. *Carbohydrate Polymers, 46*(1), 1-6. d

Klonos, P., Panagopoulou, A., Bokobza, L., Kyritsis, A., Peoglos, V., & Pissis, P. (2010). Comparative studies on effects of silica and titania nanoparticles on crystallization and complex segmental dynamics in poly(dimethylsiloxane). *Polymer, 51*(23), 5490-5499.

Koppensteiner, J., Schranz, W., & Carpenter, M. A. (2010). Revealing the pure confinement effect in glass-forming liquids by dynamic mechanical analysis. *Physical Review B, 81*(2).

Krüger, J. K., Holtwick, R., le Coutre, A., & Baller, J. (1999). On the influence of nano-scaling on the glass transition of molecular liquids. *Nanostructured Materials, 12*(1), 519-522.

Kwei, T. K. (1984). The effect of hydrogen bonding on the glass transition temperatures of polymer mixtures. *Journal of Polymer Science: Polymer Letters Edition, 22*(6), 307-313.

Labuza, T. P., & Altunakar, L. (2008). Water Activity Prediction and Moisture Sorption Isotherms *Water Activity in Foods* (pp. 109-154): Blackwell Publishing Ltd.

Lang, K. W., & Steinberg, M. P. (1980). Calculation of moisture content of a formulated food system to any given water activity. *Journal of Food Science, 45*(5), 1228-1230.

Lazzús, J. A. (2012). A group contribution method to predict the glass transition temperature of ionic liquids. *Thermochimica Acta, 528*, 38-44.

Levi, G., & Karel, M. (1995). Volumetric shrinkage (collapse) in freeze-dried carbohydrates above their glass transition temperature. *Food Research International, 28*(2), 145-151.

Lewis, G. N., & Randall, M. (1924). Thermodynamics and the free energy of chemical substances. Von G. N. Lewis und M. Randall. MacGraw-Hill publishing Co.,

London 1923. *Zeitschrift für Elektrochemie und angewandte physikalische Chemie, 30*(21-22), 553A-554.

Liapis, A. I., & Bruttini, R. (2014). Freeze Drying *Handbook of Industrial Drying, Fourth Edition* (pp. 259-282): CRC Press.

Liu, P., Yu, L., Liu, H., Chen, L., & Li, L. (2009). Glass transition temperature of starch studied by a high-speed DSC. *Carbohydrate Polymers, 77*(2), 250-253.

Liu, Y., Bhandari, B., & Zhou, W. (2006). Glass Transition and Enthalpy Relaxation of Amorphous Food Saccharides: A Review. *Journal of Agricultural and Food Chemistry, 54*(16), 5701-5717.

Liu, Y., Heying, E., & Tanumihardjo, S. A. (2012). History, Global Distribution, and Nutritional Importance of Citrus Fruits. *Comprehensive Reviews in Food Science and Food Safety, 11*(6), 530-545.

Lozano, J. E. (2006). Processing of Fruits: Ambient and Low Temperature Processing *Fruit Manufacturing: Scientific Basis, Engineering Properties, and Deteriorative Reactions of Technological Importance* (pp. 21-54). Boston, MA: Springer US.

Lu, Q., & Zografi, G. (1997). Properties of citric acid at the glass transition. *Journal of Pharmaceutical Sciences, 86*(12), 1374-1378.

Lu, X., & Weiss, R. A. (1992). Relationship between the glass transition temperature and the interaction parameter of miscible binary polymer blends. *Macromolecules, 25*(12), 3242-3246.

Mandelkern, L. (2002). *Crystallisation of Polymers: Volume 1. Equilibrium Concepts* (2 ed.): Cambridge University Press

Masters, K. (1991). *Spray Drying Handbook 5th Edition*. Harlow, England: Longman Scientific & Technical

Matveev, Y. I., Grinberg, V. Y., Sochava, I. V., & Tolstoguzov, V. B. (1997). Glass transition temperature of proteins. Calculation based on the additive contribution method and experimental data. *Food Hydrocolloids, 11*(2), 125-133.

Matveev, Y. I., Grinberg, V. Y., & Tolstoguzov, V. B. (2000). The plasticizing effect of water on proteins, polysaccharides and their mixtures. Glassy state of biopolymers, food and seeds. *Food Hydrocolloids, 14*, 425-437.

McNamee, B. F., O'Riorda, E. D., & O'Sullivan, M. (2001). Effect of Partial Replacement of Gum Arabic with Carbohydrates on Its Microencapsulation Properties. *Journal of Agricultural and Food Chemistry, 49*(7), 3385-3388.

Miller, D. P., de Pablo, J. J., & Corti, H. (1997). Thermophysical Properties of Trehalose and Its Concentrated Aqueous Solutions. [journal article]. *Pharmaceutical Research, 14*(5), 578-590.

Mosquera, L. H., Moraga, G., & Martínez-Navarrete, N. (2012). Critical water activity and critical water content of freeze-dried strawberry powder as affected by maltodextrin and arabic gum. *Food Research International, 47*(2), 201-206.

Murti, R. A. (2006). *The effect of lactose source on the stickiness of dairy powders.* (M.E.), Massey University, Palmerston North.

Nakamura, S., Todoki, M., Nakamura, K., & Kanetsuna, H. (1988). Thermal analysis of polymer samples by a round robin method. *Thermochimica Acta, 136*, 163-178.

Nanasombat, S., Piumnoppakun, N., Atikanbodee, D., & Rattanasuwan, M. (2010). Combined Effect of Cinnamon Essential Oil and Water Activity on Growth Inhibition of Rhizopus stolonifer and Aspergillus fl avus and Possible Application in Extending the Shelf Life of Bread *Water Properties in Food, Health, Pharmaceutical and Biological Systems: ISOPOW 10* (pp. 545-550): Wiley-Blackwell.

Niness, K. R. (1999). Inulin and Oligofructose: What Are They? *The Journal of Nutrition, 129*(7), 1402S-1406S.

Orford, P. D., Parker, R., & Ring, S. G. (1990). Aspects of the Glass Transition Behaviour of Mixtures of Carbohydrates of Low Molecular Weight. *Carbohydrate Research, 196*, 11-18.

Orford, P. D., Parker, R., Ring, S. G., & Smith, A. C. (1989). Effect of Water as a Diluent on the Glass Transition Behaviour of Malto-Oligosaccharides, Amylose and Amylopectin. *International Journal of Biological Macromolecules, 11*, 91-96.

Ozmen, L., & Langrish, T. A. G. (2003). An Experimental Investigation of the Wall Deposition of Milk Powder in a Pilot-Scale Spray Dryer. *Drying Technology, 21*(7), 1253-1272.

Painter, P. C., Graf, J. F., & Coleman, M. M. (1991). Effect of hydrogen bonding on the enthalpy of mixing and the composition dependence of the glass transition temperature in polymer blends. *Macromolecules, 24*(20), 5630-5638.

Palzer, S. (2005). The effect of glass transition on the desired and undesired agglomeration of amorphous food powders. *Chemical Engineering Science, 60*(14), 3959-3968.

Paterson, A. H. J., & Bröckel, U. (2015). Caking Development in Lemon Juice Powder. *Procedia Engineering, 102*(0), 142-149.

Paterson, A. H. J., Bronlund, J. E., Zuo, J. Y., & Chatterjee, R. (2007). Analysis of Particle Gun Derived Dairy Powder Stickiness Curves. *International Dairy Journal, 17*(7), 860-865.

Paterson, A. H. J., Brooks, G. F., Foster, K. D., & Bronlund, J. E. (2005). The development of stickiness in amorphous lactose at constant T-Tg levels. *International Diary Journal, 15*, 513-519.

Pedrosa, P., Pomposo, J. A., Calahorra, E., & Cortazar, M. (1994). On the glass transition behavior, interaction energies, and hydrogen-bonding strengths of binary poly(p-vinylphenol)/polyether blends. *Macromolecules, 27*(1), 102-109.

Pikal, M. J., Mascarenhas, W. J., Akay, H. U., Cardon, S., Bhugra, C., Jameel, F., & Rambhatla, S. (2005). The Nonsteady State Modeling of Freeze Drying: In-Process Product Temperature and Moisture Content Mapping and Pharmaceutical Product Quality Applications. *Pharmaceutical Development and Technology, 10*(1), 17-32.

Pinal, R. (2008). Entropy of Mixing and the Glass Transition of Amorphous Mixtures. *Entropy, 10*(3), 207.

Piotr, P. L. (2009). Data and Models of Water Activity. II *Food Properties Handbook, Second Edition*: CRC Press. R

Privalov, P. L., & Plotnikov, V. V. (1989). Three generations of scanning microcalorimeters for liquids. *Thermochimica Acta, 139*, 257-277.

Rahman, M. S. (2009). Chapter 8. Glass Transition Data and Models of Foods. In M. S. Rahman (Ed.), *Food Properties Handbook, Second Edition* (pp. 247-285).

Redlich, O., & Kister, A. T. (1948). Algebraic Representation of Thermodynamic Properties and the Classification of Solutions. *Industrial & Engineering Chemistry, 40*(2), 345-348.

Research, P. a. F. (2019). New Zealand Food Composition Database: New Zealand Foodfiles 2016 Version 01 (Database). from The New Zealand Institute for Plant and Food Research Limited

Reutner, P., Luft, B., & Borchard, W. (1985). Compound formation and glassy solidification in the system gelatin-water. [journal article]. *Colloid and Polymer Science, 263*(7), 519-529.

Roos, Y. (1993a). Melting and glass transitions of low molecular weight carbohydrates. *Carbohydrate Research, 238*, 39-48.

Roos, Y., & Karel, M. (1991a). Water and Molecular Weight Effects on Glass Transitions in Amorphous Carbohydrates and Carbohydrate Solutions. *Journal of Food Science, 56*(6), 1676-1681.

Roos, Y. H. (1993b). Melting and Glass Transitions of Low Molecular Weight Carbohydrates. *Carbohydrate Research, 238*, 39-48.

Roos, Y. H. (1995). CHAPTER 4 - Water and Phase Transitions *Phase Transitions in Foods* (pp. 73-107). San Diego: Academic Press.

Roos, Y. H. (2006). Phase Transitions and Transformations in Food Systems *Handbook of Food Engineering, Second Edition* (pp. 287-352): CRC Press.

Roos, Y. H. (2008). Water Activity and Glass Transition *Water Activity in Foods* (pp. 29-45): Blackwell Publishing Ltd.

Roos, Y. H., & Karel, M. (1990). Differential scanning calorimetry study of the phase transitions affecting the quality of dehydrated materials. *Biotechnology Progress, 6*, 159-163.

Roos, Y. H., & Karel, M. (1991b). Amorphous state and delayed ice formation in sucrose solutions. *International Journal of Food Science and Technology, 26*, 553-566.

Roos, Y. H., & Karel, M. (1991c). Phase transitions of mixtures of amorphous polysaccharides and sugars. *Biotechnology Progress, 7*, 49-53.

Roos, Y. H., & Karel, M. (1991d). Plasticizing effect of water on thermal behavior and crystallization of amorphous food models. *Journal of Food Science, 56*(1), 38-43.

Roos, Y. H., & Karel, M. (1992). Crystallization of Amorphous Lactose. *Journal of Food Science, 57*(3), 775-777.

Roussenova, M., Andrieux, J.-C., Alam, M. A., & Ubbink, J. (2014). Hydrogen bonding in maltooligomer–glycerol–water matrices: Relation to physical state and molecular free volume. *Carbohydrate Polymers, 102*, 566-575.

Ruan, R., Long, Z., Chen, P., Huang, V., Almaer, S., & Taub, I. (1999). Pulse NMR Study of Glass Transition in Maltodextrin. *Journal of Food Science, 64*(1), 6-9.

Ruiz-Cabrera, M. A., Rivera-Bautista, C., Grajales-Lagunes, A., González-García, R., & Schmidt, S. J. (2016). State diagrams for mixtures of low molecular weight carbohydrates. *Journal of Food Engineering, 171*, 185-193.

Ruiz-Cabrera, M. A., & Schmidt, S. J. (2015). Determination of glass transition temperatures during cooling and heating of low-moisture amorphous sugar mixtures. *Journal of Food Engineering, 146*, 36-43.

Saavedra-Leos, M. Z., Grajales-Lagunes, A., González-García, R., Toxqui-Terán, A., Pérez-García, S. A., Abud-Archila, M. A., & Ruiz-Cabrera, M. A. (2012). Glass Transition Study in Model Food Systems Prepared with Mixtures of Fructose, Glucose, and Sucrose. *Journal of Food Science, 77*(5), E118-E126. d

Saleki-Gerhardt, A., & Zografi, G. (1994). Non-isothermal and isothermal crystallization of sucrose from the amorphous state. *Pharm. Res., 11*(8), 1166-1173.

Sanchez-Moreno, Sonia De Pascual-Teresa, Begona De Ancos, & Cano, M. P. (2012). Nutritional Quality of Fruits. In Nirmal k. Sinha, Jiwan S. Sidhu, james S.B. Wu, Jozsef Barta & M. P. Cano (Eds.), *Handbook Fruit and Fruit Processing*.

Schneider, H. A. (1988). The Gordon-Taylor equation. Additivity and interaction in compatible polymer blends. *Die Makromolekulare Chemie, 189*(8), 1941-1955.

Schneider, H. A. (1997). Conformational Entropy Contributions to the Glass Temperature of Blends of Miscible Polymers. *Journal of Research of the National Institute of Standards and Technology, 102*(2), 20.

Schneider, H. A., & Di Marzio, E. A. (1992). The glass temperature of polymer blends: comparison of both the free volume and the entropy predictions with data. *Polymer, 33*(16), 3453-3461.

Seo, J.-A., Kim, S. J., Kwon, H.-J., Yang, Y. S., Kim, H. K., & Hwang, Y.-H. (2006). The glass transition temperatures of sugar mixtures. *Carbohydrate Research, 341*(15), 2516-2520.

Shamblin, S. L., Taylor, L. S., & Zografi, G. (1998). Mixing Behavior of Colyophilized Binary Systems. *Journal of Pharmaceutical Sciences, 87*(6).

Shamblin, S. L., & Zografi, G. (1998). Enthalpy Relaxation in Binary Amorphous Mixtures Containing Sucrose. *Pharmaceutical Research, 15*(12), 1828-1834.

Shaw, M. T., & MacKnight, W. J. (2005). Transitions and Relaxation in Amorphous Polymers *Introduction to Polymer Viscoelasticity* (pp. 129-164): John Wiley & Sons, Inc.

Shrestha, A. K., Ua-arak, T., Adhikari, B. P., Howes, T., & Bhandari, B. R. (2007). Glass Transition Behavior of Spray Dried Orange Juice Powder Measured by Differential Scanning Calorimetry (DSC) and Thermal Mechanical Compression Test (TMCT). *International Journal of Food Properties, 10*(3), 661-673.

Simha, R., & Boyer, R. F. (1962). On a General Relation Involving the Glass Temperature and Coefficients of Expansion of Polymers. *The Journal of Chemical Physics, 37*(5), 1003-1007.

Simon, F. (1930). Fünfundzwanzig Jahre Nernstscher Wärmesatz *Ergebnisse der exakten naturwissenschaften* (pp. 222-274). Berlin, Heidelberg: Springer Berlin Heidelberg.

Soesanto, T., & Williams, M. C. (1981). Volumetric Interpretation of Viscosity for Concentrated and Dilute Sugar Solutions. *Journal of Physical Chemistry, 85*, 3338-3341.

Sopade, P. A., Bhandari, B. R., D'Arcy, B., Halley, P., & Caffin, N. (2002). A study of vitrification of Australian honeys at different moisture contents In H. Levine (Ed.), *Amorphous Food and Pharmaceutical Systems* (1st ed., pp. 168-183): Royal Society of Chemistry.

Sperling, L. H. (1986). Glass-Rubber transition behaviour. In L. H. Sperling (Ed.), *Introduction to physical polymer science* (pp. 224-295). New York: Wiley.

Sperling, L. H. (2005). Glass-Rubber Transition Behavior *Introduction to Physical Polymer Science* (pp. 349-425): John Wiley & Sons, Inc.

Struik, L. C. E. (1978). *Physical aging in amorphous polymers and other materials.* (PhD), TU Delft.

Takeiti, C. Y., Kieckbusch, T. G., & Collares-Queiroz, F. P. (2010). Morphological and Physicochemical Characterization of Commercial Maltodextrins with Different Degrees of Dextrose-Equivalent. *International Journal of Food Properties, 13*(2), 411-425.

Tang, X., & Pikal, M. J. (2004). Design of freeze-drying processes for pharmaceuticals: practical advice. *Pharmaceutical Research, 21*(2), 191-200.

Tedeschi, C., Leuenberger, B., & Ubbink, J. (2016). Amorphous–amorphous phase separation in hydrophobically-modified starch–sucrose blends I. Phase behavior and thermodynamic characterization. *Food Hydrocolloids, 58*, 75-88.

Telis, V. R. N., & Martínez-Navarrete, N. (2009). Collapse and Color Changes in Grapefruit Juice Powder as Affected by Water Activity, Glass Transition, and Addition of Carbohydrate Polymers. *Food Biophysics, 4*(2), 83-93.

Telis, V. R. N., & Martínez-Navarrete, N. (2012). Biopolymers Used as Drying Aids in Spray-Drying and Freeze-Drying of Fruit Juices and Pulps *Biopolymer Engineering in Food Processing* (pp. 279-326): CRC Press.

Timothy, A. G. L. (2010). Mathematical Modeling Spray Dryers *Mathematical Modeling of Food Processing* (pp. 301-329): CRC Press.

Tonon, R. V., Baroni, A. F., Brabet, C., Gibert, O., Pallet, D., & Hubinger, M. D. (2009). Water sorption and glass transition temperature of spray dried açai (Euterpe oleracea Mart.) juice. *Journal of Food Engineering, 94*(3–4), 215-221.

Townrow, S., Roussenova, M., Giardiello, M.-I., Alam, A., & Ubbink, J. (2010). Specific Volume−Hole Volume Correlations in Amorphous Carbohydrates: Effect of Temperature, Molecular Weight, and Water Content. *The Journal of Physical Chemistry B, 114*(4), 1568-1578.

Truong, V. (2003). *Modelling of the glass transition temperature of sugar-rich foods and its relation to spray drying of such products* (PhD thesis), The University of Queensland.

Truong, V., Bhesh, B., Howes, T., & Adhikari, B. (2002). Analytical Model for the Prediction of Glass Transition Temperature of Food Systems. In H. Levine (Ed.), *Amorphous Food and Pharmaceutical Systems*: The Royal Society of Chemistry 2002.

Tucker, G. A. (1993). Introduction. In G. B. Seymour, J. E. Taylor & G. A. Tucker (Eds.), *Biochemistry of Fruit Ripening* (pp. 1-51). Dordrecht: Springer Netherlands.

Ubbink, J. (2010). Carbohydrates in Amorphous States: Molecular Packing, Nanostructure, and Interaction with Water *Water Properties in Food, Health, Pharmaceutical and Biological Systems: ISOPOW 10* (pp. 353-371): Wiley-Blackwell.

Ubbink, J., Giardiello, M., & Limbach, H. J. (2007). Sorption of Water by Bidisperse Mixtures of Carbohydrates in Glassy and Rubbery States. *Biomacromolecules, 8*(9), 2862-2873.

Utracki, L. A., & Favis, B. D. (1989). Polymer Alloys and Blends. In N. P. Cheremisinoff (Ed.), *Handbook of Polymer Science and Technology*: Marcel Dekker Inc.

van der Berg, C., & Bruin, S. (1981). Water activity and its estimation in food systems: theoretical aspects A2. In G. F. Stewart (Ed.), *Water Activity: Influences on Food Quality* (pp. 1-61): Academic Press.

van der Sman, R. G. M. (2013a). Moisture sorption in mixtures of biopolymer, disaccharides and water. *Food Hydrocolloids, 32*(1), 186-194.

van der Sman, R. G. M. (2013b). Predictions of Glass Transition Temperature for Hydrogen Bonding Biomaterials. *The Journal of Physical Chemistry B, 117*(50), 16303-16313.

van der Sman, R. G. M. (2016). Sugar and polyol solutions as effective solvent for biopolymers. *Food Hydrocolloids, 56*, 144-149.

van der Sman, R. G. M. (2017). Predicting the solubility of mixtures of sugars and their replacers using the Flory–Huggins theory. [10.1039/C6FO01497F]. *Food & Function, 8*(1), 360-371.

Vanamala, J., Reddivari, L., Yoo, K. S., Pike, L. M., & Patil, B. S. (2006). Variation in the content of bioactive flavonoids in different brands of orange and grapefruit juices. *Journal of Food Composition and Analysis, 19*(2–3), 157-166.

Vanhal, I., & Blond, G. (1999). Impact of Melting Conditions of Sucrose on its Glass Transition Temperature. *Journal of Agricultural and Food Chemistry, 47*, 4285-4290.

Verma, A., & Singh, S. V. (2015). Spray Drying of Fruit and Vegetable Juices—A Review. *Critical Reviews in Food Science and Nutrition, 55*(5), 701-719.

Viganó, J., Azuara, E., Telis, V. R. N., Beristain, C. I., Jiménez, M., & Telis-Romero, J. (2012). Role of enthalpy and entropy in moisture sorption behavior of pineapple pulp powder produced by different drying methods. *Thermochimica Acta, 528*, 63-71.

Vrentas, J. S., & Vrentas, C. M. (1991). Sorption in glassy polymers. *Macromolecules, 24*(9), 2404-2412.

Weng, L., Vijayaraghavan, R., MacFarlane, D. R., & Elliott, G. D. (2014). Application of the Kwei Equation tomodel the T(g) Behavior of Binary Blends of Sugars and Salts. *Cryobiology, 68*(1), 155-158.

Willems, J. L., & Low, N. H. (2016). Oligosaccharide formation during commercial pear juice processing. *Food Chemistry, 204*, 84-93.

Wunderlich, P. D. B. (2005). *Thermal Analysis of Polymeric Materials*: Springer

Wungtanagorn, R., & Schmidt, S. J. (2001a). Phenomenological study of enthalpy relaxation of amorphous glucose, fructose, and their mixture. *Thermochimica Acta, 369*(1–2), 95-116.

Wungtanagorn, R., & Schmidt, S. J. (2001b). Thermodynamic Properties and Kinetics of the Physical Ageing of Amorphous Glucose, Fructose, and Their Mixture. [journal article]. *Journal of Thermal Analysis and Calorimetry, 65*(1), 9-35.

Yu, L. (2001). Amorphous pharmaceutical solids: preparation, characterization and stabilization. *Advanced Drug Delivery Reviews, 48*(1), 27-42.

Zallen, R. (2007). The Formation of Amorphous Solids *The Physics of Amorphous Solids* (pp. 1-32): Wiley-VCH Verlag GmbH.

Zeleznak, K. J., & Hoseney, R. C. (1987). the glass transition in starch. *American Association of Cereal Chemists, 64*(2), 5.

Zhang, J., & Zografi, G. (2000). The Relationship Between "BET"- and "Free Volume"-Derived Parameters for Water Vapor Absorption into Amorphous Solids. *Journal of Pharmaceutical Sciences, 89*(9), 1063-1072.

Zhang, J., & Zografi, G. (2001). Water vapor absorption into amorphous sucrose-poly(vinyl pyrrolidone) and trehalose–poly(vinyl pyrrolidone) mixtures. *Journal of Pharmaceutical Sciences, 90*(9), 1375-1385.

Zhang, S. H., Jin, X., Painter, P. C., & Runt, J. (2004). Composition-dependent dynamics in miscible polymer blends: influence of intermolecular hydrogen bonding. *Polymer, 45*(11), 3933-3942.

Zuo, J., Paterson, A. H. J., Bronlund, J., & Truong, T. (2004). *Push your Spray Dryer to the Limit*. Paper presented at the The 2nd International Symposium on Spray Drying of Milk Products, Cork, Ireland, 19th- 21st October. 2004. Also presented at SCENZ conference June 2005. Christchurch, New Zealand and at PackTech FoodTech 2006 show, Auckland, New Zealand. 17-19 October 2006.